DE NOVO INITIATED RNA SYNTHESIS BY THE HEPATITIS C VIRUS RNA-

DEPENDENT RNA POLYMERASE

A Dissertation

by

SREEDHAR REDDY CHINNASWAMY

Submitted to the office of Graduate Studies of
Texas A&M University
in partial fulfillment of the requirements for the degree of

DOCTOR OF PHILOSOPHY

May 2010

Major Subject: Biochemistry

DE NOVO INITIATED RNA SYNTHESIS BY THE HEPATITIS C VIRUS RNA-

DEPENDENT RNA POLYMERASE

A Dissertation

by

SREEDHAR REDDY CHINNASWAMY

Submitted to the office of Graduate Studies of
Texas A&M University
in partial fulfillment of the requirements for the degree of

DOCTOR OF PHILOSOPHY

Approved by:

Co-Chairs of Committee,	Cheng C. Kao
	Ryland F. Young
Committee Members,	Julian L. Leibowitz
	Martin J. Scholtz
Head of Department,	Gregory D. Reinhart

May 2010

Major Subject: Biochemistry

ABSTRACT

De Novo Initiated RNA Synthesis by the Hepatitis C Virus RNA-dependent RNA

Polymerase. (May 2010)

Sreedhar Reddy Chinnaswamy, B.V.Sc. & A.H., University of Agricultural Sciences,

Bangalore; M.V.Sc., Indian Veterinary Research Institute; MS, New Mexico State

University at Las Cruces.

Co-Chairs of Advisory Committee,   Dr. Cheng C. Kao
                                Dr. Ryland F. Young

Hepatitis C Virus (HCV) is a positive-strand RNA virus that has infected more than 3% of the world population. Chronic infections by the virus lead to cirrhosis and hepatocellular carcinoma. HCV is currently the leading cause for liver transplantation in the US. The nonstructural protein NS5B of HCV is the RNA-dependent RNA polymerase (RdRp) that replicates the viral RNA on host derived membranous structures.

Structurally NS5B has the characteristic fingers, thumb and palm domains seen in all polymerase proteins. However, extensive interactions between the fingers and thumb domains completely encircle the active site of NS5B as seen in solved X-ray diffraction crystal structures. These interactions are primarily mediated by a short (35 residues) flexible loop called the $\Delta 1$ loop. NS5B produced from heterologous systems can initiate RNA synthesis by a de novo initiation mechanism from 3'ends of RNA templates or can also extend from 3' ends of primers that are annealed stably to a template RNA in biochemical assays. The closed conformation of NS5B as per X-ray crystal structures can only accommodate a ssRNA but not a dsRNA, hence necessitating a conformational

change between de novo initiation and elongation. The details of these conformational changes are not known and will prove to be important to design potent polymerase inhibitors. The study performed for this dissertation focused on the conformational requirements of NS5B during de novo initiation and primer extension (or elongation). Biochemical assays utilizing template RNAs that can lead to both de novo initiation and primer extension products were utilized, and a systematic mutational analysis of the template channel of the RdRp was performed. Mutants W397A and H428A were identified that showed only primer extension but no de novo initiation. Structural analysis of NS5B suggested that these residues were important contact points in the Δ1 loop and thumb domain interactions. A deletion mutant, m26-30 with a five amino acid deletion at the apex of the Δ1 loop also failed in de novo initiation but not primer extension reactions. Biophysical and gel shift assays showed that m26-30 was in a more open conformation than the WT enzyme. Furthermore, oligomerization of NS5B was demonstrated and its role in RNA synthesis was examined. It was found that the de novo initiation competent conformation of NS5B is maintained by oligomeric contacts between individual subunits, likely by stabilizing the Δ1 loop and thumb domain interactions. Mutations disrupting the Δ1 loop and thumb domain interactions as well as those in the allosteric GTP binding site induced conformational changes in the protein partially explaining the defect in de novo initiation activity in enzymes carrying those mutations. These results not only contribute to the overall mechanism of RNA synthesis in viral RdRps but also open new avenues for developing HCV polymerase inhibitors.

DEDICATION

I dedicate this dissertation to: My wife and son without whom I may not have come to this stage in education; my loving mother and father; and my mentor Dr. Cheng Kao.

ACKNOWLEDGEMENTS

My heartfelt thanks will go to Dr. Cheng Kao, for his support, guidance and exceptional mentorship. I thank my committee members, Dr. Ryland Young, Dr. Julian Leibowitz and Dr. Martin Scholtz for being on my committee and helping me in the course of this study. I would also like to thank Dr. Mike Kladde, Dr. Paul Fitzpatrick and Dr. William D. Park who were associated with me at various stages in the program, for their help.

I would like to thank and acknowledge the people who have been associated with me during my degree program at Texas A&M. My thanks are due to the members of the Kao lab: Drs Ranjith, Murali, Kanchan, Guanghui, Hui and Gopinath. I would like to remember the help of Ian, Robert and Peng; the association with Drs Yvonne, Hema, Xiaopeng, Koki and Kirti will be fondly remembered. I shall cherish the time spent with Liting, Yahong and Rongsu. My special thanks to the Kao family: Laura, Addy and Rene for their nice influence on me.

I would like to thank our collaborators: Dr. Stanley Lemon and Dr. Hengli Tang for including me in their work. My thanks to Dr. William Lott, my MS advisor for his encouragement.

Finally, I thank my wife Prathibha and son Kushal for their love.

ABBREVIATIONS

BME   beta-mercaptoethanol

BN-PAGE   Blue native-polyacrylamide gel electrophoresis

BVDV   Bovine viral diarrhea virus

CsA   Cyclosporine A

Cyp   Cyclophilin

DLS   Dynamic light scattering

EM   Electron microscopy

ER   Endoplasmic reticulum

HCV   Hepatitis C virus

IC   Initiation complex

IFN   Interferon

IMP   Inosine monophosphate

IRES   Internal ribosome entry site

JFH   Japanese fulminant hepatitis

MOA   Mechanism of action

NI   Nucleoside inhibitors

NNI   Non-Nucleoside inhibitors

Ni-NTA   Nickel nitrilotriacetic acid

NS   Nonstructural

NTPs   Nucleotide triphosphates

PE	Primer extension
pRb	Retinoblastoma protein
RC	Replication complex
RdRp	RNA-dependent RNA polymerase
REM	Replication enhancing mutations
RIG-I	Retinoic acid inducible gene I
SAR	Structure activity relationships
SDS-PAGE	Sodium dodecyl sulphate- polyacrylamide gel electrophoresis
SELEX	Systematic evolution of ligands by exponential amplification
UTR	Untranslated region
TMD	Trans membrane domain
Tris	tris(hydroxymethyl) aminomethane

TABLE OF CONTENTS

LIST OF FIGURES

LIST OF TABLES

CHAPTER I

INTRODUCTION*

Hepatitis C virus (HCV) was first identified as the causative agent of non-A non-B viral hepatitis in the late 1970's. It was estimated in the year 2000 that HCV had infected over 170 million people worldwide (*1*). Infection can be through injection drug use, contaminated blood transfusion, needle pricks and also unprotected sex. A majority of the acute infections lead to chronic conditions characterized by cirrhosis and hepatocellular carcinoma (*2*). HCV is the leading cause for liver transplantation in the US. A humoral immune response is raised by the host in acute infections, but does not lead to elimination of the virus in 80% of cases and results in chronic infection. Men are about twice less likely to clear the virus during the acute phase of infection than women (*3*). It is also common that HCV can cause an acute infection more than once in the same individual, due to the virus changing its antigenic properties frequently because of an error prone RNA polymerase that can readily incorporate mutations into the genome (referred to as quasispecies) (*4*). The molecular clone of the virus was isolated in 1989 by Michael Houghton's Lab at Chiron Corporation (*5*). Subsequent to this discovery, significant progress has been made in understanding HCV biology (*6*), although a vaccine for prevention and a safe and potent drug for treatment of HCV infections

_____

This dissertation follows the style of *Biochemistry.*
*Fig. 3 in this chapter is reprinted in part with permission from "Replication of hepatitis C virus" by Moradpour, D., Penin, F., and Rice, C. M. (2007). *Nature Reviews Microbiolgy.* **5**, 453-463. Copyright [2009] by Nature Publishing Group.

is not yet available. This chapter provides an introduction to HCV; briefly reviews the

problems encountered in HCV research; introduces the RNA polymerase of HCV with

an emphasis on its structure and function; discusses the mechanism of RNA synthesis in

different viral RdRps and concludes with a discussion on the scope of the research that is

the basis for this dissertation.

LIFE CYCLE AND GENOME ORGANIZATION OF HCV

HCV is an enveloped positive-strand RNA virus that belongs to the family

Flaviviridae, which includes other human viruses like Dengue virus and West Nile virus.

To our knowledge, HCV can successfully infect only humans and chimpanzees. Unlike

the other members of the family which involve complex life cycles with arthropod

vectors as intermediate hosts, HCV does not have insect or other known intermediate

hosts (Fig. 1). HCV infects hepatocytes but can infect other cell types like lymphocytes

and astrocytes in the brain by a receptor mediated endocytosis pathway involving mainly

the CD81 receptor and Claudin-1 receptors (*7*). The RNA genome of HCV is ~9.6 kb in

length and encodes a polyprotein that is cleaved by host and viral proteases into

structural and non-structural components (Fig. 2). The 5' and 3' UTRs of the HCV

genome are highly structured. The 5' UTR contains an internal ribosome entry site

(IRES) that recruits host ribosomes to translate the viral genome. The 5' UTR, 3' UTR

and even the coding region have important cis-acting replication elements needed to

initiate genomic RNA synthesis (*8*).
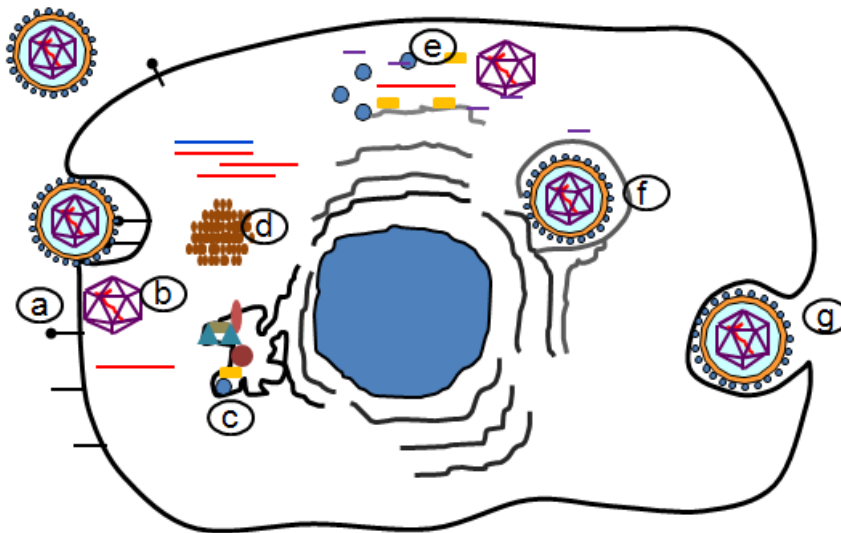
Figure 1: HCV life cycle in an infected cell. Virus binding to receptors and receptor mediated endocytosis a); uncoating of the viral structural proteins and release of genomic RNA (red line) b); translation of viral polyprotein and cleavage into its individual components c); assembly of viral replication complexes (RC) on 'membranous webs' which are composed of host derived membranes and proteins; and production of negative strand RNA (blue line) and positive-strand RNA (red line) d); assembly of new virus particles e); maturation of virus particles f); new virus particles exit the cells by budding g); This figure is adapted from reference (7). The nucleus is in blue and ER membranes are shown as dark lines while the 'membranous web' structures are shown as brown oval structures. The translated viral proteins are in different shapes and colors on the putative ER structures. The receptors that bind and internalize HCV are shown as dark straight lines with blunt or round ends on the plasma membrane. HCV is shown as an icosahedral particle (a clear explanation for the arrangement of the capsid including the triangulation number is not available largely due to an inability to produce and assemble sufficient amounts of the capsids in vitro) encapsidating the genome (red). The icosahedron is made of core protein (purple lines) while the E1 and E2 (see below) surround the core protein and are shown as blue spheres and a yellow layer.
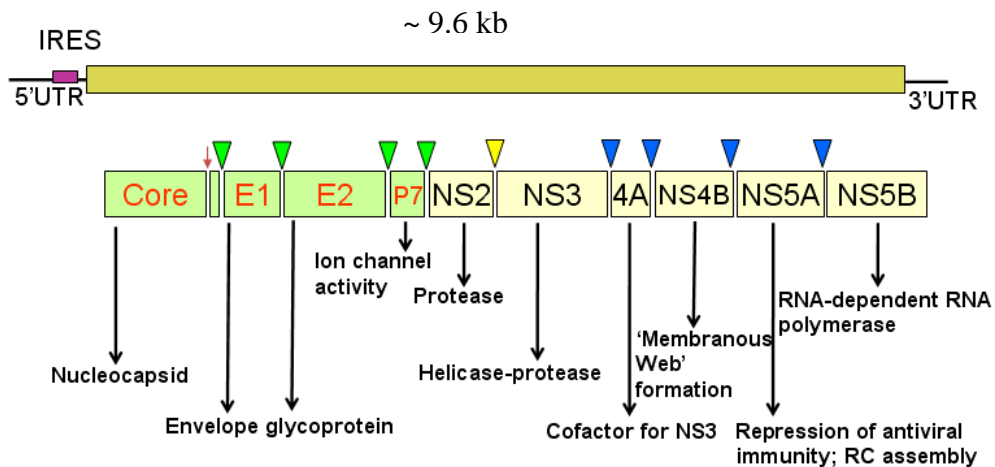
Figure 2: HCV polyprotein cleavage. The positive-sense RNA is schematically depicted on the top with the size of the genome indicated. The internal ribosome entry site (IRES) is depicted as a purple box in the 5' UTR. A schematic of the arrangements of the mature HCV proteins is shown below the RNA. The polyprotein coding sequence is shown in green and yellow blocks (green for structural proteins and yellow for non-structural proteins). The green inverted triangles represent cleavage by the host signal peptidases. The core protein is further processed at its C-terminus by the ER signal peptide peptidase (brown arrow). The NS2 protease separates itself from NS3 and the remaining polyprotein by autoproteolysis (yellow inverted triangle). The remaining polyprotein is cleaved by NS3 protease by using NS4A as the cofactor (blue inverted triangles). The putative functions of the individual proteins are indicated below each protein. RC-replication complex.

The core, E1 and E2 proteins form the structural components of the HCV virion and are processed by endoplasmic reticulum (ER) proteases. The core protein surrounds the viral genome forming the nucleocapsid and has a basic N-terminus and a hydrophobic C-terminus (*9*). E1 and E2 are glycosylated proteins and have important immunogenic regions including the hypervariable region (HVR) in E2 which is responsible for immune evasion (*10*). E1 and E2 spike the nucleocapsid throughout the surface and are responsible for membrane fusion and viral entry (*11*). p7 is a ~60 amino acid protein that is required for viral replication in vivo and has ion channel activity (*12*).

The nonstructural proteins NS2, NS3, NS4A, NS4B, NS5A and NS5B are processed by NS2 protease and NS3-4A protease (Fig. 3). NS2 is an autoprotease that cleaves the NS2-3 junction. There is evidence to suggest that NS2 is active as a dimer (*13*), and recent evidence implicates NS2 in virus assembly (*14*). NS3 is a bifunctional enzyme with a serine protease activity at its N-terminus and an ATP dependent helicase activity at the C-terminus. The protease activity cleaves the nonstructural proteins from NS3 to NS5B in the polyprotein sequence by using NS4A as a cofactor. NS3-4A also cleaves the adaptor proteins that function in innate immunity signaling and helps the virus evade host immune responses (*15*). NS4B is a membrane-associated protein and is needed to form 'membranous webs', the sites of HCV replication complexes (RC) in the endoplasmic reticulum (ER) (*16*). These structures are unique to HCV infected cells which are made of ER derived membranes and are defined as tight structures made of tiny vesicles in a membranous matrix or sponge-like inclusion bodies (*16*). NS5A is an

Figure 3: The HCV proteins and their membrane association. This figure is reproduced with permission from reference (*7*). The known structures of the proteins are depicted as ribbon diagrams while the unsolved structures are shown as grey spheres and transmembrane domains are shown as helices buried in the membrane. The semi-circular arrow denotes NS2 autoproteolytic cleavage. The straight arrows indicate NS3 cleavage regions. Almost all the HCV proteins have at least one transmembrane domain or a membrane associated amphipathic helix. The core protein has two amphipathic helices and a C-terminal signal peptide (green). The scissors indicate cleavage by ER associated signal peptidases. (Signal peptide peptidase cleavage is shown by the scissor on the cytosolic side). The glycosylation of the envelope proteins E1 and E2 heterodimers are shown as green spots. The p7 protein has an extended and a short transmembrane domain. The NS2 dimer (catalytic domains are shown as blue and pink ribbons) is tethered to the membrane at their N-terminal hydrophobic domains (*13*). The NS3 protease domain is shown in blue and its catalytic residues are shown as purple spheres. The amphipathic helix in NS3 protease is in green and the N-terminal transmembrane domain and NS3 associated domain of NS4A are in gold. NS3 helicase is shown connected to the protease domain and its three domains are colored orange, blue and grey. The NS4B structure is not available and is shown as a membrane protein with a cytosolic C-terminal domain. The dimerized domain I of NS5A are shown as ice blue and magenta ribbons while the N-terminal amphipathic helix is shown as orange and blue ribbons. Domains II and III of NS5A are shown as grey ovals. NS5B C-terminal transmembrane domain is in magenta and the thumb, palm and fingers domain are in green, orange and blue. The detailed description of the specifics in generating this figure is found in reference (*7*) and the references therein.
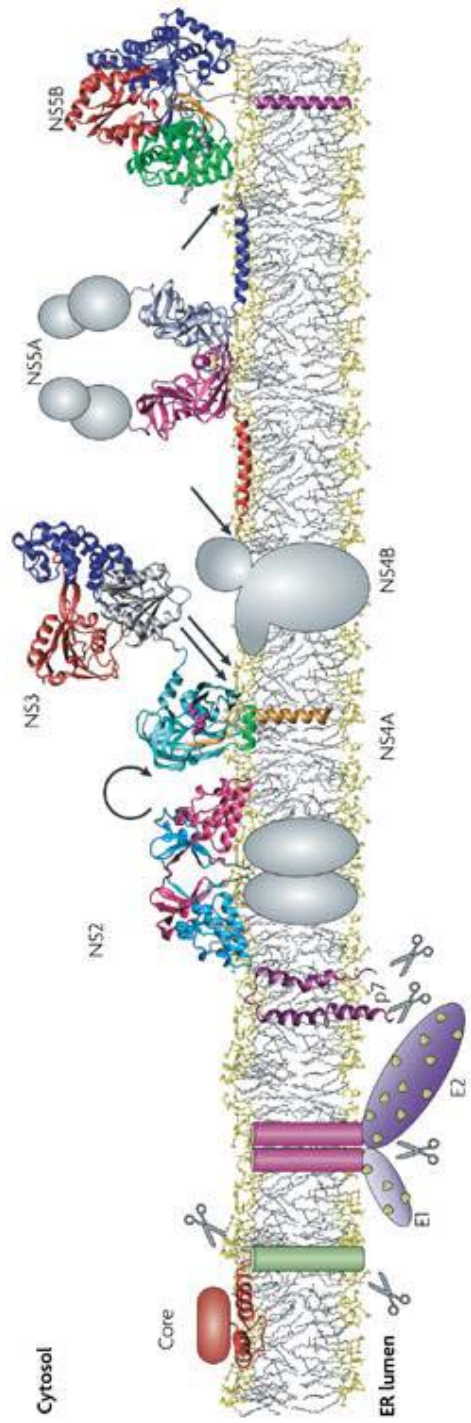
RNA binding protein that exists in a phosphorylated form in cells, is known to suppress anti-viral immunity (*17*), and may have a role in modulating the dependence of HCV on cyclophilins (*18*). NS5B is the RNA-dependent RNA polymerase (RdRp) that synthesizes viral RNA in the RC. The RC also contains other viral nonstructural proteins as well as host proteins and is associated with 'lipid rafts' (*19*), and 'lipid droplets' (*20*) in HCV infected cells. Lipid rafts and lipid droplets are specialized membrane microdomains that are detergent-resistant, with the latter showing a characteristic staining with oil red O stain. It has also been noted that a large portion of the HCV NS proteins do not participate in replication of the viral genome (*21*), suggesting that some of them may have additional functions like interactions with host factors and modulating the host environment. NS5B is known to bind and down-regulate the abundance of the master tumor suppressor Retinoblastoma protein (pRb) (*22*).

PROBLEMS IN HCV RESEARCH

A prophylactic vaccine and effective therapeutic options are not yet available for HCV, despite determination of the HCV sequence 20 years ago and extensive research efforts. This speaks of how intractable HCV has been both in the clinic and in the laboratory. HCV exists as a quasispecies, due to an error prone RNA polymerase that lacks proof-reading activity, making targeted therapies difficult (*23*). There are also six HCV genotypes (named as genotypes 1 to 6) and several subtypes in each genotype (named as a, b, c, etc) that respond differently or not at all to the standard therapy of pegylated interferon and ribavirin. As mentioned above, HCV can modulate the immune

responses from the host. Altogether these features of HCV have made it refractory to vaccine development (*24-26*).

Two additional challenges had plagued the early phase of HCV research. Firstly there is no natural, small animal model for studies of the infection and pathologies. Indeed, even infected chimpanzees exhibit only minimal pathologies, unlike humans(*27*) . Second, prior to 2005, HCV could not efficiently infect cultured cells. Therefore, studies of HCV in the laboratory were limited to infecting chimpanzees and working on recombinant portions of the HCV genome.

A breakthrough came in 1999, when Lohmann et al., developed the subgenomic replicon system for HCV (*28*). Subgenomic replicons are viral mini-genomes that lack the genes encoding structural proteins but have genes encoding fully functional nonstructural proteins that can replicate RNA in cell culture and can express reporter genes (*28*). Mutations in NS5A, NS3 and NS4B were necessary for the replicons to multiply in cells to sufficient levels (named as replication enhancing mutations or REMs) (*29*). These adaptive mutations also helped the full-length viral genome to replicate in cells but they failed to produce infectious viral particles (*30*). Nonetheless, these replicons taught us important features about HCV replication and served as the initial systems for the identification of HCV inhibitors.

Studies of HCV replicons revealed an important interaction with the innate immunity system. A subgenomic replicon system was initially established in the human hepatoma cell line (Huh-7) for the genotype 1b virus (con 1 isolate). Curing the Huh-7 cells with interferon has led to cell lines like Huh-7.5 that allowed HCV replicons to

replicate to higher levels. Characterization of the Huh-7.5 cells led to the identification of a defect in the innate immunity receptor, RIG-I (*31*), that allowed more efficient HCV subgenomic replication. REMs were later identified in the NS3 and NS5A region of genotype 1a HCV that supported subgenomic replication in Huh-7.5 cells (*31*).

A major breakthrough in HCV research was the isolation of a genotype 2a HCV strain that caused fulminant hepatitis in a Japanese patient (named JFH1) and the subsequent establishment of cell culture infections using this strain (*32-33*). JFH1 could successfully infect Huh-7.5 cells and multiply without the need for REMs. The JFH1 isolate opened the door for researchers to study the complete cycle of the HCV infection, especially viral entry. A feature of the JFH1 virus, however, is that it was not pathogenic in chimpanzees (*34*), and the prevalence of the 1a and 1b HCV infection in the western world precluded 2a from serving as a vaccine strain. In studies on HCV RNA replication, the subgenomic replicon system, along with NS5B protein expressed from heterologous systems, remains to be extensively used to understand the mechanism of RNA synthesis and also to develop inhibitors targeting NS5B.

NS5B, THE RNA-DEPENDENT RNA POLYMERASE OF HCV

NS5B is the key enzyme for HCV replication and is the focus of this dissertation project. Like other polymerases, NS5B has the characteristic divalent metal binding motif, GDD that contains two consecutive aspartates in the palm domain consistent with the notion that all polymerases use the two-metal ion mechanism of catalysis (*35*). The 591-amino acids NS5B protein has a hydrophobic C-terminal tail (21 amino acids)

needed to tether the protein on to the membranes (Fig. 3). These residues are dispensable for enzymatic activity but needed for viral replication in cells (*36-37*). NS5B lacking the C-terminal hydrophobic 21 amino acids (referred as Δ21) or 55 amino acids (referred as Δ55) is widely used in biochemical assays both for mechanism studies and inhibitor studies (*36, 38-42*). No significant differences between the enzyme kinetics of the full-length versus Δ21 enzymes were observed (*36, 43*). Δ21 however, is several fold more active than the full-length protein in both de novo initiation and primer extension assays. This may be due to efficient template binding and turnover since the K_M for the different NTPs were the same for both proteins (*43*).

HCV NS5B was initially identified based on homology with the RdRps of other viruses with positive-strand RNA genomes (*44*). The first report on the enzymatic activity of HCV NS5B was published in 1996 by Behrens et al. (*45*). In this report baculovirus expressed HCV RdRp was characterized to have a primer extension activity with heterologous RNA templates. The primer in this RNA was formed by a 'looping-back' of the 3' end of the template RNA. Lohmann et al., (*46*) demonstrated that a recombinant NS5B was able to copy the full-length HCV positive-strand genomic RNA by a 'copy-back' synthesis from the 3' end of the template. Although these works established the polymerase activity of HCV RdRp, the mechanism of initiation on the natural viral genomic templates remained unclear. The reported 'loop-back' primer extension activity does not represent a mechanism relevant to HCV RNA replication and the 'loop-back' structure is present at the 3' end of plus-strand but not minus-strand HCV genomic RNA (*47-48*). During this time a related RdRp from the Bovine Viral

Diarrhea Virus (BVDV) was reported to initiate RNA synthesis by a de novo mechanism, suggesting the possibility that a similar mechanism existed for HCV RdRp (*49*). De novo initiation was soon demonstrated with recombinant HCV NS5B using both short synthetic RNA templates as well as from the full-length and truncated positive-strand HCV genomic RNA (*50-53*). Kao et al., showed that a stable secondary structure is needed at the 3' end of the template RNA for efficient de novo RNA synthesis (*50*). GTP and ATP, but not UTP or CTP, were preferred as the initiation nucleotides (*40, 53-54*) in de novo initiation RNA synthesis. High levels of GTP but not other NTPs were found to stimulate de novo initiation (*55*). A low affinity GTP-binding site was later identified in NS5B, suggesting that GTP may act at this allosteric site to stimulate de novo initiation (*38*).

Three groups independently solved the X-ray diffraction crystal structures of the C-terminally truncated versions of NS5B in the year 1999 (*56-58*). NS5B was shown to have a thumb, fingers and the palm domains similar to all the other known polymerases (Fig. 4) (*59*). The palm domain has the conserved GDD residues that coordinate the divalent metal ions and carry out the nucleotidyl transfer reaction. Several crystal structures of NS5B in complex with inhibitors, NTPs and also with a short 5-nt ssRNA have been reported but, thus far, no structural information is available for the ternary complexes involved in initiation and elongation (*60-64*).

A unique feature of the HCV RdRp and that of related viral RdRps (*65-66*), is that the thumb and the fingers domains are bridged by two loops called the Δ1 loop and
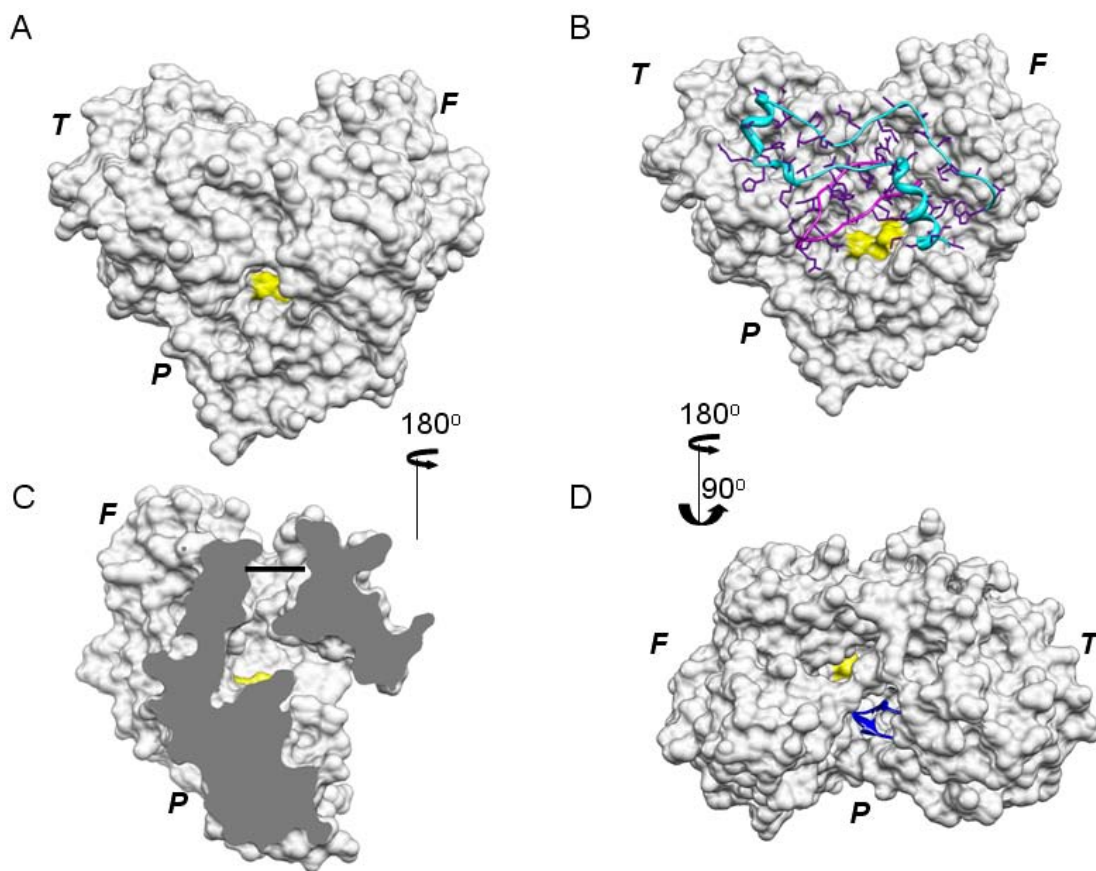
Figure 4: NS5B is crystallized in the closed conformation. Surface representation of the crystal structure of HCV NS5B Δ35 (PDB ID 1QUV). (A) The front view of the polymerase showing the encircled active site (yellow). (B) Front view of NS5B and the Δ1 loop is shown as a ribbon in cyan. Helix A in the Δ1 loop is the short helix at the tip of the loop that holds the thumb domain mainly by hydrophobic contacts. Δ2 loop is shown as a ribbon in magenta. The side chains of the two loops are in purple. (C) A cut away representation of the polymerase exposing the template channel (the tunnel running from the top towards the active site depicted in yellow). The channel is only wide enough to accommodate a ssRNA (the thick line is shown to indicate that the width of the channel at its widest point is less than 10Å distance). GDD in the active site is colored yellow. (D) Top view of NS5B showing the β loop as a blue ribbon. T: thumb domain, F: fingers domain, and P: palm domain.

Δ2 loop (also referred as finger-loops) (Fig. 4). These two loops are responsible for the

closed conformation of the enzyme that results in a complete encircling of the active site

from the front side (front side is viewed with the thumb domain at the left and fingers

domain at the right side of the viewer in Fig. 4). The back side is covered by another

loop designated as the β loop which forms part of the template channel and the β loop

extends towards the metal coordinating residues in the active site (Fig. 4). This

encircling of the active site will result in a well defined but narrow template channel that

can accommodate a ssRNA but not a dsRNA (Fig. 4C) (*63*).

Since the ternary complex of the RdRp involved in elongation will contain

dsRNA, the closed structure solved by X-ray crystallography should transition to the

more open one during elongation stage of RNA synthesis. It was initially proposed that

the β loop is used by the polymerase for this transition (*57*). In fact, a study showed that

a deletion of eight residues in the β loop allowed productive elongation from dsRNA

templates whereas the WT enzyme was not able to perform primer extension (*67*).

However, if the β loop is pushed out of the template channel to accommodate the

dsRNA a large rotation of the thumb domain is thought to be necessary (*56, 64*).

The model in which the unique closed conformation of the enzyme was proposed to

be engaged in de novo initiation was based on work on the ternary structure of the RdRp

from phage φ6 (see below) (*68*). Furthermore, mutations that disrupted the Δ1 loop and

thumb domain interactions, and thereby altered the closed conformation of the enzyme

were detrimental for RNA synthesis (*69*). Therefore, it was speculated that this

interaction is stable during the catalytic cycle of polymerization and that it may be used

for the 'clamping movement' of the polymerase on the RNA template during elongation (*69*). If true, this mechanism would be unique to HCV and related viral RdRps that have a Δ1 loop like structure since there is no precedent for a bridging interaction between the thumb and fingers domains during elongation RNA synthesis of other polymerases (*59, 70*). The Δ1 loop in HCV NS5B (Fig. 4B) contains 35 residues and is largely a coil structure except for the region that contacts the thumb domain where a small helix (helix A) fits into a pocket defined by amino acids H428, I432, W397, A396 and several other hydrophobic residues.

RNA synthesis in the HCV RdRp can be divided into at least four sequential stages in vitro: 1) Assembly of productive initiation complexes (de novo initiation or primer extension complexes); 2) Nucleotidyl transfer to synthesize the first or first few phosphodiester bonds; 3) Processive elongation; and 4) Termination of RNA synthesis. The first two steps are collectively called initiation events and are the rate limiting steps in the polymerase reaction. Different conformations of the RdRp are thought to be involved in de novo initiation and primer extension/elongation due to large differences observed in the K_M values for the NTPs involved in these two phases of RNA synthesis (*71*) (Fig. 5). In vitro, the RdRp can also switch templates before termination, although the relevance of this activity in HCV replication has not been reported. Under certain conditions, the HCV and other viral RdRps can also add non-templated nucleotides to the 3' terminus of the template (*39, 72*). While this activity can be relevant in the repair of deleted ends of the RNA, its biological relevance to HCV infection remains to be demonstrated. In vivo however, de novo initiation is the relevant mechanism of HCV
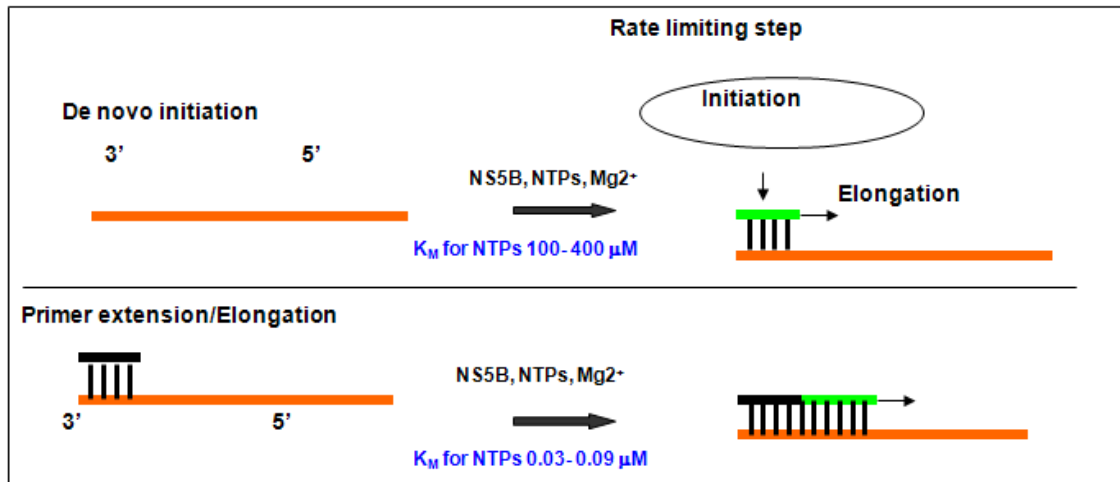
Figure 5: RNA synthesis mechanisms in NS5B. De novo initiation versus primer extension/elongation in NS5B. De novo initiation involves the recognition of the 3' end of the template RNA (red) by NS5B and initiation of RNA synthesis without the need for a primer. De novo initiation has two steps: Initiation (involves the synthesis of a primer of 5-6 nt, shown as green) and Elongation. Initiation is thought to be rate limiting. By contrast Primer extension/Elongation involves extension of a primer (black) along the length of a template (red) from a preformed primer-template RNA complex akin to the elongation step in de novo initiation. The newly extended RNA is shown as green. The K_M values shown are obtained from Ferrari et al.(*71*)

replication and it is likely that the 3' end of the RNA threads into the closed conformation of the polymerase with assistance from other viral nonstructural proteins like NS3. This process may involve changes in the Δ1 loop and thumb domain interactions within a monomeric NS5B for a better gripping of the template in the active site. A higher order structure of NS5B can stabilize the Δ1 loop and thumb domain interactions to selectively stimulate de novo initiation as several reports have shown that NS5B can oligomerize both in vitro and in vivo (*73-76*). Prior to the start of this dissertation project, the closed conformation of NS5B was proposed to be needed for de novo initiated RNA synthesis while a more open one may be suitable for assembly of primer extension complexes and also when the polymerase is engaged in elongation (*56-57*). In 2006, Ranjith-Kumar et al., showed that the HCV RdRp was able to direct de novo initiated RNA synthesis from a circularized template (*77*). Since a circularized RNA cannot thread a terminus into the active site, this observation suggests that the HCV polymerase could undergo a transition from the closed to an open conformation before template recognition (Fig. 6).

MECHANISM OF RNA-DEPENDENT RNA SYNTHESIS

Although the HCV RdRp is a relatively recent addition to the list of viral RdRps, it has proved to be a good model system especially to study de novo initiation RNA synthesis. The ease of obtaining an active enzyme in a recombinant form and its lack of template specificity are some of the reasons for the HCV RdRp to be used as a model
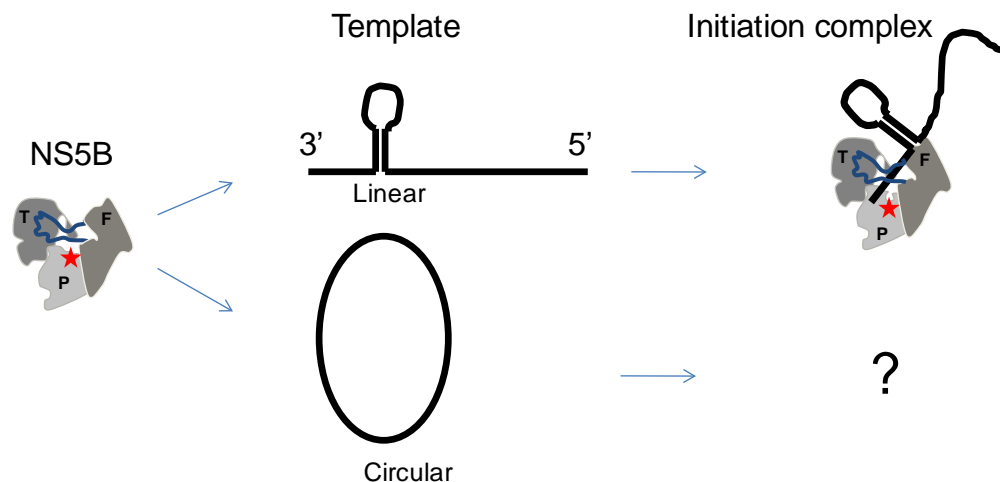
Figure 6: A closed to open transition is needed by the HCV RdRp (NS5B) to assemble the initiation complex on a circular template. The closed structure of NS5B is shown as a cartoon with the three domains: thumb, fingers and palm shown in different shades of grey and marked T, F and P respectively. The red star represents the active site located in the palm domain. The Δ1 loop connecting the fingers and thumb domains is in blue. The RNA (linear or circular) is shown as a thick black line. A linear RNA can thread its 3' terminus into the template channel to reach the active site to initiate RNA synthesis. A circular RNA can also direct de novo initiation by the HCV RdRp. Since a circular RNA cannot thread a terminus into the active site, this result clearly demonstrates that the closed polymerase structure that predominates in the crystal structure can change to an open conformation. What facilitates the close to open conformation is a central question for this dissertation project.

RdRp for structural and biochemical analyses. However, much of our initial understanding of the RdRps came from viral replicases (Replicases are RdRps that are complexed with other viral and host derived proteins. The entire complex is responsible for template recognition and RNA synthesis, although the RdRp is the catalytic subunit) from many RNA viruses infecting both prokaryotes and eukaryotes (*78*). RNA synthesis in general by the RdRps is accomplished by two major mechanisms: de novo initiation or primer-dependent RNA synthesis. In the latter class the primers can be small viral encoded peptides as in the case of the *Picornaviridae* family of viruses or the primer may be derived from the capped 5' end of a host mRNA (cap-snatching) or the 3' end of the template RNA looping back on itself to act as a short primer for the RdRp to extend. Some negative stranded segmented RNA viruses like the influenza viruses use both de novo initiation and a cap-snatching mediated primer- dependent mechanism of RNA synthesis in their life cycles (*79*). In the RdRps that initiate RNA synthesis by a de novo mechanism a short primer is synthesized in a process called abortive cycling. The polymerization begins by the generation of a short oligonucleotide (~5-6 nucleotides) and then due to a critical conformational change from initiation to elongation in the RdRp, RNA synthesis is aborted. The primers so generated are extended during the elongation phase of RNA synthesis.

  The Qβ replicase. Qβ (*Leviviridae* family) is a single-stranded positive-sense RNA bacteriophage whose replicase has served as an important model system for studies on viral RdRps especially before the advent of recombinant DNA technology which made available the individual polymerase proteins of different viruses for biochemical studies.

The Qβ replicase normally amplifies the ~ 4.2 kb RNA genome of the *E. coli* infecting

bacteriophage Qβ by a de novo initiation mechanism. RNA synthesis can approach rates

of 29 nt/sec (*80-81*) in comparison to ~3 nt/sec observed for the HCV RdRp (*67*).

The Qβ replicase contains four different subunits that total ~215 kDa in mass.

The RdRp subunit is encoded in the phage genome whereas the other three are host

encoded proteins *viz E.coli* ribosomal S1 protein and the translation elongation factors

Tu and Ts. An additional protein called 'host factor' HF, is needed for Qβ RNA

replication in phage infected cells and also to amplify Qβ RNA in vitro. The role of the

translation elongation factors seems to be structural since their protein biosynthesis

specific functions, aminoacyl tRNA binding and GTP binding are dispensable for Qβ

replication (*82*). The translation elongation factors are not required during elongation but

are absolutely needed for initiation and furthermore they can retain their function in the

Qβ replicase even after trypsinization (*83*). It is known that EF Tu and EF Ts function as

a complex in the replicase since kirromycin, an antibiotic that prevents their association,

inhibits Qβ replicase (*83*). Furthermore, both elongation factors derived from a different

bacterial species, *C. crescentus* can replace their *E. coli* counterparts in the Qβ replicase

and still be functional.

The role of S1 seems to be to enforce tighter binding between the replicase and

Qβ RNA. However, the RNA helix unwinding activity of S1 that is needed in the

ribosomes during protein biosynthesis is dispensable for Qβ replication (*84*). The S1

protein is also not needed for copying non-Qβ RNA templates (*85*). S1 can bind to two

distinct sites in the Qβ RNA (the M and S sites) which is important for replication of the RNA. The role of S1 in protein biosynthesis is to assist in the mRNA binding to the 30S ribosome. Both these roles of S1 (*i.e.* in Qβ replication and protein biosynthesis) may therefore appear to be related but S1 from *C. crescentus* or *B. subtilis* cannot substitute the *E. coli* S1 in the Qβ replicase whereas it can readily substitute the *E. coli* S1 involved in translation (*83*). HF is also needed for initiation but not elongation by the Qβ replicase and its role may be in binding to the 3' end of Qβ RNA during initiation. Interestingly the function of HF can be completely substituted by the divalent cation manganese in RNA synthesis assays in vitro (*83*).

An intriguing aspect of Qβ replicase is its high selectivity in amplifying only some RNA templates including the ~4.2 kb genome of the Qβ phage and some select RNAs that are < 250 bases long that arose from recombination events between the phage and *E. coli* RNAs (*86*). The amplification is exponential since the parent template RNA and the newly synthesized copy of the template RNA are both templates for subsequent rounds of replication. Although it has remained elusive as to what specifies RNAs for exponential amplification by the Qβ replicase, some general rules have been identified: A 5' leader stem loop structure and a free 3' region in the template; A 5' GGG sequence and a 3' CCCA sequence (The replicase adds the 3' terminal A to the product strand in a non-templated fashion and is not copied while synthesizing the complementary strand); and a stable secondary structure in the body of the template RNA (*86*). These simple rules are sufficient to allow the replicase to discriminate between the replicable RNAs

and the innumerable number of host RNAs that the replicase would encounter in the infected *E. coli* cell.

The requirement of high concentrations of the initiating nucleotide GTP is thought to confer some template specificity as different templates require varying GTP concentrations for successful initiation (*87*). A high concentration of GTP for initiation is also a feature of the HCV RdRp (*55*). Also similar to the requirements of the HCV RdRp, the divalent cation manganese can decreases the concentration of GTP required for initiation on legitimate templates by the Qβ replicase, presumably by interacting with the phosphates of the GTP (*87-88*). The specificity in template selection seems to arise at the initiation stage rather than the template binding stage as presence of short oligonucleotide primers at the 3' ends can convert many RNAs to legitimate Qβ templates (*89*). The replicase binds with high affinity to an internal site in the Qβ genome about 1500 bases upstream of the 3' terminus and the long range interactions between this site and the 3' terminus is important for replication (*90*). However the replicable minus-strand RNA does not have a specific binding site for the replicase (*91*) suggesting that the initiation of the plus versus minus-strand RNAs have distinct requirements. As mentioned, the S1 protein and the HF protein assist in exposing the 3' termini of the plus-strand RNA genome for template loading into the active site of the catalytic subunit of the replicase (*92*). These two proteins partially could be responsible for the template specificity of the Qβ replicase. However a mere presence of these two proteins will not make any RNA molecule a legitimate Qβ template for amplification

suggesting complex interactions between the replicase subunits and RNA and also within the RNA molecule.

The ability for exponential amplification of legitimate RNA templates by the Qβ replicase suggests that there is a mechanism to ensure the single-strandedness of the nascent RNA molecule, so that it is available for the next round of RNA synthesis. There should be a 'plow-like' structure near the active site of the enzyme that will help to keep the nascent RNA from annealing to the template strand. In case of the HCV RdRp, the nascent RNA remains base-paired with the template RNA at least in vitro (*93*) and in vivo, a dedicated protein such as the NS3 helicase may be responsible for unwinding dsRNA. In contrast to the Qβ replicase, the nascent RNA remains double stranded in a related RdRp from the dsRNA bacteriophage φ6 (*94*). Therefore, the Qβ replicase is unique in its ability to prevent the annealing of the nascent and the template RNA once they exit the polymerase active site when a legitimate template is being replicated. However, all legitimate templates need not necessarily be 'replicable' *i.e.* amplifiable which in turn means that the nascent RNA remains base-paired with the template RNA with some of the templates of Qβ replicase.

Ugarov et al., have characterized the Qβ templates as legitimate and illegitimate based on several criteria (*86*). The replicase bound to legitimate templates requires high concentrations of GTP for initiation and such complexes are stable as determined by their resistance to aurintricarboxylic acid (ATA), a chemical agent that prevents RNA-protein interactions. In contrast the replicase bound to illegitimate templates does not need high concentrations of GTP for initiation, can recognize and extend a 'loop-back'

RNA akin to primer extension and such template-replicase complexes are sensitive to ATA. Based on these results they hypothesized that upon binding to a legitimate template the Qβ replicase undergoes a conformational change to a 'closed' structure and this ensures the formation of a stable initiation complex. This conformational change does not take place upon recognition of an illegitimate template and the replicase will stay in an 'open' conformation which makes the replication complex ATA sensitive. This model posits that different conformations are present in the Qβ replicase which can recognize different templates and perform de novo initiation, and the conformations can depend on the nature of template. However no clear differences in the template characteristics were evident and therefore it was not clear how the replicase would become 'closed' or 'open', and as a result show different ATA sensitivities based solely on template criteria.

In a follow-up study, Ugarov and Chetverin (*95*) have shown that functional circularity is a defining criteria for a legitimate template. The 5' end and 3' portion of the template molecule must interact (the 5' and 3' ends need not be covalently connected: i.e., they need to be functionally circular) to form a legitimate template that can form an ATA resistant elongation complex with the Qβ replicase. Point mutations in the 5' end of a legitimate template can make the elongation complex unstable and conversely mutations which establish 5-3' base-pairing within a template molecule can give rise to a more stable elongation complex. These results suggested that the functional circularization along with conformational changes in the replicase is important in determining the legitimacy of a template. This also can explain how the nascent RNA

product of Qβ replicase retains its single-stranded nature since the nascent RNAs will need to compete with the intramolecular interactions at the terminal portions of the template. Atomic resolution structure of the Qb RdRp remains to be determined and this along with elucidation of the replicase structure as a whole should further advance the field of RNA-dependent RNA synthesis.

The φ6 RdRp. The polymerase from the φ6 phage has also served as a model RdRp. φ6 is a dsRNA virus from the family *Cystoviridae*. The φ6 RdRp is a single polypeptide chain and copies the genomic RNA by a de novo initiation mechanism. The replication of the genomic RNA occurs within the capsid structure in which an RdRp is pre-packaged. The RdRp from φ6 was co-crystallized with a five nucleotide RNA from the 3' end of the plus-strand genomic RNA and GTP was soaked into the crystals revealing the first structure of the quaternary complex of an RdRp consisting of all of the components needed for initiation (*68*). In this landmark report, it was seen that the RdRp is in a closed conformation with the finger-loops bridging the fingers and thumb domains and the 3' end of the template initially overshoots in the polymerase active site but in presence of GTP, it reverses and forms the initiation complex. This led to the speculation that the closed conformation may be the de novo initiation-competent conformation in all other viral RdRps. However, a dsRNA could not be modeled into the structure as steric clashes arose with the C-terminal domain (an observation also made for the HCV RdRp (*57*)), and it is not clear how a dsRNA is accommodated within the template channel during elongation in this RdRp as is the case with the HCV RdRp (*68*).

The C-terminal domain was proposed to act like a platform for the assembly of the initiation complex.

The φ6 phage has to replicate a dsRNA without the need for a helicase activity; initiation in this case should also involve melting the 3' end of the template from the 5' end of the non-template for assembly of the initiation complex (*96*). However the specific structure(s) that contribute to this event in the RdRp is not clear. The φ6 RdRp also initiates by utilizing GTP as the initiating nucleotide and it prefers a stretch of Cs at the 3' end of the template (*97*). Similar to the HCV RdRp the φ6 RdRp can also perform efficient primer extension that does not depend on high concentrations of GTP.

The BVDV is used as a surrogate system for studying HCV replication and its RdRp is also structurally and functionally well characterized (*49, 65*). The BVDV RdRp was crystallized in different conformational states in two different crystal forms (*65*). The finger-loop region was present in different states in five different monomers further providing evidence that this region in the RdRp is highly flexible. A second GTP binding site close to the active site within the palm domain was identified in the BVDV RdRp, (*98*) in contrast to the reported allosteric GTP binding site in the thumb domain of the HCV RdRp (*38*). Studies on the dengue viral RdRp have shown evidence for the hypothesis that different conformations of the RdRp are responsible for de novo initiation and primer extension (*99*). In a study by Ackermann et al., a higher temperature selectively inhibited de novo initiation while not affecting primer extension reactions, suggesting a thermal regulation of RdRp conformation (*99*). However, this effect was not observed for the HCV RdRp (*88*).

The polioviral RdRp is another well studied polymerase (*100*). The polioviral

RdRp is a primer dependent enzyme and uses a viral encoded protein primer for

initiation (*101*). Structurally this RdRp and the related RdRps from the rabbit

hemorrhagic disease virus (RHDV) and foot and mouth disease virus (FMDV) are

characterized by a relatively large entrance to the template channel as they lack the β

loop structure that covers the back of the HCV RdRp (*102-103*) (Fig. 4D). This large

cavity at the entrance of the channel is needed to accommodate a dsRNA or the protein

primer for elongation by the RdRp.

The majority of RdRps encountered in RNA viruses however begin RNA synthesis

by a de novo initiation mechanism (*78*). In RdRps that initiate by a de novo mechanism a

common feature is that the initiating nucleotide (referred to as NTPi) is a purine

nucleotide. An initiation complex comprises the divalent cation-bound RdRp and the

template RNA with its 3' end in the active site of the enzyme, base-paired to the NTPi

and NTPi + 1 nucleotide (Fig. 7). GTP is the NTPi in the HCV RdRp initiation complex

comprising the minus-strand RNA template. GTP bound to the initiation site (NTPi

site) and in the appropriate orientation initiates the reaction by a nucleophilic attack from

its hydroxyl group on the phosphodiester bond between the α and the β phosphate of the

NTPi+1 nucleotide. The divalent cations lower the pKa of the hydroxyl group of GTP to

cause its deprotonation (*104*) and initiate the nucleophilic attack. The divalent metals

also facilitate the release of the pyrophosphate from the active site while protonation of

the pyrophosphate is mediated by an active site amino acid (*105*). Magnesium is the

metal ion that is thought to be required by polymerases for nucleotidyl transfer in vivo,
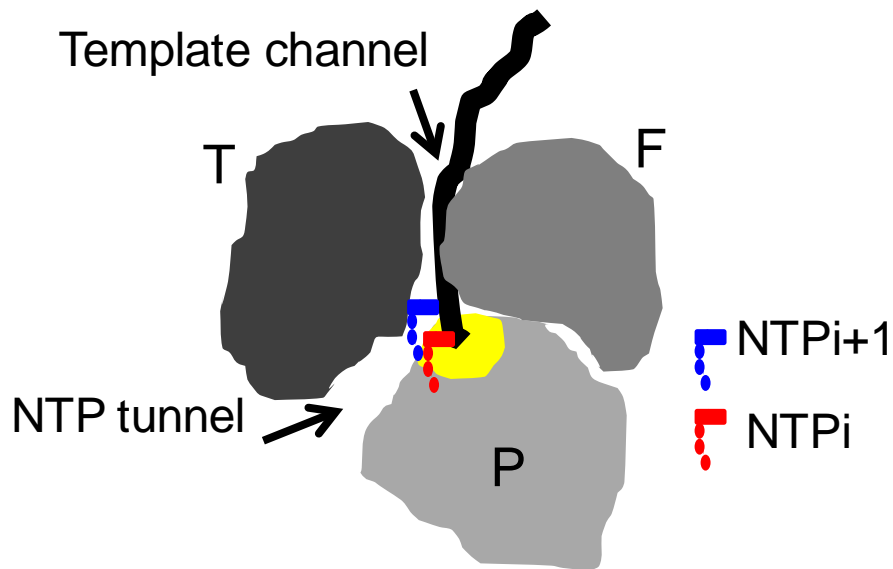
Figure 7: De novo initiation complex in an RdRp. Template RNA (thick black line) positions itself in the divalent cation metal-bound active site of the RdRp (yellow) such that the 3' end is base paired to the ultimate and penultimate nucleotides (NTPi and NTPi+1 respectively). The NTPi is usually GTP, which initiates the RNA synthesis reaction with its 3' OH group attacking the phosphodiester bond between the α and β phosphate group of NTPi+1. (The three RdRp domains: thumb, fingers and palm are shown as T, F and P in different shades of grey). The NTP tunnel is a positively charged cavity at the junction of the thumb and palm domains. It is thought to feed NTPs into the active site (yellow) during catalysis.

while manganese has been reported to substitute for magnesium in in vitro biochemical assays involving RdRps (*88, 106*). In HCV NS5B, manganese selectively stimulates de novo initiation (*88*). Manganese was recently shown for the φ6 RdRp to structurally affect the active site by making it more flexible (*107*). This flexibility may increase the efficiency of NTPi utilization during initiation in RdRps. Presence of manganese however is known to decrease the fidelity of RdRps (*106*) and may even be used by viruses to enforce mutations in their genomes, that will allow them to exist as quasispecies.

SCOPE OF THE STUDY

The focus of this study is primarily on the de novo initiation RNA synthesis by the HCV RNA polymerase. This is the likely mechanism used by the HCV NS5B to initiate genomic RNA synthesis in infected cells. Several studies have shown that NS5B purified from recombinant sources can efficiently de novo initiate from the 3' ends of ssRNA. Consistent with this, the K_M values for NTPs during initiation are about ten thousand fold higher during initiation than during elongation (*71*), supporting the notion that different conformations of NS5B participate in de novo initiation and primer extension. However, the mechanistic and structural details of these steps, especially the mechanism of transition from de novo initiation to elongation by NS5B has remained elusive. The Kao laboratory had been dedicated to understanding the interaction between the RdRp, the template and the nascent RNA involving de novo initiation RNA synthesis by the HCV NS5B (*78*). Significant progress has been made in terms of defining the template,

NTP and metal ion requirements by NS5B during de novo initiation (*40, 50, 88*). Importantly the demonstration that the polymerase could transition from the closed to open conformation before initiation (*77*) laid the foundation for the present work. The NS5B protein has also been reported to function as oligomers (*74-76*) and how oligomerization affects de novo initiation RNA synthesis was not clear.

The work conceptualized and performed for this dissertation seeks to build on the current understanding of the mechanism of de novo initiation by HCV NS5B, and the associated conformational requirements in the enzyme. The results from the current study should help us better understand the mechanism of action (MOA) of the HCV NS5B inhibitors that block initiation stage of RNA synthesis. Chapter II summarizes the current knowledge concerning the inhibitors of NS5B, with emphasis on their MOA. Defining the structural element in the RdRp that regulates de novo initiation and elongation by the HCV RdRp is the focus of Chapter III, and this work was published in the *Journal of Biological Chemistry* in 2008. The role of NS5B oligomerization in de novo initiation was also investigated, and is presented in Chapter IV. The manuscript involving this work is in review at the *Journal of Virology*. Chapter V deals with the different conformational states in a monomeric NS5B, and a discussion of its relevance in inhibitor studies. This manuscript was recently accepted for publication in *Virus Adaptation and Treatment*. In appendix I the effect of mutations in NS5B that prevent its interaction with the tumor suppressor Retinoblastoma (pRb) protein is presented. This collaborative work has been published in the *Journal of Virology in* 2009. In appendix II, the effect of mutations in NS5B that conferred Cyclosporine A (CsA) resistance to

HCV in infected cells, on the in vitro RdRp activity is examined and this work was published in the journal *Hepatology* in 2009. In appendix III, the results of the screening of a nucleoside mimic compound library from a commercial source for binding and inhibition of NS5B are presented.

CHAPTER II

HCV NS5B INHIBITORS

There is an urgent need to develop potent drugs against HCV as the conventional therapy, a combination of pegylated IFN and ribavirin, is associated with severe side effects and also not effective in 50% of the patients. HCV causes a progressive disease typically over a 20-30 years span, but shows a sustained viremia from the acute infection stage onwards. Therefore drugs that can block the virus replication are needed to control the disease. HCV is not cytopathic, but the major damage to the liver is brought on by the immune system, which suggests that an alternative strategy to control the disease is to modulate the immune system. However, such advanced therapies are not yet available for liver diseases and controlling the virus replication in the host is the currently available option.

The Hepatitis C virus polymerase is the key enzyme for the replication of the HCV genome and has been the target of numerous inhibitor studies (reviewed in (*108*)). The rationale for targeting the HCV polymerase is based on the paradigm of established therapies that target the polymerases encoded by other viruses like the human immunodeficiency virus (HIV), hepatitis B virus, and herpes viruses (*109*). Many of the HCV NS5B inhibitors have been identified from screening proprietary compound libraries either in vitro or in cell-based assays rather than being developed based on rational structure-based design. Thus, the effective compounds provide an unbiased means to assess how structure influences function. In addition, studies to probe the

mechanism of RNA synthesis by HCV NS5B such as the one undertaken for this dissertation should complement drug discovery efforts. As proof of concept, the results presented in Chapter III help us to better understand the MOA of the benzimidazole and indole class of drugs that were previously identified to inhibit HCV NS5B. This chapter reviews, and seeks to summarize recent knowledge on the inhibitors of HCV NS5B and in that context attempts to gain a better understanding of the mechanism of RNA synthesis.

The inhibitors of HCV NS5B can be broadly classified into four classes based on their chemical composition and/or mode of action. The first class consists of nucleoside or nucleotide analogs that act as competitors of NTPs during RNA synthesis. This class also includes the purine analog ribavirin, the only FDA approved small molecule drug for the treatment of HCV, although it exerts its action by multiple mechanisms (see below). The second class consists of non-nucleoside inhibitors that allosterically target the NS5B, and the majority of them inhibit the initiation stage of RNA synthesis. Other inhibitors which have a distinct MOA than the inhibitors from the first two classes are presented in the third class. A fourth and rapidly emerging class consist of compounds that target cellular proteins needed for HCV polymerase function. This class may be advantageous in that the virus cannot rapidly evolve resistance to the inhibitors.

NUCLEOSIDE INHIBITORS (NI)

Nucleoside or nucleotide mimics are usually designed to cause premature chain termination during viral nucleic acid synthesis. Phosphorylation of the nucleoside

prodrugs to their triphosphorylated forms is required for inhibitory activity. Several nucleoside analogs have been studied in vitro, with the recombinant NS5B protein and in cells expressing HCV subgenomic replicons, and also in animal models. A number of these compounds have progressed to clinical trials and can act in synergy with the interferon-ribavirin combination therapies (*108*).

A simple 2' ribose modification of cytidine (2'-O-methyl) and adenosine (2'- C-methyl) (Fig. 8) nucleosides will result in potent inhibitors of HCV subgenomic replicons acting as 'non-obligate' chain terminators of RNA synthesis by NS5B (non-obligate chain terminators have an intact ribose 3'OH group for elongation but they can induce structural constraints in the active site to lead to chain termination) (*110*). A resistant mutation S282T in the NS5B region was identified for the 2' ribose modified nucleoside analogs (*111*). Biochemical characterization revealed that the resistance was due to reduced affinity to the compound and also due to an increased ability by the mutant polymerase to incorporate the nucleotide analog during elongation.

Migliaccio et al., reported good oral bioavailability and synergistic inhibitory activity of 2'-C-methyl guanosine (2'-C-mG) and interferons (*111*). However, a 7-deaza modified 2'-C-mG suffered from poor cell penetration and inefficient phosphorylation by cellular kinases whereas a 7-deaza modification of 2'-C-methyl-adenosine resulted in a compound with improved pharmacokinetic properties and low toxicity than its unmodified form (*112*). MK0608 (7-deaza-2'-C-methyladenosine) has an EC_{50} of 0.25 μM in replicons and has showed promising results in animal studies (*113*).
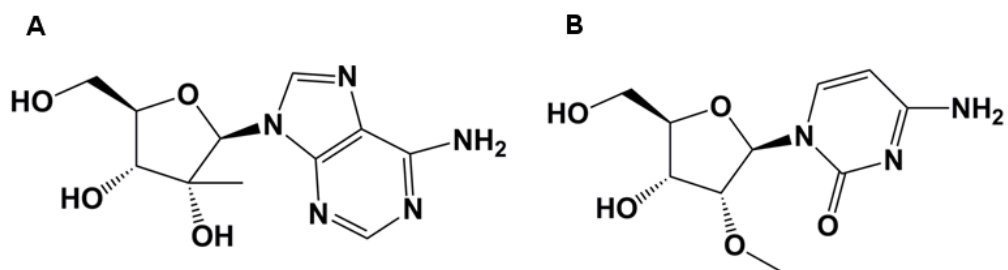
Figure 8: The structures of (A) 2′-C-methyladenosine and (B) 2′-O-methylcytidine.

Other modifications including halogenation have improved the potency of 2' ribose modified nucleoside analogs. PSI-6130 (2;-deoxy-2'fluoro-2'-C-methylcytidine) (and R7128, a prodrug of PSI-6130) has been reported by Stuyver et al., (*114*) to be active against the HCV NS5B subgenomic replicon with an EC_{90} of ~4.5 μM but did not affect the BVDV NS5B in subgenomic replicons.

A 4' ribose modified nucleoside (4'-azidocytidine (R1479) or the modified version of 4'-azidocytidine (R1626)) has also been reported (*115*), to be able to chain-terminate RNA synthesis by HCV NS5B. This analog had a similar IC_{50} (in the range of 1.12-1.3 μM) to 2'-C-methyl-cytidine in subgenomic HCV replicon-expressing cells while concentrations as high as 2 mM were not toxic to cells (*115*). S282T mutation apparently did not affect the inhibitory effect of R1479. The development of this analog has been discontinued due to safety issues (*113*).

3'-deoxy modified nucleoside analogs especially 3'-deoxy-GTP and 3'-deoxy-CTP are good chain terminators of HCV NS5B RNA elongation in vitro, but they suffered from poor activation into their triphosphate forms in cells (*116*).

2'-C-methylcytidine (NM107) was found to inhibit BVDV polymerase with a Ki of 160 nM. However, this drug did not have good oral bioavailability but a modification at the 3' OH of ribose (3'-O-valinyl-2'-C-methylcytidine, valopicitabine or NM283) led to enhanced pharmacokinetic properties and has showed promise initially in clinical studies in HCV infection especially when combined with peg-IFN and ribavirin (*113*). However, due to associated serious side effects FDA has suspended the clinical trials for NM283 in the US, but the trials are on in the European union (*108*).

The resistance mutations to NI include S282T, S96T and N142T (Fig. 9) (*111, 117*). The S282T mutation confers resistance to 2' C-methyl cytidine and 2' C-methyl-adenosine and the presence of this mutation in subgenomic replicons reduces the replicative capacity to ~20% to that of WT (*111*). S96T and N142T mutations confer resistance to R1479 (see above) and their presence severely debilitates subgenomic replicon capacity (*117*) and do not confer any cross resistance to 2' C-methyl cytidine suggesting a specific interaction in the binding pocket. S282 residue is in close proximity to the NTPi (initiation nucleotide (*78*)) binding residues identified in co-crystal structures of NS5B and GTP (Fig. 9). Mutations involving the NTPi binding residues have yielded polymerases that are decreased in de novo initiation but unaffected for primer extension activity (*118*) providing another hint about a different conformation of NS5B involved in these two activities. This will also suggest that the NTP binding pocket in the active site is more flexible during elongation than during de novo initiation. S282 residue therefore should have a very specific interaction with the nucleotide analog inhibitors in the NTP binding pocket in order for S282T to confer resistance. None of the mutations conferring resistance to NI lie outside the template channel (Fig. 9) suggesting that they do not allosterically influence the polymerase function unlike non-nucleoside inhibitors (see below). Dinucleotide analogues targeting de novo initiation by NS5B have also been reported (*119*), but no further progress has been reported in their development. The purine analog ribavirin (Fig. 10) is an FDA approved drug for treatment of HCV in humans and has been in use for more than a decade.
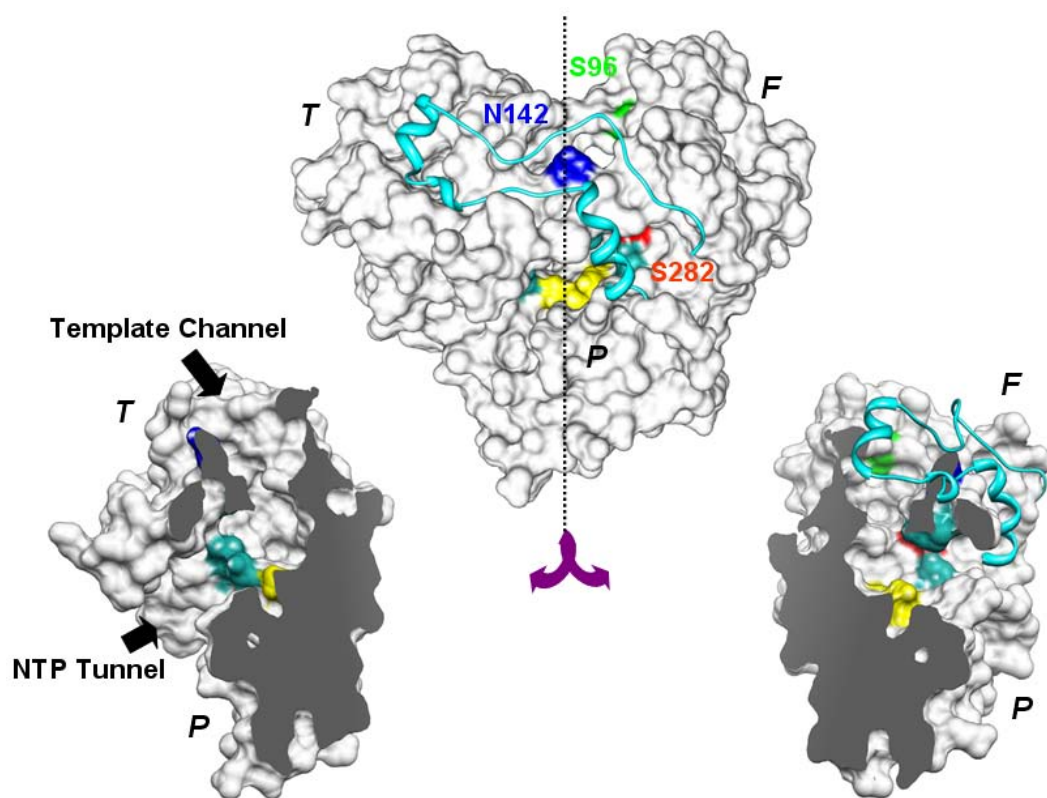
Figure 9: The NTPi site and the resistance mutations to NI in HCV NS5B. The top image is a front side representation of HCV NS5B (PDB ID 1QUV), while the bottom images shows a cut away representation of the top image on a vertical axis (dashed line) in order to expose the template channel (an enclosed channel in the polymerase that extends from the cavity formed by thumb and fingers domain junctions at the top, to the cavity formed between the thumb and palm domain junction. The latter cavity is also called as the NTP tunnel). The NTPi site (or initiation GTP binding site) residues D225, R48, R158, R386, R394 and S367 are colored in light green. Amino acid S282 is (in red) mutated in polymerases which are resistant to 2'-me-C and 2'-me-A to a threonine. Amino acids S96 and N142 are in green and blue respectively. S96T and N142T mutations confer resistance to compound R1479. T, P and F refer to thumb, palm and fingers domains respectively. The Δ1 loop is shown as a ribbon in cyan. The active site metal coordinating residues are in yellow.
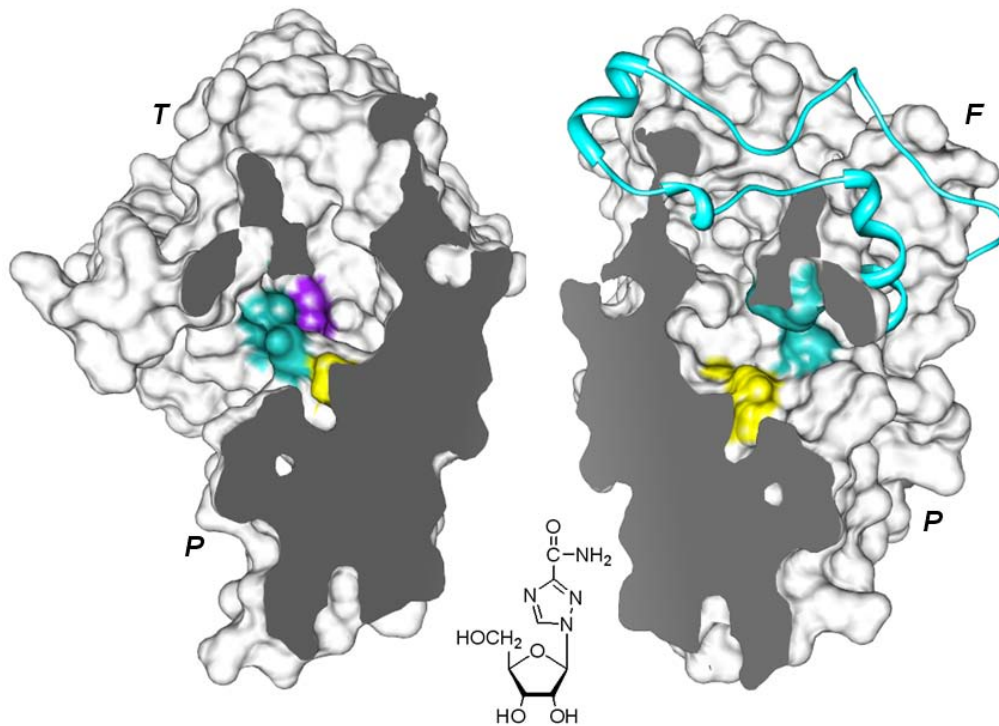
Figure 10: Ribavirin resistance mutation maps to the NTPi binding pocket in NS5B. Cut away representation of HCV NS5B (PDB ID 1QUV) as in Fig. 9. Δ1 loop is shown as a ribbon in cyan, while the active site GDD residues are colored yellow. The NTPi binding residues D225, R48, R158, R386, R394 and S367 are in light green, and Y415 is in purple. Y415F has been reported to confer resistance to ribavirin, a purine analog (structure is shown).

In conjunction with pegylated interferon, ribavirin can clear HCV from patients but in only 50% of the cases and also involves many side effects (*120*). The mechanism of action of ribavirin is not clear. It is thought that ribavirin may act by more than one mechanism like causing an 'error catastrophe' in the virus population and also by participating in immune modulation (reviewed in (*121*)). It may also act by inhibiting the host IMP dehydrogenase, which will in turn, lower the GTP levels in the cell. Interestingly, Y415F mutation has been mapped in the template channel that can confer resistance to this purine analog, providing strong evidence for binding of ribavirin to NS5B (*122*) (Fig. 10).

NON-NUCLEOSIDE INHIBITORS (NNI)

While NI act by interfering with the nucleotide addition by the HCV polymerase, several NNI have been identified that primarily target the initiation phase of RNA synthesis by NS5B, likely by preventing critical conformational adjustments in the enzyme in association with RNA binding and initiation. The NNI target different sites both on the surface and in the template channel of NS5B. NNI can be broadly classified into three different subclasses based on the location of their binding sites: Site 1 involves the Δ1 loop and thumb domain interface. Site2 is a pocket in the thumb domain that is present beneath Site 1. Site 3 unlike the other two sites is in the template channel and involves the 'primer-grip site' and the β loop and binds different classes of drugs (Fig. 11).

Class	Compounds	Inhibition stage
Site 1	benzimidazoles/ Indoles	Initiation
Site 2	thiophenes pyranindoles	NA Elongation
Site 3	benzothiadiazines/ benzofurans	Initiation
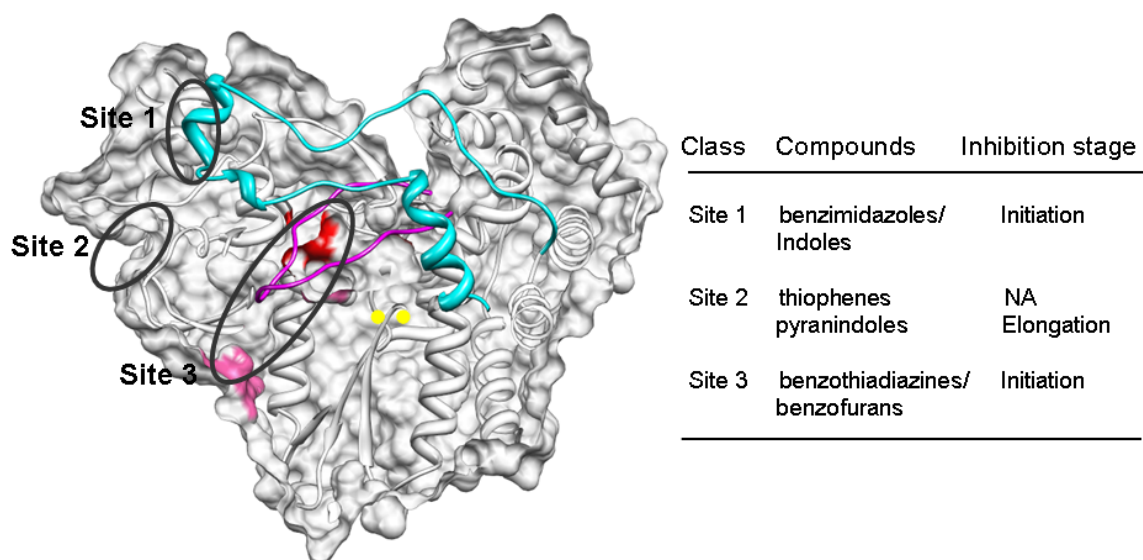
Figure 11: NNI binding sites in NS5B. The location of the different NNI sites is shown on a partial surface and ribbon representation of HCV NS5B Δ55 (PDB ID 1QUV). Site 1 and Site 2 are on the surface of the thumb domain of NS5B while Site 3 is located within the polymerase template channel. In Site 3 the representative drug binding residues in the template channel 414, 415 and 556 are colored red while the 'primer-grip' (a region that is thought to help in holding the primer during RNA synthesis) site (residues 360-380) is highlighted in pink. The active center of NS5B is shown as two yellow spheres representing the metal ions that are coordinated by the conserved GDD motif. The table in the right summarizes the three classes of NNI and their mechanism of action.

Site 1: Benzimidazoles and indole derivatives bind to this site and inhibit the initiation

stage of RNA synthesis by NS5B. Benzimidazoles were identified by Boehringer

Ingelheim (Canada) (*123*) to inhibit NS5B noncompetitively with NTPs with a

low microomolar IC_{50} value. The binding site for this compound and the related indole-

N-acetamides is at the binding interface between the Δ1 loop and the thumb domain (*62,

124*). This site also overlaps with the allosteric site that putatively binds GTP (*38*) (Fig.

12). Inhibitor binding at this site will result in a disruption of the inter-domain

communication and displacement of the Δ1 loop (*62*).

Biochemical characterization revealed that these compounds did not inhibit NS5B

during elongative mode of RNA synthesis and also were ineffective on preformed

NS5B-RNA complexes (*125-126*). Interestingly, the presence of RNA was required for

binding of benzimidazoles to NS5B, although prolonged incubation of NS5B and RNA

abolished inhibitor binding (*126*). Together with the fact that prolonged incubation of

NS5B with RNA increases primer extension activity of the enzyme (*71, 126*), the

observation that benzimidazoles do not bind to preincubated binary complexes suggests

a stepwise loss of Δ1 loop-thumb domain interaction as a function of preincubation time.

Notably, two residues that were identified in this study (see Chapter II) W397 and H428,

that are critical for de novo initiation by NS5B have side chains that chemically

resemble the two classes of NNI that act at site 1 (imidazole ring in H428 with

benzimidazoles and indole ring in W397 with indoles). Resistance mutations for the

benzimidazole class of NNI include P495A and P495L (*126*). Plant derived

phytoestrogens have been shown to be effective against NS5B in biochemical assays

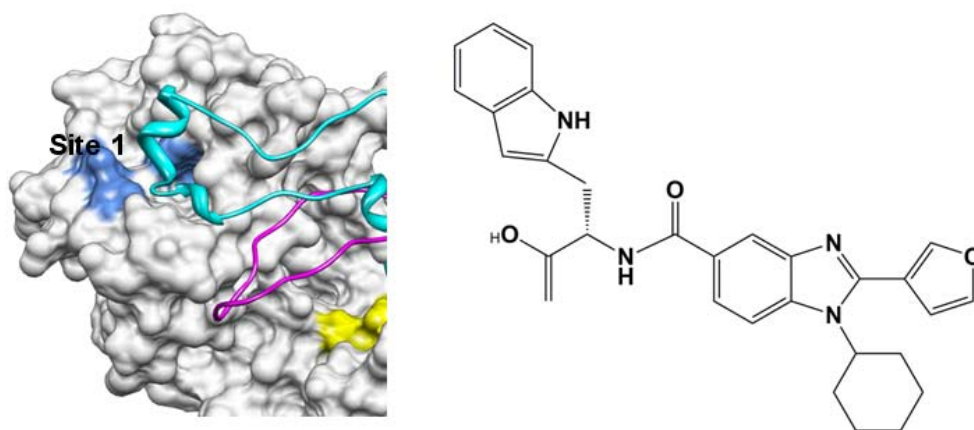Figure 12: NNI site 1. The location of the binding site for benzimidazole and indole based NNI (residues P495 and H428 are colored blue) at the interface of the apex of the Δ1 loop and thumb domain. The Δ1 loop is shown as a ribbon in cyan while Δ2 loop is colored magenta and the metal coordinating GDD residues are in yellow (PDB ID 1QUV) (Left). A representative scaffold of the benzimidazole NNI (Right).

(*127*) and act as non-competitive inhibitors of NTPs and the template RNA. The MOA is thought to be similar to that of benzimidazole compounds based on SAR studies.

Site 2: Compounds based on the thiophene scaffold were identified (*128*) to bind to NS5B in the thumb domain and inhibit its activity. Compounds derived from the leads in this class are generally hydrophobic due to the nature of their binding site which involves residues L419, M423, L474 and W528 (Fig. 13). In the genotype 1b NS5B, no gross change in the conformation of the enzyme was observed in presence of the inhibitor (*61, 128*), but genotype 2a NS5B showed a pronounced change with the disruption of the helix A in the Δ1 loop that resulted in the formation of a β sheet (*60*). Despite the availability of several crystal structures for the NS5B-inhibitor complex (*60-61, 128-129*) a clear MOA has not been elucidated for this class of inhibitors. This site may be involved with NS5B oliomerization (*60-61, 129*), and also inhibitor binding at this site may perturb GTP binding at the allosteric site (*128*). Another report has shown that pyranoindoles that putatively bind at Site 3 inhibited the elongation stage of RNA synthesis (*130*). Resistance mutations to Site 2 NNI include L419M and M423T (*131*). A minor population of drug resistant clones carrying M423I and I482L were also observed in subgenomic replicons. When the mutations were introduced into WT replicons all of them showed resistance to thiophene-2-carboxylic acid derivatives. Although some inhibitors that act at Site 2 have shown low nanomolar IC_{50} values in biochemical assays they generally show micromolar IC_{50} values in cell-based assays. Clinical trials involving the NNI binding to this site are currently in progress.
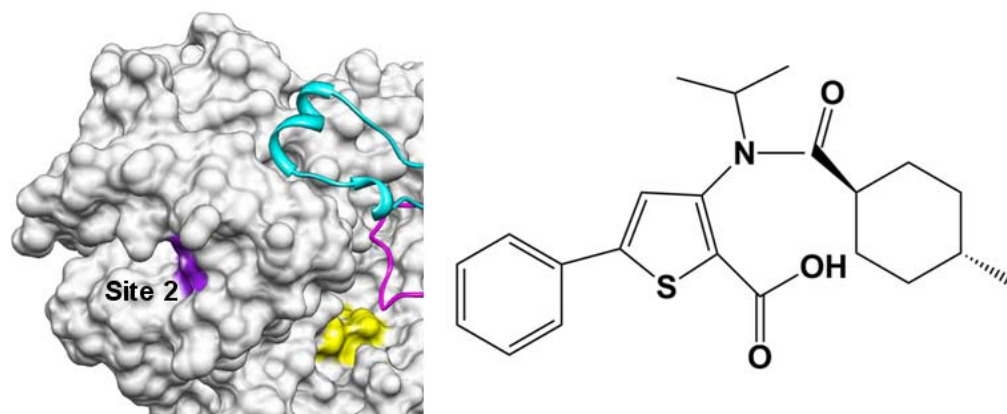
Figure 13: NNI Site 2. The location of the binding site for NNI in Site 2. Residues L419, M423 that bind to thiophene-carboxylic acids are colored purple. The coloring scheme is the same as in Fig.7 (Left). A representative scaffold of thiophene based NNI (Right).

Site 3: Different classes of compounds have been described to be binding to this site and inhibiting NS5B (Fig. 14). The first consists of derivatives of benzothiadiazines initially identified from the GlaxoSmithKline proprietary compound library (*132*) with 0.5 μm IC_{50} values in subgenomic replicons of genotype 1b. These compounds inhibit the initiation phase of RNA synthesis but do not affect elongation or preformed initiation complexes of purified NS5B and RNA (*42, 133*). Benzothiadiazines inhibited de novo initiation by WT Δ21 with IC_{50} values about 5-10 fold lesser than those for primer extension (*42*). Benzothiadiazines appear to act allosterically, as the inhibition is noncompetitive with GTP and RNA (*42, 132*), and may involve disruption of the movement of the thumb and palm domains essential for the assembly of the initiation complex. Resistance mutations arising in HCV genotype 1b replicons when treated with benzothiadiazines include: M414T, C451R, G558R and H95R (Fig. 11) (*42*). The mutant replicons M414T and H95R were not affected for replication efficiency compared to the WT replicons. Interestingly, C451R and G558R mutant replicons replicated at very low levels in absence of compounds but were increased in replication in the presence of compounds (*42*), in a dose-dependent manner. In biochemical RdRp assays however, only M414T showed significant rescue from inhibition of RNA synthesis while H95R, C451R and G558R did not.

A second class of drugs that bind at this site is the potent inhibitor benzofuran-C3-carboxamide (HCV796) (IC_{50} ~9 nM in replicon cells). This compound binds several residues in the 'primer-grip' site (Fig. 11) apart from L314, C316, C366 and M414 and
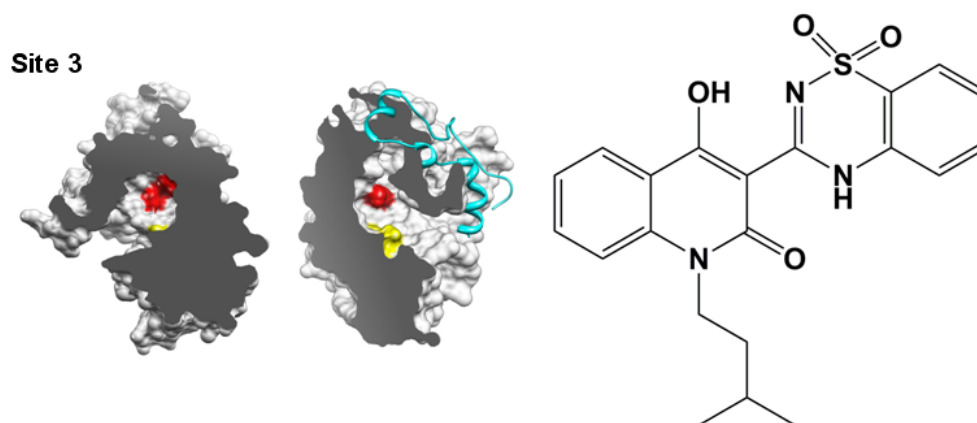
Figure 14: NNI Site 3. The location of benzothiadiazine binding site in the template channel. The NS5B Δ55 structure (PDB ID 1QUV) is split in vertical axis exposing the template channel. The drug binding residues 414, 415 and 556 are colored red. The Δ1 loop is in cyan, active site GDD residues are in yellow (Left). A representative scaffold of a benzothiadiazine compound is shown (Right). The structure was drawn using ChemDraw.

mutations in these residues renders NS5B resistant to HCV796 both in replicons and

in biochemical enzymatic assays (*134*). HCV796 showed excellent inhibitory profiles in

the chimeric mouse model (*135*) and later on was approved by the FDA to enter phase II

clinical trials. However, it showed severe hepatocellular toxicity in humans and its

development has therefore been discontinued (*136*).

A third class consisting of 1,5-benzodiazepines were also reported to bind to Site

3 and inhibit NS5B in vitro with IC_{50} values in the range of 3-9 μM (*137*) and a much

higher range in HCV replicon cells.

Several of the NNI binding to all the three sites described above are currently in

clinical trials (*113*). Compounds binding to Site 1 (JTK-003 and JTK-009) from Japan

Tobacco Inc., Japan, are some examples of NNI in clinical trials while the details about

others are not available.

MISCELLANEOUS NS5B INHIBITORS

Other classes of inhibitors based on aminorhodanine scaffold have been reported

to inhibit NS5B by covalently modifying C366 in the 'primer-grip' site (Fig. 11) (*138*).

Dicarboxylic and diketo acid derivatives could bind in the active site of NS5B (*139-140*).

The MOA of these drugs is by chelating the active site magnesium ions as they act as

pyrophosphate analogs. These compounds generally have poor cell permeability and

may involve toxicity hence have not been developed further (*113*).

INHIBITORS THAT ACT INDIRECTLY ON NS5B

Cyclosporine A (CsA) was discovered to be effective against HCV replication in subgenomic replicon cells (*141*). CsA has been used as an immunosuppressant in organ transplantation patients. Surprisingly, it was also able to inhibit HCV replication. Several reports have shown subsequently that CsA acts on HCV replication in part by disrupting the association of NS5B with Cyclophilin A (CypA), although NS3 and NS5A may also require CypA (*142-143*). CypA may recruit NS5B to the replication complexes in the membranes, and increases RNA binding by NS5B through its prolyl-peptidyl isomerase activity (*143*). Given that the NS5B conformation and oligomerization are intricately linked (this study, Chapter IV), CypA may act by assisting the conformational changes needed for proper template loading in highly oligomerized states of NS5B in the RC. Notably, the CsA resistance mutations include I11V, I432V which are within or in very close proximity to the Δ1 loop (*144*). However mutations like Q438R, E440G which are associated with the β loop were also found to confer CsA resistance (*144*). CsA derivatives like NIM-811 and SCY-635 have recently created a lot of interest in this novel class of NS5B inhibitors (*145-146*). A recent report points out an association between estrogen receptors and NS5B in HCV replicon carrying cells and the anti-estrogen drug tamoxifen disrupted this association similar to the role of CsA (*147*). However it is not known if tamoxifen directly associates with NS5B, and it is interesting to note here that phytoestrogens were able to inhibit NS5B by a mechanism similar to that of Site 1 NNI (*127*).

THE ALLOSTERIC SITE OF NS5B AND NUCLEIC ACID INHIBITORS

GTP is known to stimulate RNA synthesis by HCV NS5B at high concentrations (*55, 64*). HCV NS5B has at least two GTP binding sites both identified by X-ray crystallography (*38*) (Fig. 9, 10 and 15A). The NTPi binding site at the active site cleft of the enzyme can bind to all four NTPs but the low affinity NTP binding site at the surface of the thumb domain (referred as the allosteric site hereafter) adjacent to the interacting pocket of the Δ1 loop is specific for GTP. The K_D for GTP at this site is estimated to be between 200-400 μM (*38*). GTP is used as the initiating nucleotide for de novo initiation at a higher efficiency than ATP (*40*). In order to examine the importance of the allosteric site in NS5B activity, Cai et al., (*148*) performed a systematic mutagenesis analysis of this site, but surprisingly found that none of the point mutations at the allosteric site affected de novo initiation activity of NS5B in vitro. However, all of the mutations affected the replication of subgenomic replicons to various degrees, suggesting that the allosteric site on NS5B is important for HCV replication in cells. The site seems to be a 'hot-spot' in the NS5B structure for the following reasons: 1) It is adjacent to the Δ1 loop binding pocket in the thumb domain (Fig. 12A); 2) It is overlapping with the critical residues required for binding the Site 1 NNI (*126*); 3) It overlaps with one of the residues (H502) known to be essential for homomeric interactions between NS5B subunits (*75*); 4) It is needed for replication of HCV subgenomic replicons (*148*); 5) A DNA aptamer inhibitor was identified by SELEX to bind NS5B at the allosteric site and inhibit its activity (*149*).
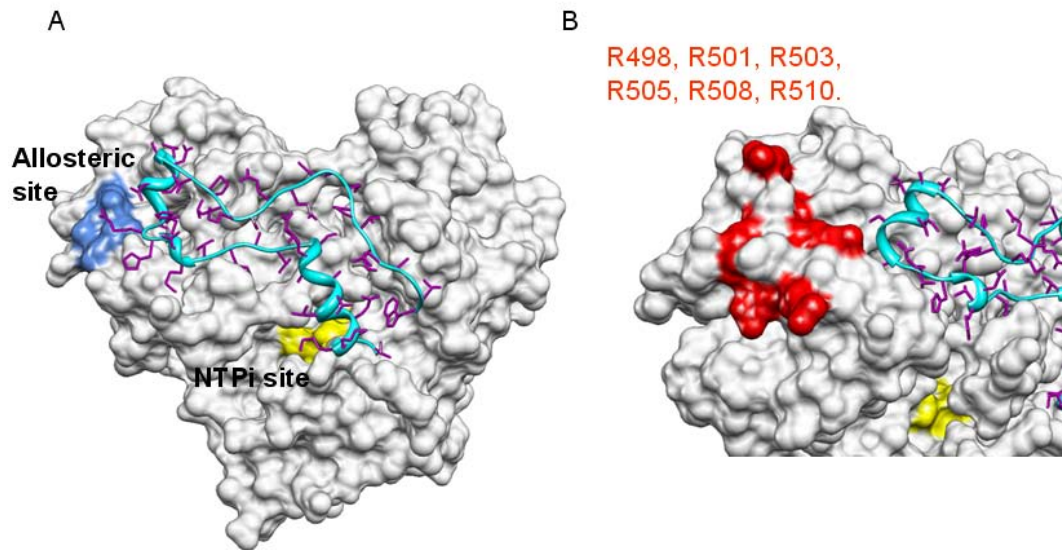
Figure 15: The allosteric site and the exposed 'basic-patch' of NS5B. (A) The allosteric GTP binding site (*38*). GTP binding residues in the thumb domain (P495, V499 and R503) are colored blue in the crystal structure of Δ35 (PDB ID 1QUV) (Two other residues binding to GTP, S29 and R32 are in the helix A of Δ1 loop and not highlighted). The Δ1 loop is in ribbon and colored cyan. The active site GDD residues are in yellow and the NTPi site that binds to all four NTPs is located within the active site close to the GDD residues. (B) The exposed 'basic-patch' in the thumb domain of NS5B. Helix-T (residues 497-513) has six basic residues and all are surface exposed. The arginines are colored red and positions are indicated at the top. The Δ1 loop and GDD residues are as in A.

RNA aptamers have also been identified to bind NS5B and inhibit its activity in biochemical assays and in HCV infected cells (*150*). One aptamer, 27v, was competitive with RNA for binding to NS5B and prevented both initiation and elongation. A second aptamer, 127v, was non-competitive with RNA and inhibited only pre-elongation events in RNA synthesis by NS5B. It is likely that 127v also binds to the allosteric site and inhibits NS5B in a mechanism similar to Site 1 NNI.

HCV GENOTYPIC VARIATION IN INHIBITOR RESPONSE

HCV exists as six known genotypes and a number of subtypes. Within the infected individual, significant differences in the viral sequences are commonly encountered, demonstrating that each subtype is a quasispecies (*151*). NI that inhibit NS5B mainly act as chain terminators and therefore target elongation stage of RNA synthesis unlike the majority of NNI which target the initiation stage. NI are effective to comparable levels among all HCV genotypes unlike NNI that have genotypic differences in responses (*108, 151-155*). In fact, significant differences in response to NNI have been noted within different viral sequences isolated from the same individual patient (*151*). This may suggest either mechanistic differences in the initiation complex assembly process between NS5B of different isolates (since most NNI target the initiation stage of RNA synthesis), or just variations in binding sites for these NNI. Gu et al., have shown differences in oligomeric properties and enzymatic activities in NS5B from genotype 1a and 1b (*74*). It is likely that differences exist in the binding constants for NS5B oligomerization across genotypes that may have a role in initiation. But, it is difficult to

reconcile major genotypic differences in the events that occur during initiation complex assembly in terms of requirement of oligomerization or intramolecular interactions. Consistent with this idea, binding site polymorphisms have been proposed to be the reason for discrepancies in the response to NNI from NS5B of different genotypes.

There is evidence in support of differential sensitivities to inhibitors. Pauwels et al., (*154*) used biochemical assays to show that among the NNI, benzimidazoles did not show much variation in IC_{50} values across genotypes except that they were about 100-fold higher for genotype 2a and 2b. In comparison, Site 2 and Site 3 inhibitors showed significant genotypic variation in responses, consistent with an altered binding site being responsible for the observed differences. For example a polar residue at position 414 was not tolerated by the 2a NS5B to bind benzothiadiazines while a Q414M mutation partially restored the inhibition. In a similar observation 1,5-benzodiazipines were effective against only genotype 1a and 1b NS5B while Q414M mutation led to only a partial inhibition of the genotype 2a NS5B (*137*). In another study the NS5B sequences from patient sera were amplified, and cloned into a genotype 1b con1 background subgenomic replicon plasmids, and were assessed for sensitivity to different NI and NNI (*151*). While NI affected all the individual replicons equally, differences existed in the response to NNI. The response to benzimidazoles showed that within the same individual, viruses with NS5B sequences that responded with a difference of almost 20-fold to the drug were present. This difference was more pronounced with the patients with genotype 1b infection than with genotype 1a infection. In the same study benzothiadiazines were not effective on isolates from a patient with genotype 1b

infection at three times the EC_{50} value (EC_{50} was determined for a consensus con1 NS5B). The response to thiophenes was somewhat uniform among different isolates in the same study.

Herlihy et al., (*153*) found a variation of 0-7% at the amino acid level in the NS5B sequences from the viral population present in each patient. In this study replicons were constructed with a con1 background containing consensus NS5B sequences from non-genotype 1 viruses obtained from patient sera to evaluate the response to different NI and NNI. While NM107 (2'-C-methylcytidine) and a NS3 protease inhibitor elicited an almost similar response from chimeric replicons containing NS5B from different genotypes, differences were clear when NNI were tested. Benzimidazoles showed a similar response from genotypes 1b, 3a, 4a and 5a but up to a 30- fold reduction in response from genotype 2a and 2b. Thiophenes had an 8-fold reduction in response from genotype 5a compared to 1b, while genotypes 2b, 3a and 4a did not have any significant response. Benzothiadiazines did not show significant response from any of the genotypes at concentrations that were inhibitory to genotype 1b replicons. Interestingly, HCV796 (Benzofuran) that binds to Site 3 had a comparable response from all genotype 1 and non-genotype 1 NS5B containing replicons.

These results collectively demonstrate the role that the viral quasispecies can play at the clinical level in therapeutic failures (Fig. 16). NNI target the initiation complex formation in NS5B, and therefore are dependent on strict conservation of their binding sites for binding and inhibition. Since NS5B itself does not have a proof reading activity and readily incorporates mutations in the genome, polymorphisms are common in the
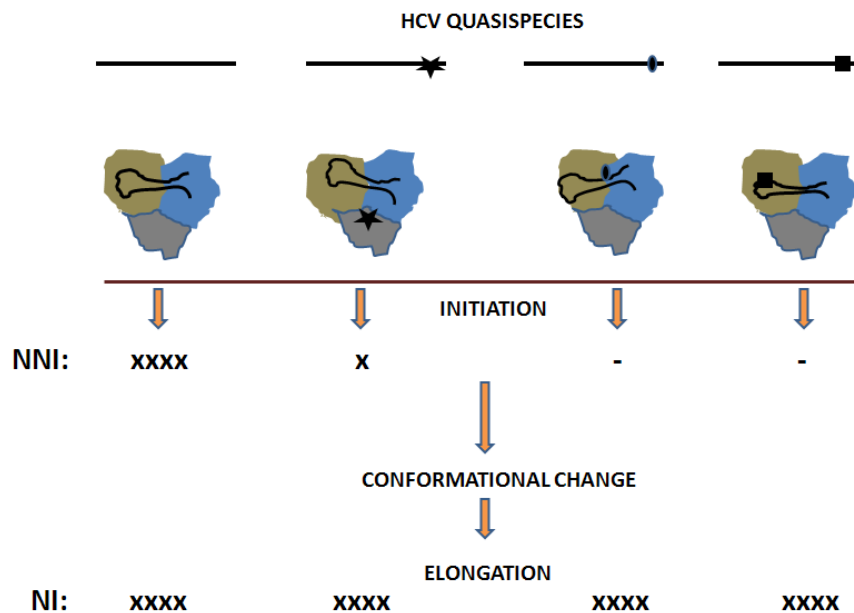
Figure 16: Role of HCV quasispecies in effectiveness of polymerase inhibitors. Presence of mutations in the viral genome (black line) in the region encoding NS5B is shown as a star, an oval or a filled box. The resulting polymerases (the three domains are in different colors and the Δ1 loop is shown as a black line) have different conformations due to polymorphisms involving the drug binding sites and also in other regions. NNI act during the initiation stage and their effect (denoted by Xs) is less or abolished in polymerases that have mutations in their binding sites or are different in their conformations. A conformational change occurs after initiation in NS5B and elongation ensues. NI that act as chain terminators target the elongating polymerase active site and get incorporated in the nascent RNA chain, hence are not affected by the polymorphisms in NS5B and therefore equally effective against NS5B of all genotypes.

NNI binding sites (*154*). In contrast, NI are nucleotide analogs and hence compete for binding with the NTPs which make them equally effective against all the HCV genotypes.

Even though a handful of NI and NNI have shown promise in clinical trials, the majority of them have suffered from safety issues and have been withdrawn from further study (*108*). Ribavirin-interferon combination therapy remains the only however, imperfect choice available against HCV infections. The 'non-responders' to this combination therapy interestingly have viruses that have about 3-fold more of hydrophobic sequences in the viral proteins along with a pattern of covarying networks among them (*156*). Clearly, more genomic analysis as well as studies in chimpanzee, or mice transplanted with human livers (*157*) needs to be carried out in order to improve the strategies for antiviral development against HCV. At the same time it is important to build and improve on the foundations laid in HCV structural and molecular biology, to identify new drug targets and to improve upon the hits to the current ones.

CHAPTER III

THE Δ1 LOOP AND DE NOVO INITIATION IN HCV NS5B*

INTRODUCTION

All RNA viruses encode their own RdRps that direct viral RNA replication and transcription. Similar to other template-dependent polymerases, the shape of a right hand is a useful description of the structures of viral RdRps (*59*). The finger and the thumb subdomains guide the template, whereas the palm contains the active site for nucleotidyl transfer. The HCV NS5B provides a useful model system to study viral RNA-dependent RNA synthesis. In contrast to a partially open conformation, the HCV RdRp structure has extensive interactions between the thumb and finger subdomains, resulting in the formation of a closed hand structure with a prominent template channel (*56-57*).

This closed conformation is also found in other viral RdRps (*65, 68, 102-103, 158-161*).Modeling studies and analysis of the ternary RdRp complex of the bacteriophage Φ6 suggest that the template RNA threads into the channel. Functional studies of various template RNAs also reveal a shared requirement for single-stranded sequence in RNA-dependent RNA synthesis (*50, 78, 162-163*). Thus, viral RdRps, unlike DNA-dependent DNA polymerases and reverse transcriptases, may use a defined channel as part of the mechanism to recognize templates (*35*).

In addition, since the channel contains the active site, it must participate in contacting the nascent RNA during elongative synthesis.

Although the template channel provides an elegant solution for the specific recognition of the initiation sequence for RNA synthesis, the diameter of this channel within the crystal structure of the HCV RdRp (ranging from 6 to 20 Å, see below) is too narrow to accommodate the duplex formed by the template and newly synthesized nascent RNA without a significant conformational change. In addition, there is growing evidence that the HCV NS5B protein undergoes a transition into an open structure to accept the template RNA (*60, 130, 164-165*). Indeed, the HCV RdRp can initiate *de novo* RNA synthesis from a circular template that cannot possibly be threaded into the template channel, functionally demonstrating that a transition between closed and open conformation can occur during template recognition (*77*).

Different conformations of the HCV RdRp may also affect its interactions with cellular proteins. The retinoblastoma tumor suppressor protein (pRb) is one interesting example, since it is targeted by DNA tumor viruses and by HCV as a means to deregulate cell cycle progression (*166*). pRb-binding proteins contain an L*X*C*X*E motif. In NS5B, this motif overlaps the residues that coordinate divalent metals in the catalytic pocket (*22*). Thus, the NS5B residues that are putatively involved in the interaction with pRb are not surface-exposed, suggesting the need for a conformational change in NS5B to accommodate the binding of pRb.

Cyclophilins are cellular peptidyl isomerases that are required for replication of several viruses, including human immunodeficiency virus and HCV (*167-169*). The

peptide drug cyclosporine, which binds cyclophilins, was found to inhibit HCV RNA replication (*170-173*), and some mutations that render resistance to cyclosporine mapped to NS5B (*172*). Cyclophilin A (CypA) and CypB have been shown to co-precipitate with the HCV NS5B protein (*172*), but RNA silencing experiments have yielded conflicting results as to whether CypB and/or CypA are required for HCV replication.

We have carried out a series of experiments aimed at determining how mutations in the template channel of the HCV RdRp affect RNA synthesis and its interactions with cellular proteins. Three of the mutations affected an interaction between a surface loop and the outer lining of the template channel. Furthermore, the interaction appears to regulate the transition between the conformations that are needed for *de novo* initiation and primer extension (PE). Furthermore, we show that RNA synthesis by the PE-competent and presumably the more open conformation is preferentially inhibited by pRb.

MATERIALS AND METHODS

Reagents, Site-directed Mutagenesis, and Protein Purification. Recombinant pRb was purchased from QED Biosciences, Inc. Oligoribonucleotides were chemically synthesized by Dharmacon, Inc. Wild-type and mutant versions of the HCV RdRp were expressed with a C-terminal His_6 tag in *Escherichia coli* and purified first by metal ion affinity chromatography, followed by chromatography with polyuridylate resin (Sigma) (*163*). The purified proteins were stored in 50 mM Tris (pH 7.9), 400 mm NaCl, 1 mm dithiothreitol, and 10% (v/v) glycerol at -80 °C. Protein concentrations were determined

by staining SDS-PAGE with Coomassie Blue and comparing the bands to those of

bovine serum albumin at known concentrations. Amino acid substitutions were

introduced in the plasmid encoding HCV Δ21 using the QuikChange site-directed

mutagenesis protocol recommended by Stratagene. The entire open reading frame was

sequenced to confirm the presence of directed mutation and the absence of unintended

mutations.

HCV Subgenomic Replicon Assay. All of the mutations except m26-30 were introduced

into the subgenomic replicon by using the appropriate BglII DNA fragment from the

pET21B plasmid that can express the mutant protein to replace the comparable fragment

in the wild-type subgenomic HCV replicon (pFK/I$_{389}$neo/NS3-3'/5.1). To introduce the

m26-30 mutation into the replicon, an EcoRI-SpeI fragment from the wild-type

subgenomic HCV replicon was subcloned into pBSK$^-$ plasmid (Stratagene), and

mutations were introduced by site-directed mutagenesis. The subcloned fragment was

reintroduced into pFK/I$_{389}$neo/NS3-3'/5.1, replacing the comparable DNA fragment. The

presence of the mutation in the HCV subgenomic replicon was confirmed by DNA

sequencing.

Subgenomic HCV replicon RNAs were transcribed using the T7 Ampliscribe kit

(Epicenter, Madison, WI) from plasmids linearized with ScaI. The subgenomic HCV

replicon RNAs were transfected into Huh7 cells by electroporation with a GenePulser

system (Bio-Rad) as described by Krieger *et al.* (*29*). Briefly, 1 μg of the *in vitro*

transcribed RNAs along with 9 μg of total RNA from naive Huh-7 cells were

electroporated at 960 microfarads and 270 V into ~1×10^6 Huh7 cells in 0.4 ml of ice-

cold Cytomix. The cells were immediately transferred to 8 ml of complete Dulbecco's modified Eagle's medium containing 1.25% DMSO and seeded in a 10-cm dish. 24 h after transfection, the cell culture medium was replaced with complete Dulbecco's modified Eagle's medium supplemented with 0.5 mg/ml G418. The medium was changed every week for 3 weeks for the colony formation assay. The G418-resistant cell colonies were stained with 0.01% Coomassie Brilliant Blue.

Reverse Transcription-PCR Assay. The reverse transcription reaction used 400 ng of total RNA (harvested 72 and 96 h after electroporation with the RNeasy RNA isolation kit (Qiagen)). Reverse transcription reactions used the Superscript III reverse transcriptase (Invitrogen), incubated at 50 °C for 60 min. 15% of the reaction mixture was used directly for PCR with an initial denaturation step at 94 °C for 2 min, followed by 30 cycles of 94 °C for 30 °C s, 50 °C for 30 s, and 72 °C for 90 s. The final extension was at 72 °C for 5 min. PCR products were separated in a 1% agarose gel. Primers used had the sequence 5'-CTCGATGTCCTACACATG-3' (plus-strand primer) and 5'-ATTGACTGGAGTGTGTCTAG-3' (minus-strand primer).

RdRp Activity Assays. Standard RdRp assays consisted of 1 pmol of linear template RNA and 0.04 μm NS5B (unless stated otherwise) in a 20-μl reaction containing Core buffer (20 mm sodium glutamate (pH 8.2), 4 mm $MgCl_2$, 12.5 mm dithiothreitol, 0.5% (v/v) Triton X-100) amended with 200 mm GTP, 100 μm each of ATP and UTP, and 250 nm [α-^{32}P] CTP (Amersham Biosciences). $MnCl_2$, if used, was added to a final concentration of 1 mm. The final reaction also contained 20 mm NaCl that came from the storage buffer. RNA synthesis reactions were incubated at 25 °C for 60 min and

stopped by phenol/chloroform extraction, followed by ethanol precipitation in the presence of 5 μg of glycogen and 0.5 m ammonium acetate. Products were usually separated by electrophoresis on denaturing (7.5 m urea) polyacrylamide gels. Gels were wrapped in plastic, and radiolabel was quantified using a PhosphorImager (Amersham Biosciences). Each quantified result shown was from a minimum of three independently assayed samples.

Intrinsic Fluorescence Spectroscopy. Fluorescence measurements were done at 23-25 °C with a PerkinElmer Life Sciences LS55 spectrometer. Proteins were in a buffer of 20 mm Tris (pH 7.9), 1 mm dithiothreitol, 10% glycerol, and 400 mm NaCl. The protein concentrations were adjusted to 0.75-1.5 μm. Measurements were performed with constant stirring to minimize photobleaching. Five independent measurements were recorded per sample with 1-min intervals between scans, and the measurements were averaged. Excitation was performed at 295 nm, and the emission spectrum was collected at 1-nm intervals from 305 to 400 nm, with an integration time of 1 s and slit width of 5 nm.

Electrophoretic Mobility Shift Assays. *In vitro* transcribed double-stranded RNAs treated with alkaline phosphatase were radiolabeled with [^{32}P] ATP, using T4 polynucleotide kinase. Labeled RNA (40 fm) was incubated in a 20-μl reaction with a 40 nm final concentration of the polymerase in the Core buffer amended with 1 mm MnCl$_2$ and 0.2 mm GTP. The reactions were incubated at 25 °C for 30 min, after which a 4-μl solution containing 10 mm Tris (pH 8.1), 1 mm EDTA, 0.1% bromophenol blue, 0.1% xylene cyanol, and 30% glycerol was added. The samples were electrophoresed on a native 10%

polyacrylamide gel at 400 V for 1 h, and then the gel was autoradiographed.

Analytical Ultracentrifugation. Analytical ultracentrifugation experiments were performed at the Center for Analytical Ultracentrifugation of Macromolecular Assemblies at the University of Texas Health Science Center at San Antonio. Δ21 and W397A were analyzed by sedimentation velocity experiments performed in a Beckman XLA centrifuge using absorbance optics by measuring intensity scans at 280 nm of a 0.8 OD loading. The experiments were performed in two-channel epon centerpieces at 45,000 rpm in an AN50 Ti rotor using a buffer containing 20 mm MOPS, 100 mm NaCl, and 0.75% (w/w) glycerol at 10 and 25 °C. Data analysis was performed with the UltraScan software suite (*174*). Data were first analyzed with the two-dimensional spectrum analysis (*175*) with simultaneous time invariant noise subtraction according to Schuck and Demeler (*176*). After noise subtraction, the data were examined for heterogeneity with the enhanced van Holde-Weischet analysis (*177*) and fitted by the genetic algorithm Monte Carlo analysis (*178*) in order to obtain shape information. All computations were performed on the TIGRE cluster at the University of Texas Health Science Center at San Antonio and the Texas Advanced Computing Center at the University of Texas in Austin. Partial specific volume was estimated based on PROTEIN sequence according to Durchschlag (*179*) and was found to be 0.732 cm^3/g for both Δ21 and W397A.

Circular Dichroism Analysis. Δ21, W397A, and H428A were subject to thermal unfolding using an Aviv 202SF spectropolarimeter with temperature control and stirring units. The change in CD signal at 220 nm was measured from 2 to 97 °C with 3-min

equilibration intervals, and the data were averaged for 5 s at each interval. The

concentration of the protein samples was between 4 and 15 μm in 5 mm MOPS at pH

7.6. The data were analyzed using methods described by Grimsley *et al.* (*180*).

Molecular Modeling. The crystal structure of the wild-type HCV-RdRp (Protein Data

Bank code 1QUV) was used to construct the W397A mutant model with Modeler

(Insight II; Accelrys). Residues within a 15-Å radius of the Ala^{397} were subjected to a

medium level of simulated annealing optimization with respect to the variable target

function of Modeler. To mimic the Δ1 loop deletion, we constructed another model by

mutating the residues L26-S27-N28-S29-L30 into alanines, which were then subjected to

a medium level of simulated annealing optimization. The mutant models were

superimposed onto the 1QUV structure using USCF Chimera (available on the World

Wide Web).

RESULTS

Mutational Analysis of the Template Channel in the HCV RdRp. An unusual aspect of

the crystallographic structures of viral RdRps is the presence of a RNA template channel

that can lead the template RNA to the active site (*56-57, 63*). The template channel has

areas that are more constricted, with the narrowest part having a diameter of ~5.5 Å

when measured from the surfaces of the channel (Fig. 17A). To probe how the template

channel might regulate RNA synthesis, we mutated many of the polar or aromatic

residues that line the channel, typically to alanine. The locations of these mutations and

their relationship to the channel are shown in Fig. 17A.

Template LE19 was used to assess the effects of the mutations on RNA synthesis. The 19-nt LE19 can exist either as a hairpin with a single-stranded 3' sequence that directs *de novo* initiation from the 3'-terminal cytidylate or as a partially duplexed dimer that can be primer-extended to result in a 32-nt product (Fig. 17B). Higher molecular mass bands that are multiples of 19 nt are also produced and have been characterized as template switch products (*88, 181*). Given that these are extended from the nascent RNA, they should be considered primer extension products.

Compared with the wild-type Δ21 NS5B protein, several mutants demonstrated significantly decreased RNA synthesis, including D225A, T389A, and Q436A. D225 and T389 are residues that are 6 and 16 Å, respectively, from the active site (the measurement was to the center of the respective side chains from the side chain of D318), but N436 resides at a distance of 32.4 Å from the active site, at the tip of the thumb domain. Unexpectedly, 14 of 33 mutants demonstrated increased RNA synthesis. When mapped onto the template channel, these mutations tend to be located at the entry and exit portions as well as the constricted region of the channel (Fig. 17A, *blue residues*). Thus, the observed increase in RNA synthesis suggests that these residues lining the channel may function to restrict access of inappropriate templates. Two substitutions, W397A and H428A, resulted in severely decreased de novo initiation but had little impact on PE (Fig. 17C). Both W397 and H428 are more than 20 Å from the GDD motif that coordinates divalent metals and therefore should not affect binding of the initiation GTP (*118*). Our reactions contained 1 mm Mn^{2+}, the presence of which generally decreases the effects of mutations of the NTPi-binding residues.

Figure 17: Mutational analysis of the RNA channel in the HCV RdRp**. *A*, *a ribbon diagram representation* of the structure of the HCV RdRp molecule (Protein Data Bank code 1QUV) and a *cut away representation* of the template channel. The thumb, finger, and palm subdomains are identified by the letters *T, F*, and *P*, respectively. The amino acids in the template channel mutated to alanine are shown with their side chains in different colors. The yellow residues are the aspartates that bind the divalent metals and are intended to serve as a landmark in the catalytic pocket. The blue residues identify substitutions that increased RNA synthesis. The *red residues* were inactive. The purple residues are defective in de novo initiation but competent for extension from a primed template. The mutations that did not significantly affect RNA synthesis (Table 1) are not shown in this figure. Distances shown were measured as follows: 18 Å is from OE1 of Q446 to OE of K98; 21.5 Å is from CB of S556 to OD1 of D352; 4.5 Å is from NE2 of Q446 to OE1 of D143; 16.5 Å is from NE2 of Q355 to CG of K155. *B*, the sequence and predicted secondary structures of LE19, a template for RNA-dependent RNA synthesis. LE19 exists in two conformations, a stem-loop structure that can direct *de novo* initiation and a partially base-paired dimer that can direct primer extension. *C*, image of the products of RNA synthesis by the mutant RdRps. Mutant proteins tested in each reaction are shown at the *top* of the gel image. The purified proteins used in each reaction, resolved on 4-12% SDS-polyacrylamide gels and stained with Coomassie Brilliant Blue are shown *below* the autoradiogram images. The protein molecular weight markers are the SeeBlue standards from Bio-Rad. The sizes of the RdRp products for *de novo* initiation (19 nt), PE (32 nt), and the purified HCV RdRps (65 kDa) are shown to the *left* of the gel images.
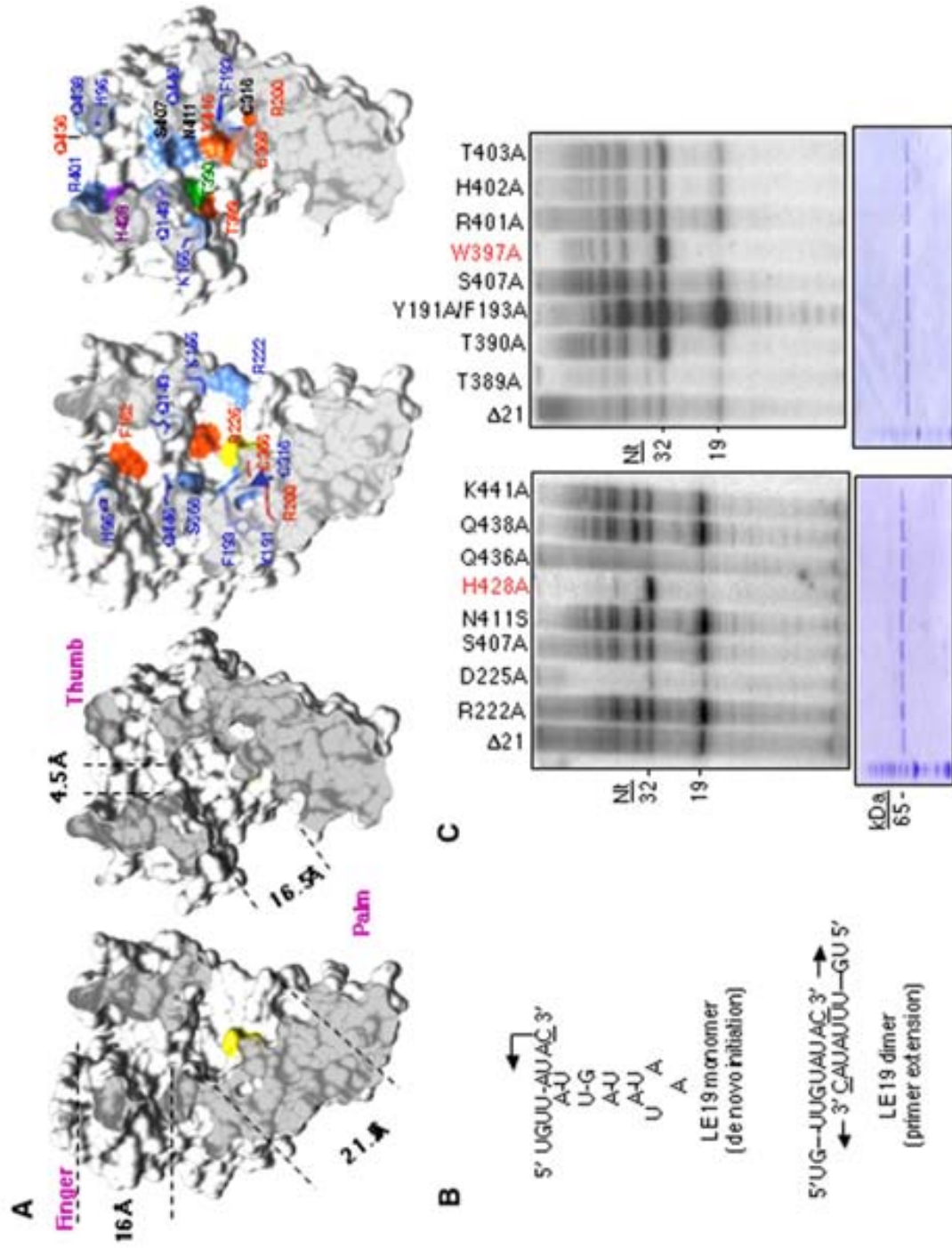
Table 1: A summary of the effects of mutations in or near the template channel of HCV RdRp. The mutants are classified according to the five groups distinguished in function. d n, *de novo* initiation. PE- primer extension. Fold synthesis is shown as follows: ++++, >10.0-fold; +++, 5.1-10.0-fold; ++, 3.1-5.0-fold; +, 1.3-3.0-fold; 0, 0.9-1.2-fold; -, 0.6-0.8-fold; -|-, 0.1-0.5-fold; -|-|-, 0-0.1-fold.

Functinal subclass	d n	PE
Increased activity		
Q438A	++	++
Y191/F193A	++++	++++
S407A	++	++
R401A	++	+
R222A	+	++
N411S	+	++
K155A	+++	++++
Q446A	++	++
S556A	+	++
E143A	+++	+
H95A	++	+++
C316A	+	++
Y191/F3/Y448A	+	+
D559A	++	+++
Increased PE		
T390A	0	++++
H402A	-	+
M139A	-	
		+

Functional subclass	d n	PE
No *de novo* initiation		
H428A	—	++
W397A	—	++++
W397A/A396W	—	++++
H428A/I432W	—	++++
m26-30	—	+
Decreased activity		
T389A	-|-	-|-
D225A	-|-	-|-
Q436A	-|-	-|-
Y415A	0	-|-
C366Y	-|-|-	-|-|-
R200A	-|-	-|-
F162A	-|-	-|-
Minimal effect		
C146A	-	0
T403A	0	+
K441A	0	0
Y448A	0	+

Therefore, these residues are not directly involved in NTPi recognition (*118*).

To further characterize the defects in *de novo* initiation manifested by H428A and W397A mutants, we manipulated the concentration of the initiation GTP. LE19 has a cytidylate only at the 3' initiation site; hence, GTP is required for initiation but not PE (Fig. 17B). The absence of GTP in the reaction mix did not affect the abundance of the 32-nt PE product produced by the mutants (Fig. 18A, *lanes 7* and *11*). In contrast, the wild-type Δ21 protein failed to initiate RNA synthesis *de novo* without GTP (Fig.18A, *lane 3*). To demonstrate that the 32-nt products resulted in PE, we used LE19P, which is identical to LE19 but has a puromycin blocking the 3' terminus. H428A and W397A did not produce the 32-mer from LE19P (Fig. 18A, *lanes 6* and *10*), confirming that products were made by extension from the 3' terminus of LE19.

Next, we used the 115 nt from the 3' end of minus-strand HCV RNA as a template to confirm the defect in *de novo* initiation with W397A and H428A. This RNA, designated H115, forms extensive secondary structures (Fig. 18C) but can direct *de novo* RNA synthesis (*148*). H428A and W397A failed to generate the expected 115-nt products from this template (Fig. 18B, compare *lane 1* with *lanes 2* and *3*). However, a related template RNA, H115 + PE46, which provides a "looped back" primer allowing for PE, restored RNA synthesis by W397A and H428A to 34 and 9%, respectively, of the level seen with Δ21. Truncated products from H115 + PE46 were not observed, suggesting that the low level of synthesis was not due to premature termination. The reduction in PE observed with the H115 + PE46 template suggests that mutants W397A and H428A may have additional defects in RNA synthesis that are not as evident with

Figure 18: H428 and W397 interact with the Δ1 loop. *A*, RNA products made by mutant and Δ21 using templates and reaction conditions to examine *de novo* initiation and PE. The proteins, templates, and the GTP concentrations used in the reactions are indicated *above* the gel image. LE19P is a version of LE19 that has a covalently attached 3′-puromycin. The *lane numbers* are indicated at the *bottom* of the gel image. The *de novo* initiated (19 nt) and primer extension products (32 nt) are indicated to the *left* of the gel image. *B*, RNA synthesis by the HCV RdRp with template derived from HCV. RNA H115 contains the 3′ 115 nt of HCV minus-strand RNA. RNA H115 + PE46 contains the PE46 sequence (*boxed*) fused to the 3′ end of H115. Whereas H115 can direct *de novo* initiation, H115 + PE46 is capable of primer extension. The gel images show the reaction products of the enzymes using H115 or H115 + PE46 as template, which were run on a 10% urea denaturing polyacrylamide gel. The divalent metal ion manganese was left out of the reaction mix in the assays with H115 and H115 + PE46 templates. The *lane numbers* are shown at the *bottom*, and the *enzyme names* are shown at the *top* of the *lanes*. The lengths of the products are shown to the *left* of the image; the 115 nt band corresponds to a *de novo* initiation product of H115, and the 275 nt band corresponds to the PE product of H115 + PE46. *C*, interaction between H428, W397, and the Δ1 loop. The Δ1 loop is rendered as a *blue ribbon* with the network of primarily hydrophobic interaction residues *below*, indicated in *red*, except for H428 and W397, which are in *purple*. The *box* contains a *ribbon representation* of the Δ1 loop (residues *underlined*) interacting with the helices in the thumb domain. The apex of the Δ1 loop is *colored gold*.

shorter templates.

Δ1 Loop Participates in the Open and Closed Transition States by the HCV RdRp. W397
and H428 have their side chains pointing away from the active site and are part of a
hydrophobic surface overlaid with a structure named the Δ1 loop. In the closed RdRp
conformation, the Δ1 loop protrudes at the tip of the fingers domain and contacts the
thumb domain by packing its short α-helix (helix A) against the α-helices O (residues
388-401) and Q (residues 418-437) (Fig. 19B). H428 contacts the side chains of residues
S29 and L30 in helix A. The aromatic side chain of W397 stacks against the
hydrophobic pocket formed by the side chains of residues L21, P22, V37, and A39
of the Δ1 loop (Fig. 18C) (data not shown). These interactions suggest that the contact
between the Δ1 loop and the outside surface of the template channel are required for *de
novo* initiation. Consistent with this model, inhibitors that bind to a groove in the thumb
subdomain disrupt interdomain communication mediated by the Δ1 loop and cause
conformational changes in the 2a and 1b HCV RdRps (*60, 62*). To determine whether
the Δ1 loop is required for *de novo* initiation, we deleted the five residues of helix A
within the Δ1 loop. The resultant protein, designated m26-30, was capable of PE when
tested with the LE19 template (Fig. 18A, *lanes 13-16*). This result confirms that *de novo*
initiation requires the interaction between the Δ1 loop and the underlying residues that
help to form the template channel. Furthermore, the presence of higher levels of the
template in the reaction increased in preferential accumulation of the primer extension
products (not shown). Two additional mutants, I432W/H428A and A396W/W397A,
were made in an attempt to restore this interaction.
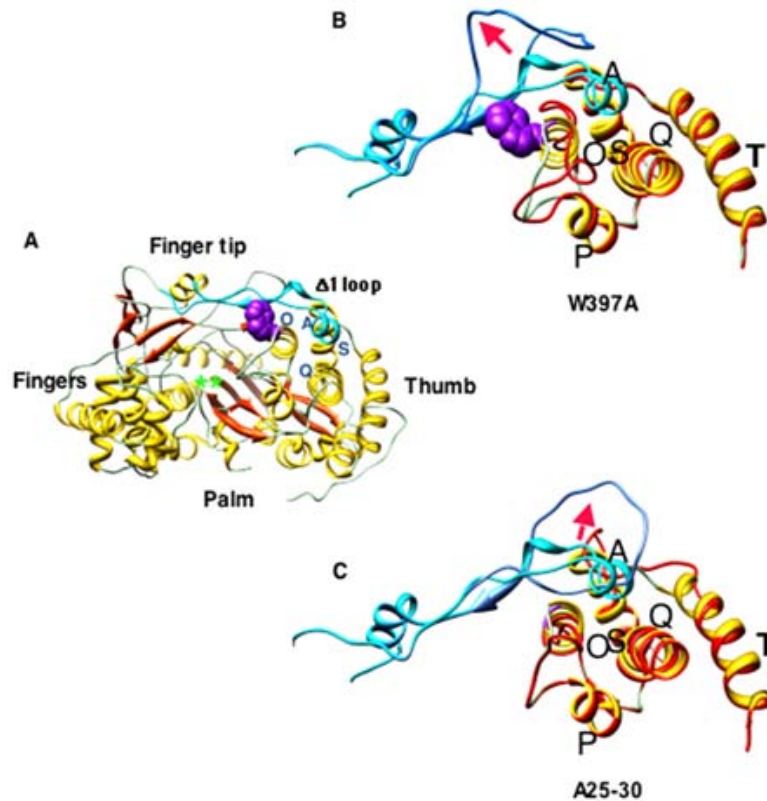
Figure 19: Molecular modeling of the HCV RdRp, emphasizing the effect of the substitution on the Δ1 loop. *A*, location of Δ1 loop (*colored* in *cyan*) with respect to the thumb, palm, and fingers is shown in the crystal structure (1QUV) of the HCV NS5B protein. The Δ1 loop protrudes at the tip of the fingers domain and contacts the thumb domain by packing its short α-helix (helix A) against the α-helices O (residues 388-401) and Q (residues 418-437) of the thumb domain. The W397 residue is shown in *purple*. The active site is indicated by *green stars. B*, superposition of the W397 mutant model (*red* and *sky blue*) of NS5B and the WT structure (*yellow* and *cyan*). Only Δ1 loop and its contact regions are shown. The side chain of W397 stacks into the Δ1 loop. In the W397A mutant model, the key interactions are lost, and the Δ1 loop moves significantly away from its contact region. The *red arrow* indicates the movement. *C*, superposing a mutant in helix A of the Δ1 loop (L26A/S27A/N28A/S29A/L30A) and the wild-type protein; the Δ1 loop moves away from the thumb domain, and the helix A widens into a loop. The *arrow* indicates the direction of the movement.

However, although both of these mutants were found to be competent for PE, they were defective for *de novo* initiation (Table 1), perhaps due to a requirement for additional interactions between the outer surface of the template channel and the Δ1 loop that will not be addressed in this work.

W397A, H428A, and the m26-30 and HCV Replication in Cells. We next introduced several of these mutations into cDNA encoding a subgenomic HCV replicon in order to assess their effects on replication of HCV RNA in cultured human hepatoma cells. *In vitro* transcribed RNAs produced from these mutant plasmids were transfected into Huh7 cells, and colonies supporting replication of the viral RNA were selected by growth in the presence of G418. The H428A mutant failed to form colonies, whereas the wild-type replicon and an unrelated mutant replicon formed a significant number of colonies (Fig. 20A). To further examine the functional impact of the NS5B mutations, subgenomic replicons containing the H428A and W397A substitutions and the m26-30 deletion were transfected into Huh7 cells, and the level of replicon RNAs was examined semiquantitatively using reverse transcription-PCR. The WT subgenomic replicon RNA could be detected at 72 and 96 h after transfection, but an active site GAA mutant and all three mutants of interest failed to produce a detectable signal with two independent sets of primers specific to HCV cDNA (Fig. 20B and C). These results demonstrated that the *in vitro* competence of NS5B for *de novo* initiation is correlated to HCV RNA replication in cells.

Molecular Modeling of the Mutant Polymerases. We used molecular modeling to examine the effects of the W397A substitution.
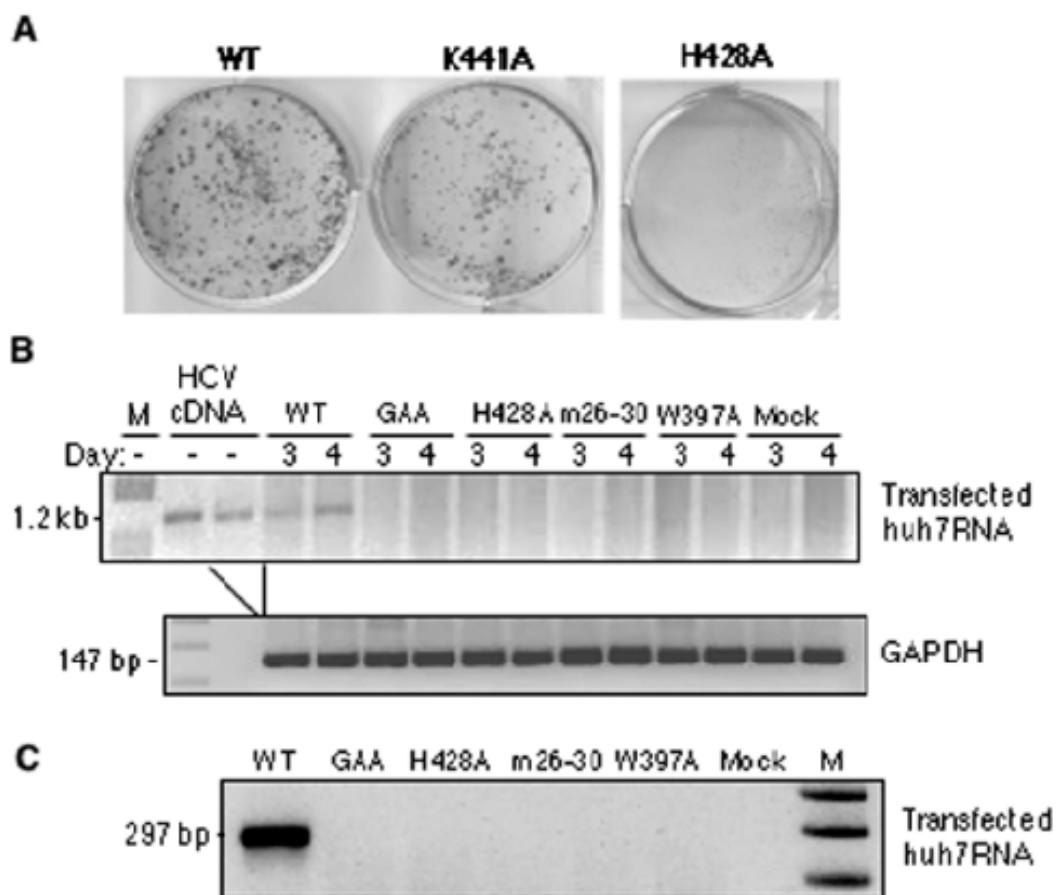
Figure 20: W397, H428 and the helix A residues are required for HCV subgenomic replication in Huh7 cells. A) Formation of G418-resistant colonies in cells electroporated with the wild-type and mutant HCV subgenomic replicons. The plates were stained with Coomassie Blue three weeks after electroporation. B) RT-PCR result of the HCV RNAs produced in WT and mutant cells. The DNA bands were visualized by staining the agarose gel with ethidium bromide. The 146-bp fragments were from the GAPDH mRNA that was amplified from the same samples. These bands serve as loading controls. C) Amplification of a 297-bp fragment from the HCV replicon. This experiment was performed with only the RNAs harvested 96 h after electroporation. The smaller DNA fragment was able to increase the signal from the HCV replicon and show that the mutant replicons were unable to replicate.

Residues within a 15-Å radius of W397A were subjected to a medium level of simulated annealing optimization using the variable target function of Modeler. W397A resulted in the Δ1 loop moving away from the thumb domain, with a maximum deviation of 12 Å. In fact, helix A unwinds into a loop during the energy optimization and loses contact to the neighboring helix Q (Fig. 19A and B). Similar results were obtained when we analyzed the structure of an HCV RdRp that had the helix A residues 26-30 in the Δ1 loop (sequence LSNSL) replaced with alanines (Fig. 19C). These changes in the Δ1 loop were predicted to alter the structure of the template channel, making it more accessible to solvents. These predicted changes in the structure of the HCV RdRp could account for the functional differences we observed between the mutant RdRps and the wild-type Δ21 polymerase.

Biophysical Characterizations. We sought biophysical evidence in support of these hypothesized differences in the conformations of Δ21 and the mutant RdRps generated by computational modeling. The HCV RdRp has been reported to form oligomers (*75-76*). Therefore, we examined the masses of Δ21 and W397A in solution at 10 and 25 °C using velocity sedimentation analytical centrifugation. Enhanced van Holde-Weischet analyses indicated that both protein samples were homogeneous and had *S* values between 4.1 and 4.2 (Fig. 21A). Results from a global genetic algorithm Monte Carlo analysis of each sample suggested that the proteins are globular in shape with frictional coefficients between 1.1 and 1.25, which correspond to an average molecular mass of 67.7 kDa, an excellent fit with monomers. Slight differences in the sedimentation of the two proteins exist at 25 °C, but it is difficult to assess whether this is due to significant

Figure 21: Biophysical and biochemical analyses of the mutant RdRps**.** *A*, analytical ultracentrifugation to examine the oligomerization state of W397A and Δ21 at two temperatures. The profiles for the two proteins largely overlap, suggesting that both are homogeneous and monomeric in solution. *B*, intrinsic fluorescence of the Δ21, W397A, H428A, and m26-30. The W397A has a spectrum indistinguishable from Δ21. H428A and m26-30 show a pronounced red shift in the spectrum between 349 and 363 nm. *C*, partial rescue of *de novo* initiation by dinucleotide primers. Shown is an autoradiograph of the RdRp products from template LE19 in the presence or absence of GTP or the NTPi mimic, GpU, as indicated *above* the gel image. *D*, PE from template PE46 in the presence of heparin. *E*, double-stranded RNA binding by Δ21 and the mutant RdRps. The gel image is from a 10% nondenaturing gel. The sequence of the probe used, RIII46, is shown *above* the gel image.
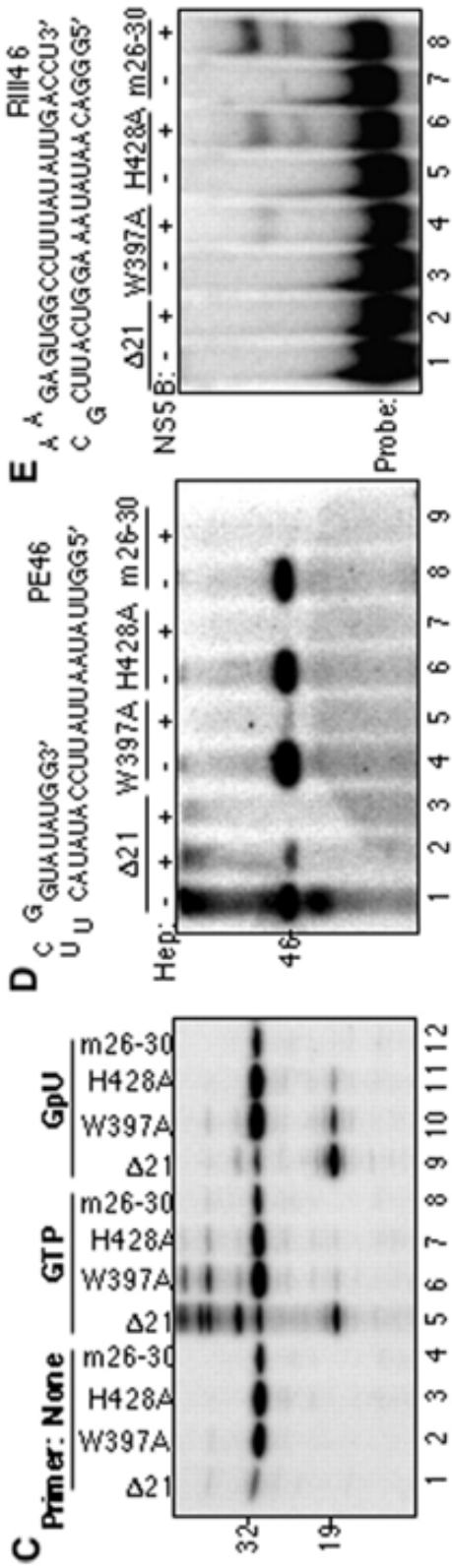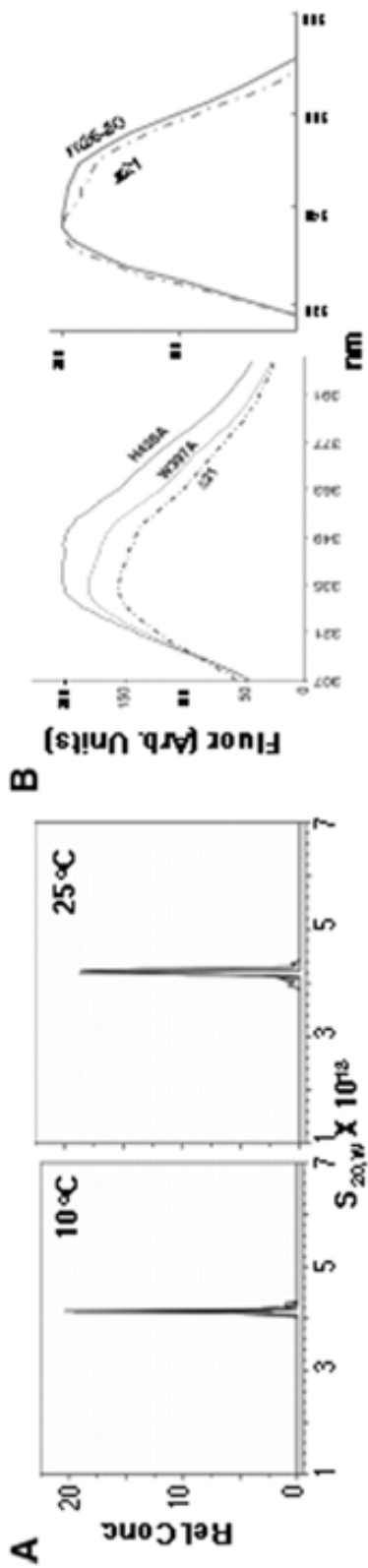
conformational changes within the monomers. Nonetheless, these results establish that the mutation W397A, which renders it unable to initiate *de novo*, is not through an effect on the oligomerization state of the protein.

Next, we characterized the intrinsic fluorescence of the wild-type and mutant RdRps. The environment of aromatic residues, especially tryptophans, can affect their fluorescence (*182*). The intrinsic fluorescence spectra of several independent preparations of the H428A and m26-30 mutants exhibited a pronounced red shift in comparison with the wild-type Δ21 protein (Fig. 18B, *both panels*). Such a red-shifted spectrum is indicative of the presence of tryptophan residues in a more polar environment (*183*) and provides evidence for an altered conformation in H428A and m26-30. However, this red shift was not seen with the mutant W397A, despite its sharing a common defect in *de novo* initiation. These results suggest that the three mutant RdRps are not in identical conformations (Fig. 21B, *graph* on the *left*). We attempted to examine the relative stabilities of Δ21 and the mutant proteins using circular dichroism spectroscopy with increasing temperature. H428A and W397A demonstrated smooth two-state transitions, with T_m values of 43 and 46 °C, respectively. In contrast, Δ21 demonstrated multiple transitions, probably due to some of the protein precipitating during the experiment (Fig. 22). Altogether, these biophysical and modeling results show that the mutant proteins have physical properties that differ from the wild-type Δ21. Furthermore, the mutant proteins are not in identical conformations. *Additional Functional Characterizations.* We hypothesized that the different conformations assumed by the mutant and wild-type HCV RdRps are related to the

conformational states required for distinct stages of RNA synthesis by the HCV RdRp. The closed conformation with a defined template channel could be responsible for *de novo* initiation, whereas the open conformation would permit elongation. The template channel will expand to accommodate the duplex of the nascent and template RNA by releasing the interaction with the Δ1 loop. To examine this hypothesis, we characterized how Δ21 and the mutant RdRps interacted with RNA. Dinucleotides can replace the NTPi and can improve the stability of the ternary complex and rescue some defects in RNA synthesis (*40*). We investigated whether RNA synthesis by the mutants could be restored with the dinucleotide (GpU in place of GTP. GpU is complementary to the first two nucleotides at the 3' terminus of LE19). The presence of GpU increased *de novo* initiated RNA synthesis by W397A and H428A by 27- and 12-fold, respectively, in comparison with GTP (Fig. 21C). However, GpU failed to rescue *de novo* initiation by m26-30.

To examine whether template binding by the mutant RdRps was affected, we performed RNA synthesis in the presence of heparin, a template mimic (*184*). RNA PE46 was selected for this analysis, because it is capable of directing only PE, thus eliminating possible effects on *de novo* initiation. The enzymes were preincubated with PE46 for 5 min to form a binary complex before the addition of heparin and rNTPs. Heparin reduced PE by the wild-type protein, Δ21, to ~10%, whereas W397A, H428A, and m26-30 were capable of PE at less than 0.5% of the amount seen in the absence of heparin (Fig. 21D, *lanes 2, 5, 7*, and *9*).
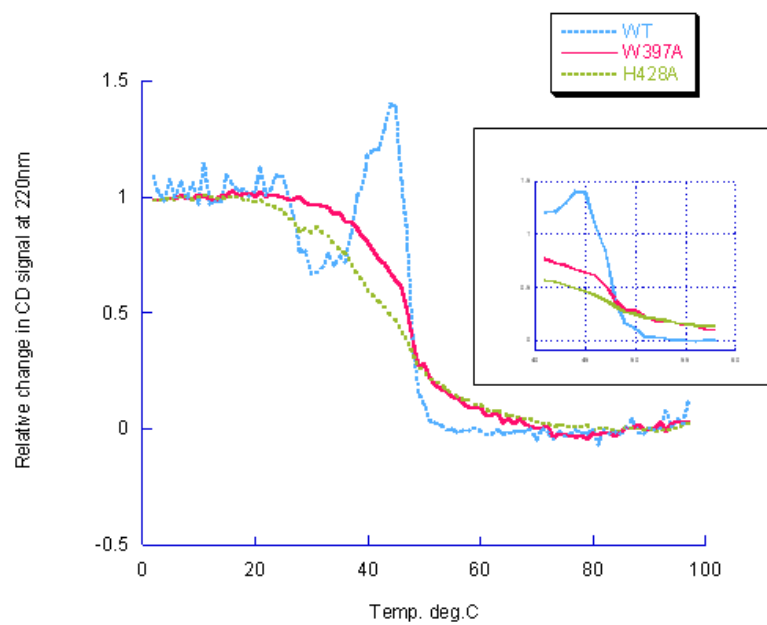
Figure 22: CD spectroscopy to analyze the thermal melts for Δ21 and the PE+ mutant RdRps. The complex denaturation pattern of Δ21 suggests that the protein may exist in more than one conformation or oligomeric state.

However, when heparin and PE46 were added simultaneously to Δ21 before rNTP addition, no RNA synthesis was observed (Fig. 21D, *lane 3*). These results show that Δ21 can form a more stable binary complex with RNA than the mutant RdRps and suggest that the mutant polymerases might have reduced affinity for single-stranded RNA as compared with Δ21 and/or a reduced capacity to form a productive complex as compared with Δ21. Together, these results suggest that the interaction between the Δ1 loop and the thumb subdomain can affect binary complex formation with single-stranded RNA, probably accounting for the defect in RNA synthesis.

Last, we compared the abilities of Δ21 and the mutant RdRps to bind double-stranded RNAs in an electrophoretic mobility shift assay. For these experiments, we used the RIII46 RNA, which can form a stable 21-nt hairpin (*185*) (Fig. 21E). Δ21 failed to form a shifted band. However, the three mutant enzymes bound detectably to RPIII46, in increasing quantities from W397A to H428A and m26-30 (Fig. 21E). These results are consistent with the model that the mutant RdRps are in more open conformations when compared with Δ21.

Interaction with Cyclophilins and Retinoblastoma. Several cellular proteins have been shown to interact with the HCV NS5B in pull-down and co-immunoprecipitation assays, including CypB and CypA and the cell cycle regulator, pRb (*22, 141, 170, 172*). CypB interacts with the C-terminal domain of NS5B and has been reported to increase template binding in pull-down assays (*141, 172*). However, Robida *et al.* (*172*) did not observe a significant effect on HCV replication with the silencing of CypB, suggesting that another cyclophilin, perhaps CypA, has a role. An *et al.* (*167*) found that

polymorphisms in CypA affected HCV replication.

The addition of purified CypA resulted in a concentration-dependent inhibition of RNA synthesis by the HCV RdRp from Δ21, m26-30, and I432V, a cyclosporin A-resistant mutation in NS5B (Fig. 23B) (*172*). However, both *de novo* initiation and PE were inhibited, indicating that CypA does not preferentially target a particular mode of RNA synthesis. The presence of purified CypB resulted in a more pronounced shut-off of RNA synthesis than CypA. A molar ratio of three CypA to one RdRp reduced RNA product accumulation to approximately half, whereas the same amount of CypB reduced product formation 10-fold (Fig. 23C). In addition, the inhibitory effect of CypB was slightly stronger on the PE products than the *de novo* initiation products, although both were inhibited at higher CypB concentrations. These results demonstrate that both CypA and CypB can affect RNA synthesis by the HCV RdRp *in vitro*, although the effects are distinct. Several other proteins, such as bovine serum albumin and the RNA-binding proteins, PusA and App1, that affected brome mosaic virus RNA replication (*186*) did not affect HCV RNA synthesis (not shown). The putative binding site for pRb lies deep within the catalytic pocket of the HCV RdRp (Fig. 23A, *green residue*) (*22, 166*). This location suggests that the closed conformation of the HCV RdRp should be more resistant to inhibition by pRb. Purified pRb inhibited RNA synthesis by Δ21 but demonstrated a substantially stronger inhibitory effect on the PE products than on the *de novo* initiated products (Fig. 23D, *graph*). PE by m26-30 and W397A were also inhibited by pRb (data not shown).
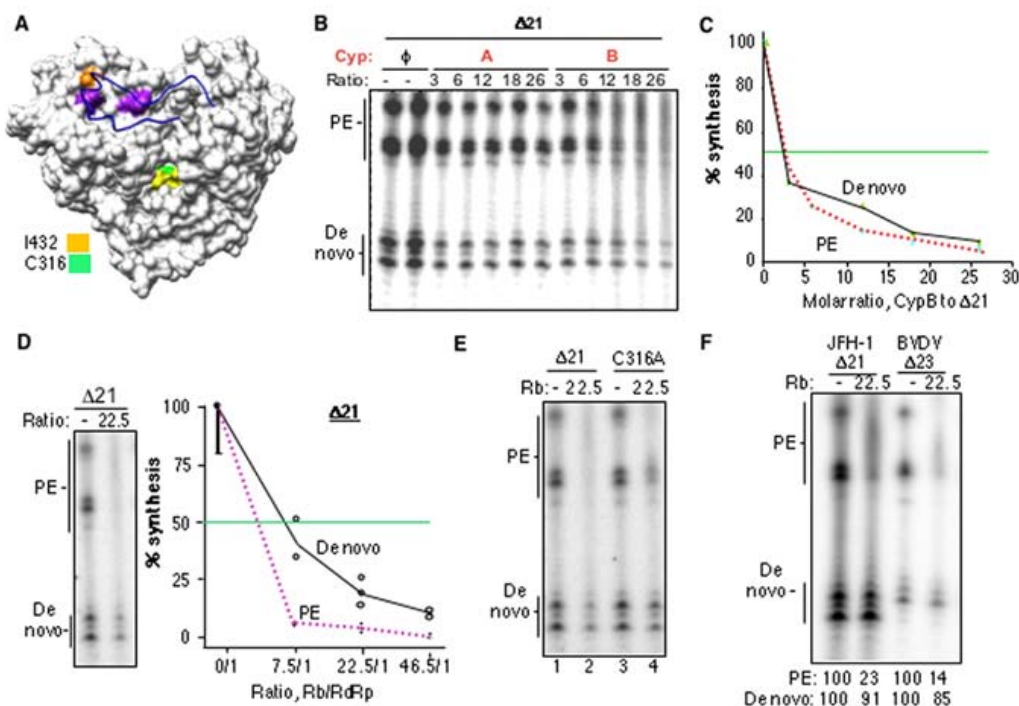
Figure 23: Effects of recombinant cyclophilin A and pRb on RNA synthesis by the HCV RdRp. *A*, model of the HCV RdRp with the locations of residues that affect the activity of CypA or pRb in HCV-infected cells. The locations of W397 and H428 are in *purple*, and the catalytic aspartates responsible for coordinating divalent metals are in *yellow*. I432, which has been identified to confer resistance to cyclosporin, the small peptide inhibitor of CypA, is in *orange*. C316, which probably contacts pRb , is in *light green. B*, CypA can inhibit the HCV RdRp products made by *de novo* initiation and PE. The molar ratios of CypA or CypB to RdRp used in the reactions are listed *above* the gel image. *C*, quantification of the effects of CypB on *de novo* initiated and PE by Δ21. *D*, pRb can preferentially inhibit primer extension by Δ21. The gel image shows qualitatively the production of the *de novo* and primer extension products. The *graph* is from a related experiment, where pRb was titrated in increasing concentrations. All products made in three independent samples in the absence of pRb were set as 100%. *E*, effect of pRb on Δ21 and the mutant C316A, a part of the pRb binding site in NS5B. Where present, pRb was at a molar ratio of 22.5:1 to the RdRps. *F*, effects of pRb on RNA synthesis by the RdRps from JFH-1 2a HCV and BVDV. A 22.5:1 molar ratio of pRb to RdRp was used.

A substitution of C316 to an alanine within the putative pRb binding site (Fig. 23A) decreased the inhibitory effect of pRb on *de novo* initiation and also on PE (Fig. 23E, *lanes 7* and *8*). The differential effect of pRb on these two modes of RNA synthesis suggests that it preferentially interacts with and inhibits the open conformation of the HCV RdRp. Furthermore, mutant C316A was less affected by pRb for primer extension compared with Δ21, consistent with the idea that Δ21 exists in dynamic equilibrium between open and closed conformations.

To determine whether RNA synthesis by other RdRps is also sensitive to pRb, NS5B derived from the genotype 2A JFH-1 strain of HCV, named 2a-Δ21, and from the pestivirus bovine viral diarrhea virus (BVDV) were tested (*49*). Both 2a-Δ21 and the BVDV RdRp were sensitive to the presence of pRb at levels comparable with that exhibited by Δ21 (Fig. 23F). Furthermore, the PE products of both RdRps were preferentially inhibited. These results suggest that all three of these related RdRps exist in equilibrium between a *de novo* initiation-competent closed form and a PE-competent open form. Consistent with this, the RdRps from BVDV and several other members of the *Flaviviridae* possess loops equivalent to the HCV Δ1 both in location and in primarily hydrophobic interactions with the surface of the template channel (Fig. 24).

DISCUSSION

Our mutational analysis of the HCV NS5B RdRp template channel identified an interaction between the thumb domain and the Δ1 loop that is required for *de novo* initiation of RNA synthesis. Substitutions disrupting this interaction are instructive,
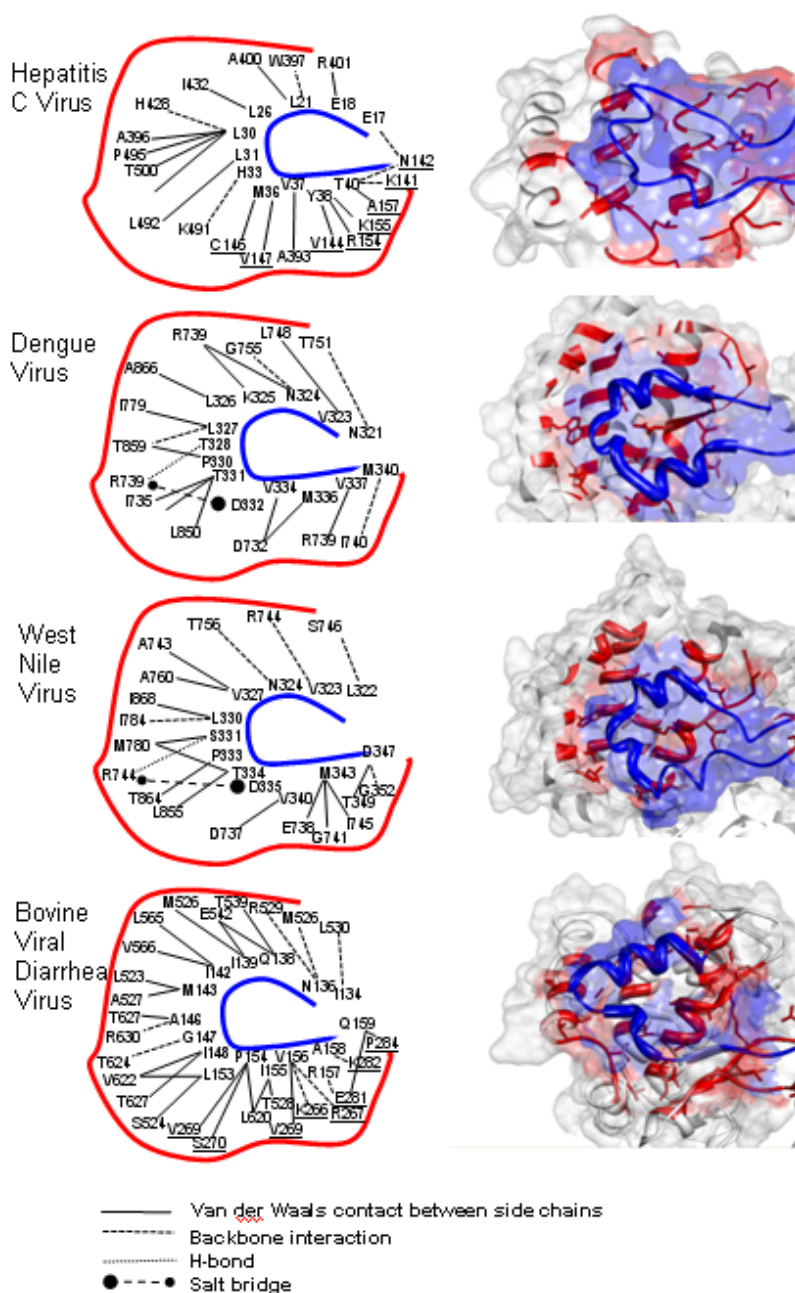
Figure 24: Δ1 loop-like structures in other viral RdRps. The *space-filling models* show the locations of the loops that could have a role comparable with that of the HCV Δ1 loop (blue ribbon) in the RdRp structures of HCV, Dengue virus, West Nile Virus (*WNV*), and BVDV. The *schematic* to the *left* shows the potential interactions that allow the comparable loops to interact with the outer surface of the template channels in the RdRps. Residues in the apex of the loop are in *boldface type*, and residues in the Δ2 loop are *underlined*. The *key* in the *box* shows the *lines* used for the different interactions.

because they reveal that the HCV RdRp requires distinct conformations for different steps in viral RNA synthesis. Furthermore, interactions between NS5B and the cellular pRb protein depend on the conformation of the HCV RdRp, suggesting that alternative conformations of the HCV RdRp are not only potential drug targets for treatment of HCV infection but may also contribute to perturbations of cellular processes.

Several lines of evidence suggest that mutant proteins W397A, H428A, and m26-30 exist in a more open, PE-competent conformation. First, molecular dynamic studies predict that mutations in either the residues on the outside of the template channel or the Δ1 loop decrease contact with helices Q and O and increase access to the catalytic pocket of the RdRp (Fig. 19). Second, the mutated RdRp proteins have discernable spectroscopic properties when compared with Δ21 and with each other, indicating that there are changes in the conformations of these proteins. Third, in comparison with Δ21, all three mutants are more sensitive to heparin in the reaction buffer in the presence of a primed single-stranded template, suggesting that they are defective in the formation of the binary complex (Fig. 21). Fourth, and perhaps the most direct evidence in support of the open conformation, the mutants have an increased ability to bind to double-stranded RNA relative to Δ21 (Fig. 21E).

The interaction between the Δ1 loop and the outer surface of the template channel provides an elegant mechanism to regulate the initiation and elongation phases of HCV RNA synthesis (Fig. 25). The closed conformation is required for *de novo* initiation (Fig. 25, *form i*). In this conformation, the template channel can orient the singlestranded template to the catalytic site (*form ii*). In fact, since substitutions at the most constricted

portion of the template channel increased RNA synthesis, the template channel may function to restrict access to more structured or otherwise inappropriate RNAs. The addition of the NTPi and a nucleotide complementary to the second template nucleotide will stabilize the ternary complex (Fig. 25, *form iii*). The nascent RNA will then grow with polymerization until the duplex reaches a length where steric constraints force the release of the Δ1 loop from the thumb domain (Fig. 25, *form iv*). The open form of the polymerase allows elongation to proceed in a processive manner until the entire template is copied. At this point, the Δ1 loop may regain the ability to interact with the thumb subdomain.

Our model (Fig. 25) is consistent with results from studies of benzimidazole/indole-based nonnucleoside inhibitors that have been shown to specifically bind to the pocket in the thumb subdomain and inhibit the polymerase at a step before the elongation phase of RNA synthesis (*42, 124-127, 133, 187*). Interestingly, pyranoindole small molecule inhibitors that bind to a site different from the Δ1 loop-thumb domain interface inhibit elongation but not *de novo* initiation and cause an accumulation of 5-mer products, indicating that elongation might involve additional changes in the overall structure of the polymerase (*130*). There is evidence that supports the concept that the HCV RdRp normally exists in equilibrium between closed and open conformations. Biswal *et al.* (*60*) crystallized two distinct conformations of the 2a form of the HCV RdRp, which retains the Δ1 loop, consistent with the wild-type RdRp existing in at least two distinct conformations.
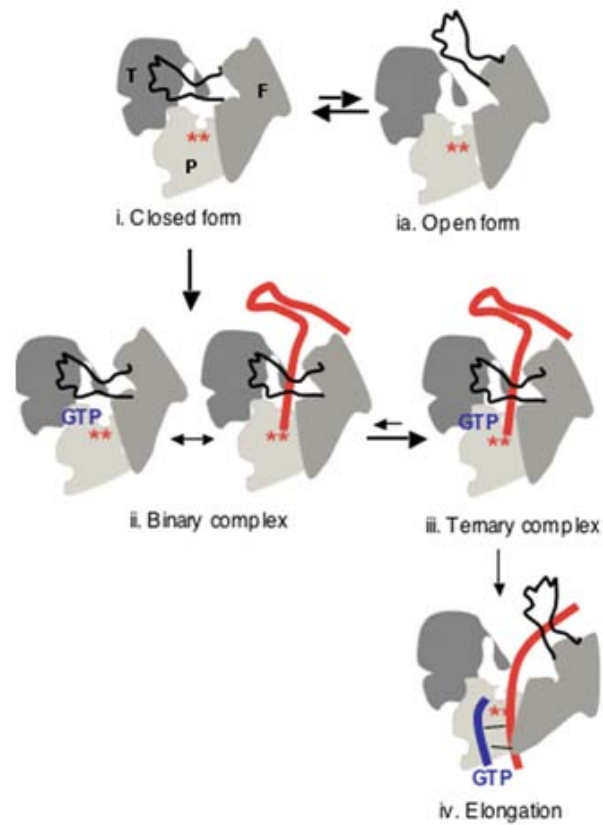
Figure 25: A model for RNA synthesis by the HCV NS5B. A schematic representation of the NS5B in the closed conformation is shown to the *left* with the thumb (*T*), fingers (*F*), and palm (*P*) domains holding a single-stranded RNA (*red*). The active site residues are shown as *red asterisks*. During elongation, the enzyme undergoes large conformational changes, including the displacement of the Δ1 loop to hold the growing nascent RNA-template hybrid (*right*).

observation that is best explained by the open conformation of the protein wrapping itself around the template (*77*).

The closed and open conformations of the HCV RdRp may regulate other activities of the NS5B protein that are only indirectly related to RNA synthesis. Viral replicases are usually capable of a high level of RNA synthesis despite low amounts of RdRp being present, thus making biochemical characterization of the replicase challenging (*188*). This raises the possibility that most of the RdRp molecules and other replicase subunits are not involved in RNA synthesis but serve to modulate the activities of other viral and also cellular proteins (*22, 166, 173, 189-191*).

In an interaction that is likely to have significant consequences for the association of liver cancer with HCV infection, NS5B can bind pRb, inducing its ubiquitination and subsequent proteasome-mediated degradation and thereby perturbing regulation of the cell cycle (*22, 166*). *In vitro*, such a protein-protein interaction resulted in the inhibition of RNA synthesis, perhaps by affecting template binding and/or catalysis. Interestingly, pRb preferentially inhibited PE by the wild-type HCV RdRp, Δ21, as well as the PE-competent mutants (Fig. 23 and not shown). pRb is not known to have nucleic acid binding domains (*192*), and our finding that a C316A substitution resulted in escape from inhibition by pRb and an increase in the PE product (Fig. 23E) confirms earlier observations of Munakata *et al.* (*22*), who demonstrated that this substitution near the active site of the RdRp inhibits its interaction with pRb. The inhibitory activity of pRb contrasts with the effects of CypA, which did not differentially affect the production of the *de novo* initiated *versus* primer-extended products of the HCV RdRp (Fig. 23B).

Given that the recombinant pRb protein made in *E. coli* was capable of inhibiting the RdRp, post-translational modification of pRb is not required for this interaction (*193-194*).

The differential inhibitory effects of pRb on different steps in RNA synthesis raise the interesting possibility that other cellular and/or viral proteins may interact with NS5B in a conformation-dependent manner. A screen for such interacting proteins or drugs that affect these interactions is now possible with the availability of mutant HCV RdRps that exist in different conformations.

The HCV RdRp has served as a model for the polymerases of other RNA viruses (*195-196*). Indeed, some common themes are emerging now that the structures of a number of RdRps are available. Notably, the RdRp of BVDV can also exist in an open conformation, with a displaced loop that regulates access to the active site (*65*). A comparison of the activities of the RdRps from other members of the family *Flaviviridae* revealed that they have generally similar properties with respect to RNA synthesis *in vitro* (*39, 88, 99, 163, 197*). Consistent with this, we also demonstrated that pRb could preferentially inhibit the synthesis of elongation products made by the BVDV RdRp (Fig. 23F), suggesting that similar interactions may exist between pRb and RdRps from other positive-strand RNA viruses.

DNA-dependent RNA polymerases, DNA-dependent DNA polymerases, and reverse transcriptases are all known to undergo transitions from open to closed states (*70, 167, 198-199*). Our results indicate that RdRps from positive-strand RNA viruses can undergo similar transitions. Whether these changes go in the same order *in vivo*

depends on how the RdRp-replicase complex locates the appropriate viral template RNA. In the case of HCV, it is possible that the RdRp first binds an internal sequence within the HCV genomic RNA and then scans for the 3' terminus. In this scenario, the RdRp will initially bind RNA in the open form. On the other hand, it is also possible that the replicase is threaded with the 3' terminus of the HCV RNA. In this case, the RdRp will first function in RNA synthesis in its closed conformation, followed by a transition to the open conformation during elongation. It is also possible that cellular protein(s), such as a cyclophilin, could mediate template loading by manipulating the RdRp conformation.

CHAPTER IV

REGULATION OF DE NOVO INITIATED RNA SYNTHESIS IN THE HEPATITIS C

VIRUS RNA-DEPENDENT RNA POLYMERASE BY INTERMOLECULAR

INTERACTIONS*

INTRODUCTION

Polymerases undergo a series of conformational changes at different stages of

nucleic acid synthesis (*70*). Of the template-dependent polymerases, the RNA-dependent

RNA polymerases (RdRps) are the least understood in terms of their mechanism of

action. RdRps are of increasing interest due to recent research showing cellular RdRps

playing important roles in the defense against non-self RNAs (*200*). In addition, virus-

encoded RdRps are important targets for the development of antivirals. A better

understanding of RNA-dependent RNA polymerases is thus important for both basic and

applied science.

Several model systems for biochemical study of viral RNA-dependent RNA

synthesis exist (*83, 201-203*). Well-characterized RdRps include those from the hepatitis

C virus (HCV) and poliovirus (*56, 158*). In the host, the RdRps are complexed with

other viral and/or cellular proteins that are usually associated with membranous

intracellular structures.

_____

*This work has been submitted to *The Journal of Virology* as: "Regulation of De
Novo Initiated RNA Synthesis in the Hepatitis C Virus RNA Dependent RNA
Polymerase by Intermolecular Interactions" by Chinnaswamy, S., Ayaluru, A., Li,
P., and Kao, C. C.

The replicases are usually difficult to study biochemically, but the catalytic RdRp subunits of several viruses can be purified for functional and structural analyses (*35*). These recombinant proteins can reproduce some of the activities of the replicases and can affect the activities of other replicase subunits in vitro (*191, 204*). Understanding how RdRp subunit structure affects function will help us understand the viral RNA replication.

RdRps form a right-hand like structure with thumb, finger, and palm subdomains. The metal-coordinating residues important for nucleotide binding are positioned within the palm subdomain (*57*). An interesting feature of viral RdRps is that they tend to exist in a closed conformation, even in the absence of template, in contrast to DNA-dependent RNA polymerases that transition from open to closed complexes upon template recognition (*205*). The closed form of the phage ϕ6 RdRp has been proposed to allow specific recognition of the single-stranded viral RNA (*68*). The template channel formed by the closed structure, however, is too narrow to accommodate the partially duplexed RNA that forms during RNA synthesis. Hence the closed conformation needs to become open in the ternary complex.

The HCV RdRp has structural features compatible with a mechanism to initiate RNA synthesis by a de novo mechanism (*56-57*). It can also extend from a primed template as well as switch templates without release of the nascent RNA (*181*). A secondary structure that extends from the finger to the thumb subdomains named the Δ1 loop has been proposed to serve as a gate to cover the template channel and regulate the switch from de novo initiation to elongation (*56*). Mutations that affect the interaction

between the Δ1 loop and the mostly hydrophobic residues that it contacts have resulted

in polymerases that are defective for de novo initiation but can bind to partially duplexed

RNA and can extend from the 3' terminus of an RNA primer (see Chapter III).

The HCV RdRp likely undergoes a change between the open and closed structure

in vivo. The HCV RdRp can bind the master cell cycle regulator, Retinoblastoma (pRb),

and cause the degradation of Rb (*22*). The pRb binding motif overlaps with the metal-

coordinating residues of the HCV RdRp in the palm domain (*22*). It stands to reason that

only the open RdRp conformation can bind pRb. Biswal et al., (*60*) have captured an X-

ray crystallographic structure of a partially open conformation of the HCV RdRp. The

BVDV RdRp was also shown to exist in a partially open conformation as a result of the

interaction between two RdRp subunits (*65*).

Two general models for de novo initiation by the HCV RdRp have been proposed

(Fig. 26). The first shows the HCV RdRp to be functional as a monomer at least during

de novo initiation because the closed template channel is needed for specific recognition

of the template ((*56, 68*) and also see Chapter III). It was presumed that the Δ1 loop and

thumb domain interaction in the HCV RdRp is stable and mutations that disrupted this

interaction would render the enzyme catalytically inactive (*69*). However, a deletion of

five residues in the tip of the Δ1 loop did not prevent RNA synthesis from a primed

template by the polymerase (see Chapter III). Furthermore, a genotype 2a RdRp was

crystallized in a form with altered interaction between the Δ1 loop and thumb domain in

comparison to the 1b RdRp (*60*). Interestingly, a low affinity GTP binding site exists on

the thumb domain close to the base of Δ1 loop binding pocket. GTP binding at this site

has been proposed to stabilize the Δ1 loop and thumb domain interactions, favoring the closed monomer model (*38*). A second model for RNA synthesis is based on the reports that HCV RdRp can oligomerize and that oligomerization increases its activity (*74-76*). In this model, an RdRp oligomer stabilizes the Δ1 loop and thumb interactions to allow formation of the template channel for de novo initiation (Fig. 26). Herein we attempt to determine whether monomers or oligomers of the HCV RdRp (from 1b HCV genotype) can better perform de novo initiation using biochemical and biophysical analyses.

MATERIALS AND METHODS

Production of the HCV RdRp. The HCV RdRp we use as a model system, named Δ21, is derived from HCV 1b isolate strain BK. Wild-type and mutant versions of the NS5B Δ21 were expressed in *E. coli* with the 6X-His tag at the C-terminus of the protein. The culture was shaken at 37°C until the OD_{600} reached 0.8-1.0, and then the temperature was changed to 16°C and IPTG was added to 0.5 mM. After a 12-16 h period, the cells were pelleted at 8000 g for 15 min., and the pellets were frozen at -70°C until needed.

RdRp purification used cells suspended in lysis buffer (20 mM Tris, pH 7.5, 300 mM NaCl, 10% glycerol, 10 mM imidazole, a protease inhibitor cocktail at the concentration suggested by the manufacturer (Sigma Inc.), 5 mM beta-mercaptoethanol (BME), and 0.1 mg/ml lysozyme. The suspension was sonicated for 2 min and clarified by centrifugation at 16,000 g for 30 min. The supernatant was loaded onto Ni-NTA columns equilibrated with 20 mM Tris, pH 7.5, 300 mM NaCl, 10% glycerol, 10 mM imidazole, and 5 mM BME. The columns were washed with the same buffer containing

De novo initiation

Model 1   Closed conformation of HCV RdRp monomer initiates RNA synthesis on 3' terminus of ssRNA

Model 2   Dimeric or oligomeric RdRp complex forms a template channel by stabilizing Δ1 loop-thumb domain interactions
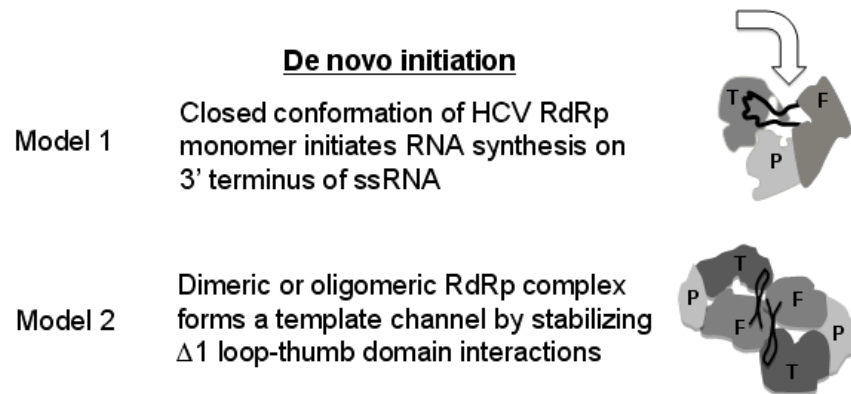
Figure 26: Two models for de novo initiation by the HCV RdRp. Model I is based on the central tenant that intramolecular interactions within a RdRp molecule regulate the modes of RNA synthesis. The thumb, fingers and palm domain are represented by the letters T, F, and P, respectively.The Δ1 loop is shown as a thick black line. The curved arrow represents the possible orientation of the template RNA. Model II is an adaptation from the dimer model of the norovirus RdRp proposed to require oligomers for de novo initiation (*206*).

20 mM imidazole followed by elution of the bound proteins with lysis buffer containing

500 mM imidazole. Δ21 purified from the NTA column was dialyzed into buffer of 20

mM Tris, pH 7.5, 100 mM NaCl, 10% glycerol, and 10 mM BME using a desalting

column and then loaded onto a MonoS column (HR 100/10, GE Healthcare) which was

pre-equilibrated with desalting buffer. Δ21 was eluted with a gradient of 100 to 600 mM

NaCl in desalting buffer. The proteins generated from these two columns were highly

pure and did not contain other bands in Coomassie blue stained gels.

Blue Native PAGE (BN-PAGE). Approximately 250 ng of proteins were mixed with the

loading dye supplied by the manufacturer (Invitrogen Inc.) and electrophoresed in 3-

12% native-PAGE gels (Invitrogen Inc.) with a Coomassie Blue-containing cathode

buffer at 4°C for 2 h according to the manufacturer's instructions. The gel was stained

with silver stain.

HCV RdRp assays. LE19 is a template typically used to measure several RNA synthesis

activities in one reaction (*88*): de novo initiation, primer extension, template switch and

nontemplated nucleotide addition. Standard RdRp reactions contained 50 nM RNA, 0.1

mM ATP and UTP, 33 nM (α-^{32}P) CTP and 0.01 mM GTP (unless stated otherwise) and

the amount of NS5B as specified. The assays also contain 20 mM sodium glutamate (pH

8.2), 4 mM MgCl2, 12.5 mM dithiothreitol, 0.5% (v/v) Triton X-100, 20 mM NaCl and

1 mM MnCl$_2$. The reactions were incubated for 1 hr at 25 °C before extracting the

products with a 1:1 mixture of phenol-chloroform and precipitated with ethanol in the

presence of 0.3 M NaOAc. The RNA was electrophoresed on 20% urea denaturing

polyacrylamide gels and the gels were wrapped in plastic and exposed to phosphor

screens prior to scanning by a phosphorimager (Molecular Dynamics).

Differential scanning fluorimetry (DSF). DSF was carried out in a Stratagene MX3005P

PCR machine with filter sets for excitation at 492 nm and emission at 610 nm. Each

sample of 25 μL contained 2 μM final concentration of protein in 300 mM Tris (pH 7.5),

80 mM NaCl and SYPRO orange (Molecular Probes) at 2.5x final concentration (the

actual concentration not revealed by MP). The samples were heated at a rate of

0.5°C/minute, from 25 to 75°C, and the MxPro software (Stratagene) was used to

calculate the Tm_{app} by plotting the negative derivative of the observed fluorescence

change over temperature.

Dynamic light scatter analysis (DLS). DLS measurements were made with Zetasizer-

NanoS (Malvern Instruments, UK) in a buffer containing 300 mM Tris (pH 7.5) and 1

μM final protein concentration. The buffer components were filtered through a 0.2 μ

pore filter (Nalgene, USA) to avoid suspended particles. The measurements were made

at 10 s intervals with the data points collected after a 1 s scan. At least three

measurements were made per sample, and the average intensity for the corresponding

peaks was plotted.

Electron microscopy and image reconstruction. The protein in a buffer containing 50

mM Tris pH 7.5, 100 mM NaCl, 5% glycerol and 1 mM BME was adjusted to ~5 ng/μL,

adsorbed to freshly glow-discharged carbon-coated copper grids (EMS), and stained

with uranyl acetate (1% w/v aqueous solution). Electron microscopy was performed

using a transmission electron microscope operated at 80 kV (JEOL 1010). Dimeric

particles of the HCV RdRp were selected using the BOXER routine in the EMAN program (*207*), filtered, and centered. Class averages were generated with these filtered and centered particles without imposed symmetry. Centered particles (about 4000) were subjected to the Multirefine program to sort the particles into an initial model. A molecular mass of 130 kDa was used for the surface-rendering threshold of the 3D structures of the dimers. 3D reconstructions were visualized using the UCSF Chimera software package (*208*).

RESULTS

Analysis of Δ21 conformations and oligomerization. Blue-native gel electrophoresis (BN-PAGE) was used to examine the oligomeric and conformational state of the HCV Δ21 protein. In this type of gel electrophoresis, proteins coated with Coomassie blue have an overall negative charge and are separated in an acrylamide gel based on a combination of size, shapes and/or oligomeric states (*209-210*). We examined the wild-type Δ21 (Fig. 27A) along with several mutants that are affected for oligomerization (E18R,(*75*)); de novo initiation (m26-30 and I432V (Chapter III and (*144*)), and GTP binding at the allosteric site (P495/V499A named as PV (*38*)). While the recombinant Δ21 migrated at the expected molecular mass of 65 kDa in SDS-PAGE, it existed as multiple bands of different intensities in a BN gel (Fig. 27B). m26-30, with a five amino acid deletion in the Δ1 loop which renders it defective for de novo initiation (Chapter III) had a different banding pattern. E18R and PV mutants deviated significantly from the banding pattern of Δ21 and exhibited some poorly resolved high molecular weight

complexes (Fig. 27B). I432V had bands in similar position to that of Δ21. The variety of bands exhibited by Δ21 and mutant RdRps in the BN-PAGE suggest that each of the RdRps exists in complex arrays of oligomeric states and/or conformations.

Dynamic light scatter spectroscopy (DLS) was used to measure the hydrodynamic diameter of Δ21 to estimate the dimensions of the protein. In a Tris buffer containing 40 mM NaCl, Δ21 existed in three peaks (Fig. 27C). The first has a mean diameter of more than 8 nm and represents more than 95% of the protein based on volume distribution of the peak. This hydrodynamic diameter was higher than expected based on the X-ray structure of the monomeric HCV RdRp, indicating polydispersity (25%). The other two peaks are likely to be high molecular weight oligomers. Increasing the concentration of monovalent salt in the buffer was reported to affect the Δ21 oligomers in solution (*211*). Higher salt concentrations slightly increased the abundance of peak I and altered the abundance and positions of the other two peaks in DLS (Fig. 27C). This is consistent with the idea that the three peaks are in equilibrium in a manner that can be affected by the monovalent salt concentration, as reported previously (*211*). Finally, Δ21 eluted as three distinct peaks in a Superdex-200 gel filtration column when in a buffer containing 100 mM monovalent salt. However, the most abundant peak eluted at a mass smaller than 65 kDa when compared with molecular mass markers (not shown). Similar observations were made by Gu et al. (*74*).

Next, we visualized Δ21 by electron microscopy after staining with uranyl acetate. Δ21 existed in particles of different sizes that are likely monomers (~6 nm average diameter), dimers, and higher order complexes with the longest diameters
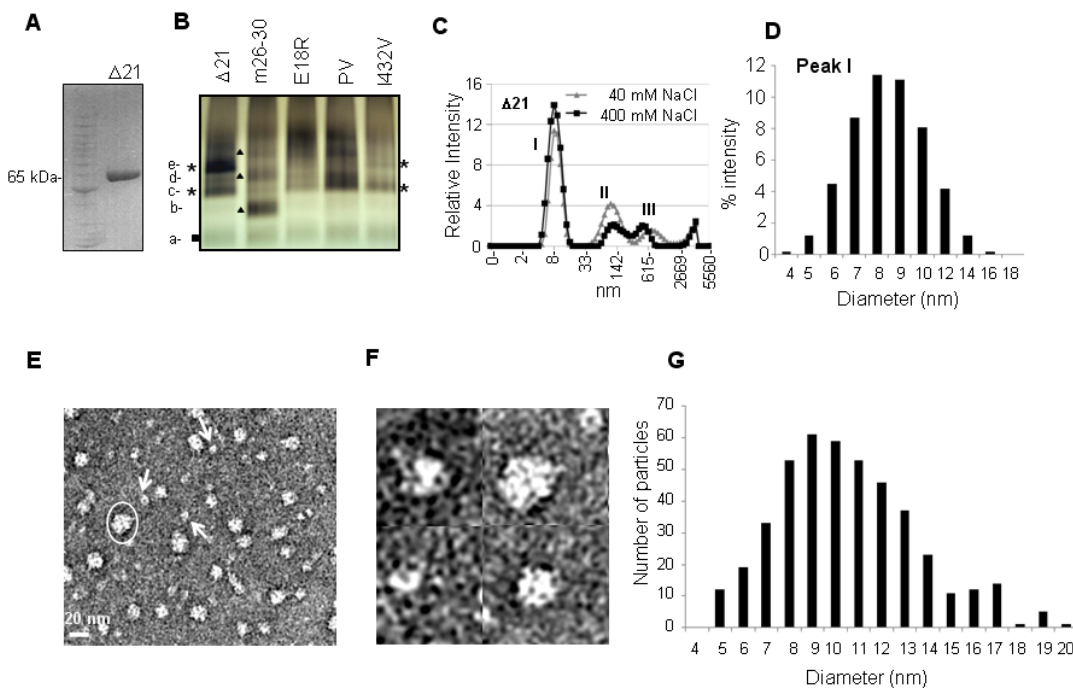
Figure 27: Analysis of the conformations and oligomeric states of the HCV RdRp. A) SDS-PAGE demonstrating the mobility of the Δ21 at ~ 65 kDa under denaturing conditions. The molecular weight markers are from Invitrogen (Benchmark protein ladder). B) Blue-native gel of Δ21 and its variants that are affected for RNA synthesis. The different bands that were distinct in mobility and intensity are labeled from a to e. Bands that were common to all proteins are indicated by a filled box; bands common to Δ21 and I432V are shown with asterisks; whereas bands in m26-30 are shown with filled triangles. C) DLS analysis of Δ21 at 40 mM and 400 mM NaCl. D) Polydisperse nature of the peak I from C. E) A representative EM image of a 5 ng/μL Δ21 in a Tris buffer containing 100 mM NaCl. The particles were stained by uranyl acetate after adsorption onto carbon grids. The scale bar shown at bottom left. The arrows point to the likely monomers based on the estimated sizes of the particles. Note that some monomeric particles may represent different orientations attached on to the grid hence appearing in different shapes. One of the oligomer is indicated with an oval. F) Magnified view of micrographs showing Δ21 monomers and oligomers. G) A histogram of the dimensions of 440 particles of Δ21 picked from different micrographs. The measurements were made manually using the image processing software ImageJ (NCBI) at a 2.35 Å/pix ratio at specimen level. Two measurements were taken each at the longest and widest dimensions of each particle at roughly perpendicular angles and the average of the two measurements is plotted as histograms.

being up to 20 nm (Fig. 27E, 27F). The diameters of ~450 Δ21 particles distributed in

several micrographs are plotted in Fig. 27G. The distribution of Δ21 particles on EM

matched with the polydisperse nature of peak 1 observed in DLS (compare Fig. 27D and

27G). In Chapter I it is shown by analytical ultracentrifugation that Δ21 is primarily a

monomer in solution while others have shown by a similar experiment that Δ21

apoenzyme is a monomer that can form dimers and tetramers in the presence of an RNA

that can direct de novo initiation (*69*). The reason for the discrepancy is unclear, but it is

likely that the oligomeric contacts are weak in the apoenzyme and do not survive

sedimentation velocity experiments.

RNA synthesis as a function of enzyme concentration. Since Δ21 can be present as an

oligomer, we wanted to examine whether oligomerization can affect a particular mode of

RNA synthesis. For this analysis we used a template LE19 to report on both de novo

initiation (producing a 19-mer RNA) and primer extension products (producing a 32-mer

RNA, Fig. 28A). The reactions had 10 μM of the initiating nucleotide GTP, 50 nM

template RNA, and from 20 to 60 nM of Δ21. Over this concentration range, we

observed a geometric increase in de novo initiation but a linear increase in primer

extension and template switch products (Fig. 28B and C). This suggested that conditions

that favor higher order RdRp complexes favored de novo initiation. To confirm the

results without the complex template switch products, we used LE19P, which can direct

de novo initiation but not primer extension due to a puromycin being attached to the 3'-

most hydroxyl of the template. A second RNA named PE46 that can only direct primer
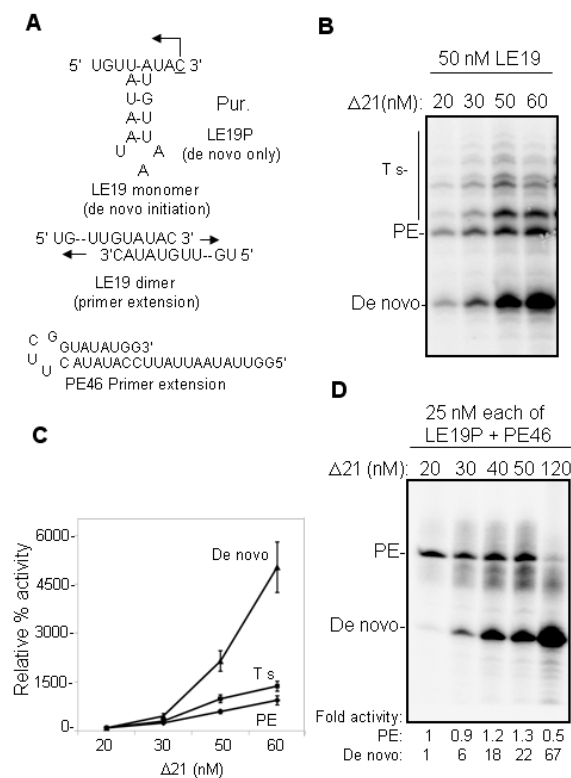
Figure 28: Higher enzyme concentrations selectively stimulated de novo initiation by Δ21. A) The templates used in the analysis. Template LE19 exists as a monomer and directs the synthesis of a 19-nt de novo initiation product from Δ21 while it can also form a dimer with another LE19 molecule and directs the synthesis of a primer extension product of 32-nt. The capital P represents a puromycin covalently attached to the 3' terminus of the RNA LE19P. PE46 is a stem loop structure that can direct a primer extension product of 46-nt. B) A representative gel image of the RdRp assay described using different concentrations of Δ21 with a constant concentration of 50 nM LE19 and 0.1 mM of ATP, UTP; 0.01 mM of GTP and 33 nM of (α - ^{32}P) CTP. PE and Ts denote primer extension and template switch, respectively. C) Quantification of products of RdRp reaction. The 19-nt product is quantified as de novo initiation product; 32-nt as primer extension (PE) product and all other higher molecular weight products as template switch (indicated as Ts in the left of the image). The error bars represent standard deviations from three reactions. The respective activities at 20 nM were normalized to 100% and the relative increase at different concentrations is plotted. D) A gel image of the products of the RdRp assay carried out as in B, but with the templates LE19P and PE46. PE-primer extension. (A). Each of the RNAs was at a concentration of 25 nM. The de novo and primer extension activity at different enzyme concentrations was normalized and compared to that of 20 nM enzyme concentration and is indicated below respective lanes.

extension was also present to allow comparative analysis of the two modes of RNA synthesis (Fig. 28A). Both RNAs were at 25 nM final concentration. Again, Δ21 concentrations from 20 to 120 nM yielded a geometric increase in de novo initiated RNAs while the primer extension product was inhibited at the highest concentration tested (Fig. 28C). These results show that the mode of RNA synthesis by Δ21 is dependent on Δ21 concentration. We note that the divalent cation manganese was required for the simulation of de novo initiation in all of these reactions while primer extension was inhibited at higher enzyme concentrations in a divalent metal independent manner (not shown). This is consistent with a previous finding that manganese has a selective effect on de novo initiation (*88*).

De novo initiation-defective mutant proteins can stimulate de novo initiation by Δ21. To examine the relationship between oligomerization and de novo initiated RNA synthesis, we needed a mutant RdRp that was defective for de novo initiation, but could retain interaction with Δ21. The Δ1 loop deletion mutant, m26-30 was selected for this activity. First, we examined whether highly purified m26-30 (Fig. 29A) was altered in conformation/oligomerization when compared to Δ21 using the differntial scanning fluorimetry (DSF) assay. The assay uses the dye SYPRO orange that fluoresces when bound to hydrophobic regions of the protein. When assayed along over a fixed rate of temperature increase, SYPRO orange fluorescence will report on the denaturation profile of proteins (*212*). A clear difference was observed between the melting profiles of Δ21 and m26-30 (Fig. 29B). Δ21 had a relatively symmetric melting curve with a maximum Tm_{app} of 45.5^{o}C; m26-30 had a more complex melting profile and a maximum Tm_{app} of
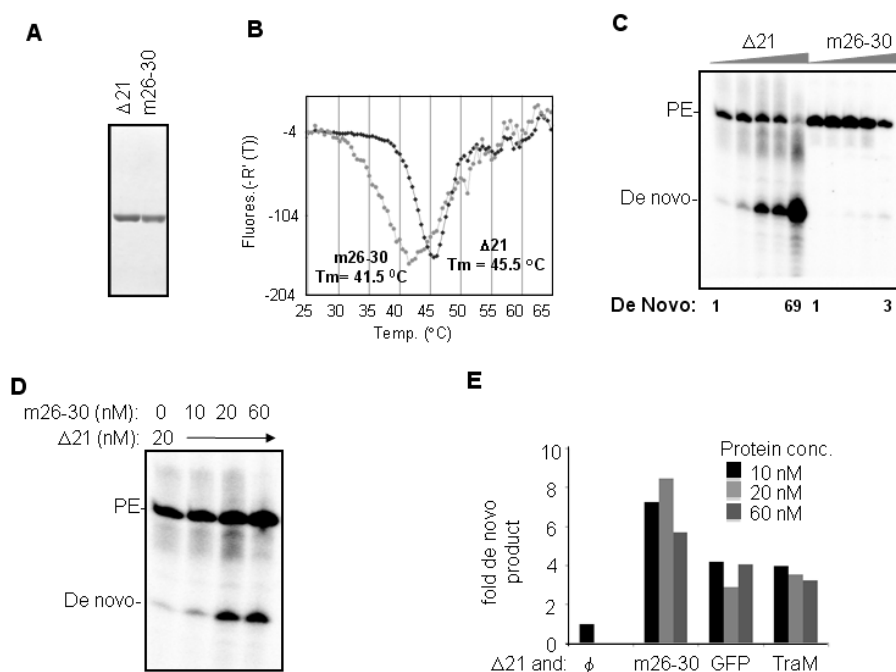
Figure 29: Intermolecular interactions in the RdRp can stimulate de novo initiation. A) Image of the SDS-PAGE of the Δ21 and the m26-30 proteins used in these studies. m26-30 has a five-amino acid deletion at the tip of the Δ1 loop (Chapter 3). B) DSF analysis of 2 μM of Δ21 or m26-30. The fluorescence increase due to SYPRO-orange dye binding to hydrophobic patches in the protein is plotted as a negative derivative on the y-axis. The plots were generated from the software package MxPro supplied with the real time PCR machine (Stratagene). The minimal point on the y-axis for each plot is considered the Tm_{app}. C) Products of RNA synthesis assays as described by Δ21 and m26-30 using a equal mix of the LE19P and PE46 templates. The primer extension (PE) and de novo initiated products are marked to the left of the gel image. The de novo products are quantified and indicated below the lanes. D) Effects of m26-30 on de novo initiation by 20 nM of Δ21. This concentration of Δ21 was selected since de novo initiation products are at a low level. The addition of m26-30, which is debilitated for de novo initiation, but could retain protein-protein interaction, was able to stimulate de novo initiation by Δ21. E) Quantification of the increase in de novo initiation by 20 nM of Δ21 in the presence of m26-30 or two unrelated proteins. The unrelated proteins are added to test for the effects of molecular crowding.

41.5°C. We next compared RNA synthesis by Δ21 and m26-30 over a range of protein

concentrations. While de novo initiation increased by 69 fold over the range of

concentrations tested for Δ21, m26-30 produced only a small increase in de novo

initiated products over the same concentration range tested (Fig. 29C). Finally, we fixed

Δ21 in the RNA synthesis reaction at 20 nM, a concentration that produces only a faint

amount of de novo initiated products and asked whether the presence of m26-30 could

stimulate de novo initiated product synthesis. Indeed, there was a concentration-

dependent increase in the de novo products when m26-30 was present with Δ21 (Fig.

29D). These results suggest that the intermolecular interaction between m26-30 and Δ21

led to increased de novo initiation by Δ21.

Lastly, we wanted to test whether the interaction is specific or could be due to a

molecular crowding effect. Hence, recombinant green fluorescent protein (GFP) and *E.*

coli TraM proteins were added to Δ21 in the same concentrations as m26-30. Both had a

more modest effect on de novo initiation by Δ21 when compared to m26-30 assayed in

the same reaction (Fig. 29E). These results suggest that molecular crowding did

contribute to higher de novo initiation by Δ21, but that m26-30 retains the ability to

interact with a WT Δ21 to increase de novo initiation.

We wanted a second de novo initiation-defective mutant to confirm that

intermolecular interactions could stimulate de novo initiation by Δ21. A closer

examination of the Δ1 loop revealed that residue E18 was a good candidate for

disrupting the interaction of the Δ1-loop with the thumb domain since it formed a salt-

bridge with R401 in the thumb domain (Fig. 30A). E18 was previously claimed to be involved in a homomeric pair with H502 (*75*). However, over 200 sequences from the 1b HCV strains revealed that the E18-R401 (or a E18-K401) salt bridge was highly conserved (data not shown), suggesting that the interaction with R401 was likely important for HCV NS5B function. We produced the E18R mutant protein and subjected it to the DSF assay in comparison to Δ21. E18R, like m26-30, has a broader denaturation peak and also a lower Tm_{app} relative to Δ21 (Fig. 30B). When tested for RNA synthesis, E18R was also defective for de novo initiation but not primer extension, except at very high concentrations of protein (Fig. 30C). Again, when co-incubated with a 20 nM Δ21 protein, E18R increased de novo initiation by Δ21 (Fig. 30D). Two mutations that are defective for producing products by de novo initiation can thus activate de novo initiation by Δ21.

Effect of GTP on conformation and de novo initiation by Δ21. Previous reports have shown that GTP stimulates de novo initiation while inhibiting primer extension (*41, 55*). However it is not clear if GTP acts at the NTPi (*78*), allosteric site on the thumb domain, or both (*38*). The low affinity GTP-binding pocket is at the base where the Δ1 loop interacts with the thumb domain, suggesting a relationship with the conformations needed for de novo initiation (Fig. 31A). To examine whether the allosteric site has an effect on de novo initiation we tested a double mutant, P495/V499A (referred to as PV) for RNA synthesis using LE9P and PE46 as templates. Both Δ21 and PV can extend from PE46 to similar levels, but the PV mutant synthesized only a fraction of the de
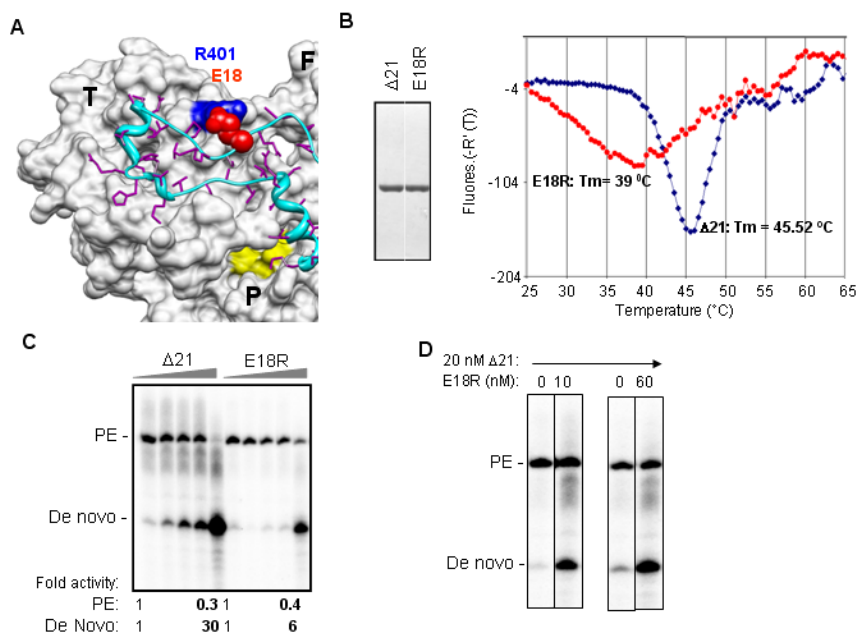
Figure 30: E18R can stimulate de novo initiation by Δ21. A) A surface and ribbon representation of the X-ray crystal structure of HCV RdRp (PDB ID 1QUV) to highlight the location of E18 (red spheres) and its interaction with R401 (blue spheres). The complete thumb domain (T); a part of the palm (P) domain and a part of the fingers (F) domain are marked. The active site metal coordinating residues in the active site are in yellow. The Δ1 loop that connects the fingers and thumb domain is in ribbon representation and is colored cyan while the side chains of its residues are in purple. B) Proteins used in the reactions shown in this figure and their behavior in a DSF reaction. C) Representative image of the products of the RdRp assay with templates LE19P and PE46 with increasing concentrations of Δ21 or E18R. The ratio of increase in the de novo initiated product has been quantified below the gel image. D) Effects of amending a RNA synthesis where Δ21 was kept constant at 20 nM while E18R was at 10 or 60 nM. The two enzymes were preincubated on ice for 30 minutes before adding the RNAs.
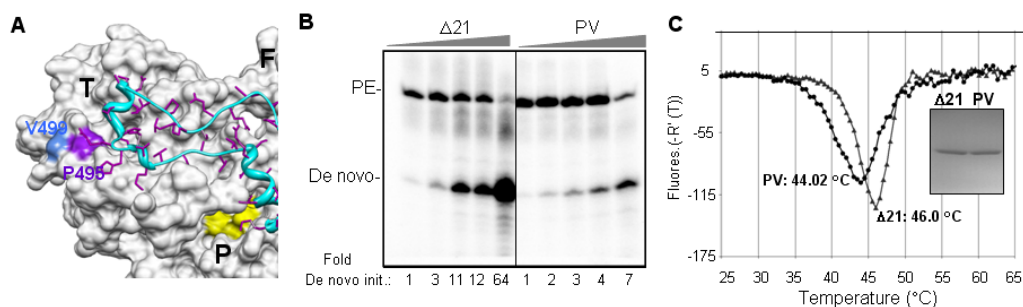
Figure 31: The allosteric GTP binding site and de novo initiation of RNA synthesis. A) The location of the low-affinity GTP binding site on the surface of the thumb domain of HCV RdRp (PDB ID 1QUV) as shown by Bressaneli et al. (*38*). The Δ1 loop is in cyan and the residues P495 and V499that were identified to bind GTP on the thumb domain are shown in different colors (residues S29, R32 and H503 which are also part of the allosteric site are not shown). B) Gel image of the RdRp reaction products using LE19P and PE46 with increasing protein concentrations. The two proteins were at 20, 30, 40, 50 and 120 nM in the assays. The amount of de novo initiated product at different enzyme concentrations was normalized and compared to that of 20 nM of either PV mutant or Δ21, as indicated below respective lanes. PE-primer extension. C) DSF analysis of Δ21 and PV mutant as in Fig. 4D to examine conformational differences between the two proteins. The inset shows SDS-PAGE of the two proteins used.

novo initiated product made by $\Delta21$ while producing more of the primer-extended product (Fig. 31B).

The DSF assay was used to examine whether PV has a change in conformation. PV has a broader melting curve than $\Delta21$ in a manner that was reminiscent of m26-30 and E18R and the Tm_{app} of PV was also 2^oC lower than that of $\Delta21$ (Fig. 31C). However, the changes conferred by the PV mutations are subtler than the changes in the $\Delta1$ loop we characterized above (Fig. 29 and 30). The DSF assay can measure the effect of ligand binding on the stability of proteins (*212*). We used it to measure the effect of increasing concentrations of GTP on the Tm_{app} of $\Delta21$. GTP increased the thermal stability of $\Delta21$ by ~2.5^oC in a concentration-dependent manner (Fig. 32A and 32B). A similar increase in stability was observed with UTP (not shown). In contrast, the PV protein had a decreased response to GTP and UTP at all concentrations tested (Fig. 32B and data not shown). These results suggest that the HCV RdRp will undergo a conformational change upon binding NTPs and that the PV mutation in the allosteric site did affect the ability of the polymerase to respond to nucleotides and undergo a conformational change, but the effect was not specific to GTP.

Lastly, we examined whether increasing GTP concentration from 10 to 200 μM could help to restore de novo initiated RNA synthesis by PV at three enzyme concentrations (Fig. 32C). At 20 nM protein, increasing GTP concentrations increased de novo initiation by $\Delta21$
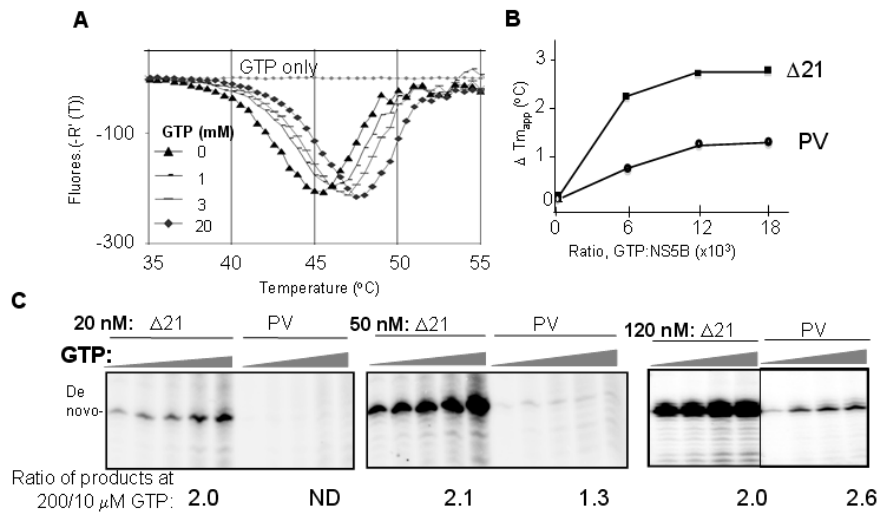
Figure 32: GTP can stabilize Δ21 conformation and increase de novo initiation. A) Tm$_{app}$ of a 2 μM concentration of Δ21 in absence or presence of increasing concentrations of GTP. The Tm$_{app}$ was 45.5, 46.05, 47.02 and 47.52 ^{o}C at 0, 1, 3 and 20 mM GTP respectively. B) Increase in Tm$_{app}$ of PV mutant in comparison to Δ21 at increasing GTP concentrations as indicated in the X-axis. The derivative of the Tm$_{app}$ at different GTP concentrations is plotted. C) Gel image of the products of RNA synthesis by Δ21 and PV mutant at three enzyme concentrations along with increasing GTP concentrations. LE19P was the template and GTP was included at 0.01, 0.05, 0.1, 0.2 and 0.5 mM while ATP and UTP were at 0.1 mM along with 33 nM of (α -^{32}P) CTP. Gel image of the products of RdRp assay of Δ21 and PV mutant at 120 nM concentration with increasing GTP concentrations (0.01, 0.05, 0.1 and 0.2 mM GTP, as represented by the grey triangles). The fold increase in de novo initiation activity of different concentrations of Δ21 and PV mutant when GTP was increased from 0.01 mM to 0.2 mM are shown at the bottom of the gel image.

significantly, whereas there was no significant rescue of de novo initiation by the PV

mutant; the de novo initiated product in the reaction with 200 μM GTP was two-fold that

of the reaction with 10 μM for Δ21, but could not be determined for PV (Fig. 32C,

leftmost panel).

The PV mutant did respond to GTP starting at 50 nm and the increase was more

obvious with 120 nM enzyme (Fig. 32C). Altogether, these results suggest that the

allosteric GTP binding site is required for optimal de novo initiation while the PV

mutant retains the ability to respond to GTP, likely through the NTPi substrate binding

site.

Reconstruction of RdRp dimers. All of the characterizations so far show that that there

are complex interactions and conformational changes associated with even RdRps that

have a single amino acid change and with the mode of RNA synthesis. The dynamic

nature of the RdRp will make it a challenge to define all of the changes necessary for

RdRp function, especially by X-ray crystallography. However, 3D reconstruction from

negative-stained particles obtained by EM can inform us about major changes in protein

conformation. This approach has already been used to define conformations of larger

molecules such as ribosomes, GroEL, and innate immune receptors (*213-215*). With the

immune receptors, we have determined that ligands can induce dramatically different

conformations, including oigomerization (*214-215*).

To capture the de novo initiation-competent structure, we first collected over 3000

individually selected dimers/oligomers of Δ21 from negative-stained electron

micrographs. However, the final models generated did not yield a good match to the

class averages of the data set and the Fourier transform over the eight rounds of refinement showed that convergence was suboptimal (data not shown). Therefore, we analyzed several other mutant RdRps and found that mutant I432V was a good choice for reconstruction. The I432V substitution was originally identified in Huh7 cells in a mutant HCV replicon that was resistant to Cyclosporin A and subsequently shown to be better at de novo initiation than the WT Δ21 especially at higher enzyme concentrations ((*144*) and Fig. 33A, 33B). Finally, the dimensions of the I432V particles were more homogenous than that of Δ21 especially measured in absence of GTP (compare Fig. 33C and 33D). The I432V mutant was thus selected for single particle reconstruction of a de novo initiation-competent HCV RdRp.

Over 4000 dimer-like particles of I432V without GTP and with GTP were picked and sorted into class averages. The particles selected had a good coverage of the potential orientations, as determined by their distributions in the asymmetry triangle (Fig. 34A and 34E). The class averages generated are shown in Fig. 34B and 34F. Several initial models were selected and used for reconstructions without symmetry and with C2 symmetry and the resulting models were congruous but the model generated with C2 symmetry had higher resolution. They are shown in Fig. 34D. The final model for the complex was at 19 Å resolution without GTP and 16 Å with GTP. The I432V molecule has the density set to the mass of 130 kDa (the mass of a Δ21 dimer) and reveals a central channel with a width of 16 Å that could accommodate RNA (Fig. 34D).
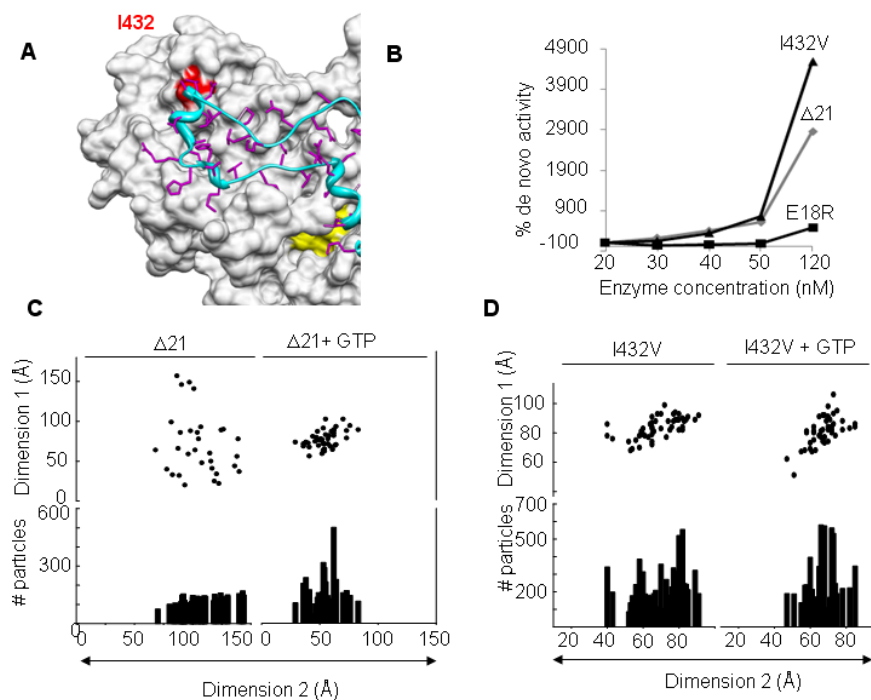
Figure 33. Selection of I432V for reconstruction of dimeric RdRp molecules. A) The location of I432 in relation to the Δ1 loop (cyan ribbon) on the thumb domain of HCV RdRp (PDB ID 1QUV). The active site residues are in yellow. B) Comparative increase in de novo initiation activity by I432V versus Δ21 and E18R at increasing enzyme concentrations as indicated. The assays were performed with LE19P and PE46 as described in Fig. 3D. Quantification- The activity at different enzyme concentrations was normalized and compared to that at 20 nM enzyme concentration and plotted as percentage values. I432V shows a higher increase in de novo initiation at 120 nM from that at 20 nM compared to other two enzymes. C) Distribution of dimensions for Δ21 with and without GTP. D) The distribution of dimensions for I432V with and without GTP. The dimensions in both C and D were taken from the class averages generated with no presumed symmetry. The maximum and minimum dimensions for each of the class averages were measured and plotted max vs. min (in top panels in C and D) and the maximum dimension against number of particles in each class was plotted in bottom panels.
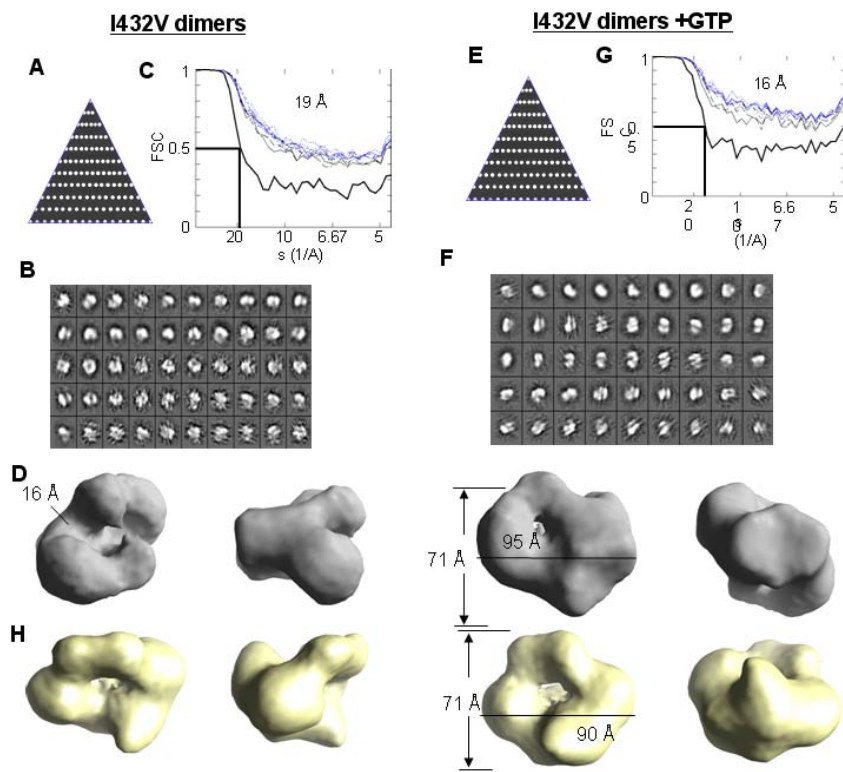
Figure 34: Single particle analysis and reconstruction of I432V dimers in presence and absence of GTP. A) Asymmetry triangle showing distribution of orientation of the particles that constitute the model for I432V dimers. B) Class averages as generated for I432V dimer complex with no presumed symmetry using EMAN's refine2d command. C) Fourier shell correlation showing the convergence of the final model for I432V to 19 Å as per 0.5 σ criterion. D) Different orientations of the final model for I432V dimers (grey). The model measures 71 Å x 95 Å with a groove of about 16 Å. E) Asymmetry triangle that shows the particle orientation for the final model of I432V dimers in the presence of GTP. F) Class averages for I432V dimers complexed with GTP with no presumed symmetry (see materials and methods). G) Fourier shell correlation for I432V dimers with GTP showing that the model has converged to 16 Å resolution. H) Different views of the final model for I432V dimers + GTP complex (yellow). The model has dimensions of 71 Å x 90 Å.

However individual monomers were difficult to be delineated in the models due to a possible combination of extensive interactions between the monomers and/or a low resolution. Interestingly, in the presence of GTP, the densities over the central channel closed and the central channel became more constricted (Fig. 34H), showing that a conformational change can reconfigure the central channel in the dimeric RdRp.

DISCUSSION

Many viral RdRps need to initiate genomic RNA synthesis de novo from the termini of their RNA genomes in order to avoid the loss of genomic information. This mechanism is fundamentally different than that of DNA-dependent polymerases and may ensure the specificity of synthesis from viral templates. In this report, we show that factors, such as GTP, and interactions between intermolecular subunits of a higher order complex can modulate the conformations of the HCV RdRp and influence the mode of RNA synthesis. We demonstrated that highly purified $\Delta 21$ is present as a polydisperse and heterogeneous protein using multiple spectroscopic, gel-based, and imaging assays. Our results further highlight the roles of the $\Delta 1$ loop, the thumb domain, and the allosteric pocket within this domain in contributing to de novo initiation, although our results suggest that the $\Delta 1$ loop and thumb interactions may be more important for assembling initiation complexes rather than the proposed clamping movement of the polymerase on the template during elongation (*56, 69*). In support of this idea, mutations in the $\Delta 1$ loop and the associated thumb domains did not adversely affect primer extension from short RNA templates.

The conformational changes in viral RdRps are just starting to be defined. However, it is important to put this in the context of RNA-dependent RNA synthesis. RNA synthesis by an RdRp in vitro can be divided into discrete steps: 1) formation of productive initiation complexes (de novo initiation or primer extension complexes), 2) formation of the first or first few phosphodiester bonds, and 3) elongation of the stable primer along the template. The first two stages are rate limiting and are collectively called as initiation events. The Km values for NTPs for initiation nucleotides are significantly lower for elongation than initiation (*71, 88*) consistent with the idea of a conformational change in the RdRp between initiation and elongation in RNA synthesis.

The template channel in Δ21 seems to be a region whose dimensions can change depending on enzyme concentration and the presence of NTPs. This will have a direct effect on the initiation events in RNA synthesis. A recent report has shown that the degree of 'closedness' of the enzyme depends on the amino acid composition in the thumb domain (*64*). This implies that a weak Δ1 loop and thumb domain interaction will result in inefficient de novo initiation (*64*) but efficient primer extension, at least from short RNA templates (Chapter III). In this work, we propose that the interactions between RdRp subunits can promote the de novo initiation in a manner that involves the Δ1 loop and the thumb domain.

A dimer and/or an oligomer of the HCV RdRp being the state for active RNA synthesis was proposed by Qin et al., (*75*) and Wang et al., (*76*). Wang et al., (*76*), showed the presence of two broad interacting interfaces in the thumb region of one molecule and the finger region of another molecule. However, Cramer et al. (*211*),

reported that a monomeric RdRp is active. This difference may be a matter of the sensitivity in detecting the de novo initiated products since we show that the HCV RdRp could exist in an array of conformations and/or oligomeric states, even at the nanomolar enzyme concentrations used in this study. Proper contacts between RdRp subunits may cause the conformational changes that will result in productive de novo initiation complex assembly. Our results from the addition of m26-30 and E18R to increase de novo initiation by $\Delta 21$ (Fig. 29, and 30) provide further support for this hypothesis.

The regulation of the HCV RdRp seems to be concentrated at the location where the $\Delta 1$ loop is interacting with the thumb subdomain. This is an elegant mechanism where a flexible loop is used to facilitate changes in polymerase structure/oligomerization state. Our results show that E18 and residues 26-30 in the $\Delta 1$ loop are key residues for proper function. Furthermore, the allosteric site in the thumb domain and also NTPs (we did not find a specific effect of GTP) could help to maintain the proper conformation for de novo initiation. All of these residues are required in vivo for replication of HCV subgenomic replicons in hepatoma cells (*148, 216*).

Residue I432 may modulate RdRp conformation through its interaction with the $\Delta 1$ loop. I432V can confer Cyclosporine A resistance to HCV (*141, 172*), suggesting that the role for the cellular Cyclophilins is likely to be to modulate conformational changes and possibly the oligomerized states of the RdRp. This role is consistent with the need for the active site of Cyclophilin A (protein isomerases) being required for HCV replication (*142*). Therefore, while we have performed biochemical studies, the residues that are important in vitro are linked to requirements for HCV infection.

Doubtless, these quasi-stable RdRp conformations could be influenced by the sequence of the HCV protein (*64, 217*), some buffer components, other HCV replicase subunits, the membrane environment, and/or the template RNA. The HCV replicase has consistently been reported to contain endogenous RNA that cannot be dissociated without loss of activity (*218-221*). Stable binding to the RNA may be of advantage to prevent the recognition of HCV replication intermediates by the host innate immunity receptors. Contact between the oligomerized polymerase subunits has been reported to increase the cooperativity in RNA synthesis in poliovirus 3D^{pol} (*222-223*), and more recently, for the Norovirus RdRp (*206*). Another proposal is that the interface contacts between poliovirus 3D polymerase monomers (thumb interface) and the poliovirus 3C protease could affect RNA synthesis through regulating protein-priming (*224*). While the mechanism needs to be examined further, it is clear that higher order structures of viral RdRps and associations with other viral proteins will be a general theme in viral RNA synthesis (*191, 204, 225*). Finally, it is interesting to note a difference between viruses that use a polyprotein processing mechanism (including HCV) and viruses that use different RNAs to express the replication proteins. The former class of viruses should, theoretically, have more comparable stoichiometries of all the viral proteins. In contrast, viruses that use distinct RNAs to express the replication proteins could have dramatically reduced expression of the RdRp without affecting the overall level of RNA synthesis (*226-227*). These two strategies will certainly allow selection for additional activities of the RdRp (such as binding of pRb) as well as distinct ways to deal with the host's innate immunity mechanisms.

CHAPTER V

CONFORMATIONS OF THE MONOMERIC NS5B: AN EM APPROACH*

INTRODUCTION

The nonstructural proteins required for HCV replication are important therapy targets in HCV. The HCV RNA-dependent RNA polymerase, NS5B is also one of the best characterized RdRps from positive-strand RNA viruses (*35, 78*). In vitro, NS5B is usually expressed without the C-terminal 21 residues to improve its solubility. The majority of the work in the Kao laboratory is with the RdRp from the 1b genotype of HCV. The structure of the 2a RdRp has also been recently reported (*64*). The vast majority of the 1b RdRps and the 2a RdRp form a structure that resembles a closed right hand, with thumb, palm, and finger subdomains. The metal coordinating residues in the RdRp active site are in the palm subdomain that is usually shielded by extensive thumb-finger interactions (*56-57*). The closed conformation in absence of template is in contrast to the DNA-dependent RNA polymerases, which can transition from an open to a closed complex upon template recognition (*205*).

A major influence in the models for viral RNA-dependent RNA synthesis comes from the ternary structure of the phage ϕ6 RdRp (*68*).

_____

Like the HCV RdRp, the ϕ6 RdRp forms a closed structure with a defined template channel. Both template channels are too narrow to accommodate the partially duplexed RNA that must form during RNA synthesis, indicating that the RdRp needs to transition to a more open conformation after initiation of RNA synthesis (Chapter III). Consistent with a need for a change in conformation, a partially open conformation was also solved by X-ray crystallography and revealed significant reconfiguration of the secondary structure in the region where the finger domain interacts with the thumb domain (*60*).

Mutations that affect the interaction between the Δ1 loop and the hydrophobic residues that it contacts have resulted in polymerases that can perform primer extension but not de novo initiation from short RNA templates (Chapter III).

The open and closed structure transition in vivo may allow or be influenced by cellular proteins. The HCV RdRp is reported to interact with the tumor suppressor Retinoblastoma (pRb) protein, to manipulate the cell cycle and cause its degradation (*22*). The L-X-C/N-X-D pRb binding motif overlaps with the metal-coordinating residues of the HCV RdRp. Therefore unless the RdRp adopts a more open conformation the pRb binding motif will remain inaccesible. The cellular protein Cyclophilin, could also interact with the HCV RdRp to affect its ability to bind RNA, perhaps through a change in NS5B conformation (*144*).

We seek to better understand how the HCV RdRp conformations relate to RNA synthesis. This type of analysis will contribute to the mechanism of action of viral RdRps and provide new insight into conformation-specific drug targets. X-ray crystallography is difficult for the analysis of the flexible conformations. We used

electron microscopy and single particle reconstruction to capture semi-stable states of the HCV RdRp. In addition, reconstruction of a mutant version of the HCV RdRp lacking the tip of the Δ1 loop resulted in a primarily open conformation. These results confirm the role of the Δ1 loop in conformational change in the HCV RdRp. Analysis of the residues in the Δ1 loop and the thumb domain identified several conserved interacting residues and differences in the interactions that formed the closed conformation of the 1b and 2a RdRps.

MATERIALS AND METHODS

Production of the HCV RdRp. The detailed procedures are described in Chapter IV, Materials and Methods. The preparation used for DSF assay was purified through the poly-U agarose column (see Chapter III, Material and Methods) after the initial Ni-column purification step.

Gel filtration. Analytical gel filtration used a Superdex-200 HR column (GE Healthcare) equilibrated with the running buffer (50 mM Tris pH 7.5, 100 mM KCl or 500 mM KCl as indicated, 5% Glycerol and 1 mM BME). The fractions obtained were analyzed by SDS-PAGE. The column was calibrated with MW standards (BioRad Inc): bovine thyroglobulin (670 kDa), bovine γ-globulin (158 kDa), chicken ovalbumin (44 kDa), horse myoglobin (17 kDa), and Vitamin B12 (1.35 kDa).

HCV RdRp assays. RNA synthesis by the HCV RdRp used a 19-nt template named LE19, which measures several RNA synthesis activities in one reaction (*88*): de novo initiation, primer extension, template switch and non-templated nucleotide addition. The RdRp reactions are as described in Chapters III and IV, Materials and Methods, except that the α-^{32}P-CTP was at 33 nM and NS5B concentrations are as specified in the legends. The buffer in the RdRp assays includes 20 mM sodium glutamate (pH 8.2), 12.5 mM dithiothreitol , 4 mM $MgCl_2$, 0.5% (v/v) Triton X-100, 20 mM NaCl and 1 mM $MnCl_2$.

Differential scanning fluorimetry. Differential scanning fluorimetry utilized a Stratagene MX3005P Real-time PCR machine as described reference (*144*), and in Chapter 4, Materials and Methods.

Electron microscopy and image reconstruction. The proteins were adjusted to ~1 ng/µL in buffer containing 50 mM Tris pH 7.5, 100 mM NaCl and 1 mM BME, adsorbed to freshly glow-discharged carbon coated copper grids (EMS), and stained with uranyl acetate (1% w/v aqueous solution). Electron microscopy was performed using either a JEOL 1200 transmission electron microscope operated at 100 kV or the JEOL 1010 at 80 kV. Micrographs containing the proper spread of the particles taken using the JEOL 1200 instrument were digitalized using an Epson Projection 3200 scanner at 1200 dpi, corresponding to 3.7 Å/pixel at the specimen level. Images from the JEOL 1010 were collected with a CCD Camera (4K X 4K) and the micrographs were taken at 50 K magnification with an effective 2.35 Å/pixel at specimen level. 3D reconstruction of the

single particles used the EMAN software package (*213*) with a Linux operating system as described by Sun et al. (*215*).

Individual particles of the HCV RdRp were selected using the BOXER routine, filtered, and centered. Class averages were generated without imposing any symmetry. Centered particles (about 38,000) were subjected to the Multirefine program to sort the particles among five models. The initial models used for the multirefinement process were generated from the HCV RdRp crystal structure (pdb: 1quv) with different noise levels to decrease constraints in the conformations. Particles from each of the models were collected separately and subjected to additional single model refinement to improve the convergence of the data set to the model. The reconstructions were iteratively refined until the structure was stable as judged by Fourier shell correlation (FSC). The convergence was examined by comparing the projections of the model with corresponding class averages. A molecular mass of 65 kDa was used for the surface-rendering threshold of the 3D structures of the monomers. 3D reconstructions were visualized using the UCSF Chimera software package (*208*).

Molecular modeling of m26-30. A crystal structure of the wild-type HCV-RdRp (Protein Data Bank code 1QUV) was used to construct a m26-30 model with Modeler (Insight II; Accelrys). In this model, residues 26-30 of the Δ1 loop deletion were substituted with glycines since the program does not allow deletions. The model was then subjected to a medium to high level of simulated annealing optimization with respect to the variable target function of Modeler with an effective radius parameter of 10-20 Å. The final model was selected based on visual inspection and its best fit to the most open EM map using UCSF chimera.

Analysis of HCV sequences. All the sequences in analysis were extracted from HCV

Sequence Databases (NIH). Then the residues of Δ1loop involving in interaction with Δ2

loop and thumb subdomain were chosen by PIC webserver (*228*).

RESULTS

HCV RdRp exists in multiple conformations or oligomeric states. Several models for

HCV RNA-dependent RNA synthesis currently exist in the literature. Some researchers

proposed that a monomer of RdRp is the form that carries out RNA synthesis (*68, 211,*

224). Others have shown that oligomers of several viral polymerases can cooperatively

interact with RNA and that there are two surfaces for RdRp-RdRp interactions that can

promote the formation of active scaffolds for RNA synthesis (*74-76, 206, 222-223, 229*).

It is likely that both forms will contribute to aspects of HCV replication, either directly,

or through interaction with other viral and cellular factors.

A highly purified preparation of HCV RdRp free from contaminating RNAs will

be necessary to understand HCV RdRp conformation. Our preparation of the HCV Δ21

protein is highly active for RNA synthesis, more than 98% pure, and soluble at

concentrations in excess of 10 mg/ml. There is also no contaminating ribonuclease as

determined by the optical density of the preparations and attempts to stain the

preparation with silver. When examined by using gel-filtration chromatography using a

Superdex-200 column (GE healthcare) at a 100 mM monovalent salt concentration, Δ21

was present in various mass/conformational states (Fig. 35A), with the first peak that

eluted at a position that corresponded to molecular mass markers of ~40 kDa (Δ21 is ~65

kDa) and other peaks being less than 30 kDa when compared to the molecular mass markers. This is likely due to interactions of the protein with column matrix. SDS-PAGE of the different column fractions from the same gel confirmed presence of Δ21 in all fractions suggesting that there are likely to be proteins with different masses or conformations in the preparation. However, when the same preparation was run under similar conditions, with 500 mM monovalent salt in the buffer, Δ21 behaved more like a homogenous protein with a single peak eluting at ~50 kDa (Fig. 35A). This further confirms that the oligomeric and the conformational state of the protein is dependent on the salt conditions in the buffer, in line with DLS results (Chapter IV, Results) and the report by Cramer et al. (*211*). Should the HCV RdRp assume alternative conformations/mass states, a DSF assay that measures the denaturaion profile of proteins should detect these changes (*212*) (see Chapter III, Materials and Methods). Since the Δ21 purified through the Mono-S column showed a single denaturation curve (see Chapter IV, Results) a Δ21 that was purified through the poly-U agarose column was used at different protein concentrations. At low protein concentrations, Δ21 had a rather broad denaturation profile, consistent with the protein existing in multiple conformations. With two- or four-fold increases in the concentration of Δ21, at least two populations of proteins with distinct Tm_{apps} can be discerned (Fig. 35B). These results suggest that the oligomerization states of the HCV RdRp and/or significant changes in conformation can be manipulated by its concentration (Fig. 35B). These results also indicate that any analysis of the HCV RdRp will have to take into account the changes in the RdRp oligomerization state and conformations.
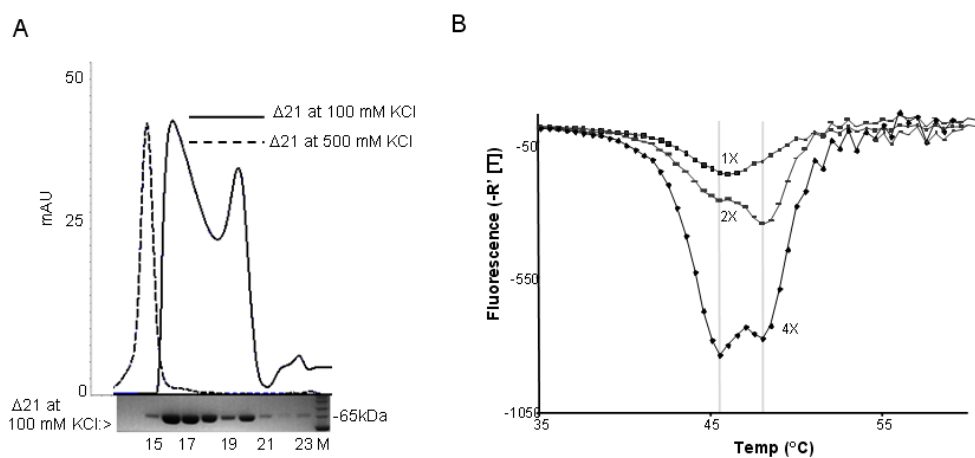
Figure 35: Gel filtration and DSF assay of Δ21. A) About 100 μg of Δ21 purified on Ni-column and Mono-S column was injected into a Superdex-200 column and chromatography was performed at a flow rate of 0.25 ml/min while the elution was monitored by absorbance at 280 nm. The Δ21 at 100 mM KCl showed multiple peaks hence all the fractions were analyzed by SDS-PAGE to check for the presence of the protein (fraction numbers at bottom of gel). B) Δ21 that was purified through Ni-column and poly-U agarose column was subjected to DSF assay (see Chapter 4, Materials and Methods) at 1, 2 and 4 μM concentrations (indicated as 1X, 2X and 4X respectively).

RNA synthesis by the HCV RdRp. RNA synthesis assays which used template named LE19 that can report on both de novo initiation and primer-extension in the same reaction was used to quantify the 19-nt product of de novo initiated and terminated RNA, and the 32-nt product generated by elongation from a primed template. Other products in the reaction are ones with terminal additions to the template (20-nt and 21-nt) that are usually of low abundance, and the more prominent template switch products that are multimers of 19-nt in length ((*181*), Fig. 36A). These last two classes of enzymatic activities are likely minor in importance in vivo when compared to de novo initiation and primer extension.

We examined whether RdRp concentration and the associated changes in conformation/oligomerization states will correlate with the mode of RNA synthesis. When a range of Δ21 concentrations for RNA synthesis was used, different requirements for de novo initiation and elongation were observed (Fig. 36B). The primer extended product was more prominent at the lower RdRp concentration and inhibited at the higher enzyme concentrations (Fig. 36B). The opposite trend was observed with the de novo initiated product. These results suggest that lower Δ21 concentrations favored extension from a primed template (akin to elongation) while the higher order structures favored de novo initiation. To confirm the effects seen with LE19, we used a 1:1 combination of LE19P and PE46. LE19P can direct the synthesis of only the 19-nt de novo initiation product but cannot give rise to the 32-nt primer extension product and also cannot be efficiently used for template switching. The 3' terminus of PE46 can be extended to form a complete hairpin of 46-nt. In a reaction with a range of Δ21 concentrations, we
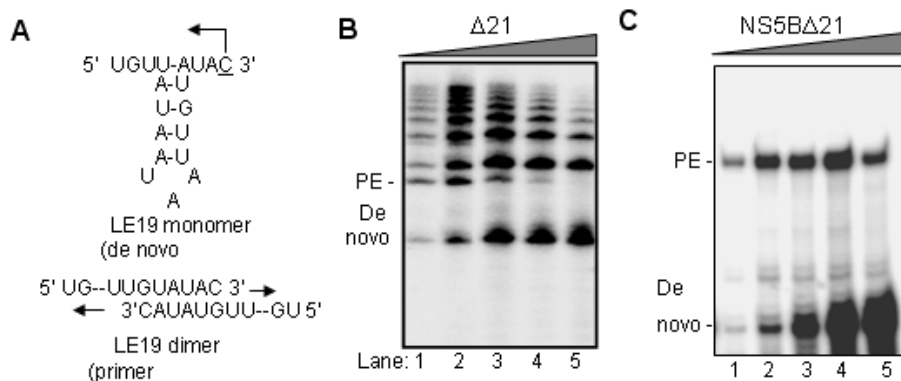
Figure 36: Concentration dependent RNA synthesis by Δ21. A) Schematic of secondary structure and depiction of the two primary modes of RNA synthesis directed by the RNA template LE19 by the HCV RdRp: de novo initiation and primer extension. B) RNA synthesis from template LE19 RNA by increasing concentrations of Δ21. Final concentrations of Δ21 were at 78, 96, 192, 384 and 780 nM in lanes 1-5. The enzyme was incubated with LE19 (50 nM) for 5 min. before initiating the RdRp reaction by adding NTPs and radiolabeled CTP in a solution containing divalent metal ions as described in the Materials and Methods. After incubating the reaction components at 25°C for 1 h, the RNA was extracted with phenol-chloroform and ethanol precipitated before running the products in a 20% urea denaturing polyacrylamide gel. The gel was subjected to autoradiography and phosphorimaging (GE Healthcare). The 19-nt de novo initiated (De novo) and 32 mer primer-extension products (PE) generated from template LE19 are identified to the left of the gel image. C) Effect of increasing concentration of Δ21 in RNA synthesis with LE19P or PE46. Δ21 was used at 10, 20, 40, 80, and 160 nM in reactions 1-5. In both panels B and C, the de novo initiated and primer-extension products are labeled to the left of the gel image to facilitate interpretation of the results.

again observed that the primer extension product was produced in larger amounts at the lower Δ21 concentrations while de novo initiation increased with Δ21 concentration (Fig. 36C). These results suggest that if the monomer of Δ21 participates in viral RNA synthesis, it is in elongation from a nascent template-primer duplex. The oligomerization state for de novo initiation will be examined in a separate work. This manuscript will focus on the monomeric forms of Δ21.

Electron microscopy and single particle reconstruction. We seek to visualize the Δ21 monomers and determine their shapes and visualize any changes in conformation. A method appropriate for this analysis is the single particle reconstruction of proteins stained with uranyl acetate. Oligomeric states and conformational changes for innate immune receptors in the absence and presence of ligands were captured using this method (*214, 230*). To enrich for the monomers, a concentration of 1 ng/uL was empirically determined to give a good spread on the EM grids (Fig. 37A). Over 200 micrographs were used to collect over 38,000 well-separated particles. We note that the particles represent different views of proteins as they land on the grid as well as possible oligomers. The particles were then centered and subjected to sorting using the Multirefine function of the EMAN suite of programs. We initially designated eight subgroups for the sorting of the particles, but inspection of the results showed that three of the groups were nearly identical to three others. Therefore, we reduced the number of classes to five for 3D model building. To examine whether the sorting was reasonable,
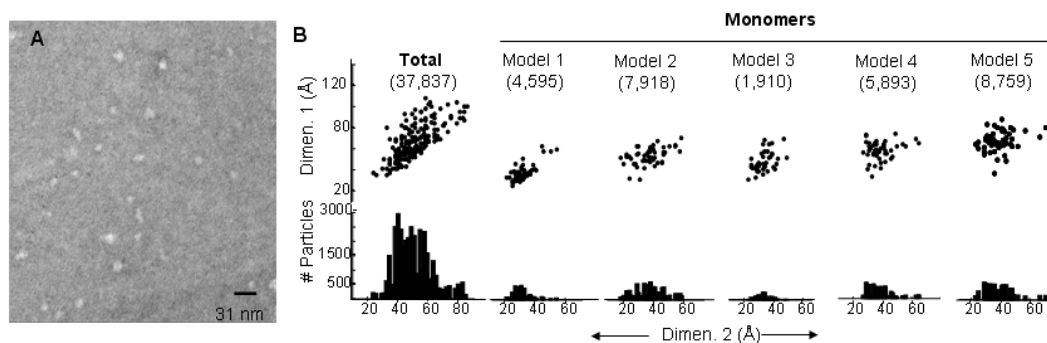
Fig. 37. Analysis of single particles of Δ21 by electron microscopy. A) A sample image of the micrographs used for the picking of single particles. Some of the particles may represent monomers, dimers, and higher order oligomers. However, it is also possible that the particles may land in various orientations on the carbon grid. The scale bar used in the imaging is shown at the lower right corner. B) Size distribution of all of the single particles for the HCV RdRp used for 3D image reconstruction and the distributions for the five models of the Δ21 monomer. More than 40,000 particles were individually picked for this analysis; 36,000 represent the five minimal classes of monomers as sorted by the multirefine program of EMAN. Each of the five sets of monomeric particles was used to generate class averages for image reconstruction. Each spot in the scatter plot depicts the longest and shortest dimensions (in angstroms) for each of the class averages. The bar graph shows the number of particles present in each class average. The total number of the particles used to generate each of the models is shown in parentheses.

we took measurements of the shortest and longest dimensions for each of the subclasses from the five models and plotted the two dimensions in the graphs shown in Fig. 37B. In the lower panel, we used a histogram to show the number of particles within each subgroup. While the entire collection of particles had a wide distribution (left-most plot), it is clear that the subgroups within each of the five models are more closely clustered, providing some confidence for the sorting of the subclasses.

Three dimensional reconstructions without presumed symmetry were performed for all five models. After the standard two sets of eight refinements, all five models converged to a resolution of 20-23 Å (Fig. 38). The final 3D models match well with the projections shown in the class averages, providing some confidence for the models. Interestingly, the five models ranged from those that are in a structure which is more closed relative to the X-ray structure (models 1 and 3), to ones similar to the X-ray structure (model B) and to two forms that appear to be more open (models 4 and 5). The more closed form may explain the elution of Δ21 at a smaller molecular mass in the gel filtration column. These models offer a snapshot of the quasi-stable conformations that the HCV Δ21 can assume in solution.

Conformation of m26-30. We hypothesize that the open and closed conformation of Δ21 is due to the loss of interaction between the Δ1 loop and the hydrophobic residues that it contacts. To gain evidence in support of this model, we sought to reconstruct the 3D structure of the m26-30 mutant protein, which lacks five residues in the tip of the Δ1 loop. Electron micrographs confirm that the majority of the particles in the m26-30
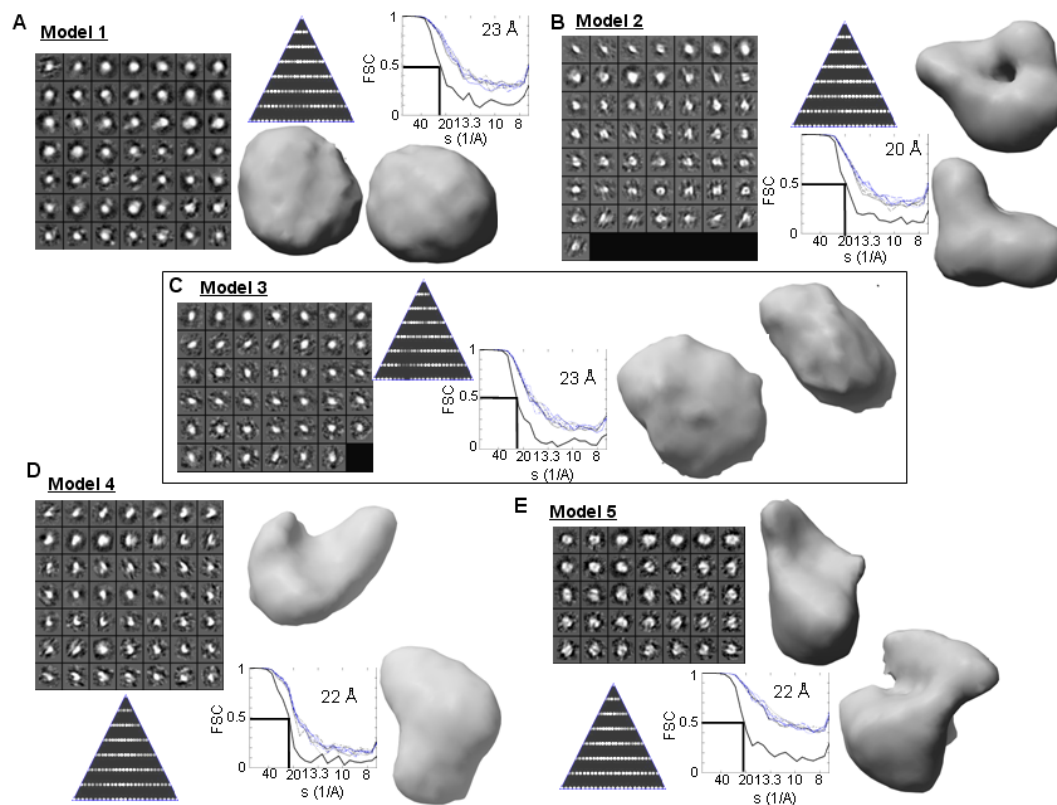
Figure 38. Data used to construct the five models depicting different conformations of the Δ21 monomer**.** Panels A-E all contain the class averages generated for each of the five monomer models, the asymmetric triangles that depicts the coverage of all of the views in each model, a Fourier shell correlation plots showing the convergence of the eight rounds of model refinement. The final calculation of the structures, and two views of the model are shown as electron density shells in grey.

preparation are also more homogenous than the particles of Δ21 (Fig. 39A).

We selected ~4000 particles from over 20 micrographs and used the EMAN program to generate a three-dimensional model. The class averages suggest that the vast majority of the particles are monomers and belonged to one model (Fig. 39B). The reconstruction of m26-30 was achieved in two independent trials using different data sets and yielded the same models between 18 and 20 Å resolution (Fig. 39C and data not shown). The particles selected were a good representation of the different views of the final reconstructed model (Fig. 39E), giving confidence to the validity of the model (compare the model in Fig. 39E to the class averages in Fig. 39B).

Protein m26-30 was predicted to exist in a predominantly open conformation based on preferential binding to dsRNA (Chapter III, Results). Putative thumb, finger, and palm subdomains can be appreciated in the model (Fig. 39E), and the exposed template channel has a width of 36 Å at the most constricted juncture, a feature compatible with the ability to bind dsRNA. To facilitate a comparison, the shape of the RdRp determined by X-ray crystallography (pdb: 1QUV) is shown in Fig. 36F. To explore further the arrangement of the subdomains, we attempted to fit the electron density of m26-30 to the existing atomic resolution structures and found that none matched with the extra protrusion observed in the model.

However the typical closed form of RdRp can generally fit into the rest of the electron density for m26-30. In Chapter III a simulated annealing model of RdRp was generated (see Chapter III, Results), which depicted a slightly open conformation with
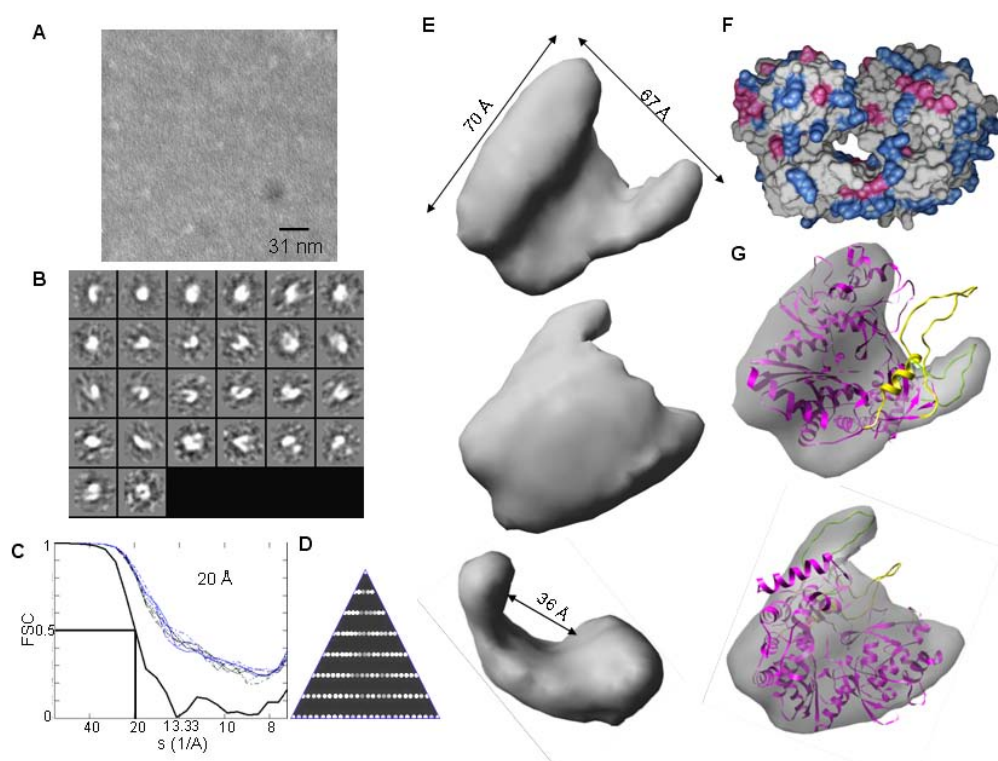
Fig. 39. 3D reconstruction of the m26-30 monomer. A) A sample micrograph of the m26-30 protein used for single particle reconstruction. B) Class averages of the ca. 4000 particles picked for this analysis. C) Fourier Shell Correlation of the refinement process and EOTEST showing that the resolution of the converged m26-30 structure was at 20 Å. D) An asymmetric triangle showing the distribution of the particles. E) Three views of the model of the m26-30 molecule. The EM envelopes of the reconstructions are shown. F) Model of a closed form of HCV RdRp intended to illustrate the difference between the open conformation of m26-30 and the closed conformation of the HCV RdRp. The surface residues that are acidic are shown in red and the basic ones in blue. G) Docking of the molecular model generated from the crystal structure of the HCV RdRp into the electron density of m26-30. Two views that differ by 180o are shown. The ribbon structure of the HCV RdRp was generated by replacing residues 26-30 of the HCV crystal structure (pdb 1quv) with glycines and then calculating the lower energy state of the resulting molecule. The altered Δ1 loop is shown in yellow.

an unfolded Δ1 loop and flexibility of the nearby helices. To improve the fit, additional

models were generated by varying the annealing temperature and effective radius for the

structures of Δ21 using initial manual fitting followed by further refinement using the

Mapfit option of Chimera (UCSF). Two views of the best fit between the calculated

structure and the m26-30 3D model are shown in Fig. 39G. The correlation of the final

fit is ~70 %. Based on the map, it seems that the fingertip region has completely moved

away from the thumb helices while the simulated model represents an intermediate

position in this movement of the loop region. There may even be changes in the

secondary structure(s) as observed by Biswal et al., (2005) (*60*) that may account for

some portions of the two molecules not fitting better. These results show that single

particle reconstruction can be used to identify conformational states of the HCV RdRp

that are difficult to capture by X-ray crystallography. This is partly confirmed in Fig. 40,

where we compare the conformations of the five states for the Δ21 monomers and the

open conformation of m26-30 along with the dimensions of the X-ray structures of a 1b

RdRp.

Residues involved in the regulation of the open and closed RdRp conformations. The

reconstruction of the m26-30 structure is consistent with findings in Chapter III

showing that the Δ1 loop is involved in the regulation of the open and closed

conformations. Recently, the crystal structure of the HCV genotype 2a RdRp was solved

and also shown to be capable of more de novo initiation than the 1b RdRp (*64*). The

increase in de novo initiation is likely due to formation of a more closed conformation.
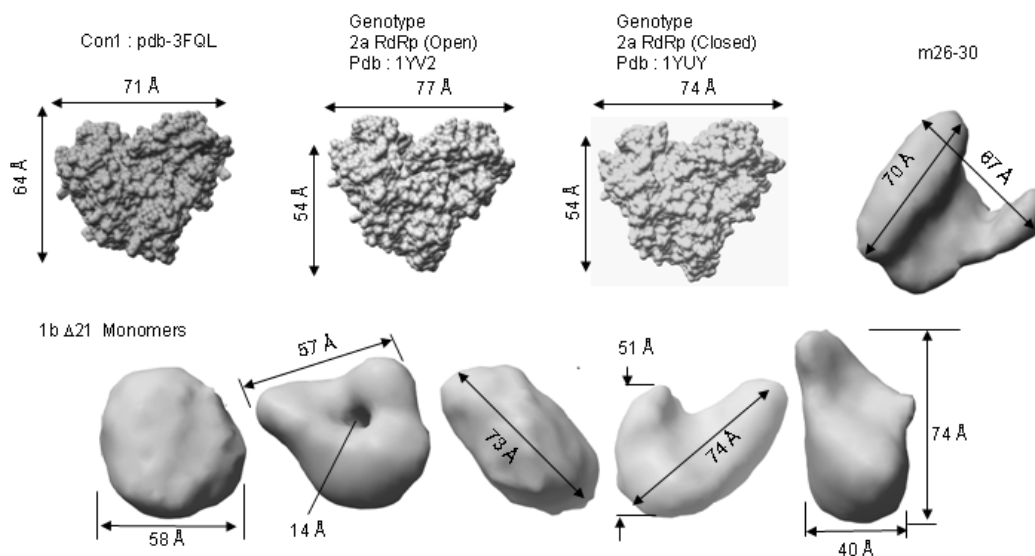
Figure. 40. A compilation of the conformations of the monomers reconstructed or reported in the crystal structure for the HCV RdRp. The crystal structures are shown with higher resolution electron density structures along with their associated pdb numbers. The dimensions for each of the particles were measured using Chimera.

The analysis of the RdRp conformations above suggests that changes in the interaction between the Δ1 loop and the regions that it contacts could be partially responsible for the differences in de novo initiation. To better understand these interactions, the sequences of the Δ1 loop of more than 230 1b and 12 2a HCV strains were analyzed to determine which residues in the Δ1 loop are conserved for interactions. Interestingly, a highly conserved portion included residues 26-35 which involves the helix-A in the Δ1 loop (Fig. 41). In addition, the sequences close to where the Δ1 loop originated from the finger domain (residues 10-18 and 40-45) were also more conserved (residues 12-18 and 40-45). We also note that the acidic or basic residues, E17, E18, R32, H34, and R43, tended to be highly conserved. With regard to a comparison between the 1b and the 2a Δ1 loops, the 2a Δ1 loop contained a Glu at position 19 (whereas a serine or threonine existed for the 1b RdRp) and a Lys at position 36 where Met or Leu normally existed in other HCV strains. The 2a Δ1 loop thus has two additional charged residues when compared to the total HCV isolate. This analysis prompted us to more closely examine how the residues in the Δ1 loop could interact with the residues in the thumb domain. We first used the PIC Webserver (*228*) program to predict the locations of potential bond forming partners within the Δ1 loops of the 1b and the 2a RdRps (Fig. 42A). As would be expected, a number of interactions are predicted in both the Δ1 loops of the 1b and the 2a RdRps. Both contained a number of interactions within the short α-helical
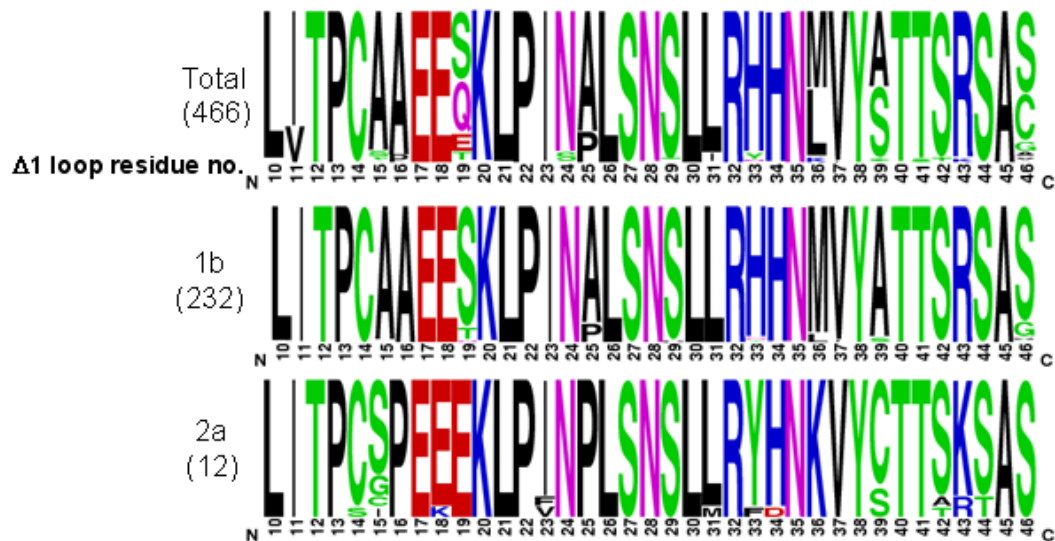
Figure 41. Sequence alignment of Δ1-loop region of NS5B found in the different isolates in the HCV database (NIH). The program WebLogo, (University of Californaia, at Berkeley) (*231*) was used to generate the alignment. The length of the one-letter name of the amino acid indicates the degree of conservation. The number of sequences used for each analysis is shown in parenthesis under the HCV genotype. N-amino terminus, C-carboxy terminus.

region, as well as between the two termini of the loop as they emerged from the finger domain. In addition, a number of additional interactions (highlighted in red, Fig. 42A, right panel) are seen with the 2a Δ1 loop. Next, we examined for possible interactions between the Δ1 loop and the rest of the RdRp. The Δ1 loop had interactions with the thumb subdomain and with the Δ2 loop. However, the interaction with the thumb subdomain was found to be critical in maintaining a closed structure required for de novo initiation. In addition, we observed that there are several new interactions within the Δ1 loop of the 2a RdRp with the Δ2 loop. Of special interest is the interaction between the Glu19 and Lys154, which adds a sidechain-sidechain hydrogen bond interaction that should be of interest for future analysis for the basis of the interactions that promote de novo initiation (Fig. 42B). A detailed summary of the interactions in the Δ1 loops of the 1b and the 2a RdRps with the thumb subdomain and the Δ2 loop are in Table 2.

There are several key residues in the interactions between the Δ1 loop and the thumb domain. In the thumb domain, a key sidechain-sidechain interaction between E18 and R401 is conserved between the two genotypes of HCV RdRps. Several thumb residues also participate in multiple conserved interactions, including W397 (interacting with L21, P22, and V37, and A39 in the 1b RdRp), and A396 and L492 that participate in multiple, primarily hydrophobic interactions with the residues in the Δ1 loop. In the Δ1 loop, I11, L21, P22, L30, L31, Y38 and V37 anchor a set of hydrophobic interactions. We note that the 1b RdRp also has M36 involved in hydrophobic interactions while this residue was replaced with a K36 in the 2a RdRp.
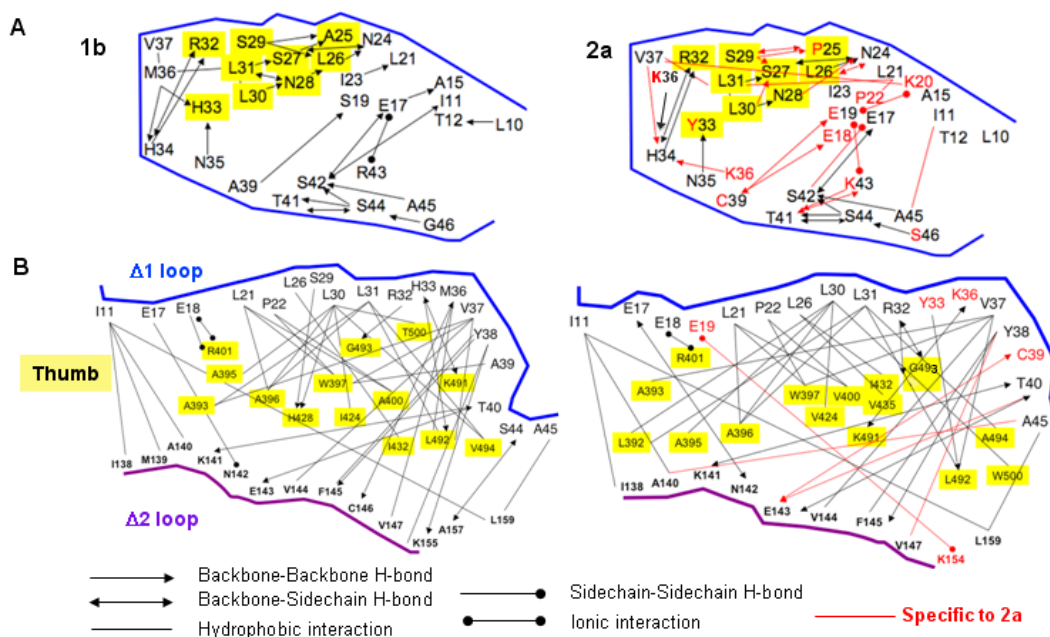
Figure 42. Analysis of the HCV RdRp sequences involved in the formation of the open or closed structures. A) Predicted interactions within the Δ1 loops for the 1b and 2a HCV RdRps. The key to the interactions are shown at the bottom of the figure. The residues highlighted in yellow are the ones that are at the tip of the Δ1 loop and contain a short a-helix. C) The interactions between the Δ1 loops of the 1b and 2a RdRps with the thumb subdomain (residues highlighted in yellow) and the Δ2 loop. Both the Δ1 and the Δ2 loops have been splayed to allow the interactions to be shown more clearly.

Table 2: Summary of intraloop interactions within the Δ1-loop of HCV NS5B (genotype 1b)

Residues in Δ1 loop		Interaction residues		Bond type
L10	L 98.7%, M 1.3%	T12	T 100%	B-B
I11	I 99.1%, V 0.9%	S42	S 99.1%, T 0.9%	B-S
		A45	A 100.0%	HI
T12	T 100%	L10	L 98.7%, M 1.3%	B-B
P13	P 100%	S42	S 99.1%, T 0.9%	S-S
C14	C 100%	NONE		
A15	A 97.8%, G 0.4%, S 0.4%, T 0.4%, V 0.9%	E17	E 100%	B-B
A16	A 99.6%, S 0.4%	NONE		
E17	E 100%	A15	A 97.8%, G 0.4%, S 0.4%, T 0.4%, V 0.9%	B-B
		S42	S 99.1%, T 0.9%	B-S
		R43	R 100%	II
E18	E 99.6%, G 0.4%	NONE		
S19	A 0.4%, N 1.7%, S 88.4%, T 9.5%	A39	A 95.7%, S 3.9%, V 0.4%	B-B
K20	A 0.4%, Q 0.4%, E 0.4% K 98.7%	NONE		
L21	L 100%	I23	I 99.6%, V 0.4%	B-B
		V37	I 2.6%, V 97.4%	HI
P22	P 100%	NONE		
I23	I 99.6%, V 0.4%	L21	L 100%	B-B
N24	N 99.6%, I 0.4%	L26	L 100%	B-B
		S27	N 0.4%, S 99.6%	B-B
				B-S
		N28	N 99.6%, Y 0.4%	B-B
A25	A 85.3%, P 14.2%, S 0.4%	S27	N 0.4%, S 99.6%	B-B
		N28	N 99.6%, Y 0.4%	B-B
		S29	P 1.7%, S 97.8%, T 0.4%	B-B
L26	L 100%	N24	N 99.6%, I 0.4%	B-B
		N28	N 99.6%, Y 0.4%	B-B
		S29	P 1.7%, S 97.8%, T 0.4%	B-B

Table 2, Continued:

S27	N 0.4%, S 99.6%	N24	N 99.6%, I 0.4%	B-S
		A25	A 85.3%, P 14.2%, S 0.4%	B-B
		L31	L 100%	B-B
N28	N 99.6%, Y 0.4%	N24	N 99.6%, I 0.4%	B-B
		A25	A 85.3%, P 14.2%, S 0.4%	B-B
		L26	L 100%	B-B
		L30	Q 0.4%, L 99.6%	B-B
		L31	L 100%	B-S
S29	P 1.7%, S 97.8%, T 0.4%	A25	A 85.3%, P 14.2%, S 0.4%	B-B
		L26	L 100%	B-B
L30	Q 0.4%, L 99.6%	N28	N 99.6%, Y 0.4%	B-B
L31	L 100%	S27	N 0.4%, S 99.6%	B-B
		N28	N 99.6%, Y 0.4%	B-S
R32	R 100%	H34	R 0.9%, H 99.1%	B-B
				B-S
H33	R 0.4%, N 1.7%, H 96.1%	N35	N 99.1%, S 0.9%	B-B
		M36	L 6.5%, K 0.4%, M 93.1%	B-B
H34	R 0.9%, H 99.1%	R32	R 100%	B-B
				B-S
		M36	L 6.5%, K 0.4% M 93.1%	B-B
		V37	I 2.6%, V 97.4%	B-B
N35	N 99.1%, S 0.9%	H33	R 0.4%, N 1.7%, H 96.1%	B-B
M36	L 6.5%, K 0.4%, M 93.1%	H33	R 0.4%, N 1.7%, H 96.1%	B-B
		H34	R 0.9%, H 99.1%	B-B
		V37	I 2.6%, V 97.4%	HI
V37	I 2.6%, V 97.4%	H34	R 0.9%, H 99.1%	B-B
Y38	Y 100%	NONE		
A39	A 95.7%, S 3.9%, V 0.4%	S19	A 0.4%, N 1.7%, S 88.4%, T 9.5%	B-B
T40	A 0.4%, T 99.6%	NONE		
T41	T 100%	S44	I 0.4%, S 99.6%	B-S
S42	S 99.1%, T 0.9%	I11	I 99.1%, V 0.9%	B-S
		P13	P 100%	B-S
		E17	E 100%	B-S

Table 2, Continued:

		S44	I 0.4%, S 99.6%	B-B
		A45	A 100%	B-B
R43	R 100%	NONE		
S44	I 0.4%, S 99.6%	T41	T 100%	B-B
				B-S
		S42	S 99.1%, T 0.9%	B-B
		G46	N 1.7%, C 0.9%, G 11.2%, S 84.5%, T 1.3%, V 0.4%	B-B
		L47	R 0.4%, Q 76.3%, L 22.8%, K 0.4%	B-B
		R48	R 100%	B-B
A45	A 100%	S42	S 99.1%, T 0.9%	B-B
G46	N 1.7%, C 0.9%, G 11.2%, S 84.5%, T 1.3%, V 0.4%	S44	I 0.4%, S 99.6%	B-B

Residues in red have one amino acid present at more than 99%

B: Backbone
R: R-group
(H): H bond
φ: hydrophobic
I : Ionic
NONE: none observed in structure

Note: Residues in blue denote mutations to similar amino acids

Altogether, while most of the interactions between the Δ1 loop and the thumb are conserved in the two RdRps, there are sufficient differences in the 1b and the 2a HCV RdRps that could account for the altered conformational changes that could result in an increase in de novo initiation by the 2a RdRp.

DISCUSSION

Viral RNA replication and transcription products are recognized by the host innate immunity receptors to signal a viral infection (*232*). Therefore, there should be strong selectional pressure to regulate viral RNA synthesis both in terms of timing, and the types and amounts of the replication and transcription products. A likely regulatory step is the conformations of the polymerase that is required for initiation and elongation. In

this work, we provide evidence to show that Δ21 exists in multiple conformations and that the interaction between the Δ1 loop and the residues that it contacts can provide regulation for the resulting conformations. This evidence includes low-resolution structures of the monomeric HCV RdRps and the open conformation formed by a mutant RdRp with a short deletion in the Δ1 loop. These conformations are likely important factors for RNA-dependent RNA synthesis and for interaction with cellular proteins, such as pRb.

RdRp conformation and RNA synthesis. The conformation of the HCV RdRp has been claimed to distinguish the modes of RNA synthesis (*64*). We note that the open and closed structures observed in the monomers could participate in extension from a primed template (which requires lower concentrations of RdRp) but the formation of oligomeric structures may be needed to direct de novo initiation. This complex scenario is necessitated by our results demonstrating that higher concentrations of the HCV RdRp is more competent for de novo initiation, suggesting that monomers may not be sufficient for the initiation of RNA synthesis. In addition, the requirements of an oligomeric HCV RdRp complex for the initiation of RNA synthesis have been previously proposed for RNA synthesis by the HCV and Poliovirus RdRps (*74-76, 206, 222-223, 229*). For the poliovirus RdRp, contact between the oligomerized polymerase subunits has been reported to increase the cooperativity in RNA synthesis (*223*). Similar results have been observed for the Norovirus RdRp (*206*). The contacts between poliovirus 3D polymerase monomers and the poliovirus 3C protease have also been proposed to regulate RNA synthesis by regulating protein-priming (*224*). We propose that the opening of the

monomers could be a key state to allow the interaction between HCV RdRp subunits, or between the RdRp and cellular proteins, such as pRb which interacts with the exposed palm domain of the HCV RdRp (*22*).

RdRp conformation and NNI interaction. The open and closed conformations of the HCV RdRp will have important implications for the design and efficacy of HCV-specific NS5B inhibitors. There are three distinct sites for the binding of nonnucleoside analog inhibitors (NNI) (Fig. 11, Chapter II). Site 1 involves the Δ1 loop and thumb domain interface. Site 2 is a pocket in the thumb domain that is present near Site 1. Site 3 lies within the template channel and involves the 'primer-grip site'. The binding of benzimidazole/indoles to Site 1 will affect the interaction between the Δ1 loop and the rest of the polymerase (*62, 124*). The binding of these compounds have led to results consistent with the mutational analyses of the HCV RdRp (*126*); the inhibitors did not affect the ability of the HCV RdRp in elongation, but prevented initiation, consistent with a closed structure (or one that requires Δ1 loop-thumb interactions between two or more RdRp subunits) needed for initiation complex assembly (*125*).

Site 2 binds compounds based on the thiophene scaffold and acts at the base of the thumb some distance from the Δ1 loop. The binding of the compounds to the 1b RdRp (to residues L419, M423, L474, and W528) did not reveal a dramatic change in RdRp conformation (*61*). However, binding to the 2a RdRp did cause a reconfiguration to the tip of the Δ1 loop structure (*60*), confirming that the 1b and 2a RdRps will have distinct interactions that could influence RNA synthesis and binding to inhibitors.

The compounds that bind to Site 3, including those from the benzothiadiazine class showed differences in response by the different HCV genotypes (*137*). We speculate that the propensity to form an open RdRp conformation and the strength of the interactions between the Δ1 loop, the thumb domain and the Δ2 loop could facilitate the entry of the inhibitors. Furthermore, the mutation of one or two key residues in or around the Δ1-loop results in polymerases severely affected for de novo initiation but not primer extension activity of Δ21 (Chapter IV, Results: E18R and PV mutants for example). Since most of the NNI target the initiation stage, the efficiency with which they can act on a given virus population may be compromised due to mutations in the key interacting residues in the Δ1-loop and thumb regions. How does the virus benefit by having these mutations when they fail in de novo initiation is a natural question that arises. Interestingly, mutant proteins that cannot themselves de novo initiate can interact with and increase de novo initiation from WT Δ21 (Chapter IV, Results).

The existing results show that the dynamic conformations of the HCV RdRp could pose an important regulatory step in RNA synthesis and, more importantly, can potentially be exploited by designing NNI that target the HCV polymerase. In addition, a number of predicted interactions, such as ones between the Δ1 loop and the Δ2 loop should be examined in detail for effects on RNA synthesis.

CHAPTER VI

PERSPECTIVES AND CONCLUSIONS

In contrast to the host DNA-dependent RNA polymerases that are mostly primer-dependent enzymes, HCV NS5B initiates RNA synthesis by a de novo mechanism and also participates in elongation. Despite the availability of numerous crystal structures and several studies involving MOA of inhibitors for the NS5B, a clear model for assembly of the initiation complexes has not emerged. Before the present study was initiated, it was believed that the closed conformation of NS5B mediated by the finger-loop interactions (involving mainly the Δ1 loop) is absolutely required for the catalytic activity of the enzyme. In the report by Labonte et al., mutations that disrupted the Δ1 loop and thumb domain interactions and therefore perturbed the closed conformation of NS5B, were detrimental for RdRp activity (*69*). However, there are sequential steps involved in RNA synthesis by RdRps and it was not clear which steps were affected by the mutations in the Δ1 loop. For instance, if only the assembly of initiation complex was adversely affected, all the other steps in the sequence will be affected. The result will be a negative effect on RNA synthesis. Moreover, several inhibitor studies that involved benzimidazole/indole scaffolds (which disrupt the Δ1 loop and thumb domain interactions) showed that the elongating polymerase was not affected by these inhibitors even though they were able to block the initiation events (*62, 124-127, 187*). This suggested that either the Δ1 loop binds to an alternate site elsewhere in the enzyme during elongation, or that the closed conformation of the enzyme was no longer retained

in the elongation phase of RNA synthesis. Experiments that can differentiate the two possibilities were needed to understand this critical piece in the overall mechanism of RNA synthesis by RdRps. Importantly, the Δ1 loop like structures are present in RdRps from other viruses like West Nile virus, Dengue virus, and poliovirus (Fig. 21, Chapter III) suggesting that the mechanism of RNA synthesis may be similar in these viruses too.

The requirement of oligomerization in the functioning of RdRps has also been unclear as conflicting reports are presented in the literature. For the poliovirus RdRp, several reports from the Kirkegaard laboratory (*222-223, 229*) showed that oligomerization is an essential requirement for polymerase function both in vitro and in virus infected cells. Pathak et al., (2002) however (*224*) concluded that the interactions of the polymerase with other replicase components were required only for the initiation of RNA synthesis by a protein-primed mechanism whereas a monomeric RdRp was capable of elongating the 3' end of a primer. In a similar case, the requirement of HCV NS5B oligomerization in RNA synthesis is not clear. Reports from several sources (*73-76*), using physical and biochemical methods have shown that HCV NS5B forms oligomeric structures and that oligomerization stimulates RNA synthesis. Ma et al., (2004) (*216*) further demonstrated that the residues critical for homomeric interactions within NS5B subunits are also required for HCV subgenomic replication. However Cramer et al., (2006) (*211*) showed that NS5B is indeed an oligomer in solution, but did not observe an oligomerization-dependent effect on RNA synthesis. The reason for this discrepancy is unclear, but it is likely that the primer-extension templates used in the study may have precluded the authors from observing an effect of NS5B oligomerization

that is more pronounced on de novo initiation templates as reported in this dissertation project.

Oligomerization is also a feature of HCV NS3 protein (*233*). The role of oligomerization in NS3 is likely to increase the processivity of the enzyme (*233-234*). Helicases have to work with two strands of nucleic acids of opposite polarity, during unwinding. It can be conceived that two subunits can bind to each strand of the RNA and unwind cooperatively. From this perspective, an oligomeric helicase must be more active than a monomeric helicase (*235*). In the RdRps however, it is unlikely that more than one active site participates in the nucleotidyl transfer; all known DNA and RNA polymerases employ a single active site during the catalytic cycle (*59, 68*).

In this context the results presented in this dissertation contribute to the mechanism of RNA synthesis by the HCV RdRp by showing that the closed conformation of the enzyme is required for de novo initiation RNA synthesis. This conclusion is based on the results from several mutations that interfered with the Δ1 loop and thumb domain contacts, like W397A, H428A, PV and the deletion mutation m26-30 (which has five residues in helix A deleted, see Chapters III and IV). These mutants were severely debilitated for de novo initiation RNA synthesis while remaining competent for primer extension activity from short RNA templates. This suggests that the closed conformation stabilizes the initiation complex while the open conformation is more suitable for elongation. This finding can also be interpreted to be that the interaction between the Δ1 loop and the thumb domain may not be stable and that additional factors may play a role in stabilizing this interaction during de novo initiation.

The results presented in Chapter IV show that oligomeric contacts beween RdRp

subunits further contribute to de novo initiation, likely by stabilizing the Δ1 loop and

thumb domain interactions. The HCV RdRp likely depends on both intramolecular and

intermolecular interactions to stabilize the de novo initiation competent conformation.

In summary the work presented in this dissertation project identified different

states of the HCV RdRp involved in different stages of RNA synthesis (Fig. 43). The

RdRp exists in at least two conformational states: open and closed as determined by

whether the Δ1 loop interacts with the thumb domain. The closed conformation is most

likely the same conformation reported in X-ray diffraction crystal structures for NS5B

(Fig. 4, Chapter I) with hydrophobic interactions holding the Δ1 loop in its binding

pocket in the thumb domain, whereas the structural details for the open conformation

remains to be determined. Since it was observed that the protein stability is affected by

disrupting the Δ1 loop and thumb domain contacts (Chapter IV, Results, Fig. 29 and 31)

a dsRNA ligand may be needed to stabilize the open conformation of the protein to make

it suitable for crystallization. In that sense, an open conformation may actually be more

suitable to capture the ternary complex of the elongating RdRp.

The number of subunits that make up the RdRp oligomer could not be determined

in this work. There was evidence for NS5B to be present as sizes corresponding to

dimers as well as higher order oligomers of ~20 nm in average diameter in negatively

stained samples from EM experiments. This is partly in agreement with the report by

Wang et al., in which the HCV RdRp was crystallized as an oligomer with two broad

interacting interfaces (*76*) (Fig. 43B, Model II).
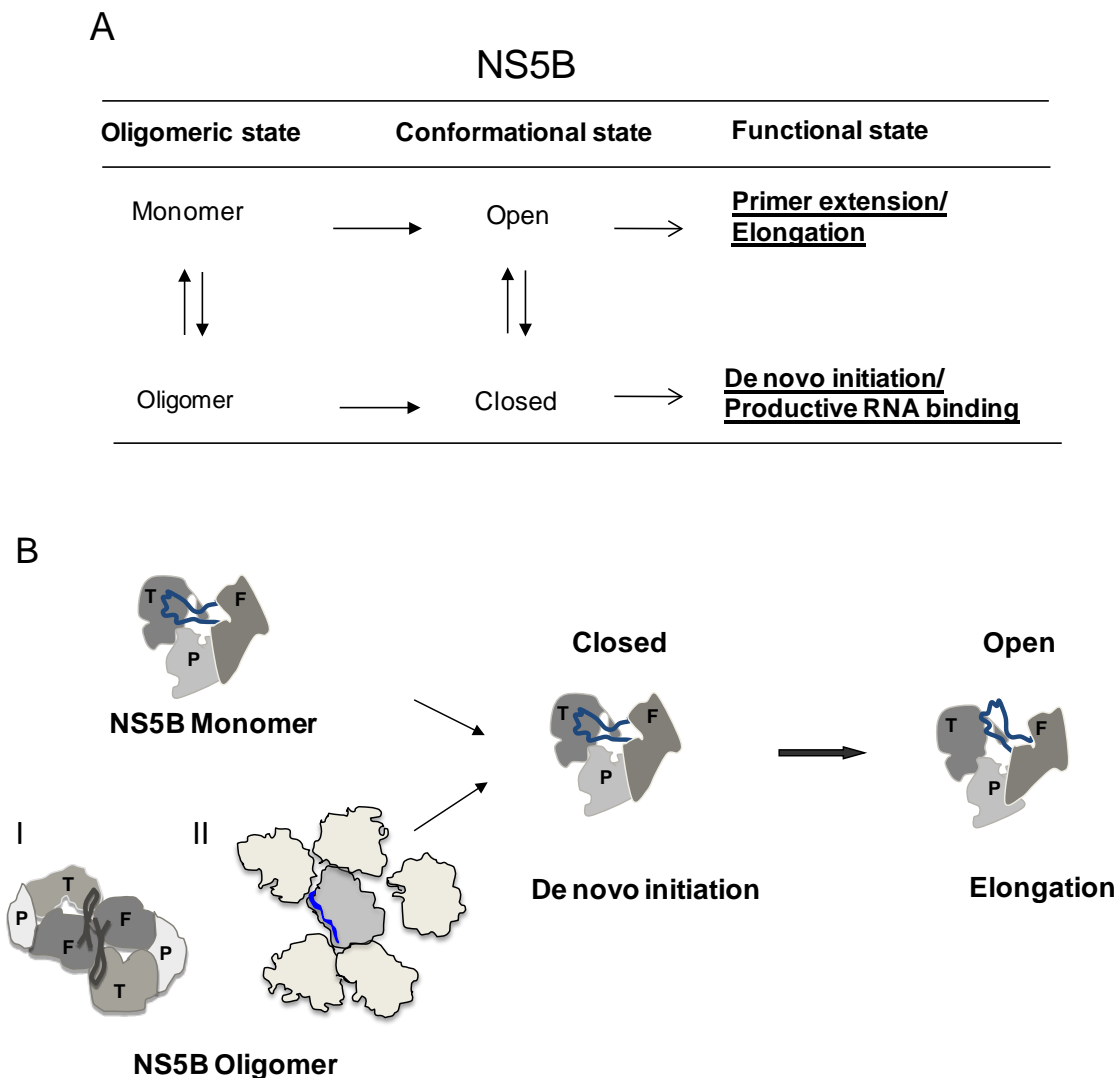
Figure 43: Summary of the major findings in this project. A) HCV NS5B exists in two conformational states: closed and open. The conformational states are guided by the oligomeric state of the protein which will in turn decide its functional state. At lower protein concentrations that favor a monomeric state of the polymerase the enzyme tends to be in the open conformation as evidenced by more primer extension and less de novo initiation at these concentrations (Chapter IV, Results). B) The two models for de novo initiated RNA synthesis by HCV NS5B: the monomer model and the oligomer model. The results from this work favor the oligomer model for de novo initiation. It was not clear if NS5B was a dimer (I) or a higher order oligomer (II) (six individual monomers making contacts with each other are shown). Model II is derived from the oligomeric crystal structure of HCV NS5B reported by Wang et al. (*76*). T, P and F refer to the three domains in NS5B and the thick line (black or blue) represents the Δ1 loop.

On the other hand, Qin et al., saw evidence for an NS5B dimer in glycerol gradient fractionation (*75*) and identified E18 and H502 as the interacting pair in the dimer. Consistently, E18R mutation prevented optimal de novo initiation from NS5B (Chapter IV, Results) and therefore E18 may be important to maintain the closed conformation of NS5B in an oligomeric complex. The Δ1 loop and its interaction with the thumb domain could be interacting as part of an interface between two RdRp subunits (Fig. 44A). This would help to explain how mutations in the Δ1 loop, such as m26-30, and even the PV mutants were either incapable of, or exhibit only a linear increase in de novo initiation activity with increasing enzyme concentrations (Chapter IV, Results). In the study by Wang et al., a Hill coefficient of 2.2 was determined for the cooperativity in NS5B during RNA synthesis suggesting 2-3 interacting surfaces between monomers which was confirmed by crystallization (*76*). An interesting experiment would be to do a mutational analysis of the "basic-patch" on the thumb domain (Fig. 15, Chapter II) near the Δ1 loop interaction pocket and analyze the effects on primer extension and de novo initiation. If this region is an oligomeric interface as predicted previously (*38*) it can be identified by the RNA synthesis assays and the blue-native PAGE assays described in Chapter IV (Fig. 27 and Fig. 29).

However, another consideration that is likely to be important in determining the oligomeric state of NS5B in vivo is how the trans-membrane domain (TMD) at the C-

Figure 44: Model showing the interacting surfaces in a putative HCV NS5B dimer. A) The closed conformation structure of HCV NS5B monomer (PDB ID 1QUV) was used to construct the dimer model (The ribbon structures of the monomers are shown as white or grey). A manual docking of two monomers is done without any constraints to get the two residues E18 and H502 reported by Qin et al., (*75*) to be involved in a dimeric pair, into close proximity. The thumb domains of each monomer dock into each other with minimal steric clashes except at the region involving the apex of the $\Delta 1$ loop (shown as residues 26-30 in gold). Interestingly a patch of positively charged residues (colored cyan) line up along the junction between the thumb domains of each monomer and could potentially help to stabilize the RNA that feeds into the template channel leading into the active site (GDD residues colored yellow). B) The dimer model shown on the surface of a membrane structure. The membrane is shown as two orange horizontal lines connected by a set of black vertical lines. The C-terminal tail of NS5B which is the trans-membrane domain (TMD) is shown as a thick black line emerging out of the active site and inserting into the membrane.
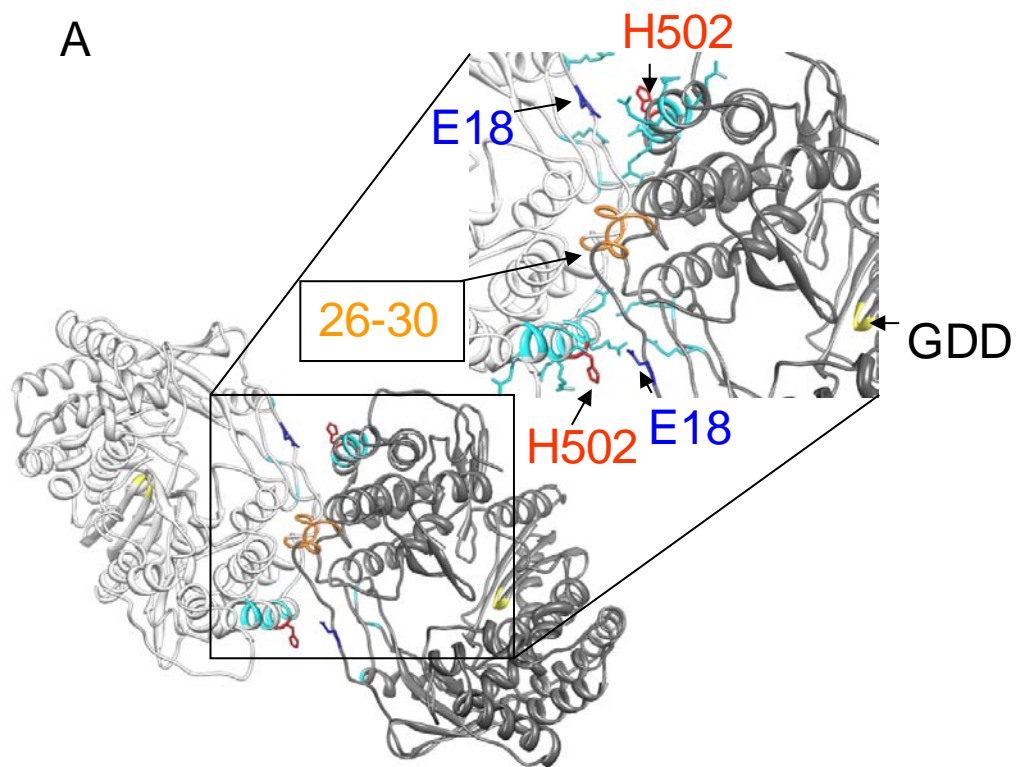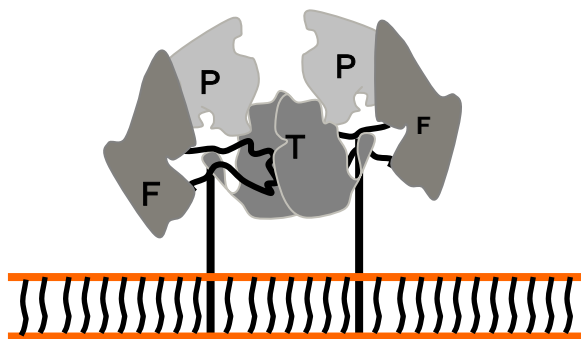
terminus of the polymerase is arranged within the membrane (Fig. 44B). The C-terminal 21 amino acids in NS5B are required for viral replication but interestingly can be partially or completely replaced by a hydrophobic sequence from the polioviral protein 3A (*236*). Polioviral 3A protein as its precursor 3AB binds to the polioviral RdRp, 3D pol and anchors it to the membranes. This will suggest that specific interactions between the TMD of HCV NS5B and other membrane components may not be important in forming the membrane associated HCV replication complex (*236*). NS5B TMD may be responsible only to physically anchor the polymerase on the membranes as no adaptive mutations were observed during serial passages of the chimeric HCV subgenomic replicons which had the NS5B TMD replaced by the polioviral 3A TMD (*236*).

Since homomeric interactions between viral protein TMDs are common (*237*) it is likely that TMDs of different subunits of NS5B interact with each other and define the arrangement of the subunits on the cytosolic side of the protein. In this context it would help the oligomerization process if there are more interacting surfaces between the subunits. It will be a challenge to determine the arrangement of the NS5B oligomers in HCV replication complexes on membranes. In any model, it will be important to take into account how the presence of other components of the HCV replicase affects NS5B oligomerization.

Host Cyclophilins may have key roles in 'remodeling' these oligomeric RdRps by way of their peptidyl-prolyl isomerase activity (*142, 238*). The cellular kinases (PRK-2) phosphorylates NS5B and may affect initiation complex formation (*239*). It will be interesting to dissect the mechanism by which cyclophilins and PRK-2 kinase affect the

function of HCV RdRp. Experiments are underway in the Kao laboratory to understand how PRK-2 phosphorylation of NS5B affects its function. Preliminary experiments have shown that the mutant polymerases characterized in Chapter III *viz*. W397A, H428A and m26-30 which were all defective for de novo initiation but not primer extension showed increased levels of phosphorylation by PRK-2 (data not shown). Phosphorylation is also a feature in another replicase protein NS5A, and in preliminary experiments it was seen that NS5A inhibits NS5B activity in vitro (not shown). How this inhibition is related to the phosphorylation of both proteins is an interesting future area of research. Since NS5A also can oligomerize, phosphate groups in both the nonstructural proteins may have roles in "remodeling" these oligomeric structures. Cyclophilins may alter the dimensions of the template channel in highly oligomeric RdRp and thereby increase RNA binding. In line with this a recent report showed that a baculovirus expressed cyclophilin was able to increase RNA synthesis from recombinant HCV RdRp (*240*). Roles for host proteins in HCV RNA synthesis are increasingly being appreciated (*141, 144, 172, 239*). Whole proteome approaches are needed to identify other host proteins that associate with HCV RdRp and facilitate NS5B activity. The information gained will surely help to identify additional targets that will lead to new therapies to treat hepatitis C.

REFERENCES

1.   Wasley, A., and Alter, M. J. (2000) Epidemiology of hepatitis C: geographic differences and temporal trends, *Semin Liver Dis 20*, 1-16.

2.   El-Serag, H. B. (2004) Hepatocellular carcinoma: recent trends in the United States, *Gastroenterology 127*, S27-34.

3.   Micallef, J. M., Kaldor, J. M., and Dore, G. J. (2006) Spontaneous viral clearance following acute hepatitis C infection: a systematic review of longitudinal studies, *J Viral Hepat 13*, 34-41.

4.   Lai, M. E., Mazzoleni, A. P., Argiolu, F., De Virgilis, S., Balestrieri, A., Purcell, R. H., Cao, A., and Farci, P. (1994) Hepatitis C virus in multiple episodes of acute hepatitis in polytransfused thalassaemic children, *Lancet 343*, 388-390.

5.   Choo, Q. L., Kuo, G., Weiner, A. J., Overby, L. R., Bradley, D. W., and Houghton, M. (1989) Isolation of a cDNA clone derived from a blood-borne non-A, non-B viral hepatitis genome, *Science 244*, 359-362.

6.   Tellinghuisen, T. L., Evans, M. J., von Hahn, T., You, S., and Rice, C. M. (2007) Studying hepatitis C virus: making the best of a bad virus, *J Virol 81*, 8853-8867.

7.   Moradpour, D., Penin, F., and Rice, C. M. (2007) Replication of hepatitis C virus, *Nat Rev Microbiol 5*, 453-463.

8.   Diviney, S., Tuplin, A., Struthers, M., Armstrong, V., Elliott, R. M., Simmonds, P., and Evans, D. J. (2008) A hepatitis C virus cis-acting replication element forms a long-range RNA-RNA interaction with upstream RNA sequences in NS5B, *J Virol 82*, 9008-9022.

9.   Kunkel, M., Lorinczi, M., Rijnbrand, R., Lemon, S. M., and Watowich, S. J. (2001) Self-assembly of nucleocapsid-like particles from recombinant hepatitis C virus core protein, *J Virol 75*, 2119-2129.

10.   Schofield, D. J., Bartosch, B., Shimizu, Y. K., Allander, T., Alter, H. J., Emerson, S. U., Cosset, F. L., and Purcell, R. H. (2005) Human monoclonal antibodies that react with the E2 glycoprotein of hepatitis C virus and possess neutralizing activity, *Hepatology 42*, 1055-1062.

11.   Pileri, P., Uematsu, Y., Campagnoli, S., Galli, G., Falugi, F., Petracca, R., Weiner, A. J., Houghton, M., Rosa, D., Grandi, G., and Abrignani, S. (1998) Binding of hepatitis C virus to CD81, *Science 282*, 938-941.

12.   Pavlovic, D., Neville, D. C., Argaud, O., Blumberg, B., Dwek, R. A., Fischer, W. B., and Zitzmann, N. (2003) The hepatitis C virus p7 protein forms an ion channel that is inhibited by long-alkyl-chain iminosugar derivatives, *Proc Natl Acad Sci U S A 100*, 6104-6108.

13.   Lorenz, I. C., Marcotrigiano, J., Dentzer, T. G., and Rice, C. M. (2006) Structure of the catalytic domain of the hepatitis C virus NS2-3 protease, *Nature 442*, 831-835.

14.   Jirasko, V., Montserret, R., Appel, N., Janvier, A., Eustachi, L., Brohm, C., Steinmann, E., Pietschmann, T., Penin, F., and Bartenschlager, R. (2008) Structural and functional characterization of nonstructural protein 2 for its role in hepatitis C virus assembly, *J Biol Chem 283*, 28546-28562.

15.   Ferreon, J. C., Ferreon, A. C., Li, K., and Lemon, S. M. (2005) Molecular determinants of TRIF proteolysis mediated by the hepatitis C virus NS3/4A protease, *J Biol Chem 280*, 20483-20492.

16.   Egger, D., Wolk, B., Gosert, R., Bianchi, L., Blum, H. E., Moradpour, D., and Bienz, K. (2002) Expression of hepatitis C virus proteins induces distinct membrane alterations including a candidate viral replication complex, *J Virol 76*, 5974-5984.

17.   Gale, M., Jr., Blakely, C. M., Kwieciszewski, B., Tan, S. L., Dossett, M., Tang, N. M., Korth, M. J., Polyak, S. J., Gretch, D. R., and Katze, M. G. (1998) Control of PKR protein kinase by hepatitis C virus nonstructural 5A protein: molecular mechanisms of kinase regulation, *Mol Cell Biol 18*, 5208-5218.

18.   Kaul, A., Stauffer, S., Berger, C., Pertel, T., Schmitt, J., Kallis, S., Zayas, M., Lohmann, V., Luban, J., and Bartenschlager, R. (2009) Essential role of cyclophilin A for hepatitis C virus replication and virus production and possible link to polyprotein cleavage kinetics, *PLoS Pathog 5*, e1000546.

19.   Shi, S. T., Lee, K. J., Aizaki, H., Hwang, S. B., and Lai, M. M. (2003) Hepatitis C virus RNA replication occurs on a detergent-resistant membrane that cofractionates with caveolin-2, *J Virol 77*, 4160-4168.

20.   Miyanari, Y., Atsuzawa, K., Usuda, N., Watashi, K., Hishiki, T., Zayas, M., Bartenschlager, R., Wakita, T., Hijikata, M., and Shimotohno, K. (2007) The

lipid droplet is an important organelle for hepatitis C virus production, *Nat Cell Biol 9*, 1089-1097.

21. Miyanari, Y., Hijikata, M., Yamaji, M., Hosaka, M., Takahashi, H., and Shimotohno, K. (2003) Hepatitis C virus non-structural proteins in the probable membranous compartment function in viral genome replication, *J Biol Chem 278*, 50301-50308.

22. Munakata, T., Nakamura, M., Liang, Y., Li, K., and Lemon, S. M. (2005) Down-regulation of the retinoblastoma tumor suppressor by the hepatitis C virus NS5B RNA-dependent RNA polymerase, *Proc Natl Acad Sci U S A 102*, 18159-18164.

23. Gomez, J., Martell, M., Quer, J., Cabot, B., and Esteban, J. I. (1999) Hepatitis C viral quasispecies, *J Viral Hepat 6*, 3-16.

24. Argentini, C., Genovese, D., Dettori, S., and Rapicetta, M. (2009) HCV genetic variability: from quasispecies evolution to genotype classification, *Future Microbiol 4*, 359-373.

25. Pawlotsky, J. M. (2003) Hepatitis C virus genetic variability: pathogenic and clinical implications, *Clin Liver Dis 7*, 45-66.

26. Domingo, E., and Gomez, J. (2007) Quasispecies and its impact on viral hepatitis, *Virus Res 127*, 131-150.

27. Kolykhalov, A. A., Agapov, E. V., Blight, K. J., Mihalik, K., Feinstone, S. M., and Rice, C. M. (1997) Transmission of hepatitis C by intrahepatic inoculation with transcribed RNA, *Science 277*, 570-574.

28. Lohmann, V., Korner, F., Koch, J., Herian, U., Theilmann, L., and Bartenschlager, R. (1999) Replication of subgenomic hepatitis C virus RNAs in a hepatoma cell line, *Science 285*, 110-113.

29. Krieger, N., Lohmann, V., and Bartenschlager, R. (2001) Enhancement of hepatitis C virus RNA replication by cell culture-adaptive mutations, *J Virol 75*, 4614-4624.

30. Pietschmann, T., Lohmann, V., Kaul, A., Krieger, N., Rinck, G., Rutter, G., Strand, D., and Bartenschlager, R. (2002) Persistent and transient replication of full-length hepatitis C virus genomes in cell culture, *J Virol 76*, 4008-4021.

31. Blight, K. J., McKeating, J. A., Marcotrigiano, J., and Rice, C. M. (2003) Efficient replication of hepatitis C virus genotype 1a RNAs in cell culture, *J Virol 77*, 3181-3190.

32.	Wakita, T., Pietschmann, T., Kato, T., Date, T., Miyamoto, M., Zhao, Z., Murthy, K., Habermann, A., Krausslich, H. G., Mizokami, M., Bartenschlager, R., and Liang, T. J. (2005) Production of infectious hepatitis C virus in tissue culture from a cloned viral genome, *Nat Med 11*, 791-796.

33.	Kato, T., Furusaka, A., Miyamoto, M., Date, T., Yasui, K., Hiramoto, J., Nagayama, K., Tanaka, T., and Wakita, T. (2001) Sequence analysis of hepatitis C virus isolated from a fulminant hepatitis patient, *J Med Virol 64*, 334-339.

34.	Kato, T., Date, T., Miyamoto, M., Furusaka, A., Tokushige, K., Mizokami, M., and Wakita, T. (2003) Efficient replication of the genotype 2a hepatitis C virus subgenomic replicon, *Gastroenterology 125*, 1808-1817.

35.	van Dijk, A. A., Makeyev, E. V., and Bamford, D. H. (2004) Initiation of viral RNA-dependent RNA polymerization, *J Gen Virol 85*, 1077-1093.

36.	Tomei, L., Vitale, R. L., Incitti, I., Serafini, S., Altamura, S., Vitelli, A., and De Francesco, R. (2000) Biochemical characterization of a hepatitis C virus RNA-dependent RNA polymerase mutant lacking the C-terminal hydrophobic sequence, *J Gen Virol 81*, 759-767.

37.	Moradpour, D., Brass, V., Bieck, E., Friebe, P., Gosert, R., Blum, H. E., Bartenschlager, R., Penin, F., and Lohmann, V. (2004) Membrane association of the RNA-dependent RNA polymerase is essential for hepatitis C virus RNA replication, *J Virol 78*, 13278-13284.

38.	Bressanelli, S., Tomei, L., Rey, F. A., and De Francesco, R. (2002) Structural analysis of the hepatitis C virus RNA polymerase in complex with ribonucleotides, *J Virol 76*, 3482-3492.

39.	Ranjith-Kumar, C. T., Gajewski, J., Gutshall, L., Maley, D., Sarisky, R. T., and Kao, C. C. (2001) Terminal nucleotidyl transferase activity of recombinant Flaviviridae RNA-dependent RNA polymerases: implication for viral RNA synthesis, *J Virol 75*, 8615-8623.

40.	Ranjith-Kumar, C. T., Gutshall, L., Kim, M. J., Sarisky, R. T., and Kao, C. C. (2002) Requirements for de novo initiation of RNA synthesis by recombinant flaviviral RNA-dependent RNA polymerases, *J Virol 76*, 12526-12536.

41.	Ranjith-Kumar, C. T., Gutshall, L., Sarisky, R. T., and Kao, C. C. (2003) Multiple interactions within the hepatitis C virus RNA polymerase repress primer-dependent RNA synthesis, *J Mol Biol 330*, 675-685.

42. Tomei, L., Altamura, S., Bartholomew, L., Bisbocci, M., Bailey, C., Bosserman, M., Cellucci, A., Forte, E., Incitti, I., Orsatti, L., Koch, U., De Francesco, R., Olsen, D. B., Carroll, S. S., and Migliaccio, G. (2004) Characterization of the inhibition of hepatitis C virus RNA replication by nonnucleosides, *J Virol 78*, 938-946.

43. Wang, Q. M., Johnson, R. B., Chen, D., Leveque, V. J., Ren, J., Hockman, M. A., Abe, K., Hachisu, T., Kondo, Y., Isaka, Y., Sato, A., and Fujiwara, T. (2004) Expression and purification of untagged full-length HCV NS5B RNA-dependent RNA polymerase, *Protein Expr Purif 35*, 304-312.

44. Miller, R. H., and Purcell, R. H. (1990) Hepatitis C virus shares amino acid sequence similarity with pestiviruses and flaviviruses as well as members of two plant virus supergroups, *Proc Natl Acad Sci U S A 87*, 2057-2061.

45. Behrens, S. E., Tomei, L., and De Francesco, R. (1996) Identification and properties of the RNA-dependent RNA polymerase of hepatitis C virus, *EMBO J 15*, 12-22.

46. Lohmann, V., Korner, F., Herian, U., and Bartenschlager, R. (1997) Biochemical properties of hepatitis C virus NS5B RNA-dependent RNA polymerase and identification of amino acid sequence motifs essential for enzymatic activity, *J Virol 71*, 8416-8428.

47. Kolykhalov, A. A., Feinstone, S. M., and Rice, C. M. (1996) Identification of a highly conserved sequence element at the 3' terminus of hepatitis C virus genome RNA, *J Virol 70*, 3363-3371.

48. Kolykhalov, A. A., Mihalik, K., Feinstone, S. M., and Rice, C. M. (2000) Hepatitis C virus-encoded enzymatic activities and conserved RNA elements in the 3' nontranslated region are essential for virus replication in vivo, *J Virol 74*, 2046-2051.

49. Kao, C. C., Del Vecchio, A. M., and Zhong, W. (1999) De novo initiation of RNA synthesis by a recombinant flaviviridae RNA-dependent RNA polymerase, *Virology 253*, 1-7.

50. Kao, C. C., Yang, X., Kline, A., Wang, Q. M., Barket, D., and Heinz, B. A. (2000) Template requirements for RNA synthesis by a recombinant hepatitis C virus RNA-dependent RNA polymerase, *J Virol 74*, 11121-11128.

51. Luo, G., Hamatake, R. K., Mathis, D. M., Racela, J., Rigat, K. L., Lemm, J., and Colonno, R. J. (2000) De novo initiation of RNA synthesis by the RNA-dependent RNA polymerase (NS5B) of hepatitis C virus, *J Virol 74*, 851-863.

52.   Oh, J. W., Ito, T., and Lai, M. M. (1999) A recombinant hepatitis C virus RNA-dependent RNA polymerase capable of copying the full-length viral RNA, *J Virol 73*, 7694-7702.

53.   Zhong, W., Uss, A. S., Ferrari, E., Lau, J. Y., and Hong, Z. (2000) De novo initiation of RNA synthesis by hepatitis C virus nonstructural protein 5B polymerase, *J Virol 74*, 2017-2022.

54.   Sun, X. L., Johnson, R. B., Hockman, M. A., and Wang, Q. M. (2000) De novo RNA synthesis catalyzed by HCV RNA-dependent RNA polymerase, *Biochem Biophys Res Commun 268*, 798-803.

55.   Lohmann, V., Overton, H., and Bartenschlager, R. (1999) Selective stimulation of hepatitis C virus and pestivirus NS5B RNA polymerase activity by GTP, *J Biol Chem 274*, 10807-10815.

56.   Bressanelli, S., Tomei, L., Roussel, A., Incitti, I., Vitale, R. L., Mathieu, M., De Francesco, R., and Rey, F. A. (1999) Crystal structure of the RNA-dependent RNA polymerase of hepatitis C virus, *Proc Natl Acad Sci U S A 96*, 13034-13039.

57.   Lesburg, C. A., Cable, M. B., Ferrari, E., Hong, Z., Mannarino, A. F., and Weber, P. C. (1999) Crystal structure of the RNA-dependent RNA polymerase from hepatitis C virus reveals a fully encircled active site, *Nat Struct Biol 6*, 937-943.

58.   Ago, H., Adachi, T., Yoshida, A., Yamamoto, M., Habuka, N., Yatsunami, K., and Miyano, M. (1999) Crystal structure of the RNA-dependent RNA polymerase of hepatitis C virus, *Structure 7*, 1417-1426.

59.   Steitz, T. A. (1999) DNA polymerases: structural diversity and common mechanisms, *J Biol Chem 274*, 17395-17398.

60.   Biswal, B. K., Cherney, M. M., Wang, M., Chan, L., Yannopoulos, C. G., Bilimoria, D., Nicolas, O., Bedard, J., and James, M. N. (2005) Crystal structures of the RNA-dependent RNA polymerase genotype 2a of hepatitis C virus reveal two conformations and suggest mechanisms of inhibition by non-nucleoside inhibitors, *J Biol Chem 280*, 18202-18210.

61.   Biswal, B. K., Wang, M., Cherney, M. M., Chan, L., Yannopoulos, C. G., Bilimoria, D., Bedard, J., and James, M. N. (2006) Non-nucleoside inhibitors binding to hepatitis C virus NS5B polymerase reveal a novel mechanism of inhibition, *J Mol Biol 361*, 33-45.

62. Di Marco, S., Volpari, C., Tomei, L., Altamura, S., Harper, S., Narjes, F., Koch, U., Rowley, M., De Francesco, R., Migliaccio, G., and Carfi, A. (2005) Interdomain communication in hepatitis C virus polymerase abolished by small molecule inhibitors bound to a novel allosteric site, *J Biol Chem 280*, 29765-29770.

63. O'Farrell, D., Trowbridge, R., Rowlands, D., and Jager, J. (2003) Substrate complexes of hepatitis C virus RNA polymerase (HC-J4): structural evidence for nucleotide import and de-novo initiation, *J Mol Biol 326*, 1025-1035.

64. Simister, P., Schmitt, M., Geitmann, M., Wicht, O., Danielson, U. H., Klein, R., Bressanelli, S., and Lohmann, V. (2009) Structural and functional analysis of hepatitis C virus strain JFH1 polymerase, *J Virol 83*, 11926-11939.

65. Choi, K. H., Groarke, J. M., Young, D. C., Kuhn, R. J., Smith, J. L., Pevear, D. C., and Rossmann, M. G. (2004) The structure of the RNA-dependent RNA polymerase from bovine viral diarrhea virus establishes the role of GTP in de novo initiation, *Proc Natl Acad Sci U S A 101*, 4425-4430.

66. Choi, K. H., and Rossmann, M. G. (2009) RNA-dependent RNA polymerases from Flaviviridae, *Curr Opin Struct Biol 19*, 746-751.

67. Hong, Z., Cameron, C. E., Walker, M. P., Castro, C., Yao, N., Lau, J. Y., and Zhong, W. (2001) A novel mechanism to ensure terminal initiation by hepatitis C virus NS5B polymerase, *Virology 285*, 6-11.

68. Butcher, S. J., Grimes, J. M., Makeyev, E. V., Bamford, D. H., and Stuart, D. I. (2001) A mechanism for initiating RNA-dependent RNA polymerization, *Nature 410*, 235-240.

69. Labonte, P., Axelrod, V., Agarwal, A., Aulabaugh, A., Amin, A., and Mak, P. (2002) Modulation of hepatitis C virus RNA-dependent RNA polymerase activity by structure-based site-directed mutagenesis, *J Biol Chem 277*, 38838-38846.

70. Doublie, S., Sawaya, M. R., and Ellenberger, T. (1999) An open and closed case for all polymerases, *Structure 7*, R31-35.

71. Ferrari, E., He, Z., Palermo, R. E., and Huang, H. C. (2008) Hepatitis C virus NS5B polymerase exhibits distinct nucleotide requirements for initiation and elongation, *J Biol Chem 283*, 33893-33901.

72.   Rubach, J. K., Wasik, B. R., Rupp, J. C., Kuhn, R. J., Hardy, R. W., and Smith, J. L. (2009) Characterization of purified Sindbis virus nsP4 RNA-dependent RNA polymerase activity in vitro, *Virology 384*, 201-208.

73.   Dimitrova, M., Imbert, I., Kieny, M. P., and Schuster, C. (2003) Protein-protein interactions between hepatitis C virus nonstructural proteins, *J Virol 77*, 5401-5414.

74.   Gu, B., Gutshall, L. L., Maley, D., Pruss, C. M., Nguyen, T. T., Silverman, C. L., Lin-Goerke, J., Khandekar, S., Liu, C., Baker, A. E., Casper, D. J., and Sarisky, R. T. (2004) Mapping cooperative activity of the hepatitis C virus RNA-dependent RNA polymerase using genotype 1a-1b chimeras, *Biochem Biophys Res Commun 313*, 343-350.

75.   Qin, W., H. Luo, T. Nomura, N. Hayashi, T. Yamashita, and S. Murakami. . (1999) Oligomeric interaction of hepatitis C virus NS5B is critical for catalytic activity of RNA-dependent RNA polymerase. , *J. Biol. Chem 277*, 2132-2137.

76.   Wang, Q. M., Hockman, M. A., Staschke, K., Johnson, R. B., Case, K. A., Lu, J., Parsons, S., Zhang, F., Rathnachalam, R., Kirkegaard, K., and Colacino, J. M. (2002) Oligomerization and cooperative RNA synthesis activity of hepatitis C virus RNA-dependent RNA polymerase, *J Virol 76*, 3865-3872.

77.   Ranjith-Kumar, C. a. K. C. (2006) Recombinant viral RdRps can initiate RNA synthesis from circular templates, *RNA 12*, 303-312.

78.   Kao, C. C., Singh, P., and Ecker, D. J. (2001) De novo initiation of viral RNA-dependent RNA synthesis, *Virology 287*, 251-260.

79.   Vreede, F. T., Jung, T. E., and Brownlee, G. G. (2004) Model suggesting that replication of influenza virus is regulated by stabilization of replicative intermediates, *J Virol 78*, 9568-9572.

80.   Chetverin, A. B., and Spirin, A. S. (1995) Replicable RNA vectors: prospects for cell-free gene amplification, expression, and cloning, *Prog Nucleic Acid Res Mol Biol 51*, 225-270.

81.   Hosoda, K., Matsuura, T., Kita, H., Ichihashi, N., Tsukada, K., and Yomo, T. (2007) Kinetic analysis of the entire RNA amplification process by Qbeta replicase, *J Biol Chem 282*, 15516-15527.

82.   Brown, S., and Blumenthal, T. (1976) Function and structure in ribonucleic acid phage Qbeta ribonucleic acid replicase. Effect of inhibitors of EF-Tu on

ribonucleic acid synthesis and renaturation of active enzyme, *J Biol Chem 251*, 2749-2753.

83.   Blumenthal, T., and Carmichael, G. G. (1979) RNA replication: function and structure of Qbeta-replicase, *Annu Rev Biochem 48*, 525-548.

84.   Cole, P. E., Sawchyn, I., and Guerrier-Takada, C. (1982) Q beta replicase containing altered forms of ribosomal protein S1, *J Biol Chem 257*, 12929-12934.

85.   Kamen, R., Kondo, M., Romer, W., and Weissmann, C. (1972) Reconstitution of Q replicase lacking subunit with protein-synthesis-interference factor i, *Eur J Biochem 31*, 44-51.

86.   Ugarov, V. I., Demidenko, A. A., and Chetverin, A. B. (2003) Qbeta replicase discriminates between legitimate and illegitimate templates by having different mechanisms of initiation, *J Biol Chem 278*, 44139-44146.

87.   Blumenthal, T. (1980) Q beta replicase template specificity: different templates require different GTP concentrations for initiation, *Proc Natl Acad Sci U S A 77*, 2601-2605.

88.   Ranjith-Kumar, C. T., Kim, Y. C., Gutshall, L., Silverman, C., Khandekar, S., Sarisky, R. T., and Kao, C. C. (2002) Mechanism of de novo initiation by the hepatitis C virus RNA-dependent RNA polymerase: role of divalent metals, *J Virol 76*, 12513-12525.

89.   Feix, G., and Hake, H. (1975) Primer directed initiation of RNA synthesis catalysed by Qbeta replicase, *Biochem Biophys Res Commun 65*, 503-509.

90.   Klovins, J., Berzins, V., and van Duin, J. (1998) A long-range interaction in Qbeta RNA that bridges the thousand nucleotides between the M-site and the 3' end is required for replication, *RNA 4*, 948-957.

91.   Barrera, I., Schuppli, D., Sogo, J. M., and Weber, H. (1993) Different mechanisms of recognition of bacteriophage Q beta plus and minus strand RNAs by Q beta replicase, *J Mol Biol 232*, 512-521.

92.   Miranda, G., Schuppli, D., Barrera, I., Hausherr, C., Sogo, J. M., and Weber, H. (1997) Recognition of bacteriophage Qbeta plus strand RNA as a template by Qbeta replicase: role of RNA interactions mediated by ribosomal proteins S1 and host factor, *J Mol Biol 267*, 1089-1103.

93.   Deval, J., D'Abramo, C. M., Zhao, Z., McCormick, S., Coutsinos, D., Hess, S., Kvaratskhelia, M., and Gotte, M. (2007) High resolution footprinting of the

hepatitis C virus polymerase NS5B in complex with RNA, *J Biol Chem 282*, 16907-16916.

94.　Makeyev, E. V., and Bamford, D. H. (2000) The polymerase subunit of a dsRNA virus plays a central role in the regulation of viral RNA metabolism, *EMBO J 19*, 6275-6284.

95.　Ugarov, V. I., and Chetverin, A. B. (2008) Functional circularity of legitimate Qbeta replicase templates, *J Mol Biol 379*, 414-427.

96.　Sarin, L. P., Poranen, M. M., Lehti, N. M., Ravantti, J. J., Koivunen, M. R., Aalto, A. P., van Dijk, A. A., Stuart, D. I., Grimes, J. M., and Bamford, D. H. (2009) Insights into the pre-initiation events of bacteriophage phi 6 RNA-dependent RNA polymerase: towards the assembly of a productive binary complex, *Nucleic Acids Res 37*, 1182-1192.

97.　Makeyev, E. V., and Bamford, D. H. (2000) Replicase activity of purified recombinant protein P2 of double-stranded RNA bacteriophage phi6, *EMBO J 19*, 124-133.

98.　D'Abramo, C. M., Deval, J., Cameron, C. E., Cellai, L., and Gotte, M. (2006) Control of template positioning during de novo initiation of RNA synthesis by the bovine viral diarrhea virus NS5B polymerase, *J Biol Chem 281*, 24991-24998.

99.　Ackermann, M., and Padmanabhan, R. (2001) De novo synthesis of RNA by the dengue virus RNA-dependent RNA polymerase exhibits temperature dependence at the initiation but not elongation phase, *J Biol Chem 276*, 39926-39937.

100.　Lescar, J., and Canard, B. (2009) RNA-dependent RNA polymerases from flaviviruses and Picornaviridae, *Curr Opin Struct Biol 19*, 759-767.

101.　Paul, A. V., van Boom, J. H., Filippov, D., and Wimmer, E. (1998) Protein-primed RNA synthesis by purified poliovirus RNA polymerase, *Nature 393*, 280-284.

102.　Ferrer-Orta, C., Arias, A., Perez-Luque, R., Escarmis, C., Domingo, E., and Verdaguer, N. (2004) Structure of foot-and-mouth disease virus RNA-dependent RNA polymerase and its complex with a template-primer RNA, *J Biol Chem 279*, 47212-47221.

103.　Ng, K. K., Cherney, M. M., Vazquez, A. L., Machin, A., Alonso, J. M., Parra, F., and James, M. N. (2002) Crystal structures of active and inactive conformations of a caliciviral RNA-dependent RNA polymerase, *J Biol Chem 277*, 1381-1387.

104. Castro, C., Smidansky, E., Maksimchuk, K. R., Arnold, J. J., Korneeva, V. S., Gotte, M., Konigsberg, W., and Cameron, C. E. (2007) Two proton transfers in the transition state for nucleotidyl transfer catalyzed by RNA- and DNA-dependent RNA and DNA polymerases, *Proc Natl Acad Sci U S A 104*, 4267-4272.

105. Castro, C., Smidansky, E. D., Arnold, J. J., Maksimchuk, K. R., Moustafa, I., Uchida, A., Gotte, M., Konigsberg, W., and Cameron, C. E. (2009) Nucleic acid polymerases use a general acid for nucleotidyl transfer, *Nat Struct Mol Biol 16*, 212-218.

106. Arnold, J. J., Gohara, D. W., and Cameron, C. E. (2004) Poliovirus RNA-dependent RNA polymerase (3Dpol): pre-steady-state kinetic analysis of ribonucleotide incorporation in the presence of Mn2+, *Biochemistry 43*, 5138-5148.

107. Poranen, M. M., Salgado, P. S., Koivunen, M. R., Wright, S., Bamford, D. H., Stuart, D. I., and Grimes, J. M. (2008) Structural explanation for the role of Mn2+ in the activity of phi6 RNA-dependent RNA polymerase, *Nucleic Acids Res 36*, 6633-6644.

108. Burton, J. R., Jr., and Everson, G. T. (2009) HCV NS5B polymerase inhibitors, *Clin Liver Dis 13*, 453-465.

109. Deval, J. (2009) Antimicrobial strategies: inhibition of viral polymerases by 3'-hydroxyl nucleosides, *Drugs 69*, 151-166.

110. Carroll, S. S., Tomassini, J. E., Bosserman, M., Getty, K., Stahlhut, M. W., Eldrup, A. B., Bhat, B., Hall, D., Simcoe, A. L., LaFemina, R., Rutkowski, C. A., Wolanski, B., Yang, Z., Migliaccio, G., De Francesco, R., Kuo, L. C., MacCoss, M., and Olsen, D. B. (2003) Inhibition of hepatitis C virus RNA replication by 2'-modified nucleoside analogs, *J Biol Chem 278*, 11979-11984.

111. Migliaccio, G., Tomassini, J. E., Carroll, S. S., Tomei, L., Altamura, S., Bhat, B., Bartholomew, L., Bosserman, M. R., Ceccacci, A., Colwell, L. F., Cortese, R., De Francesco, R., Eldrup, A. B., Getty, K. L., Hou, X. S., LaFemina, R. L., Ludmerer, S. W., MacCoss, M., McMasters, D. R., Stahlhut, M. W., Olsen, D. B., Hazuda, D. J., and Flores, O. A. (2003) Characterization of resistance to non-obligate chain-terminating ribonucleoside analogs that inhibit hepatitis C virus replication in vitro, *J Biol Chem 278*, 49164-49170.

112. Olsen, D. B., Eldrup, A. B., Bartholomew, L., Bhat, B., Bosserman, M. R., Ceccacci, A., Colwell, L. F., Fay, J. F., Flores, O. A., Getty, K. L., Grobler, J. A., LaFemina, R. L., Markel, E. J., Migliaccio, G., Prhavc, M., Stahlhut, M. W.,

Tomassini, J. E., MacCoss, M., Hazuda, D. J., and Carroll, S. S. (2004) A 7-deaza-adenosine analog is a potent and selective inhibitor of hepatitis C virus replication with excellent pharmacokinetic properties, *Antimicrob Agents Chemother 48*, 3944-3953.

113.   Raney, K.D., Gotte, M, and Cameron, C. E. (2009) Viral RNA polymerase inhibitors, *Viral Genome Replication*, Springer US, 10.1007/b135974_23, Pt.3, ISBN:978-0-387-89425-6, pp527-548.

114.   Stuyver, L. J., McBrayer, T. R., Tharnish, P. M., Clark, J., Hollecker, L., Lostia, S., Nachman, T., Grier, J., Bennett, M. A., Xie, M. Y., Schinazi, R. F., Morrey, J. D., Julander, J. L., Furman, P. A., and Otto, M. J. (2006) Inhibition of hepatitis C replicon RNA synthesis by beta-D-2'-deoxy-2'-fluoro-2'-C-methylcytidine: a specific inhibitor of hepatitis C virus replication, *Antivir Chem Chemother 17*, 79-87.

115.   Klumpp, K., Leveque, V., Le Pogam, S., Ma, H., Jiang, W. R., Kang, H., Granycome, C., Singer, M., Laxton, C., Hang, J. Q., Sarma, K., Smith, D. B., Heindl, D., Hobbs, C. J., Merrett, J. H., Symons, J., Cammack, N., Martin, J. A., Devos, R., and Najera, I. (2006) The novel nucleoside analog R1479 (4'-azidocytidine) is a potent inhibitor of NS5B-dependent RNA synthesis and hepatitis C virus replication in cell culture, *J Biol Chem 281*, 3793-3799.

116.   Shim, J., Larson, G., Lai, V., Naim, S., and Wu, J. Z. (2003) Canonical 3'-deoxyribonucleotides as a chain terminator for HCV NS5B RNA-dependent RNA polymerase, *Antiviral Res 58*, 243-251.

117.   Le Pogam, S., Jiang, W. R., Leveque, V., Rajyaguru, S., Ma, H., Kang, H., Jiang, S., Singer, M., Ali, S., Klumpp, K., Smith, D., Symons, J., Cammack, N., and Najera, I. (2006) In vitro selected Con1 subgenomic replicons resistant to 2'-C-methyl-cytidine or to R1479 show lack of cross resistance, *Virology 351*, 349-359.

118.   Ranjith-Kumar, C. T., Sarisky, R. T., Gutshall, L., Thomson, M., and Kao, C. C. (2004) De novo initiation pocket mutations have multiple effects on hepatitis C virus RNA-dependent RNA polymerase activities, *J Virol 78*, 12207-12217.

119.   Zhong, W., An, H., Barawkar, D., and Hong, Z. (2003) Dinucleotide analogues as novel inhibitors of RNA-dependent RNA polymerase of hepatitis C Virus, *Antimicrob Agents Chemother 47*, 2674-2681.

120.   Feld, J. J., and Hoofnagle, J. H. (2005) Mechanism of action of interferon and ribavirin in treatment of hepatitis C, *Nature 436*, 967-972.

121. Wohnsland, A., Hofmann, W. P., and Sarrazin, C. (2007) Viral determinants of resistance to treatment in patients with hepatitis C, *Clin Microbiol Rev 20*, 23-38.

122. Young, K. C., Lindsay, K. L., Lee, K. J., Liu, W. C., He, J. W., Milstein, S. L., and Lai, M. M. (2003) Identification of a ribavirin-resistant NS5B mutation of hepatitis C virus during ribavirin monotherapy, *Hepatology 38*, 869-878.

123. Beaulieu, P. L., Bos, M., Bousquet, Y., Fazal, G., Gauthier, J., Gillard, J., Goulet, S., LaPlante, S., Poupart, M. A., Lefebvre, S., McKercher, G., Pellerin, C., Austel, V., and Kukolj, G. (2004) Non-nucleoside inhibitors of the hepatitis C virus NS5B polymerase: discovery and preliminary SAR of benzimidazole derivatives, *Bioorg Med Chem Lett 14*, 119-124.

124. Kukolj, G., McGibbon, G. A., McKercher, G., Marquis, M., Lefebvre, S., Thauvette, L., Gauthier, J., Goulet, S., Poupart, M. A., and Beaulieu, P. L. (2005) Binding site characterization and resistance to a class of non-nucleoside inhibitors of the hepatitis C virus NS5B polymerase, *J Biol Chem 280*, 39260-39267.

125. McKercher, G., Beaulieu, P. L., Lamarre, D., LaPlante, S., Lefebvre, S., Pellerin, C., Thauvette, L., and Kukolj, G. (2004) Specific inhibitors of HCV polymerase identified using an NS5B with lower affinity for template/primer substrate, *Nucleic Acids Res 32*, 422-431.

126. Tomei, L., Altamura, S., Bartholomew, L., Biroccio, A., Ceccacci, A., Pacini, L., Narjes, F., Gennari, N., Bisbocci, M., Incitti, I., Orsatti, L., Harper, S., Stansfield, I., Rowley, M., De Francesco, R., and Migliaccio, G. (2003) Mechanism of action and antiviral activity of benzimidazole-based allosteric inhibitors of the hepatitis C virus RNA-dependent RNA polymerase, *J Virol 77*, 13225-13231.

127. Kaushik-Basu, N., Bopda-Waffo, A., Talele, T. T., Basu, A., Costa, P. R., da Silva, A. J., Sarafianos, S. G., and Noel, F. (2008) Identification and characterization of coumestans as novel HCV NS5B polymerase inhibitors, *Nucleic Acids Res 36*, 1482-1496.

128. Love, R. A., Parge, H. E., Yu, X., Hickey, M. J., Diehl, W., Gao, J., Wriggers, H., Ekker, A., Wang, L., Thomson, J. A., Dragovich, P. S., and Fuhrman, S. A. (2003) Crystallographic identification of a noncompetitive inhibitor binding site on the hepatitis C virus NS5B RNA polymerase enzyme, *J Virol 77*, 7575-7581.

129. Wang, M., Ng, K. K., Cherney, M. M., Chan, L., Yannopoulos, C. G., Bedard, J., Morin, N., Nguyen-Ba, N., Alaoui-Ismaili, M. H., Bethell, R. C., and James, M. N. (2003) Non-nucleoside analogue inhibitors bind to an allosteric site on HCV NS5B polymerase. Crystal structures and mechanism of inhibition, *J Biol Chem 278*, 9489-9495.

130. Howe, A. Y., Cheng, H., Thompson, I., Chunduru, S. K., Herrmann, S., O'Connell, J., Agarwal, A., Chopra, R., and Del Vecchio, A. M. (2006) Molecular mechanism of a thumb domain hepatitis C virus nonnucleoside RNA-dependent RNA polymerase inhibitor, *Antimicrob Agents Chemother 50*, 4103-4113.

131. Le Pogam, S., Kang, H., Harris, S. F., Leveque, V., Giannetti, A. M., Ali, S., Jiang, W. R., Rajyaguru, S., Tavares, G., Oshiro, C., Hendricks, T., Klumpp, K., Symons, J., Browner, M. F., Cammack, N., and Najera, I. (2006) Selection and characterization of replicon variants dually resistant to thumb- and palm-binding nonnucleoside polymerase inhibitors of the hepatitis C virus, *J Virol 80*, 6146-6154.

132. Dhanak, D., Duffy, K. J., Johnston, V. K., Lin-Goerke, J., Darcy, M., Shaw, A. N., Gu, B., Silverman, C., Gates, A. T., Nonnemacher, M. R., Earnshaw, D. L., Casper, D. J., Kaura, A., Baker, A., Greenwood, C., Gutshall, L. L., Maley, D., DelVecchio, A., Macarron, R., Hofmann, G. A., Alnoah, Z., Cheng, H. Y., Chan, G., Khandekar, S., Keenan, R. M., and Sarisky, R. T. (2002) Identification and biological characterization of heterocyclic inhibitors of the hepatitis C virus RNA-dependent RNA polymerase, *J Biol Chem 277*, 38322-38327.

133. Gu, B., Johnston, V. K., Gutshall, L. L., Nguyen, T. T., Gontarek, R. R., Darcy, M. G., Tedesco, R., Dhanak, D., Duffy, K. J., Kao, C. C., and Sarisky, R. T. (2003) Arresting initiation of hepatitis C virus RNA synthesis using heterocyclic derivatives, *J Biol Chem 278*, 16602-16607.

134. Howe, A. Y., Cheng, H., Johann, S., Mullen, S., Chunduru, S. K., Young, D. C., Bard, J., Chopra, R., Krishnamurthy, G., Mansour, T., and O'Connell, J. (2008) Molecular mechanism of hepatitis C virus replicon variants with reduced susceptibility to a benzofuran inhibitor, HCV-796, *Antimicrob Agents Chemother 52*, 3327-3338.

135. Kneteman, N. M., Howe, A. Y., Gao, T., Lewis, J., Pevear, D., Lund, G., Douglas, D., Mercer, D. F., Tyrrell, D. L., Immermann, F., Chaudhary, I., Speth, J., Villano, S. A., O'Connell, J., and Collett, M. (2009) HCV796: A selective nonstructural protein 5B polymerase inhibitor with potent anti-hepatitis C virus activity in vitro, in mice with chimeric human livers, and in humans infected with hepatitis C virus, *Hepatology 49*, 745-752.

136. Feldstein, A., Kleiner, D., Kravetz, D., and Buck, M. (2009) Severe hepatocellular injury with apoptosis induced by a hepatitis C polymerase inhibitor, *J Clin Gastroenterol 43*, 374-381.

137. Nyanguile, O., Pauwels, F., Van den Broeck, W., Boutton, C. W., Quirynen, L., Ivens, T., van der Helm, L., Vandercruyssen, G., Mostmans, W., Delouvroy, F., Dehertogh, P., Cummings, M. D., Bonfanti, J. F., Simmen, K. A., and Raboisson, P. (2008) 1,5-benzodiazepines, a novel class of hepatitis C virus polymerase nonnucleoside inhibitors, *Antimicrob Agents Chemother 52*, 4420-4431.

138. Powers, J. P., Piper, D. E., Li, Y., Mayorga, V., Anzola, J., Chen, J. M., Jaen, J. C., Lee, G., Liu, J., Peterson, M. G., Tonn, G. R., Ye, Q., Walker, N. P., and Wang, Z. (2006) SAR and mode of action of novel non-nucleoside inhibitors of hepatitis C NS5b RNA polymerase, *J Med Chem 49*, 1034-1046.

139. Koch, U., Attenni, B., Malancona, S., Colarusso, S., Conte, I., Di Filippo, M., Harper, S., Pacini, B., Giomini, C., Thomas, S., Incitti, I., Tomei, L., De Francesco, R., Altamura, S., Matassa, V. G., and Narjes, F. (2006) 2-(2-Thienyl)-5,6-dihydroxy-4-carboxypyrimidines as inhibitors of the hepatitis C virus NS5B polymerase: discovery, SAR, modeling, and mutagenesis, *J Med Chem 49*, 1693-1705.

140. Summa, V., Petrocchi, A., Matassa, V. G., Taliani, M., Laufer, R., De Francesco, R., Altamura, S., and Pace, P. (2004) HCV NS5b RNA-dependent RNA polymerase inhibitors: from alpha,gamma-diketoacids to 4,5-dihydroxypyrimidine- or 3-methyl-5-hydroxypyrimidinonecarboxylic acids. Design and synthesis, *J Med Chem 47*, 5336-5339.

141. Watashi, K., Ishii, N., Hijikata, M., Inoue, D., Murata, T., Miyanari, Y., and Shimotohno, K. (2005) Cyclophilin B is a functional regulator of hepatitis C virus RNA polymerase, *Mol Cell 19*, 111-122.

142. Chatterji, U., Bobardt, M., Selvarajah, S., Yang, F., Tang, H., Sakamoto, N., Vuagniaux, G., Parkinson, T., and Gallay, P. (2009) The isomerase active site of cyclophilin A is critical for hepatitis C virus replication, *J Biol Chem 284*, 16998-17005.

143. Liu, Z., Yang, F., Robotham, J. M., and Tang, H. (2009) Critical role of cyclophilin A and its prolyl-peptidyl isomerase activity in the structure and function of the hepatitis C virus replication complex, *J Virol 83*, 6554-6565.

144. Liu, Z., Robida, J. M., Chinnaswamy, S., Yi, G., Robotham, J. M., Nelson, H. B., Irsigler, A., Kao, C. C., and Tang, H. (2009) Mutations in the hepatitis C virus polymerase that increase RNA binding can confer resistance to cyclosporine A, *Hepatology 50*, 25-33.

145. Hopkins, S., Scorneaux, B., Huang, Z., Murray, M. G., Wring, S., Smitley, C., Harris, R., Erdmann, F., Fisher, G., and Ribeill, Y. (2009) SCY-635: A Novel

Non-Immunosuppressive Analog of Cyclosporin A that Exhibits Potent Inhibition of Hepatitis C Virus RNA Replication in vitro, *Antimicrob Agents Chemother*.

146.   Ma, S., Boerner, J. E., TiongYip, C., Weidmann, B., Ryder, N. S., Cooreman, M. P., and Lin, K. (2006) NIM811, a cyclophilin inhibitor, exhibits potent in vitro activity against hepatitis C virus alone or in combination with alpha interferon, *Antimicrob Agents Chemother 50*, 2976-2982.

147.   Watashi, K., Inoue, D., Hijikata, M., Goto, K., Aly, H. H., and Shimotohno, K. (2007) Anti-hepatitis C virus activity of tamoxifen reveals the functional association of estrogen receptor with viral RNA polymerase NS5B, *J Biol Chem 282*, 32765-32772.

148.   Cai, Z., Yi, M., Zhang, C., and Luo, G. (2005) Mutagenesis analysis of the rGTP-specific binding site of hepatitis C virus RNA-dependent RNA polymerase, *J Virol 79*, 11607-11617.

149.   Biroccio, A., Hamm, J., Incitti, I., De Francesco, R., and Tomei, L. (2002) Selection of RNA aptamers that are specific and high-affinity ligands of the hepatitis C virus RNA-dependent RNA polymerase, *J Virol 76*, 3688-3696.

150.   Bellecave, P., Cazenave, C., Rumi, J., Staedel, C., Cosnefroy, O., Andreola, M. L., Ventura, M., Tarrago-Litvak, L., and Astier-Gin, T. (2008) Inhibition of hepatitis C virus (HCV) RNA polymerase by DNA aptamers: mechanism of inhibition of in vitro RNA synthesis and effect on HCV-infected cells, *Antimicrob Agents Chemother 52*, 2097-2110.

151.   Ludmerer, S. W., Graham, D. J., Boots, E., Murray, E. M., Simcoe, A., Markel, E. J., Grobler, J. A., Flores, O. A., Olsen, D. B., Hazuda, D. J., and LaFemina, R. L. (2005) Replication fitness and NS5B drug sensitivity of diverse hepatitis C virus isolates characterized by using a transient replication assay, *Antimicrob Agents Chemother 49*, 2059-2069.

152.   Heck, J. A., Lam, A. M., Narayanan, N., and Frick, D. N. (2008) Effects of mutagenic and chain-terminating nucleotide analogs on enzymes isolated from hepatitis C virus strains of various genotypes, *Antimicrob Agents Chemother 52*, 1901-1911.

153.   Herlihy, K. J., Graham, J. P., Kumpf, R., Patick, A. K., Duggal, R., and Shi, S. T. (2008) Development of intergenotypic chimeric replicons to determine the broad-spectrum antiviral activities of hepatitis C virus polymerase inhibitors, *Antimicrob Agents Chemother 52*, 3523-3531.

154. Pauwels, F., Mostmans, W., Quirynen, L. M., van der Helm, L., Boutton, C. W., Rueff, A. S., Cleiren, E., Raboisson, P., Surleraux, D., Nyanguile, O., and Simmen, K. A. (2007) Binding-site identification and genotypic profiling of hepatitis C virus polymerase inhibitors, *J Virol 81*, 6909-6919.

155. Le Pogam, S., Seshaadri, A., Kosaka, A., Chiu, S., Kang, H., Hu, S., Rajyaguru, S., Symons, J., Cammack, N., and Najera, I. (2008) Existence of hepatitis C virus NS5B variants naturally resistant to non-nucleoside, but not to nucleoside, polymerase inhibitors among untreated patients, *J Antimicrob Chemother 61*, 1205-1216.

156. Aurora, R., Donlin, M. J., Cannon, N. A., and Tavis, J. E. (2009) Genome-wide hepatitis C virus amino acid covariance networks can predict response to antiviral therapy in humans, *J Clin Invest 119*, 225-236.

157. Mercer, D. F., Schiller, D. E., Elliott, J. F., Douglas, D. N., Hao, C., Rinfret, A., Addison, W. R., Fischer, K. P., Churchill, T. A., Lakey, J. R., Tyrrell, D. L., and Kneteman, N. M. (2001) Hepatitis C virus replication in mice with chimeric human livers, *Nat Med 7*, 927-933.

158. Hansen, J. L., Long, A. M., and Schultz, S. C. (1997) Structure of the RNA-dependent RNA polymerase of poliovirus, *Structure 5*, 1109-1122.

159. Love, R. A., Maegley, K. A., Yu, X., Ferre, R. A., Lingardo, L. K., Diehl, W., Parge, H. E., Dragovich, P. S., and Fuhrman, S. A. (2004) The crystal structure of the RNA-dependent RNA polymerase from human rhinovirus: a dual function target for common cold antiviral therapy, *Structure 12*, 1533-1544.

160. Malet, H., Egloff, M. P., Selisko, B., Butcher, R. E., Wright, P. J., Roberts, M., Gruez, A., Sulzenbacher, G., Vonrhein, C., Bricogne, G., Mackenzie, J. M., Khromykh, A. A., Davidson, A. D., and Canard, B. (2007) Crystal structure of the RNA polymerase domain of the West Nile virus non-structural protein 5, *J Biol Chem 282*, 10678-10689.

161. Yap, T. L., Xu, T., Chen, Y. L., Malet, H., Egloff, M. P., Canard, B., Vasudevan, S. G., and Lescar, J. (2007) Crystal structure of the dengue virus RNA-dependent RNA polymerase catalytic domain at 1.85-angstrom resolution, *J Virol 81*, 4753-4765.

162. Pogany, J., Fabian, M. R., White, K. A., and Nagy, P. D. (2003) A replication silencer element in a plus-strand RNA virus, *EMBO J 22*, 5602-5611.

163. Ranjith-Kumar, C. T., Santos, J. L., Gutshall, L. L., Johnston, V. K., Lin-Goerke, J., Kim, M. J., Porter, D. J., Maley, D., Greenwood, C., Earnshaw, D. L., Baker,

A., Gu, B., Silverman, C., Sarisky, R. T., and Kao, C. (2003) Enzymatic activities of the GB virus-B RNA-dependent RNA polymerase, *Virology 312*, 270-280.

164.   Dutartre, H., Boretto, J., Guillemot, J. C., and Canard, B. (2005) A relaxed discrimination of 2'-O-methyl-GTP relative to GTP between de novo and Elongative RNA synthesis by the hepatitis C RNA-dependent RNA polymerase NS5B, *J Biol Chem 280*, 6359-6368.

165.   Shim, J. H., Larson, G., Wu, J. Z., and Hong, Z. (2002) Selection of 3'-template bases and initiating nucleotides by hepatitis C virus NS5B RNA-dependent RNA polymerase, *J Virol 76*, 7030-7039.

166.   Munakata, T., Liang, Y., Kim, S., McGivern, D. R., Huibregtse, J., Nomoto, A., and Lemon, S. M. (2007) Hepatitis C virus induces E6AP-dependent degradation of the retinoblastoma protein, *PLoS Pathog 3*, 1335-1347.

167.   An, P., Wang, L. H., Hutcheson-Dilks, H., Nelson, G., Donfield, S., Goedert, J. J., Rinaldo, C. R., Buchbinder, S., Kirk, G. D., O'Brien, S. J., and Winkler, C. A. (2007) Regulatory polymorphisms in the cyclophilin A gene, PPIA, accelerate progression to AIDS, *PLoS Pathog 3*, e88.

168.   Li, J., Tang, S., Hewlett, I., and Yang, M. (2007) HIV-1 capsid protein and cyclophilin a as new targets for anti-AIDS therapeutic agents, *Infect Disord Drug Targets 7*, 238-244.

169.   Watashi, K., and Shimotohno, K. (2007) Chemical genetics approach to hepatitis C virus replication: cyclophilin as a target for anti-hepatitis C virus strategy, *Rev Med Virol 17*, 245-252.

170.   El-Farrash, M. A., Aly, H. H., Watashi, K., Hijikata, M., Egawa, H., and Shimotohno, K. (2007) In vitro infection of immortalized primary hepatocytes by HCV genotype 4a and inhibition of virus replication by cyclosporin, *Microbiol Immunol 51*, 127-133.

171.   Nakagawa, M., Sakamoto, N., Tanabe, Y., Koyama, T., Itsui, Y., Takeda, Y., Chen, C. H., Kakinuma, S., Oooka, S., Maekawa, S., Enomoto, N., and Watanabe, M. (2005) Suppression of hepatitis C virus replication by cyclosporin a is mediated by blockade of cyclophilins, *Gastroenterology 129*, 1031-1041.

172.   Robida, J. M., Nelson, H. B., Liu, Z., and Tang, H. (2007) Characterization of hepatitis C virus subgenomic replicon resistance to cyclosporine in vitro, *J Virol 81*, 5829-5840.

173. Watashi, K., Hijikata, M., Hosaka, M., Yamaji, M., and Shimotohno, K. (2003) Cyclosporin A suppresses replication of hepatitis C virus genome in cultured hepatocytes, *Hepatology 38*, 1282-1288.

174. Demeler, B. (2005) *Modern Analytical Ultracentrifugation: Techniques and Methods (Scott, D. J., Harding, S. E., and Rowe, A. J., eds) pp. 210-229, Royal Society of Chemistry, London.*

175. Brookes, E., Boppana, R. V., and Demeler, B. . (2006) In *Supercomputing '06: Proceedings of the 2006 ACM/IEEE Conference on Supercomputing, Tampa, Florida, November 11-17, 2006, Abst. 81, Association for Computing Machinery,* New York.

176. Schuck, P., and Demeler, B. (1999) Direct sedimentation analysis of interference optical data in analytical ultracentrifugation, *Biophys J 76*, 2288-2296.

177. Demeler, B., and van Holde, K. E. (2004) Sedimentation velocity analysis of highly heterogeneous systems, *Anal Biochem 335*, 279-288.

178. Brookes, E., and Demeler, B. . (2007) *GECCO Proceedings, London, July 7-11, 2007, pp. 361-368, Association for Computing Machinery, New York.*

179. Durchschlag, H. (1986) *Thermodynamic Data for Biochemistry and Biotechnology (Hinz, H.-J., ed) pp. 45-128, Springer-Verlag, New York.*

180. Grimsley, G. R., Huyghues-Despointes, B. M. P., Pace, C. N., and Scholtz, J. M. . (2003) in Purifying Proteins for Proteomics: A Laboratory Manual (Simpson, R. J., ed) pp. 535-566, Cold Spring Harbor Laboratory, Cold Spring Harbor, NY.

181. Kim, M. J., and Kao, C. (2001) Factors regulating template switch in vitro by viral RNA-dependent RNA polymerases: implications for RNA-RNA recombination, *Proc Natl Acad Sci U S A 98*, 4972-4977.

182. Chen, Y., and Barkley, M. D. (1998) Toward understanding tryptophan fluorescence in proteins, *Biochemistry 37*, 9976-9982.

183. Vivian, J. T., and Callis, P. R. (2001) Mechanisms of tryptophan fluorescence shifts in proteins, *Biophys J 80*, 2093-2109.

184. Sun, J. H., and Kao, C. C. (1997) Characterization of RNA products associated with or aborted by a viral RNA-dependent RNA polymerase, *Virology 236*, 348-353.

185. Pertzev, A. V., and Nicholson, A. W. (2006) Characterization of RNA sequence determinants and antideterminants of processing reactivity for a minimal substrate of Escherichia coli ribonuclease III, *Nucleic Acids Res 34*, 3708-3721.

186. Zhu, J., Gopinath, K., Murali, A., Yi, G., Hayward, S. D., Zhu, H., and Kao, C. (2007) RNA-binding proteins that inhibit RNA virus infection, *Proc Natl Acad Sci U S A 104*, 3129-3134.

187. Ma, H., Leveque, V., De Witte, A., Li, W., Hendricks, T., Clausen, S. M., Cammack, N., and Klumpp, K. (2005) Inhibition of native hepatitis C virus replicase by nucleotide and non-nucleoside inhibitors, *Virology 332*, 8-15.

188. Quinkert, D., Bartenschlager, R., and Lohmann, V. (2005) Quantitative analysis of the hepatitis C virus replication complex, *J Virol 79*, 13594-13605.

189. Burns, C. C., Lawson, M. A., Semler, B. L., and Ehrenfeld, E. (1989) Effects of mutations in poliovirus 3Dpol on RNA polymerase activity and on polyprotein cleavage, *J Virol 63*, 4866-4874.

190. Jennings, T. A., Chen, Y., Sikora, D., Harrison, M. K., Sikora, B., Huang, L., Jankowsky, E., Fairman, M. E., Cameron, C. E., and Raney, K. D. (2008) RNA unwinding activity of the hepatitis C virus NS3 helicase is modulated by the NS5B polymerase, *Biochemistry 47*, 1126-1135.

191. Zhang, C., Cai, Z., Kim, Y. C., Kumar, R., Yuan, F., Shi, P. Y., Kao, C., and Luo, G. (2005) Stimulation of hepatitis C virus (HCV) nonstructural protein 3 (NS3) helicase activity by the NS3 protease domain and by HCV RNA-dependent RNA polymerase, *J Virol 79*, 8687-8697.

192. Dick, F. A. (2007) Structure-function analysis of the retinoblastoma tumor suppressor protein - is the whole a sum of its parts?, *Cell Div 2*, 26.

193. Gibson, T. J., Thompson, J. D., Blocker, A., and Kouzarides, T. (1994) Evidence for a protein domain superfamily shared by the cyclins, TFIIB and RB/p107, *Nucleic Acids Res 22*, 946-952.

194. Lee, J. O., Russo, A. A., and Pavletich, N. P. (1998) Structure of the retinoblastoma tumour-suppressor pocket domain bound to a peptide from HPV E7, *Nature 391*, 859-865.

195. Tsai, C. H., Lee, P. Y., Stollar, V., and Li, M. L. (2006) Antiviral therapy targeting viral polymerase, *Curr Pharm Des 12*, 1339-1355.

196. Wu, J. Z., Yao, N., Walker, M., and Hong, Z. (2005) Recent advances in discovery and development of promising therapeutics against hepatitis C virus NS5B RNA-dependent RNA polymerase, *Mini Rev Med Chem 5*, 1103-1112.

197. Nomaguchi, M., Ackermann, M., Yon, C., You, S., and Padmanabhan, R. (2003) De novo synthesis of negative-strand RNA by Dengue virus RNA-dependent RNA polymerase in vitro: nucleotide, primer, and template parameters, *J Virol 77*, 8831-8842.

198. Li, Y., Korolev, S., and Waksman, G. (1998) Crystal structures of open and closed forms of binary and ternary complexes of the large fragment of Thermus aquaticus DNA polymerase I: structural basis for nucleotide incorporation, *EMBO J 17*, 7514-7525.

199. Asturias, F. J., Meredith, G. D., Poglitsch, C. L., and Kornberg, R. D. (1997) Two conformations of RNA polymerase II revealed by electron crystallography, *J Mol Biol 272*, 536-540.

200. Pikaard, C. S., Haag, J. R., Ream, T., and Wierzbicki, A. T. (2008) Roles of RNA polymerase IV in gene silencing, *Trends Plant Sci 13*, 390-397.

201. Honda, A., Mizumoto, K., and Ishihama, A. (1986) RNA polymerase of influenza virus. Dinucleotide-primed initiation of transcription at specific positions on viral RNA, *J Biol Chem 261*, 5987-5991.

202. Kao, C. C., and Sun, J. H. (1996) Initiation of minus-strand RNA synthesis by the brome mosaicvirus RNA-dependent RNA polymerase: use of oligoribonucleotide primers, *J Virol 70*, 6826-6830.

203. Nagy, P. D., and Pogany, J. (2000) Partial purification and characterization of Cucumber necrosis virus and Tomato bushy stunt virus RNA-dependent RNA polymerases: similarities and differences in template usage between tombusvirus and carmovirus RNA-dependent RNA polymerases, *Virology 276*, 279-288.

204. Piccininni, S., Varaklioti, A., Nardelli, M., Dave, B., Raney, K. D., and McCarthy, J. E. (2002) Modulation of the hepatitis C virus RNA-dependent RNA polymerase activity by the non-structural (NS) 3 helicase and the NS4B membrane protein, *J Biol Chem 277*, 45670-45679.

205. deHaseth, P. L., Zupancic, M. L., and Record, M. T., Jr. (1998) RNA polymerase-promoter interactions: the comings and goings of RNA polymerase, *J Bacteriol 180*, 3019-3025.

206. Hogbom, M., Jager, K., Robel, I., Unge, T., and Rohayem, J. (2009) The active form of the norovirus RNA-dependent RNA polymerase is a homodimer with cooperative activity, *J Gen Virol 90*, 281-291.

207. Ludtke, S. J., Baldwin, P. R., and Chiu, W. (1999) EMAN: semiautomated software for high-resolution single-particle reconstructions, *J Struct Biol 128*, 82-97.

208. Pettersen, E. F., Goddard, T. D., Huang, C. C., Couch, G. S., Greenblatt, D. M., Meng, E. C., and Ferrin, T. E. (2004) UCSF Chimera--a visualization system for exploratory research and analysis, *J Comput Chem 25*, 1605-1612.

209. Monie, T. P., Hernandez, H., Robinson, C. V., Simpson, P., Matthews, S., and Curry, S. (2005) The polypyrimidine tract binding protein is a monomer, *RNA 11*, 1803-1808.

210. Wittig, I., Braun, H. P., and Schagger, H. (2006) Blue native PAGE, *Nat Protoc 1*, 418-428.

211. Cramer, J., Jaeger, J., and Restle, T. (2006) Biochemical and pre-steady-state kinetic characterization of the hepatitis C virus RNA polymerase (NS5BDelta21, HC-J4), *Biochemistry 45*, 3610-3619.

212. Niesen, F. H., Berglund, H., and Vedadi, M. (2007) The use of differential scanning fluorimetry to detect ligand interactions that promote protein stability, *Nat Protoc 2*, 2212-2221.

213. Ludtke, S. J., Jakana, J., Song, J. L., Chuang, D. T., and Chiu, W. (2001) A 11.5 A single particle reconstruction of GroEL using EMAN, *J Mol Biol 314*, 253-262.

214. Murali, A., Li, X., Ranjith-Kumar, C. T., Bhardwaj, K., Holzenburg, A., Li, P., and Kao, C. C. (2008) Structure and function of LGP2, a DEX(D/H) helicase that regulates the innate immunity response, *J Biol Chem 283*, 15825-15833.

215. Sun, J., Duffy, K. E., Ranjith-Kumar, C. T., Xiong, J., Lamb, R. J., Santos, J., Masarapu, H., Cunningham, M., Holzenburg, A., Sarisky, R. T., Mbow, M. L., and Kao, C. (2006) Structural and functional analyses of the human Toll-like receptor 3. Role of glycosylation, *J Biol Chem 281*, 11144-11151.

216. Ma, Y., Shimakami, T., Luo, H., Hayashi, N., and Murakami, S. (2004) Mutational Analysis of Hepatitis C Virus NS5B in the Subgenomic Replicon Cell Culture, *J Biol Chem 279*, 25474-25482.

217. Weng, L., Du, J., Zhou, J., Ding, J., Wakita, T., Kohara, M., and Toyoda, T. (2009) Modification of hepatitis C virus 1b RNA polymerase to make a highly active JFH1-type polymerase by mutation of the thumb domain, *Arch Virol 154*, 765-773.

218. El-Hage, N., and Luo, G. (2003) Replication of hepatitis C virus RNA occurs in a membrane-bound replication complex containing nonstructural viral proteins and RNA, *J Gen Virol 84*, 2761-2769.

219. Hardy, R. W., Marcotrigiano, J., Blight, K. J., Majors, J. E., and Rice, C. M. (2003) Hepatitis C virus RNA synthesis in a cell-free system isolated from replicon-containing hepatoma cells, *J Virol 77*, 2029-2037.

220. Lai, V. C., Dempsey, S., Lau, J. Y., Hong, Z., and Zhong, W. (2003) In vitro RNA replication directed by replicase complexes isolated from the subgenomic replicon cells of hepatitis C virus, *J Virol 77*, 2295-2300.

221. Yang, G., Pevear, D. C., Collett, M. S., Chunduru, S., Young, D. C., Benetatos, C., and Jordan, R. (2004) Newly synthesized hepatitis C virus replicon RNA is protected from nuclease activity by a protease-sensitive factor(s), *J Virol 78*, 10202-10205.

222. Lyle, J. M., Bullitt, E., Bienz, K., and Kirkegaard, K. (2002) Visualization and functional analysis of RNA-dependent RNA polymerase lattices, *Science 296*, 2218-2222.

223. Pata, J. D., Schultz, S. C., and Kirkegaard, K. (1995) Functional oligomerization of poliovirus RNA-dependent RNA polymerase, *RNA 1*, 466-477.

224. Pathak, H. B., Ghosh, S. K., Roberts, A. W., Sharma, S. D., Yoder, J. D., Arnold, J. J., Gohara, D. W., Barton, D. J., Paul, A. V., and Cameron, C. E. (2002) Structure-function relationships of the RNA-dependent RNA polymerase from poliovirus (3Dpol). A surface of the primary oligomerization domain functions in capsid precursor processing and VPg uridylylation, *J Biol Chem 277*, 31551-31562.

225. Ahlquist, P., Wu, S. X., Kaesberg, P., Kao, C. C., Quadt, R., DeJong, W., and Hershberger, R. (1994) Protein-protein interactions and glycerophospholipids in bromovirus and nodavirus RNA replication, *Arch Virol Suppl 9*, 135-145.

226. Noueiry, A. O., Chen, J., and Ahlquist, P. (2000) A mutant allele of essential, general translation initiation factor DED1 selectively inhibits translation of a viral mRNA, *Proc Natl Acad Sci U S A 97*, 12985-12990.

227. Yi, G., Letteney, E., Kim, C. H., and Kao, C. C. (2009) Brome mosaic virus capsid protein regulates accumulation of viral replication proteins by binding to the replicase assembly RNA element, *RNA 15*, 615-626.

228. Tina, K. G., Bhadra, R., and Srinivasan, N. (2007) PIC: Protein Interactions Calculator, *Nucleic Acids Res 35*, W473-476.

229. Hobson, S. D., Rosenblum, E. S., Richards, O. C., Richmond, K., Kirkegaard, K., and Schultz, S. C. (2001) Oligomeric structures of poliovirus polymerase are important for function, *EMBO J 20*, 1153-1163.

230. Ranjith-Kumar, C. T., Murali, A., Dong, W., Srisathiyanarayanan, D., Vaughan, R., Ortiz-Alacantara, J., Bhardwaj, K., Li, X., Li, P., and Kao, C. C. (2009) Agonist and antagonist recognition by RIG-I, a cytoplasmic innate immunity receptor, *J Biol Chem 284*, 1155-1165.

231. Crooks, G. E., Hon, G., Chandonia, J. M., and Brenner, S. E. (2004) WebLogo: a sequence logo generator, *Genome Res 14*, 1188-1190.

232. Takeuchi, O., and Akira, S. (2009) Innate immunity to virus infection, *Immunol Rev 227*, 75-86.

233. Sikora, B., Chen, Y., Lichti, C. F., Harrison, M. K., Jennings, T. A., Tang, Y., Tackett, A. J., Jordan, J. B., Sakon, J., Cameron, C. E., and Raney, K. D. (2008) Hepatitis C virus NS3 helicase forms oligomeric structures that exhibit optimal DNA unwinding activity in vitro, *J Biol Chem 283*, 11516-11525.

234. Rajagopal, V., and Patel, S. S. (2008) Single strand binding proteins increase the processivity of DNA unwinding by the hepatitis C virus helicase, *J Mol Biol 376*, 69-79.

235. Jennings, T. A., Mackintosh, S. G., Harrison, M. K., Sikora, D., Sikora, B., Dave, B., Tackett, A. J., Cameron, C. E., and Raney, K. D. (2009) NS3 helicase from the hepatitis C virus can function as a monomer or oligomer depending on enzyme and substrate concentrations, *J Biol Chem 284*, 4806-4814.

236. Lee, H., Liu, Y., Mejia, E., Paul, A. V., and Wimmer, E. (2006) The C-terminal hydrophobic domain of hepatitis C virus RNA polymerase NS5B can be replaced with a heterologous domain of poliovirus protein 3A, *J Virol 80*, 11343-11354.

237. Li, X., McDermott, B., Yuan, B., and Goff, S. P. (1996) Homomeric interactions between transmembrane proteins of Moloney murine leukemia virus, *J Virol 70*, 1266-1270.

238. Chatterji, U., Bobardt, M., Lim, P., and Gallay, P. (2010) Cyclophilin A-Independent Recruitment of NS5A and NS5B Into HCV Replication Complexes, *J Gen Virol*.

239. Kim, S. J., Kim, J. H., Kim, Y. G., Lim, H. S., and Oh, J. W. (2004) Protein kinase C-related kinase 2 regulates hepatitis C virus RNA polymerase function by phosphorylation, *J Biol Chem 279*, 50031-50041.

240. Heck, J. A., Meng, X., and Frick, D. N. (2009) Cyclophilin B stimulates RNA synthesis by the HCV RNA dependent RNA polymerase, *Biochem Pharmacol 77*, 1173-1180.

APPENDIX I

Impaired Replication of Hepatitis C Virus Containing Mutations in a Conserved NS5B Retinoblastoma Protein-Binding Motif[▽]

David R. McGivern,[1] Rodrigo A. Villanueva,[1]† Sreedhar Chinnaswamy,[2]
C. Cheng Kao,[2] and Stanley M. Lemon[1]*

Center for Hepatitis Research, Institute for Human Infections and Immunity, and Department of Microbiology and Immunology,
University of Texas Medical Branch, Galveston, Texas 77555-0610,[1] and Department of Biology, Indiana University,
Bloomington, Indiana 47405-3700[2]

Hepatitis C virus (HCV) downregulates the retinoblastoma tumor suppressor protein (Rb), a central cell cycle regulator which is also targeted by oncoproteins expressed by DNA tumor viruses. HCV genome replication is also enhanced in proliferating cells. Thus, it is possible that HCV interactions with host cell cycle regulators, such as Rb, have evolved to modify the intracellular environment to promote viral replication. To test this hypothesis and to determine the impact of viral regulation of Rb on HCV replication, we constructed infectious viral genomes containing mutations in the Rb-binding motif of NS5B which ablate the ability of HCV to regulate Rb. These genomes underwent replication in transfected cells but produced variably reduced virus yields. One mutant, L314A, was severely compromised for replication and rapidly mutated to L314V, thereby restoring both Rb regulation and replication competence. Another mutant, C316A, also failed to downregulate Rb abundance and produced virus yields that were about one-third that of virus with the wild-type (wt) NS5B sequence. Despite this loss of replication competence, purified NS5B-C316A protein was two- to threefold more active than wt NS5B in cell-free polymerase and replicase assays. Although small interfering RNA knockdown of Rb did not rescue the replication fitness of these mutants, we conclude that the defect in replication fitness is not due to defective polymerase or replicase function and is more likely to result from the inability of the mutated NS5B to optimally regulate Rb abundance and thereby modulate host gene expression.

Chronic infection with hepatitis C virus (HCV) is associated with an increased risk for development of hepatocellular carcinoma (11). However, unlike most viruses associated with cancer, HCV has an RNA genome and an exclusively cytoplasmic life cycle. The precise mechanisms by which HCV infection leads to carcinogenesis are unclear. Although chronic inflammation is suspected to play a role, transgenic mice that express a low abundance of the entire HCV polyprotein do not exhibit hepatic inflammation and yet have an increased incidence of hepatocellular carcinoma (10). These data suggest that HCV proteins may have a direct oncogenic effect. Consistent with this, several structural and nonstructural proteins encoded by HCV (core, NS3, NS5A, and NS5B) have been shown to regulate host cell cycle regulators and tumor suppressor proteins, including p53 and the retinoblastoma protein (Rb) (7, 8, 14, 17; for a recent review, see reference 16).

Rb has many important functions in cell cycle control, including the repression of transcription factors needed for the transition from G_1/G_0 to S phase. Rb is targeted by a number of DNA oncoviruses, including adenovirus (27), simian virus 40 (3), and human papillomavirus (5). These small DNA viruses exploit host cell machinery to facilitate genome replication, and they encode oncoproteins that can sequester Rb or downregulate its abundance. This results in the release of the Rb-imposed repression of various transcription factors that are needed to express genes required for DNA replication, such as proliferating cell nuclear antigen and thymidine kinase (4). In this way, the DNA oncoviruses can induce expression of cellular genes that promote their replication. The regulation of Rb by these DNA viruses is likely to contribute substantially to their oncogenic potential.

Although HCV does not require the host DNA replication machinery to replicate its RNA genome, several in vitro observations suggest that HCV RNA replication and genome accumulation are enhanced in proliferating cells (19, 20, 26). This is an intriguing feature of HCV, since its primary target cell, the hepatocyte, is generally quiescent and, while very active metabolically, demonstrates very slow turnover in the noninfected liver. Our previous studies have shown that HCV has evolved a mechanism to downregulate the Rb protein. The HCV RNA-dependent RNA polymerase (RdRp), NS5B, interacts with Rb, targeting it for E6-associated protein-dependent ubiquitination and proteasomal degradation, thereby promoting cell cycle progression (17, 18). The interaction between NS5B and Rb thus represents an interesting parallel with the oncoproteins of DNA tumor viruses. Like many cellular and viral proteins, HCV NS5B interacts with Rb through a conserved Rb-binding motif (LxC/NxD) homologous to Rb-binding domains found in DNA virus oncoproteins (17, 18). Surprisingly, this Rb-binding motif overlaps with the Gly-Asp-Asp sequence in NS5B that coordinates the binding of divalent metals near the active site of the polymerase.

* Corresponding author. Mailing address: Center for Hepatitis Research, 6.200 Galveston National Laboratory, University of Texas Medical Branch, 301 University Blvd., Galveston, TX 77555-0610. Phone: (409) 747-6500. Fax: (409) 747-6514. E-mail: smlemon@utmb.edu.
† Present address: Programa de Virología, Instituto de Cs. Biomédicas (ICBM), Facultad de Medicina, Universidad de Chile, Santiago, Chile.
▽ Published ahead of print on 20 May 2009.

In order to better understand the role of Rb regulation in the HCV life cycle, we investigated the impact of mutations within the LxC/NxD motif of NS5B on HCV RNA replication and virus production. We show that viruses with mutations in the NS5B Rb-binding site are incapable of regulating Rb abundance and also variably impaired in replication fitness. Additional data suggest that the defect in replication fitness is not due to a direct loss of polymerase or replicase complex activity but may reflect the inability of these viruses to regulate Rb abundance and thereby modulate host gene expression.

MATERIALS AND METHODS

Cells. Human hepatoma Huh-7 cells and the Huh-7 derivatives Huh-7.5 and FT3-7 were cultured as described previously (28, 29).

Plasmid construction, HCV genome transfection, and virus production. Plasmid pHJ3-5, previously referred to as pH-NS2/NS3-J(Y361H/Q1251L) (29), carries a chimeric infectious HCV genome consisting of sequence encoding the structural proteins of the genotype 1a H77S virus within the background of the genotype 2a JFH-1 virus. This plasmid contains mutations in E1 (Y361H) and NS3 (Q1251L) that enhance virus production (13). The HCV genome carried by this plasmid was selected as the "wild-type" (wt) HCV for the purpose of this study and will be referred to as HJ3-5 in this study. For mutagenesis of the NS5B sequence, the JFH-1 sequence from nucleotide (nt) 8014 to the end of the genome was released from pHJ3-5 by digestion with HpaI and XbaI and the fragment was inserted into pUC20 at SmaI and XbaI sites in the polylinker. The resulting subclone served as a template for mutagenesis of NS5B using the QuikChange site-directed mutagenesis kit (Stratagene, La Jolla, CA). The mutated NS5B sequence was digested with SnaBI and XbaI and inserted back into similarly digested, full-length pHJ3-5. The sequences of mutated regions in the resulting plasmids were confirmed by direct DNA sequencing. Mutations were named with reference to the amino acid number of the JFH-1 NS5B protein.

HCV infectivity assay. HCV RNAs were transcribed in vitro using the Megascript T7 kit (Ambion, Austin, TX) and electroporated into cells, and cell culture supernatants containing infectious virus were harvested as described previously (29). The titer of infectious virus released from cells following RNA transfection or virus infection was determined using a focus-forming assay, as described previously (30). Briefly, 100-μl aliquots of cell culture supernatants were used to inoculate naïve Huh-7.5 cells seeded 24 h earlier in eight-well chamber slides at 4×10^4 cells/well. Cells were incubated at 37°C, 5% CO$_2$ and fed with 200 μl medium after 24 h. At 48 h after virus inoculation, cells were washed twice in 1× phosphate-buffered saline (PBS), fixed in methanol-acetone (1:1) for 9 min, and washed again with 1× PBS. Cells were then incubated for 3 h at 37°C with monoclonal antibody to the core protein (C7-50; Affinity Bioreagents, Golden, CO) diluted 1:500 in 3% bovine serum albumin (BSA)–1× PBS. Cells were washed three times in 1× PBS before incubation for 1 h at 37°C with 1:200 dilution of fluorescein isothiocyanate-conjugated goat anti-mouse immunoglobulin G (IgG) antibody (Southern Biotech, Birmingham, AL). Cells were washed three times in 1× PBS and mounted in Vectashield (Vectorlabs, Burlingame, CA).

Analysis of viral RNA replication and sequences of progeny viruses. Total RNA was extracted from transfected cells using the RNeasy mini kit (Qiagen, Valencia, CA) according to the manufacturer's instructions. Viral RNA abundance was measured by quantitative real-time reverse transcription PCR (qRT-PCR) as previously described (13). Primers DRM59 (GGGGCCGTTA ACCACATCAAGTCCGTG; corresponding to JFH-1 nt 8007 to 8032) and DRM61 (TGGCGCCCCAAGTTTTCTGAG; nt 9151 to 9131) targeting the NS5B region were used to amplify a fragment of approximately 1.1 kb containing the Rb-binding motif. RT-PCR products were sequenced directly.

Expression and purification of proteins. wt and mutant JFH-1 NS5B proteins were expressed in *Escherichia coli* and purified as described previously (24). Briefly, *E. coli* BL21(DE3) cells transformed with NS5B constructs in pET303 plasmids were grown in LB medium to an optical density at 600 nm of −1.0 and induced for expression by treatment with 1 mM IPTG (isopropyl-β-D-thiogalactopyranoside) for 24 h at 16°C. The cells were subsequently pelleted by centrifugation and lysed by sonication in buffer L (50 mM Tris [pH 7.6], 300 mM NaCl, 1 mM β-mercaptoethanol, 10% glycerol, 1 mM phenylmethylsulfonyl fluoride, and 20 mM imidazole). The clarified lysate was applied to a 1-ml His-Trap affinity purification column (GE Healthcare). The column was washed with the sample application buffer, and the bound proteins were eluted in the same buffer

containing 500 mM imidazole. The fractions containing the protein were pooled, and the salt concentration was adjusted to 100 mM before applying the sample onto poly(U)-agarose (Sigma, St. Louis, MO). The bound proteins were eluted in buffer A (20 mM Tris [pH 7.6], 10% glycerol, 3 mM dithiothreitol [DTT], and 1 mM phenylmethylsulfonyl fluoride) containing 400 mM NaCl. The proteins were subjected to sodium dodecyl sulfate-polyacrylamide gel electrophoresis (SDS-PAGE) along with known concentrations of BSA to determine the concentrations.

RdRp activity assays. RdRp assay mixtures contained 1 pmol of linear template RNA or 30 pmol of circular (C) template RNA and 0.04 μM of NS5B protein (2, 23). The assays were carried out in 20-μl reaction mixtures containing 20 mM sodium glutamate (pH 8.2), 0.5 mM DTT, 4 mM MgCl$_2$, 12, 0.5% (vol/vol) Triton X-100, 200 μM ATP and UTP, and 250 nM [α-^{32}P]CTP (MP Biomedicals). GTP was used at a final concentration of 0.2 mM unless specified. MnCl$_2$ was included in all the assay mixtures at a final concentration of 1 mM. Reaction mixes also contained 20 mM NaCl that came from the protein storage buffer. RNA synthesis reaction mixtures were incubated at 25°C for 60 min. The reactions were stopped by phenol-chloroform extraction, followed by ethanol precipitation of the RNA in the presence of glycogen and 0.5 M ammonium acetate. Products were separated by electrophoresis on denaturing (7.5 M urea) 20% polyacrylamide gels. Gels were wrapped in plastic, and quantification of radiolabeled bands was performed using a PhosphorImager (GE Healthcare).

Circularization of RNA. The protocol to circularize linear RNA was as described previously (23). Briefly, 2 nmol of a 16-mer linear RNA named "L" was incubated with T4 RNA ligase (Ambion, Austin, TX) according to the manufacturer's specifications for 3 h at 37°C in a 20-μl reaction mixture. An aliquot of the reaction mixture was run on a 20% polyacrylamide–7.5 M urea denaturing gel along with the linear RNA as a control. The gel was stained briefly in toluidine blue, and the RNA was visualized, showing a clear electrophoretic mobility difference between the linear (L) and the circularized (C) molecules (data not shown). The circularized RNA was excised from the gel, eluted using 0.3 M ammonium acetate overnight, and then purified by phenol-chloroform extraction and ethanol precipitation. The concentration of the RNA was measured by its absorbance at 260 nm.

Immunoblot analysis. Preparation of protein extracts, SDS-PAGE, and subsequent immunoblotting were done as described previously (18) using mouse monoclonal antibodies against β-actin (AC-15; Sigma, St Louis, MO), Rb (G3-245; BD Biosciences, San Jose, CA), and core (C7-50; Affinity BioReagents, Golden, CO); rabbit polyclonal antibodies against NS5B (A266-1 [Virogen, Watertown, MA] or, in replicase assays, ab35586 [Abcam, Cambridge, MA]) and β-tubulin (ab6046; Abcam, Cambridge, MA); and goat polyclonal antibodies against NS3 (ab21124; Abcam). The endoplasmic reticulum marker Rab1b was detected using rabbit polyclonal antibody G-20 (sc-599; Santa Cruz Biotechnology, Santa Cruz, CA). Immunoblots were visualized either by chemiluminescence or by direct detection of infrared fluorescence on an Odyssey infrared imaging system (Li-Cor, Lincoln, NE).

Indirect immunofluorescence microscopy. Infected or mock-infected cells were seeded onto glass chamber slides at 6×10^4 cells per well and allowed to grow for 24 h. Cells were washed twice with 1× PBS and fixed in methanol-acetone (1:1) at −20°C for 10 min. Fixative was removed and slides air dried in a fume hood for 1 h. For the images shown in Fig. 3C, cells were fixed in 4% paraformaldehyde for 30 min and permeabilized in 0.2% Triton X-100–1× PBS for 12 min. Cells were washed twice in 1× PBS before blocking for 1 h in 10% goat serum (Sigma, St. Louis, MO) in 1× PBS. The slides were then washed twice in 1× PBS and incubated overnight at 4°C with primary antibodies diluted in 1% BSA–1× PBS. A mouse monoclonal antibody was used to detect Rb (G3-245; BD Biosciences, San Jose, CA), and either a human polyclonal anti-HCV serum or a rabbit polyclonal antibody to NS5A (a gift from Craig Cameron) was used for detection of HCV antigens. Slides were washed three times for 10 min each in 1× PBS and incubated in darkness for 1 h at 37°C with secondary antibodies diluted in 1% BSA–1× PBS. Secondary antibodies were Alexa Fluor 488-conjugated goat anti-mouse IgG and Alexa Fluor 594-conjugated goat anti-rabbit IgG (Invitrogen, Carlsbad, CA) or Texas red-conjugated donkey anti-human IgG (Jackson Immunoresearch Laboratories, West Grove, PA). The slides were washed three times for 10 min each in 1× PBS, counterstained with DAPI (4',6'-diamidino-2-phenylindole), and mounted in Vectashield (Vectorlabs, Burlingame, CA). Fluorescence images were obtained using a Zeiss Axiophot II fluorescence microscope. Confocal fluorescence images were obtained using a Zeiss LSM 510 UV META laser-scanning confocal microscope in the University of Texas Medical Branch Infectious Disease and Toxicology Optical Imaging Core. Recorded digital images and related controls were uniformly enhanced for brightness and contrast using Photoshop CS2 (Adobe Systems, San Jose, CA).

Isolation of heavy membrane fractions containing HCV replication complexes. Heavy membrane fractions were isolated from cells infected with virus following electroporation of viral RNAs and from stable Huh-7 cell lines containing dicistronic, subgenomic genotype 1a or 2a HCV replicon RNAs. Cells were grown to 70 to 90% confluence, trypsinized, washed twice with PBS, and resuspended in hypotonic lysis buffer containing 10 mM HEPES (pH 7.9), 10 mM KCl, 5 mM DTT, and EDTA-free protease inhibitors (Roche, Mannheim, Germany). Cells were kept at 4°C for 20 min and disrupted by repetitive passage (40 times) through a 25-gauge needle. Nuclei were removed by centrifugation (1,000 × g, 10 min, 4°C). Postnuclear homogenates were centrifuged at 16,000 × g for 30 min at 4°C. Pellets of heavy membranes containing HCV replication complexes (P16) were resuspended in hypotonic buffer containing 10% glycerol and stored at −80°C.

Cell-free HCV RNA synthesis by membrane-bound replicase complexes. Aliquots of P16 fractions were incubated at 37°C for 3 h in standard transcription mixtures containing 50 mM HEPES (pH 7.9); 5 mM MgCl$_2$; 50 mM KCl; 10 mM DTT; 15 µg/ml actinomycin D; 1 mM spermidine; 800 U RNasin (Promega, Madison, WI) per ml; 1% dimethyl sulfoxide; 1 mM GTP, ATP, and UTP; 10 µM CTP; and 1 mCi of [α-^{32}P]CTP per ml. Total RNA was extracted using the RNeasy mini kit, precipitated with isopropanol, and resolved on a 1% agarose gel containing glyoxal (NorthernMax-Gly; Ambion, Austin, TX).

Gene knockdown by RNA interference. Small interfering RNAs (siRNAs) were purchased from Dharmacon (Lafayette, CO). An siRNA oligonucleotide SMARTpool, containing four siRNA oligonucleotides specific for the human retinoblastoma gene (L-003296-00), and four individual siRNAs (no. 5, 6, 7, and 9; D-003296-05, -06, -07, and -09, respectively) were used to target Rb. A pool of four siRNAs (D-001206-13) that are not specific for the Rb message and individual control siRNAs 1 and 2 (D-001230-01 and D-001220-01, respectively) were used as negative controls. For knockdown experiments, FT3-7 or Huh-7.5 cells were seeded at 30% confluence in six-well plates and transiently transfected with 50 nM siRNA using Lipofectamine 2000 (Invitrogen, Carlsbad, CA) according to the manufacturer's instructions. Duplicate transfections were used for either HCV infection or supertransfection with DNA plasmids and preparation of protein extracts for immunoblot analysis at 72 to 120 h after transfection.

Plasmid DNA transfection and reporter gene assays. FT3-7 cells were seeded at 6 × 10^4 cells per well in 48-well plates at 48 h following siRNA transfection. Cells were transfected with plasmid DNA using Lipofectamine 2000 according to the manufacturer's instructions. The reporter plasmids, pMAD2-Luc, p107-Luc (18), and pIFN-β-Luc (12) (a gift from John Hiscott), were used to transfect cells at 0.2 µg/well, together with pCMV-β-galactosidase at 0.1 µg/well. Cells were harvested at 48 h posttransfection and lysed in reporter lysis buffer (Promega, Madison, WI). Quantification of luciferase and β-galactosidase activities was accomplished with commercial enzyme assay kits according to the manufacturer's instructions (Promega, Madison, WI).

RESULTS

Replication competence of HCV mutants with substitutions in the Rb-binding domain of NS5B. The downregulation of Rb by HCV is dependent upon the viral RdRp, NS5B, which interacts with Rb through a conserved LxC/NxD motif near the active site of the polymerase (18). Since HCV RNA replication is enhanced in proliferating cells (20, 26), we hypothesized that the NS5B interaction with Rb may have evolved to create an intracellular environment permissive for viral replication. To test this hypothesis, we constructed a series of HCV genomes containing mutations in the conserved Rb-binding domain of NS5B within the background of a chimeric viral genome, HJ3-5 (here considered wt), encoding the nonstructural proteins of JFH-1 virus, which replicates efficiently in cell culture (Fig. 1A). The mutations were selected based on prior studies that demonstrated their ability to ablate NS5B binding to Rb (18). We examined the effect of the mutations on replication competence and infectious virus yield in viral RNA transfection and virus infection experiments. Huh-7 human hepatoma cells were electroporated with synthetic RNAs representing each of the mutated viral genomes. Cells were harvested and the supernatant fluids were collected at 96 h postelectroporation to

assess virus yield. Viral RNA abundance in cell lysates was determined by qRT-PCR (Fig. 1B), while the titer of infectious virus released from the cells was determined by a fluorescent-focus assay (Fig. 1C).

Four of the mutants contained single amino acid substitutions in NS5B, while one contained two substitutions (Fig. 1A). Since the Rb-binding domain overlaps with the divalent metal-coordinating Gly-Asp-Asp residues in the HCV RdRp (18), the mutations within the Rb-binding domain could also negatively influence polymerase activity. Indeed, viral RNA accumulation was reduced in cells infected with each of the five mutants, as determined by the qRT-PCR assay (Fig. 1B). The L314A mutant produced only 1/10 of the RNA abundance achieved by the wt RNA by 120 h after transfection, while replication of the double mutant, L314A/C316A, was severely compromised and resulted in no detectable increase in viral RNA in this assay (Fig. 1B). Consistent with these results, virus production was also reduced with each of the mutants (Fig. 1C), with the most dramatic reduction being observed with the L314A mutant and the double mutant, L314A/C316A. As expected, D318N, which is mutated in the NS5B active site, was unable to produce infectious virus. The C316A mutant, with a substitution in the center of the Rb-binding domain of NS5B, had the least effect on virus production, with virus yields averaging 33% of that from the parental wt RNA. This mutant was further examined in a multicycle infection analysis (Fig. 1D). Virus production by C316A-infected cells was reduced throughout the 144-h assay period compared to that by cells infected in parallel at the same multiplicity of infection (MOI) as the parental wt virus.

Viruses with mutations in the LxCxD domain do not downregulate Rb abundance. Previously, we have shown that ectopic expression of wt NS5B in human hepatoma cells results in an interaction of NS5B with Rb, targeting Rb for proteasome-dependent degradation in an E6-associated protein-dependent fashion (17, 18). In contrast, ectopic expression of mutant NS5B with substitutions in the LxCxE-like Rb-binding motif does not induce changes in Rb abundance (18). We have also shown that Rb is downregulated in HCV-infected Huh-7 cells (17). It was therefore of interest to determine whether HCVs with mutations in the Rb-binding motif of NS5B are able to downregulate Rb. We initially selected the C316A mutant for study, since it was the least impaired for replication and therefore most likely to be comparable to the parental wt virus in terms of the abundance of viral proteins expressed within infected cells. FT3-7 cells were infected at an MOI of 1 with either wt or C316A virus. After 3 days, the cells were trypsinized and seeded into eight-well chamber slides, and 1 day later they were fixed and immunostained for NS5A and Rb as described in Materials and Methods. NS5A was detected in almost all cells in both the wt- and C316A-infected cultures. Fluorescence microscopy demonstrated that Rb was sharply reduced in abundance in cells infected with wt virus but not in cells infected with the C316A mutant (Fig. 2A).

We also examined cells infected with wt, C316A, or L314A virus by confocal microscopy (Fig. 2B, left panel). Cells were infected at a low MOI (<0.01) and passaged for 8 days prior to fixation and antibody labeling of Rb and HCV antigens. While Rb was found to be predominantly nuclear in its localization in cells infected with each of these viruses, a substantial amount
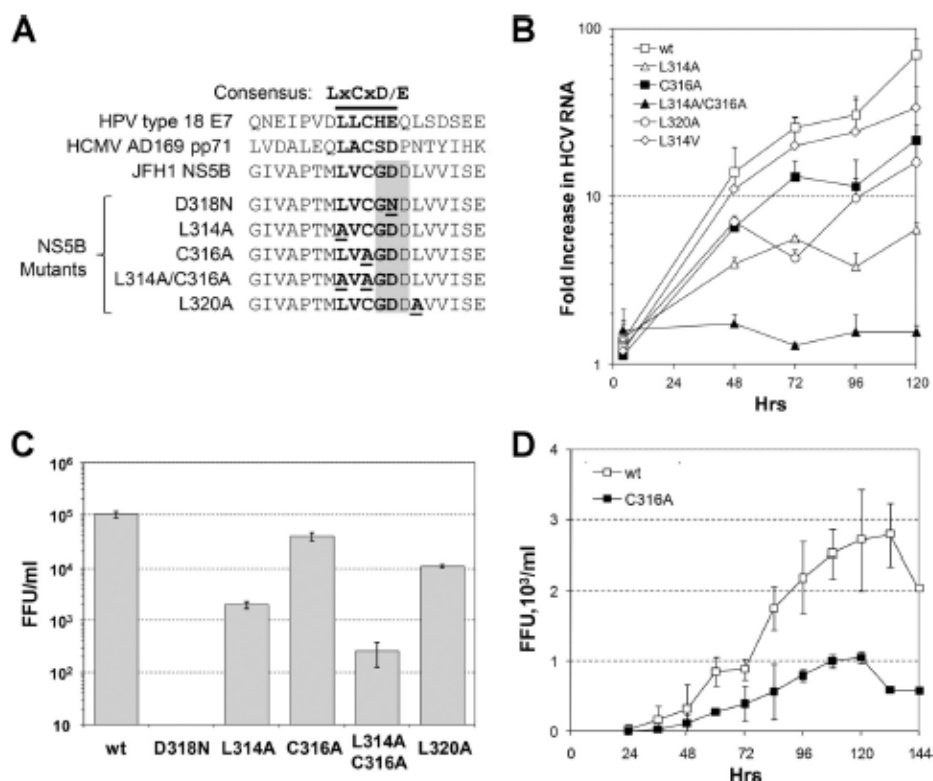
FIG. 1. Mutations in the Rb-binding motif of NS5B reduce RNA replication and replication of HCV. (A) Top, alignments of amino acids 307 to 325 of JFH-1 NS5B (present in the intergenotypic chimeric HJ3-5 virus used as the wt in these studies) and the Rb-binding domains of the E7 protein of human papillomavirus type 18 and pp71 of human cytomegalovirus strain AD169. The Rb-binding motif is shown in bold, while the overlying GDD motif in the NS5B polymerase is shaded. Bottom, amino acid sequences of the NS5B Rb-binding motif mutants used in this study. The mutated residues are underlined. (B) qRT-PCR analysis of HCV RNA accumulated in FT3-7 cells. The cells were transfected with wt HJ3-5 transcript or mutant derivatives as shown and harvested for analysis after 4, 48, 72, 96, and 120 h. Results are shown as the fold increase in viral RNA abundance relative to the replication-incompetent D318N RNA, which was transfected in parallel. (C) Infectious virus released by RNA-transfected FT3-7 cells. Serial dilutions of cell culture supernatant fluids (harvested from FT3-7 cells 96 h after the initial transfection with wt or mutant transcripts) were used to inoculate naïve Huh-7.5 cells. Cells expressing HCV core protein were detected by immunofluorescence analysis, and infectious foci were counted to determine the number of focus-forming units (FFU) per ml. The limit of detection in this assay is 10 FFU/ml. (D) The growth kinetics of mutant C316A were compared to those of the wt in a multicycle infection assay. FT3-7 cells were infected with wt or C316A virus at an MOI of 0.05. Cell culture supernatants were collected every 12 h from 24 to 144 h postinfection. Infectious virus release was measured as described for panel C. Results shown represent the means and standard deviations from three independent infections.

of Rb could be detected within the cytoplasm of many cells infected with the wt virus (Fig. 2B). This finding is consistent with previous observations demonstrating the cytoplasmic accumulation of Rb in cells expressing NS5B, a phenomenon that is enhanced by inhibition of the proteasome and is likely to be due to the trapping of Rb in cytoplasmic complexes with NS5B (17). Importantly, this abnormal, partially cytoplasmic distribution of Rb was never observed in mock-infected cells or in cells infected with the L314A or C316A virus, in which Rb was detected exclusively within the nucleus.

Immunoblots of cell lysates confirmed the downregulation of Rb in cells infected with wt virus and the lack of an effect on Rb abundance in cells infected with the C316A mutant (Fig. 2C). Importantly, the absence of downregulation of Rb in the C316A-infected cells could not be attributed to reduced ex-

pression of NS5B, as the abundances of NS5B in the wt and C316A-infected cells were comparable by 120 h after infection (Fig. 2C). Thus, consistent with previous results from experiments involving ectopic expression of NS5B (18), mutations that ablate the Rb-binding motif in NS5B result in infectious viruses that can no longer downregulate Rb abundance.

Stability of the LxCxD domain mutants. To assess the stability of the C316A mutation, total RNA was isolated from cells at 96 h after transfection with the mutant genome and used as template to amplify a 1.1-kb fragment of the NS5B-coding region (nt 8007 to 9151 of the JFH-1 virus; GenBank accession no. AB047639). The sequence of this fragment retained the engineered mutation and contained no additional changes (data not shown). The stabilities of the other mutations engineered in the Rb-binding domain were also exam-
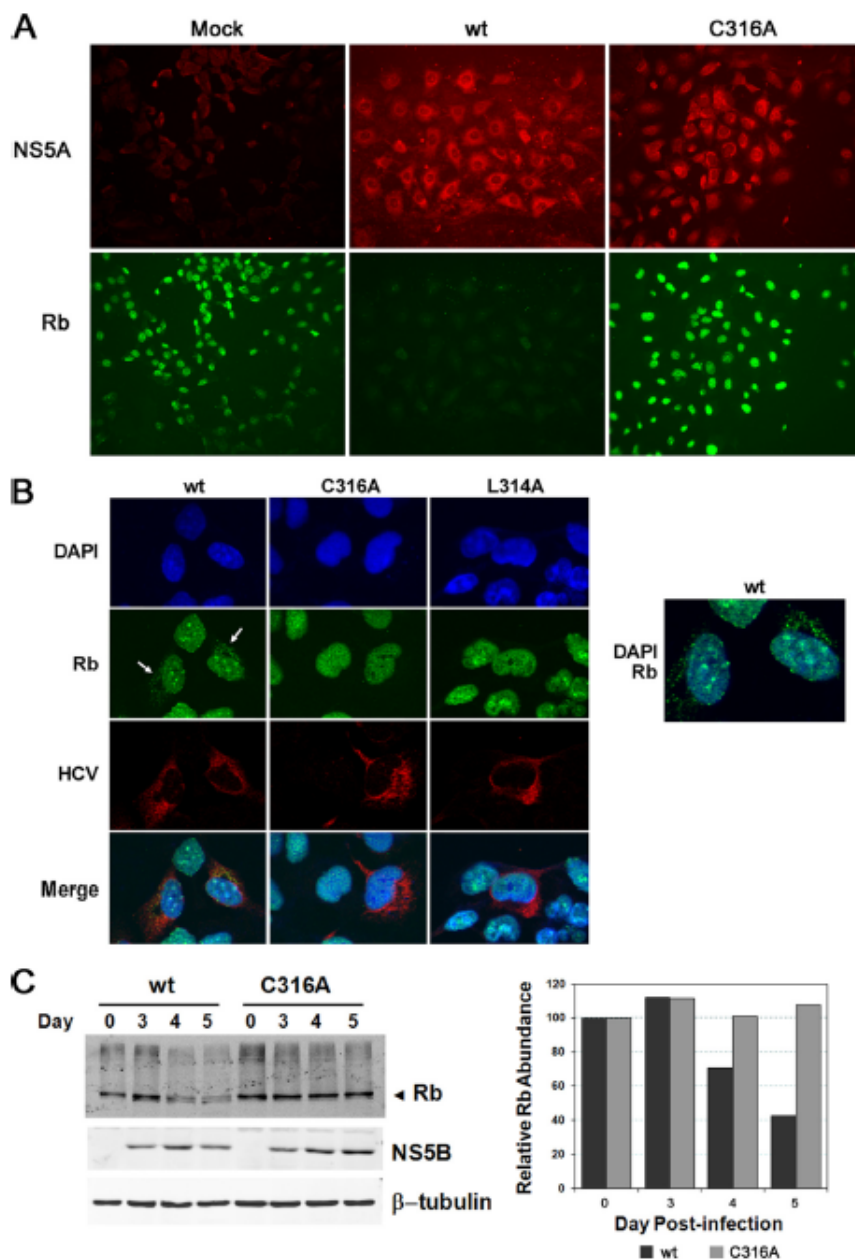
FIG. 2. Analysis of Rb abundance in cells infected with either wt or LxCxD domain mutant viruses. (A) Immunofluorescence analysis of cells infected with wt or C316A virus. FT3-7 cells were infected at an MOI of 1 and incubated for 4 days. Infected cells were fixed and immunostained for NS5A and Rb. (B) Laser-scanning confocal microscopy of cells infected with wt, C316A, and L314A viruses. Left panel, cells were labeled with a murine anti-Rb MAb (green) or human polyclonal anti-HCV sera (red). Nuclei were labeled with DAPI. The arrows indicate the presence of cytoplasmic Rb in cells infected with wt virus, a phenomenon not observed in uninfected cells or cells infected with mutant virus. Right panel, expanded view of the wt virus-infected cells showing merged DAPI and Rb images with cytoplasmic Rb. (C) Infrared immunoblot analysis of Rb in lysates from cells infected with wt or C316A virus. Left panel, cells were infected at an MOI of 1 to 2, and lysates collected on the day indicated postinfection were analyzed by immunoblotting using antibodies specific for Rb, NS5B, and β-tubulin (loading control). Right panel, quantitation of the infrared immunoblot, showing the abundance of Rb relative to β-tubulin at various times following infection with the wt or C316A virus.
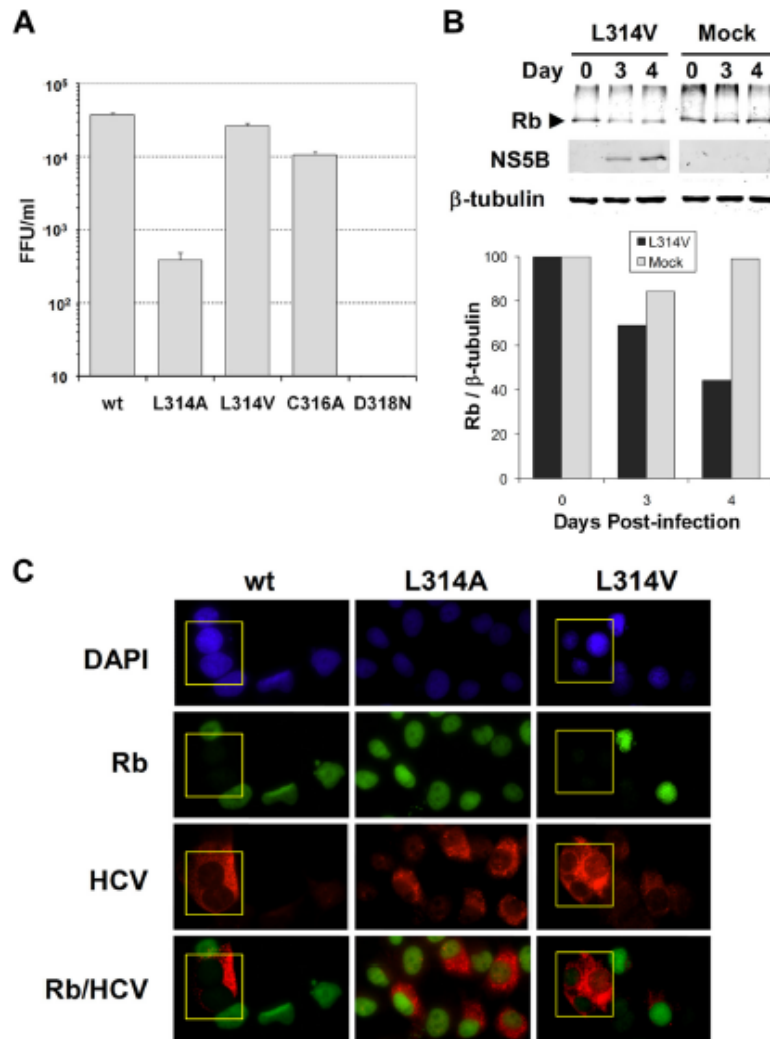
FIG. 3. Analysis of a partial revertant of the L314A mutant. (A) Virus released into cell culture medium following transfection with HJ3-5, L314A, L314V, C316A, or D318N RNA. Error bars indicate standard deviations. FFU, focus-forming units. (B) Infrared immunoblot analysis of Rb in lysates from cells infected with L314V. Left panel, cells were infected with L314V or mock infected, and lysates collected on the indicated day postinfection were analyzed by immunoblotting using antibodies specific for Rb, NS5B, and β-tubulin (loading control). Right panel, quantitation of the infrared immunoblot, showing the abundance of Rb relative to β-tubulin at the indicated time points. (C) Immunofluorescence analysis of cells infected with HJ3-5, L314A, or L314V. Huh-7.5 cells were infected at an MOI of 0.1 and incubated for 4 days before fixation and staining for Rb or NS5A.

ined over several passages of cell-free virus mutants. With the exception of L314A, each of the mutations was stable for at least three passages after electroporation. In cells infected with the L314A mutant, an Ala-to-Val change was detectable by passage 1 and became present in the majority of the viral sequences examined by passage 2 (data not shown). This new mutant contained a single nucleotide transition (C to T) at nt

8607. In order to determine the effect of the L314V mutation on virus production, it was reconstructed within the wt genome. In FT3-7 cells, the yield of L314V virus was approximately 50% of that of the wt virus, representing a dramatic increase in yield compared to L314A virus (~1%) (Fig. 3A). The L314V virus yield was consistently greater than that obtained with the C316A virus in three independent experiments,

although the differences in the yields of these two mutants were modest. Consistent with these results, L314V RNA accumulation was greater than that of C316A but lower than that of the wt when measured by qRT-PCR (Fig. 1B). These data suggest that the selection of the Ala-to-Val mutation in cells infected with the L314A mutant was due to the enhanced replication efficiency of the L314V virus.

To determine whether the L314V revertant had regained the ability to regulate Rb, we assessed Rb abundance in Huh-7.5 cells at 3 or 4 days after infection with the virus. Compared with that in mock-infected cells, Rb abundance was downregulated in immunoblots of lysates from L314V-infected cells (Fig. 3B). This was confirmed by fluorescence microscopy of cells infected at a low MOI with the L314A mutant, L314V revertant, or wt virus. These studies revealed substantial decreases in nuclear Rb abundance in most cells infected with the wt or L314V virus, while no difference in the nuclear Rb signal was apparent in cells infected with L314A or in noninfected cells adjacent to those infected with wt or L314V virus (Fig. 3C). Some L314V-infected cells showing weak HCV antigen expression appeared to retain a normal nuclear Rb abundance, but in aggregate these data indicate that the L314V revertant had at least partially regained the ability to downregulate Rb.

Mutations that ablate Rb binding do not necessarily impair RdRp activity. It was important to determine whether the mutations in NS5B affected polymerase activity directly or acted in an indirect fashion to impair replication of the virus through the failure of the LxCxD motif mutants to modulate Rb abundance. To address this question, we purified bacterially expressed wt and mutant NS5B proteins and compared their activities in an in vitro polymerase assay.

The wt JFH-1 NS5B, which is identical to that in the wt HJ3-5 virus, was expressed without the C-terminal 21 residues (named J-Δ21). Four derivatives with mutations as described above, i.e., L314A, L314V, C316A, and the double mutant L314A/C316A, were purified to ~ 90% homogeneity (Fig. 4A) after separation on an Ni-nitrilotriacetic acid column and a poly(U) column. The L320A mutant could not be purified from the *E. coli* proteins despite repeated attempts and was not analyzed further. The RNA synthesis activities of the four proteins were first assessed using a 19-nt linear RNA template named LE19. LE19 was designed to report on four distinct activities of the HCV RdRp (Fig. 4B, top): RNA synthesis by de novo initiation (generating a 19-nt RNA product), terminal nucleotide addition (generating 20- and 21-nt RNAs), extension from a primed template (generating a 32-nt RNA that is formed from a partial duplex of two LE19 molecules), and generation of a template switch product (of 38 nt and sometimes longer) (9, 22, 24). J-Δ21 has all four of the activities, which have been previously documented for the genotype 1b RdRp (25) (Fig. 4C, lane 1). In the absence of GTP, the putative initiation nucleotide, the de novo initiation product decreased more severely than the primer extension product, which does not require GTP with the LE19 template (Fig. 4C, lane 3).

Reproducible results were obtained with the L314A, L314V, C316A, and L314A/C316A mutants in five independent assays (Fig. 4D). The results revealed that the C316A mutant produced higher levels of both the de novo-initiated product and the primer extension product than the wt J-Δ21 protein. The L314A mutant had slightly lower RNA synthetic activity than

the wt protein, while the double mutant, L314A/C316A, which demonstrated a severely debilitated replication phenotype (Fig. 1B and C), was severely defective in RNA synthesis in vitro (Fig. 4C, lanes 21 to 23). Thus, while it is apparent that some mutations in the Rb-binding domain cause reduced polymerase activity, this is not true for all mutants. The results obtained with the C316A mutant demonstrate in particular that the Rb-binding function of NS5B is not important for polymerase activity.

We challenged the RdRps with two additional templates to assess whether the mutations may have caused more subtle defects. First, each RdRp was tested with the template LE19p, which has a puromycin covalently linked to the 3′-terminal hydroxyl of LE19, thus rendering it competent for de novo initiation but not primer extension. With the LE19P template, J-Δ21 and each of the mutant RdRps with single amino acid substitutions retained the ability to initiate RNA synthesis by the de novo mechanism (Fig. 4C, lanes 2, 7, 12, and 17). The L314A/C316A mutant was inactive. Next, we assessed the ability of the HCV RdRp to direct RNA synthesis from linear (L) or circular (C) 16-nt templates. Since a circularized template cannot thread a 3′ terminus into the RdRp active site, this template can be recognized only by the RdRp in an open conformation, which then closes for initiation (2). Again, both the wt J-Δ21 and the mutant proteins with single amino acid substitutions retained the ability to generate products, while L314A/C316A was far less active (Fig. 4C, lanes 5, 10, 15, 20, and 25). The products generated from a circularized RNA were different than those from the linear version of the same RNA, demonstrating that the J-Δ21 RdRp can undergo a transition between the open and closed conformations (2). Thus, with respect to each of the NS5B activities that we assessed in these experiments, mutations that disrupt the interaction of NS5B with Rb do not necessarily have a negative effect on RNA synthesis in vitro.

Effects of Rb-binding site mutations on HCV replicase activity. The finding that the C316A mutant was approximately twice as active in RNA synthesis in vitro was unexpected, given that the virus carrying this mutation is impaired for replication (Fig. 1B) and produces less virus in either RNA-transfected or virus-infected cells (Fig. 1C and D). Therefore, we compared RNA synthesis in cell-free reaction mixtures containing replicase complexes isolated from wt or C316A virus-infected cells. For these experiments, FT3-7 cells were electroporated with wt or C316A genomic RNA and passaged until they were 70 to 90% infected as judged by immunofluorescence detection of core antigen. Cells transfected with the replication-incompetent D318N genomic RNA were passaged in parallel as a control. We sequenced viral RNA extracted from the cells and confirmed that neither the wt nor the C316A virus had acquired mutations in the NS5B-coding region during passage. The cells were then harvested, and heavy membrane fractions containing HCV replicase complexes were isolated in order to measure replicase activity (Fig. 5A), as described in Materials and Methods. In this assay, the viral RNA polymerase uses endogenous viral RNA as template. For comparison between the different heavy membrane preparations, [^{32}P]CTP incorporation into RNA was assessed quantitatively by PhosphorImager analysis (Fig. 5B) and then normalized to NS5B abundance as determined in immunoblots (Fig. 5C). As
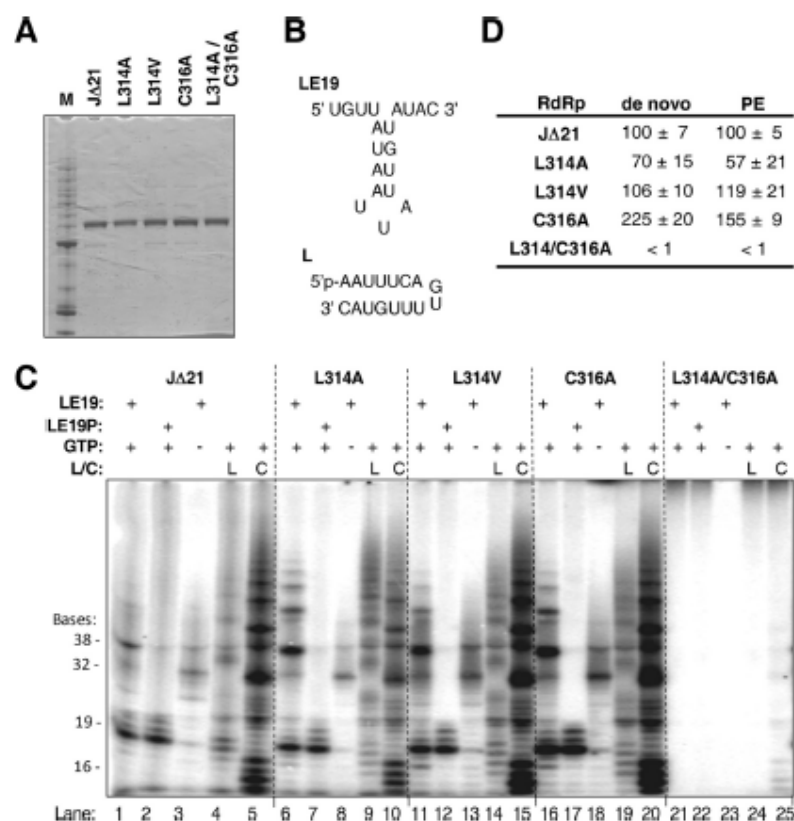
A

M JΔ21 L314A L314V C316A L314A/C316A

B

LE19
5' UGUU AUAC 3'
        AU
        UG
        AU
        AU
   U   A
        U

L
5'p-AAUUUCA G
3' CAUGUUU U

D

RdRp	de novo	PE
JΔ21	100 ± 7	100 ± 5
L314A	70 ± 15	57 ± 21
L314V	106 ± 10	119 ± 21
C316A	225 ± 20	155 ± 9
L314/C316A	< 1	< 1

C

	JΔ21	L314A	L314V	C316A	L314A/C316A

LE19:   +   +   +   +   +   +   +   +   +   +
LE19P: +   +   +   +   +
GTP: + + - + +   + + - + +   + + - + +   + + - + +   + + - + +
L/C: L C   L C   L C   L C   L C

Bases:
38 -
32 -
19 -
16 -

Lane: 1 2 3 4 5 6 7 8 9 10 11 12 13 14 15 16 17 18 19 20 21 22 23 24 25

FIG. 4. Effect of mutations in NS5B on RNA synthesis in vitro. (A) SDS-PAGE of the purified proteins. The proteins were expressed in *E. coli* and purified through two affinity columns (see Materials and Methods). Lane M contains the Benchmark protein molecular weight marker (Invitrogen). (B) Sequence of template LE19, which can direct de novo-initiated RNA synthesis by NS5B. LE19 can also form a partially duplexed dimer that can direct primer extension to result in a 32-nt product. The single-stranded RNA named "L" is the molecule that can be ligated to form the circularized RNA named "C" (see text for additional details on templates). (C) Autoradiograph of the products of an RdRp assay run on a 20% polyacrylamide–7.5 M urea denaturing gel. The templates used are specified above each lane, and the GTP, where present, is at a 0.2 mM final concentration. The sizes of the RNA products are denoted at the left. (D) Quantification of the de novo initiation (19-nt) and primer extension (PE) (32-nt) products of the RdRp assay using LE19 as template. Four replicate reactions were used to quantify the products; results are shown as means ± standard deviations. Both the de novo initiation and primer extension products generated by all the mutant polymerases were normalized to that of the wt, whose activity was set at 100%.

an additional measure of nonstructural protein abundance in these replicase preparations, we also analyzed immunoblots for NS3 protein (Fig. 5C). In three experiments, the replicase complexes from cells transfected with the C316A mutant synthesized an average of 2.21-fold (±0.48-fold) more labeled product than replicase complexes from the wt RdRp (Fig. 5A and B), consistent with the enhanced in vitro synthetic activity of the recombinant C316A protein described above (Fig. 4C). The increased activity of the C316A mutant relative to the wt was evident across the range of protein concentrations tested in the cell-free reaction (Fig. 5B). As expected, there was no RNA synthesis by heavy membrane fractions prepared from D318N-transfected cells.

Effects of Rb knockdown on HCV infection. The results obtained thus far indicated that NS5B mutations that ablate the interaction with Rb do not necessarily reduce the ability of the enzyme to direct HCV RNA synthesis. Given that the same mutations impair HCV RNA replication and virus production, we hypothesized that the lack of regulation of Rb might in some way limit the efficiency of virus replication. To test this, we used RNA silencing to knock down the intracellular abundance of Rb and then examined the impact of this on replication of the virus. Transfection of FT3-7 cells with a pool of siRNAs targeting Rb led to undetectable levels of Rb when assessed by immunoblotting 3 to 5 days later (Fig. 6A). Surprisingly, however, analysis of the culture medium from cells infected with wt or C316A virus (MOI of 2) at 3 days after siRNA knockdown of Rb revealed a modest decrease, and not an increase, in the yields of both wt and C316A viruses compared to cells treated with control siRNAs (Fig. 6B). A similar
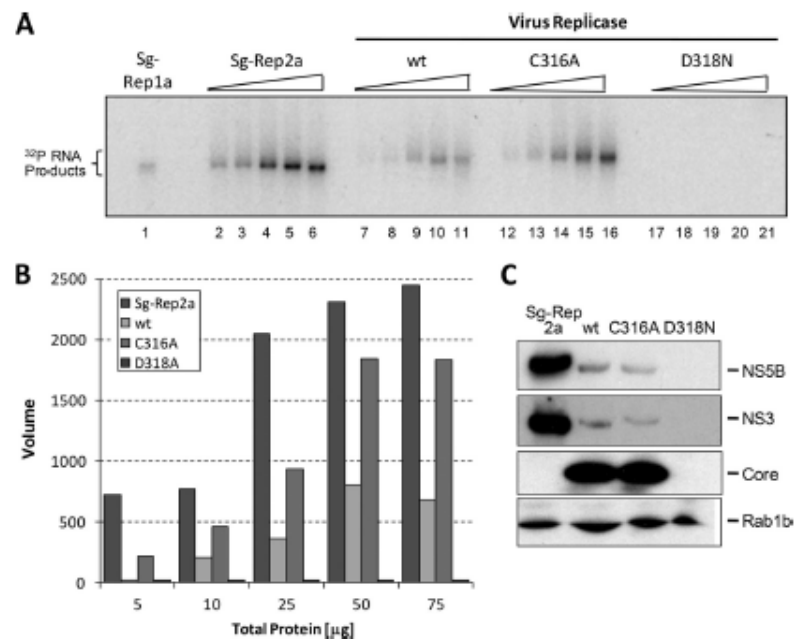
FIG. 5. In vitro RNA synthesis assay from heavy membrane fractions containing functional HCV replication complexes. (A) Heavy membrane fractions isolated from cells infected with wt or C316A virus, or mock-infected cells, were incubated in a transcription reaction mixture containing α-^{32}P-labeled CTP. Heavy membrane fractions from genotype 1a and 2a subgenomic replicon-bearing cell lines (Sg-Rep) were included as positive controls. Labeled products were resolved on a denaturing agarose gel and visualized by autoradiography. (B) Quantification of products from panel A by PhosphorImager analysis. (C) Immunoblot analysis of HCV proteins NS3, NS5B, and core in the heavy membrane fractions used for panel A. The blots were also probed for Rab1b, an endoplasmic reticulum marker, as a loading control for the heavy membrane fractions.

experiment was performed using four individual siRNAs targeting Rb and two nontargeting control siRNAs. Again, cells transfected with siRNAs targeting Rb demonstrated a negligible abundance of Rb compared to the control siRNA-transfected cells at 4 days posttransfection (Fig. 6C). With three of the four siRNAs, the virus yield was reduced ~50% compared to that for control siRNA-transfected cells, although one of the Rb-specific siRNAs caused a ~90% reduction in virus yield (Fig. 6D, no. 9). Similar results were obtained in three independent experiments.

As an alternative experimental strategy, cells were first infected at an MOI of 0.1 with wt, C316A, or L320A virus, and the cells were grown for 7 days prior to transfection with either the pool of siRNAs specific for Rb or the pool of nontargeting control siRNAs. Cell culture supernatants were harvested at 3 days after transfection with siRNA (10 days postinfection), and the titer of virus released from the cells was determined. Immunoblots of cell lysates confirmed efficient knockdown of Rb as before (data not shown). Again, for each of the three viruses, the amount of virus released from cells transfected with Rb-specific siRNAs was lower than that from cells transfected with the nontargeting control siRNAs (Fig. 6E).

To further examine the effect of Rb gene knockdown on HCV replication, we determined the effect of Rb knockdown on the spread of HCV infection in Huh-7.5 cells. Cells were infected with serial dilutions of the wt virus at 3 days after

transfection with Rb-specific or control siRNAs and then analyzed 3 days later for the number and size of foci of infected cells identified by core protein-specific immunofluorescence. Immunoblotting confirmed efficient knockdown of Rb (Fig. 7A). Consistent with the results shown in Fig. 6, Rb knockdown resulted in a reduction in the number of infectious foci to less than 50% of that developing in control cells (Fig. 7B). Furthermore, foci of infected cells were approximately 50% smaller in the cells in which Rb expression had been silenced, compared with cells transfected with control siRNA (Fig. 7C).

To confirm that siRNA-mediated Rb knockdown had, as expected, resulted in activation of E2F-responsive promoters in these experiments, we determined the activities of two cellular promoters that are subject to Rb regulation using luciferase reporter assays. The promoters for MAD2 and p107 are both suppressed by Rb through an inhibitory effect of the tumor suppressor on E2F transcription factors (18). Consistent with this, MAD2 and p107 promoter activities were increased by 3.4- and 2-fold, respectively, in cells transfected with Rb-targeting siRNA compared to cells transfected with control siRNA (data not shown). Furthermore, we did not observe an effect on the beta interferon promoter with either siRNA, consistent with the absence of a major effect of Rb on this promoter. These results confirm that the siRNAs used in these experiments were effective in downmodulating both Rb abundance and Rb function.
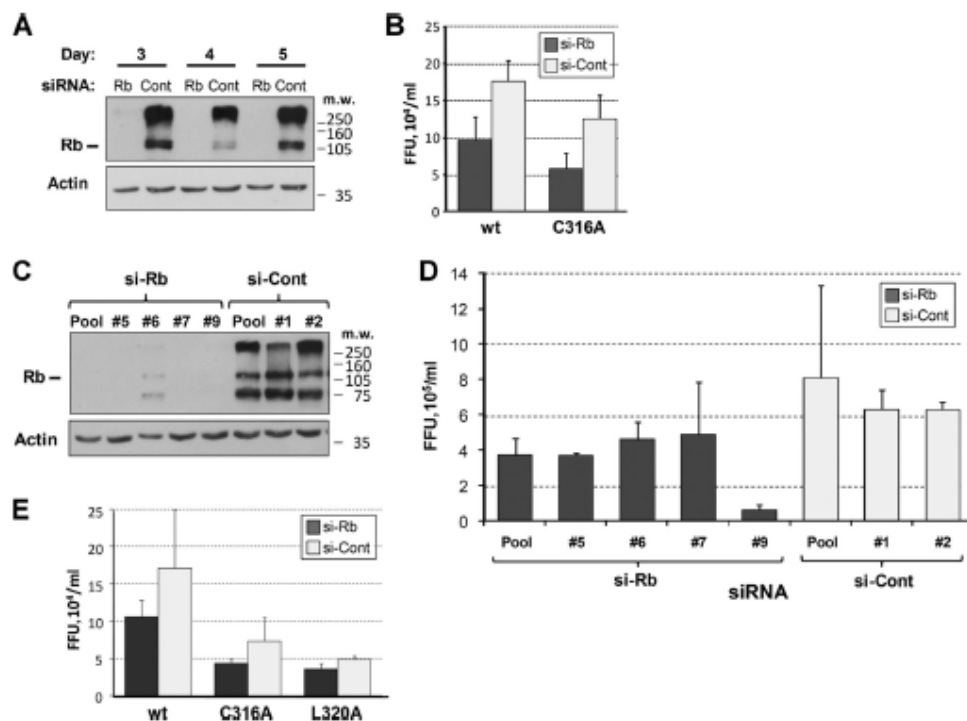
FIG. 6. Effects of Rb knockdown by siRNA on virus replication. (A) Immunoblot analysis of lysates from FT3-7 cells transfected with a pool of siRNAs targeting Rb or pooled control siRNAs. Rb was efficiently knocked down to undetectable levels at 3, 4, and 5 days post transfection (top). The same blot was also probed for actin as a loading control (bottom). (B) FT3-7 cells transfected with a pool of siRNAs targeting Rb or a similar pool of control siRNAs were infected with either wt or C316A virus at 3 days posttransfection at an MOI of 2. Cell culture supernatants were harvested at 2 days postinfection. Virus released into supernatant fluids of infected cells was determined. Immunoblot analysis of protein from a parallel transfection performed at the same time is shown in panel A. (C) Immunoblot analysis of lysates from FT3-7 cells transfected with individual siRNAs targeting Rb or nonspecific control siRNAs. Lanes: 1, Rb siRNA pool; 2, Rb siRNA no. 5; 3, Rb siRNA no. 6; 4, Rb siRNA no. 7; 5, Rb siRNA no. 9; 6, control siRNA pool; 7, control siRNA no. 1; 8, control siRNA no. 2. (D) FT3-7 cells transfected with various siRNAs for Rb or control siRNAs were infected with wt HJ3-5 virus at 3 days posttransfection at an MOI of 2. Infectious virus in cell culture supernatants was quantitated by focus-forming assay. Immunoblot analysis of protein from a parallel transfection performed at the same time is shown in panel C. (E) FT3-7 cells were infected with either wt, C316A, or L320A virus at an MOI of 0.1. At 6 dpi, cells were seeded into six-well plates and transfected with a pool of siRNAs specific for Rb or pooled control siRNAs. At 10 days postinfection, cell culture supernatants were harvested from the transfected cells and virus titers were determined. Error bars indicate standard deviations. FFU, focus-forming units.

Overall, these studies indicate that siRNA-mediated Rb knockdown reduces HCV replication in Huh-7 cells, despite the fact that NS5B interacts with Rb and targets it for degradation in infected cells (17, 18). There are several possible explanations that may account for this apparent paradox, as discussed below.

DISCUSSION

The HCV RdRp, NS5B, interacts with and downregulates the cellular abundance of Rb, an important tumor suppressor and cell cycle regulator (18). Here, we have shown that viruses containing mutations in NS5B that disrupt the Rb-binding motif are impaired for replication in cultured Huh-7 hepatoma cells (Fig. 1B and C). Importantly, we have also shown that the loss of fitness was not necessarily accompanied by reduced

RdRp function in cell-free RNA synthesis assays. The discordant changes that we observed in the viral fitness and RdRp activities of these NS5B LxCxD domain mutants suggest that the Rb-binding activity of NS5B is not required for polymerase function per se but rather that the regulation of Rb by NS5B may have evolved as a mechanism to orchestrate cellular gene expression in such a manner as to create an intracellular environment that is conducive to HCV replication. We attempted to demonstrate this by assessing the impact of siRNA-mediated knockdown of Rb on the replication of two Rb-binding mutants (C316A and L320A), but we found that this reduced rather than enhanced replication fitness (Fig. 6). Thus, although we believe that a role in modulating cellular gene expression remains the most likely explanation for the regulation of Rb by HCV, there is no simple, straightforward relationship between Rb abundance and viral replication fitness.
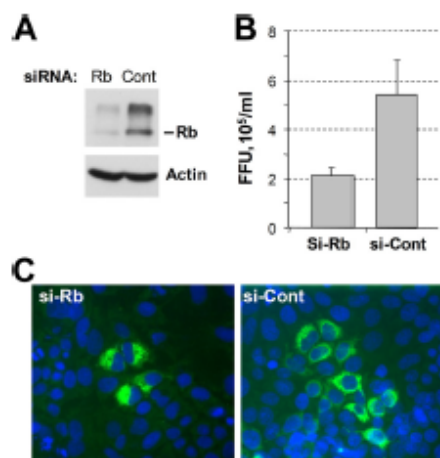
FIG. 7. (A) Immunoblot analysis of lysates from Huh-7.5 cells transfected with a pool of siRNAs targeting Rb or pooled control siRNAs. Cells were harvested at 3 days posttransfection. Parallel transfections were trypsinized, seeded into eight-well chamber slides after 2 days (4×10^4 cells per well), and infected with serial dilutions of wt HJ3-5 virus at 3 days posttransfection. Cells were fixed and stained for core antigen at 2 days postinfection. (B) The number of focus-forming units (FFU) counted on cells transfected with control siRNAs was greater than twofold higher than that on cells transfected with Rb-specific siRNAs. Error bars indicate standard deviations. (C) Examples of foci are shown to demonstrate the size of foci.

Role of the Rb-binding site in NS5B. Since the LxCxE-like motif overlaps with the GDD active-site motif of NS5B, it was important to examine whether mutations in the LxCxD motif directly affect NS5B activity. To do this, we first measured RNA synthesis in vitro by bacterially expressed wt and mutant NS5B proteins. Although C316A virus was moderately impaired in replication competence (Fig. 1B and C), the NS5B-C316A RdRp was twice as active and retained all of the in vitro activities of the wt NS5B protein (Fig. 4). We also examined RNA synthesis by fully formed membrane-bound replicase complexes extracted from virus-infected cells and confirmed that replicase containing NS5B with the C316A substitution was at least as active (if not more active) for RNA synthesis as the JFH-1 replicase from the parental wt virus used in these studies (Fig. 5). These results confirm that Rb binding is not directly important for NS5B polymerase activity and thus has evolved for other reasons. A very likely scenario is that NS5B may function in two or more populations: one that participates in RNA synthesis as part of the replicase and a second that regulates cellular processes, including the abundance of Rb. This is consistent with estimates from biochemical studies that only a small proportion of NS5B is actively engaged in RNA synthesis in HCV replicon cells (21).

The genomes of each of the LxCxD domain mutants that we constructed contained two or more nucleotide changes from the wt RNA sequence. As a result, they were generally stable and did not revert to the wt sequence on passage. However, the L314A mutant, which was severely handicapped in replication (Fig. 1B and C), underwent additional mutation to L314V on passage, thereby restoring replication fitness to close to that of

the wt (Fig. 3A). Interestingly, the increased replication fitness of L314V was associated with restoration of the ability of the virus to downregulate Rb, as assessed by immunoblotting and fluorescence microscopy (Fig. 3B and C). However, the data do not allow us to say whether these two attributes of L314V, enhanced replication fitness and restored ability to regulate Rb, are in any way related to each other. Although the L314V mutation fully corrected the modest defect in function observed with the NS5B L314A mutant in the cell-free polymerase assays (both in de novo initiation and in primer extension) (Fig. 4A), it did not restore viral fitness completely to wt levels (Fig. 1B and 3A).

The Rb-binding motif is LxCxD in most HCV strains and is LxNxD in a subset of genotype 1b viruses (18). Despite the fact that the C316A mutant appears to possess increased polymerase activity compared to the wt protein (Fig. 4C and D), 316A is not found commonly in the RdRps of naturally occurring HCV strains. This suggests that any benefit it might confer upon the enzymatic activity of the NS5B polymerase may be outweighed by the abolition of Rb binding in the context of viral replication. Mutations at L314 and C316 have been found in HCV replicons selected for resistance to a benzofuran inhibitor of NS5B, HCV796, but in agreement with the present study, these mutants were found to have reduced fitness compared to the wt replicon (6). The impact of these resistance mutations on the ability of NS5B to bind Rb is not known.

Rb abundance and optimal HCV replication. If the ability of NS5B to downregulate Rb has evolved because it facilitates virus replication, it might be expected that HCV replication would be increased in cells in which Rb abundance is reduced by other means. However, downregulation of Rb by siRNA knockdown resulted in no increase, and in fact a modest decrease, in the replication of both wt HCV and mutated HCV lacking a functional Rb-binding domain in NS5B (Fig. 6 and 7). The role of Rb in HCV infection is thus likely to be quite complex, and any effects on the efficiency of HCV replication in Huh-7 cells may be interwoven with other processes regulated by Rb. An important caveat in these experiments is that the only available cell culture systems that are sufficiently robust to study HCV infection in vitro use Huh-7-derived cell lines. Huh-7 cells are known to express high levels of a mutant p53 gene (1) and are thus likely to be defective in other aspects of normal cell cycle regulation. They also contain a constitutively activated NF-κB signaling pathway. Although the expression of wt NS5B, but not NS5B containing Rb-binding motif mutations, was able to downregulate Rb and activate E2F-responsive promoters in Huh-7 cells (18), cell culture systems that more closely mimic primary hepatocytes will be required to fully understand the effects on Rb abundance and cell cycle regulation exerted by HCV. Importantly, our previous studies failed to find any difference in cell cycle regulation in Huh-7-derived cell lines containing replicating, genome-length RNA replicons and their interferon-cured progeny (26). In contrast, we found previously that ectopic expression of NS5B (to an abundance similar to that in replicon cells) stimulates cell proliferation and S-phase entry in U2OS osteosarcoma cells that possess functional Rb and p53 pathways (18).

In vivo, downregulation of Rb might benefit HCV in a number of ways. In addition to its role as a central cell cycle regulator, Rb interacts with several transcription factors. Mi-

croarray studies have shown that downregulation of Rb leads to both upregulation of genes required for cell cycle progression and downregulation of genes involved in the modulation of immune functions (15). Over 500 different genes were differentially regulated by the acute loss of Rb in these studies. It is possible that the interaction between NS5B and Rb acts to fine-tune the level of Rb protein in the cell. That is, too much Rb (or too much hypophosphorylated Rb) may be detrimental to HCV infection due to its block in cell cycle progression. However, too little Rb could lead to altered gene expression that also disfavors HCV RNA replication. Given the possibility of such a scenario, it is not surprising to find that RNA silencing of the Rb gene would fail to regulate Rb abundance at the level that is optimal for viral replication. This is particularly so in Huh-7 cells, in which pathways regulating the cell cycle are intrinsically abnormal. Further studies will be needed to sort through these various possibilities and to ascertain the mechanism(s) responsible for the presumed benefit to viral fitness that underlies the evolution of Rb regulation by NS5B.

ACKNOWLEDGMENTS

REFERENCES

1. Bressac, B., K. M. Galvin, T. J. Liang, K. J. Isselbacher, J. R. Wands, and M. Ozturk. 1990. Abnormal structure and expression of p53 gene in human hepatocellular carcinoma. Proc. Natl. Acad. Sci. USA 87:1973–1977.
2. Chinnaswamy, S., I. Yarbrough, S. Palaninathan, C. T. Kumar, V. Vijayaraghavan, B. Demeler, S. M. Lemon, J. C. Sacchettini, and C. C. Kao. 2008. A locking mechanism regulates RNA synthesis and host protein interaction by the hepatitis C virus polymerase. J. Biol. Chem. 283:20535–20546.
3. DeCaprio, J. A., J. W. Ludlow, J. Figge, J. Y. Shew, C. M. Huang, W. H. Lee, E. Marsilio, E. Paucha, and D. M. Livingston. 1988. SV40 large tumor antigen forms a specific complex with the product of the retinoblastoma susceptibility gene. Cell 54:275–283.
4. DeGregori, J., T. Kowalik, and J. R. Nevins. 1995. Cellular targets for activation by the E2F1 transcription factor include DNA synthesis- and G1/S-regulatory genes. Mol. Cell. Biol. 15:4215–4224.
5. Dyson, N., P. M. Howley, K. Munger, and E. Harlow. 1989. The human papilloma virus-16 E7 oncoprotein is able to bind to the retinoblastoma gene product. Science 243:934–937.
6. Howe, A. Y., H. Cheng, S. Johann, S. Mullen, S. K. Chunduru, D. C. Young, J. Bard, R. Chopra, G. Krishnamurthy, T. Mansour, and J. O'Connell. 2008. Molecular mechanism of hepatitis C virus replicon variants with reduced susceptibility to a benzofuran inhibitor, Hcv-796. Antimicrob. Agents Chemother. 52:3327–3338.
7. Ishido, S., and H. Hotta. 1998. Complex formation of the nonstructural protein 3 of hepatitis C virus with the p53 tumor suppressor. FEBS Lett. 438:258–262.
8. Kao, C. F., S. Y. Chen, J. Y. Chen, and Y. H. Wu Lee. 2004. Modulation of p53 transcription regulatory activity and post-translational modification by hepatitis C virus core protein. Oncogene 23:2472–2483.
9. Kim, M. J., and C. Kao. 2001. Factors regulating template switch in vitro by viral RNA-dependent RNA polymerases: implications for RNA-RNA recombination. Proc. Natl. Acad. Sci. USA 98:4972–4977.
10. Lerat, H., M. Honda, M. R. Beard, K. Loesch, J. Sun, Y. Yang, M. Okuda, R. Gosert, S. Y. Xiao, S. A. Weinman, and S. M. Lemon. 2002. Steatosis and liver cancer in transgenic mice expressing the structural and nonstructural proteins of hepatitis C virus. Gastroenterology 122:352–365.
11. Levrero, M. 2006. Viral hepatitis and liver cancer: the case of hepatitis C. Oncogene 25:3834–3847.
12. Lin, R., C. Heylbroeck, P. M. Pitha, and J. Hiscott. 1998. Virus-dependent phosphorylation of the IRF-3 transcription factor regulates nuclear translocation, transactivation potential, and proteasome-mediated degradation. Mol. Cell. Biol. 18:2986–2996.
13. Ma, Y., J. Yates, Y. Liang, S. M. Lemon, and M. Yi. 2008. NS3 helicase domains involved in infectious intracellular hepatitis C virus particle assembly. J. Virol. 82:7624–7639.
14. Majumder, M., A. K. Ghosh, R. Steele, R. Ray, and R. B. Ray. 2001. Hepatitis C virus NS5A physically associates with p53 and regulates p21/waf1 gene expression in a p53-dependent manner. J. Virol. 75:1401–1407.
15. Markey, M. P., J. Bergseid, E. E. Bosco, K. Stengel, H. Xu, C. N. Mayhew, S. J. Schwemberger, W. A. Braden, Y. Jiang, G. F. Babcock, A. G. Jegga, B. J. Aronow, M. F. Reed, J. Y. Wang, and E. S. Knudsen. 2007. Loss of the retinoblastoma tumor suppressor: differential action on transcriptional programs related to cell cycle control and immune function. Oncogene 26:6307–6318.
16. McGivern, D. R., and S. M. Lemon. 2008. Tumor suppressors, chromosomal instability, and hepatitis C virus-associated liver cancer. Annu. Rev. Pathol. 4:399–415.
17. Munakata, T., Y. Liang, S. Kim, D. R. McGivern, J. M. Huibregtse, A. Nomoto, and S. M. Lemon. 2007. Hepatitis C virus induces E6AP-dependent degradation of the retinoblastoma protein. PLoS. Pathog. 3:1335–1347.
18. Munakata, T., M. Nakamura, Y. Liang, K. Li, and S. M. Lemon. 2005. Down-regulation of the retinoblastoma tumor suppressor by the hepatitis C virus NS5B RNA-dependent RNA polymerase. Proc. Natl. Acad. Sci. USA 102:18159–18164.
19. Nelson, H. B., and H. Tang. 2006. Effect of cell growth on hepatitis C virus (HCV) replication and a mechanism of cell confluence-based inhibition of HCV RNA and protein expression. J. Virol. 80:1181–1190.
20. Pietschmann, T., V. Lohmann, G. Rutter, K. Kurpanek, and R. Bartenschlager. 2001. Characterization of cell lines carrying self-replicating hepatitis C virus RNAs. J. Virol. 75:1252–1264.
21. Quinkert, D., R. Bartenschlager, and V. Lohmann. 2005. Quantitative analysis of the hepatitis C virus replication complex. J. Virol. 79:13594–13605.
22. Ranjith-Kumar, C. T., L. Gutshall, M. J. Kim, R. T. Sarisky, and C. C. Kao. 2002. Requirements for de novo initiation of RNA synthesis by recombinant flaviviral RNA-dependent RNA polymerases. J. Virol. 76:12526–12536.
23. Ranjith-Kumar, C. T., and C. C. Kao. 2006. Recombinant viral RdRps can initiate RNA synthesis from circular templates. RNA 12:303–312.
24. Ranjith-Kumar, C. T., Y. C. Kim, L. Gutshall, C. Silverman, S. Khandekar, R. T. Sarisky, and C. C. Kao. 2002. Mechanism of de novo initiation by the hepatitis C virus RNA-dependent RNA polymerase: role of divalent metals. J. Virol. 76:12513–12525.
25. Ranjith-Kumar, C. T., J. L. Santos, L. L. Gutshall, V. K. Johnston, J. Lin-Goerke, M. J. Kim, D. J. Porter, D. Maley, C. Greenwood, D. L. Earnshaw, A. Baker, B. Gu, C. Silverman, R. T. Sarisky, and C. Kao. 2003. Enzymatic activities of the GB virus-B RNA-dependent RNA polymerase. Virology 312:270–280.
26. Scholle, F., K. Li, F. Bodola, M. Ikeda, B. A. Luxon, and S. M. Lemon. 2004. Virus-host cell interactions during hepatitis C virus RNA replication: impact of polyprotein expression on the cellular transcriptome and cell cycle association with viral RNA synthesis. J. Virol. 78:1513–1524.
27. Whyte, P., K. J. Buchkovich, J. M. Horowitz, S. H. Friend, M. Raybuck, R. A. Weinberg, and E. Harlow. 1988. Association between an oncogene and an anti-oncogene: the adenovirus E1A proteins bind to the retinoblastoma gene product. Nature 334:124–129.
28. Yi, M., and S. M. Lemon. 2004. Adaptive mutations producing efficient replication of genotype 1a hepatitis C virus RNA in normal Huh7 cells. J. Virol. 78:7904–7915.
29. Yi, M., Y. Ma, J. Yates, and S. M. Lemon. 2007. Compensatory mutations in E1, p7, NS2, and NS3 enhance yields of cell culture-infectious intergenotypic chimeric hepatitis C virus. J. Virol. 81:629–638.
30. Yi, M., R. A. Villanueva, D. L. Thomas, T. Wakita, and S. M. Lemon. 2006. Production of infectious genotype 1a hepatitis C virus (Hutchinson strain) in cultured human hepatoma cells. Proc. Natl. Acad. Sci. USA 103:2310–2315.

APPENDIX II

Mutations in the Hepatitis C Virus Polymerase that Increase RNA Binding Can Confer Resistance to Cyclosporine A

Zhe Liu,[1]* John M. Robida,[1]* Sreedhar Chinnaswamy,[2] Guanghui Yi,[2] Jason M. Robotham,[1] Heather B. Nelson,[1] Andre Irsigler,[1] C. Cheng Kao,[2] and Hengli Tang[1]

Hepatitis C virus (HCV) infection leads to acute and chronic liver diseases, and new classes of anti-HCV therapeutics are needed. Cyclosporine A (CsA) inhibits HCV replication and CsA derivatives that lack the immunosuppressive function are currently in clinical trials as candidate anti-HCV drugs. Here we characterize several independently derived HCV replicons with varying levels of CsA resistance due to mutations in nonstructural protein 5B (NS5B), the HCV-encoded polymerase. Mutant HCV replicons engineered with these mutations showed resistance to CsA. The mutations reside in two distinct patches in the polymerase: the template channel and one face of a concave surface behind the template channel. Mutant NS5B made by cells expressing the HCV replicon had increased ability to bind to RNA in the presence of CsA. Purified recombinant NS5B proteins containing the mutations were better at *de novo* initiated RNA synthesis than the wild-type control. Furthermore, the mutant proteins were able to bind RNA with ≈8-fold higher affinity. Last, mutation near the template channel alleviated the lethal phenotype of a mutation in the concave patch, P540A. This intramolecular compensation for the HCV replicase function by amino acid changes in different domains was further confirmed in an infectious cell culture-derived virus system. *Conclusion:* An increased level of CsA resistance is associated with distinct mutations in the NS5B gene that increase RNA binding in the presence of CsA, and the intramolecular communications between residues of the thumb and the C-terminal domains are important for HCV replicase function. (HEPATOLOGY 2009;50:25-33.)

Cyclosporine A (CsA), a commonly used immunosuppressant for transplant patients, has recently emerged as a potential new anti-hepatitis C virus (HCV) therapeutic. CsA and its derivatives potently in-hibit HCV replication both in cell-culture systems and in mice with transplanted human liver,[1-3] although no consensus has emerged on the *in vivo* benefits of using CsA over Tacrolimus (FK506), a compound that lacks anti-HCV effect *in vitro*, for HCV-infected liver-transplant patients.[4-9] More recent clinical trials with a CsA derivative, DEBIO-025, yield promising results in human immunodeficiency virus (HIV) and HCV-coinfected patients, but drug resistance *in vivo* has not been studied.[10]

Studies of the antiviral effect of CsA on HCV replicons has led to the identification of cyclophilin (CyP) as an essential cofactor for HCV replication[11-13]; point mutations in nonstructural protein 5B (NS5B) and NS5A are associated with CsA resistance *in vitro*.[14,15] In addition, NS5B interacts with both CyPA and CyPB both *in vitro* and *in vivo*.[12,13] These data establish NS5B as an indirect viral target for the CsA-mediated inhibition of HCV replication. The CyPA-NS5B interaction has also been shown to be the principal mediator of cyclosporine resistance *in vitro*.[12]

How CyPA affects NS5B function is unclear. The crystal structure of HCV NS5B lacking the C-terminal transmembrane domain has been solved. It adopts a typical right-handed shape that contains finger, palm, and thumb domains surrounding the active site.[16-18] Characterization of allosteric, nonnucleoside inhibitors revealed extensive communication between the different domains.[19] Here, we identify a series of mutations in NS5B that conferred resistance to CsA and show that the mutations can affect RNA binding and synthesis by the HCV polymerase.

Materials and Methods

Compounds and Cell Lines. Cyclosporine A was purchased from Alexis (San Diego, CA). GS5- and CsA-resistant replicons have been described.[14,20] All replicon cells are routinely cultured in Dulbecco's Modified Eagle Medium (DMEM) with 10% fetal bovine serum (FBS) and 500 μg/mL of G418.

Replicon Sequencing, Site-Directed Mutagenesis, and Replication Assays. These experiments were performed using published procedures.[14,20] Detailed information on these methods can be found in the Supporting Methods. Primer sequences used in the cloning and sequencing are shown in Supporting Tables 1 and 2.

Molecular Biology Assays. Transient replication was measured by isolation of total cellular RNAs from cells 7 hours, 4 days, and 10 days after electroporation of the Rep1b or JFH-1 RNA. We performed real-time reverse-transcriptase polymerase chain reaction (RT-PCR) with a SYBR Green PCR kit (Applied Biosystems) to detect HCV IRES and GAPDH expression. Sequences of the qRT-PCR primers are shown in Supporting Table 3.

In vitro transcription, electroporation, colony formation, and Poly-U RNA binding assays were performed as described.[12,14]

Infections and Fluorescence Staining. Infection of Huh-7.5 cells by cell culture-derived virus was performed as described.[21] Immunostaining of infected Huh-7.5 cells was carried out according to standard methods with a mouse monoclonal antibody against the core protein (Affinity Bioreagents, Golden, CO) and an Fluoresbrite Carboxylate YG (FITC)-conjugated goat antimouse secondary antibody for detection (Sigma, St. Louis, MO).

Protein Purification and RNA-Dependent RNA Polymerase (RdRp) Assays. Wild-type (wt) and mutant versions of the NS5B Δ21 were expressed in *E. coli* as C-terminal 6xHis tagged proteins and purified first by a metal ion chromatography and then with polyuridylate resins. Standard RdRp assays were performed as described.[22] Protein concentrations were determined by comparison with known concentrations of bovine serum

albumin (BSA) in Coomassie blue-stained sodium dodecyl sulfate-polyacrylamide gel electrophoresis (SDS-PAGE).

Differential Scanning Fluorimetry. Differential scanning fluorimetry was performed in a Stratagene MX3005P machine with an excitation of 492 nm and emission of 610 nm. Each sample was prepared in a total volume of 50 μL containing solutions of protein at 2.5 μM final concentration, SYPRO orange (Molecular Probes) at 2.5 $\times$ final concentration. The samples were heated at a rate of 0.5°C/minute, from 25°C to 95°C, and the T_m values were calculated from the maximum of the first derivative with KaleidaGraph software (Synergy Software, Reading, PA).

Fluorescence Anisotropy Assay. Measurements were made with an LS55 spectrometer (Perkin-Elmer) and cuvettes with an optical pathlength of 0.4 cm at 22°C. The fluorescein-labeled RNA SL-UC was at 0.2 μM in 50 mM Tris-Cl (pH 7.5) and 25 mM NaCl. The final volume of protein added did not exceed 5% of the initial sample volume. The excitation wavelength was 495 nm, and each emission was scanned from 510 to 560 nm. The average of 10 scans was taken per data point and the data were analyzed by nonlinear least-square fitting using KaleidaGraph.

Results

Isolation of Replicon RNA with Distinct Levels of CsA Resistance. We have recently isolated CsA-resistant replicons using a combination of antibiotic selection and cell sorting.[14] When single-cell clones of the resistant population were analyzed, various levels of CsA resistance were observed (Fig. 1A). The three single-cell clones with the highest levels of resistance were RS1-2, RS1-8, and RS1-9 (Fig. 1A); other clones had lower levels of resistance, similar to that of RS1-10 (Supporting Fig. 1A). To confirm that the CsA resistance of these single-cell clones was indeed conferred by the replicon RNA, we introduced total RNAs isolated from these cells, which contain the replicon RNAs, into naïve Huh-7.5 cells. The new replicons are designated RS1-2.2, RS1-8.2, RS1-9.2, and RS1-10.2, respectively. The replicon RNAs from all these clones phenocopied the resistant phenotype to the new replicon cells (Supporting Fig. 1B). Importantly, the relative level of resistance was maintained in the progeny replicons, demonstrating that the replicon RNAs in these clones contain distinct mutations that are responsible for the resistant phenotype.

Identification of Point Mutations in NS5B that Confer Resistance. The HCV NS5B gene, which encodes the viral RdRp, has been implicated in the CsA-
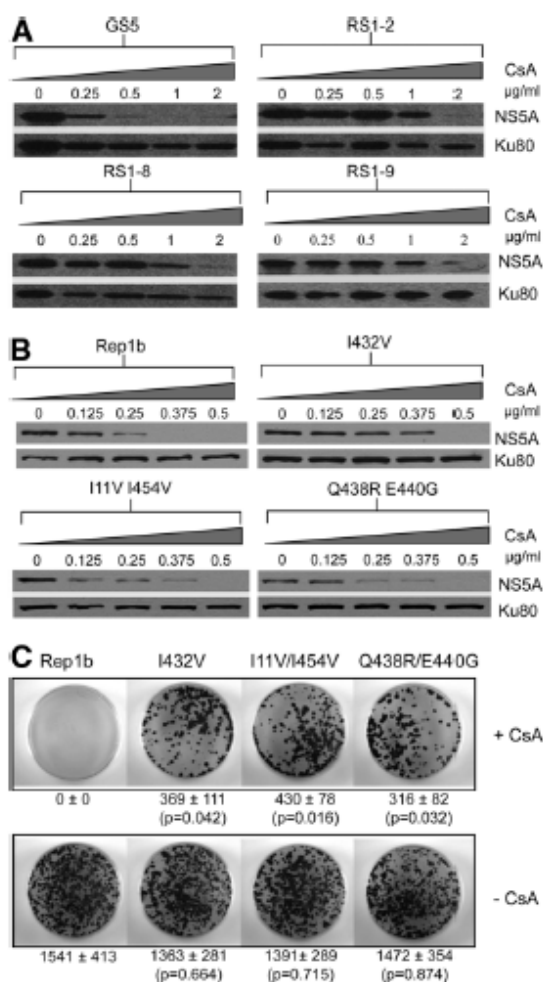
Fig. 1. NS5B mutations that confer CsA-resistance. (A) Single-cell clones exhibit distinct levels of CsA resistance. The replicon cells were treated with increasing concentrations of CsA for 4 days before being analyzed by western blotting to detect NS5A expression. (B) Point mutations in NS5B confer resistance to a Con1 replicon without GFP. The wt replicon (Rep1b) and its derivatives containing the indicated NS5B mutations were treated with CsA for 4 days. The cells were then lysed and analyzed by SDS-PAGE and western blotting for NS5A and a cellular protein, Ku80. (C) Colony formation assay. One μg of in vitro transcribed replicon RNAs was electroporated into Huh-7.5 cells. The transfected cells were then selected for 3 weeks with 500 μg/mL of G418 in the presence or absence of 0.375 μg/mL of CsA. Statistical analysis was performed using Student's t test to compare the number of colonies formed by each mutant with that by wt replicon in the presence or absence of CsA.

mediated inhibition of HCV and CsA resistance *in vitro*.[12-15] We sequenced the NS5B region of the single cell clones and compared them to the wt sequence represented by GS5 replicon. Despite having a similar level of

resistance, RS1-8, RS1-9, and RS1-2 contained different mutations in the NS5B coding region. A single common I432V mutation was found in RS1-2 NS5B, whereas combinations of two mutations, I11V/I454V and Q438R/E440G, were found in RS1-8 and RS1-9, respectively. To determine whether these mutations could confer CsA resistance, we engineered them into a wt genotype 1b replicon, Rep1b, and assayed the resultant constructs for CsA resistance. Expression of the NS5A protein of Rep1b was below the detectable level when the replicon was treated with 0.375 μg/mL of CsA. In contrast, NS5A could be detected when the mutant replicons were treated with the same concentration of CsA (Fig. 1B). This result was confirmed with a colony-formation assay. In the absence of CsA treatment, electroporated replicon RNAs resulted in formation of G418-resistant colonies as a result of the expression of the neomycin phosphotransferase gene carried by these replicons. Inclusion of 0.375 μg/mL of CsA abolished the ability of the wt replicon (Rep1b) to form colonies, whereas the three mutant replicon RNAs retained colony formation (Fig. 1C). No significant differences were observed between the mutant and wt replicons' ability to form colonies in the absence of CsA. These results demonstrate that these NS5B mutations are sufficient to confer increased CsA resistance without enhancing replication. However, the full level of CsA resistance of the original resistant isolates may require mutations in other genes (compare the CsA dosages in Fig. 1A and Fig. 1B and see Supporting Table 4).

CsA-Resistance Mutations Locate to Two Functionally Related Regions in NS5B Structure. All of the mutations lie within two regions of the NS5B structure (Fig. 2A). First, mutations I432V, I11V, and V405L are within the template channel or the $\Delta 1$ loop that extends from the finger subdomain to the thumb subdomain to form a latch over the template channel. This locking mechanism is primarily due to hydrophobic interactions between the $\Delta 1$ loop and the residues on the outer surface of the template channel.[22] The second group of mutations, Q438R, E440G, I454V, and W550R, lie along one side of a concave surface at the back of the template channel, along a groove. Mutation R556V could not be mapped because it was not present in the crystal structure, but the trajectory of the C-terminal tail is projected to be near the template channel. To extend this analysis, we also examined the locations of the two mutations in NS5B identified by Fernandes et al.,[15] S556G and P538T. S556G is located within the template channel and P538T is within the same side of the concave surface of NS5B, lining the aforementioned groove. A compilation of all nine mutations in the NS5B structure is shown in Fig. 2B,
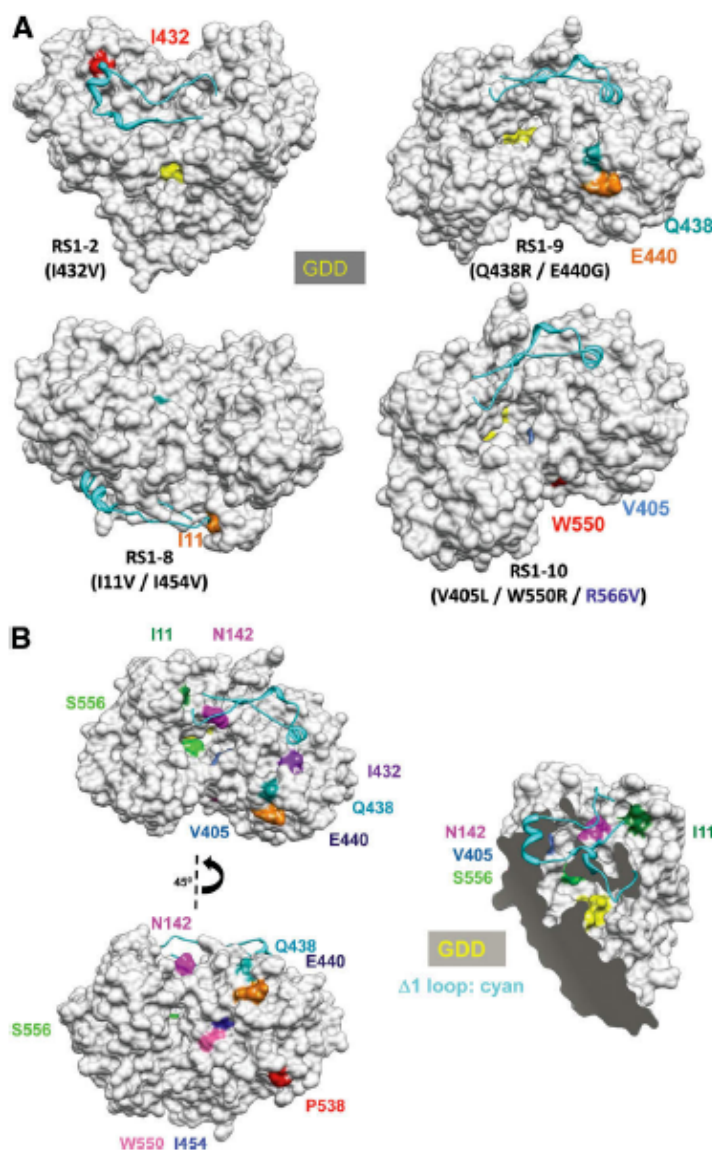
Fig. 2. Locations of the mutations in NS5B that conferred resistance to CsA. (A) Models of the mutations in NS5B from RS1-2, RS1-8, RS1-9, and RS1-10. The structure of the NS5B protein is from Ago et al.[16] (pdb: 1QUV). Several features in the structures serve as landmarks. The $\Delta 1$ loop that extends from the thumb to the finger subdomains is colored cyan. The GDD residues that coordinate divalent metals for catalysis are shown in yellow. Note that the active site within the enclosed template channel was obscured in some views. The back of the template channel includes a concave surface, the location of several of the mutations. (B) CsA mutations exist in two regions within the NS5B protein. The mutations include those identified in this study and the two from Fernandes et al.,[15] which also conferred resistance to CsA, and the mutation N142S from Wiedmann et al.[34] The first region is in or near the template channel (I11, N142, V405, I432, and S556) and the second is within one face of the concave surface (Q438, E440, I454, P538, and W550). A cut-away view of the molecule is shown to allow visualization of the mutations in the template channel.

including a cut-away view that better exposes the locations of the mutations within the template channel.

RNA Binding by HCV Replication Proteins in the Presence of CsA. On the basis of their locations in the NS5B structure, we hypothesize that the mutations could affect RNA binding by NS5B. To test this hypothesis, we assayed whether NS5B produced in cells could bind poly-U (pU) RNA *in vitro* in a CsA-sensitive manner.[13] Cell lysates were incubated with pU resin, then washed and subjected to western blot analysis with antiserum to NS5B. Binding to protein G Sepharose served as a negative control. All NS5B variants were able to bind pU RNA in the absence of CsA (Fig. 3A). The interaction between the wt NS5B and pU RNA was reduced by more than 90% upon CsA treatment. In contrast, all three of the NS5B proteins produced by mutant replicons retained pU RNA binding when treated with CsA (Fig. 3A). The reductions in RNA binding by mutant proteins containing I432V, Q438R/E440G, and I11V/I454V were 0%, 5%-10%, and 40%-50%, respectively (Fig. 3B). Note
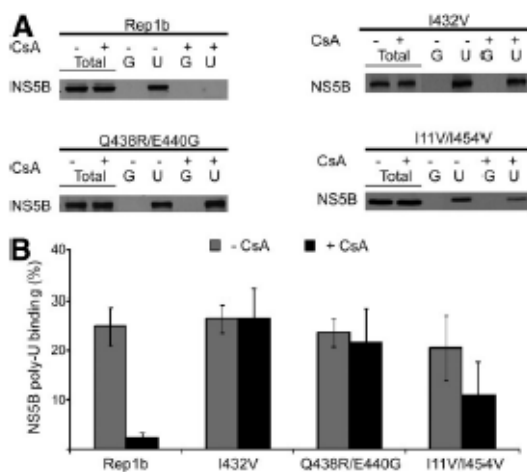
Fig. 3. CsA-resistant RNA binding of the mutant NS5B proteins. (A) An in vitro poly-U RNA binding by NS5B. Cell lysates of CsA-treated (8 μg/mL) or untreated Rep1b or mutant replicon cells were incubated with either poly-U RNA-conjugated Sepharose or protein G Sepharose beads in the presence or absence of 32 μg/mL of CsA. NS5B bound to poly-U RNA was detected with anti-NS5B antibody. The amount of input lysate used for binding was three times that of the "total." "U": poly U RNA; "G": protein G. (B) The percentage of the NS5B bound to RNA was calculated by quantification of the intensities of the western blot bands. The ratio of "bound" to "total" accounted for the 3-fold difference in loading. The error bars represent the standard derivation of three experiments.

that these cells were treated with CsA for only 22 hours, a time at which total NS5B protein level has not yet decreased. Longer treatment with CsA (>24 hours) would have resulted in a reduction in total NS5B.

To further determine if the mutations in NS5B that confer resistance to CsA affect NS5B activity, we expressed several of the mutants in E. coli in a form that lacked the C-terminal transmembrane domain (NS5B Δ21). The mutant proteins include I432V, I11V/I454V, Q438R/E440G, and a mutant that contained all five mutations (I11V, I432V, I454V, Q438R, and E440G), named Mut5 (Fig. 4A).

The HCV RdRp can initiate RNA synthesis de novo from the 3′ end of the viral genome[23,24] or by extension from a primed template.[25] Both activities could be measured in the same reaction with RNA LE19 that exists in equilibrium between a monomer and a dimer. The monomer forms an intramolecular hairpin that directs de novo initiation to produce a 19-nucleotide (nt) product. A dimer can serve as the template-primer complex for an extension reaction 32 nt in length[22] (Fig. 4B). In addition, template-switch products that are multimers of the 19-nt RNA are also produced from some of the de novo initiated 19-mers will.[26] All mutant proteins retained the ability to synthesize the de novo transcript, the primer-extended

products, and the template switch products (Fig. 4C), indicating that the mutations that conferred resistance to CsA did not affect residues of the polymerase that are essential for catalytic activity.

The mutant proteins had more subtle differences with regard to RNA synthesis. First, RNA synthesis by I432V was increased several-fold (Fig. 4C). Higher template concentrations were previously reported to inhibit RNA synthesis by Δ21 protein.[21] In contrast, I432V was not inhibited in RNA synthesis at higher ligand concentrations (Supporting Fig. 2). Second, mutants Q438R/E440G, I11V/I454V, and Mut5 produced up to 4.6-fold more of the 19-nt de novo initiated RNA than of the 32-nt primer-extension product (Fig. 4D). Notably, I432V produced a ratio of the de novo-initiated and the primer-extended products similar to that of Δ21, suggesting that I432V is functionally distinct from the other mutants. Because Mut5 also contained the I432V mutation, the effects of the other mutations on the ratio of RNA synthesis appear to dominate that of I432V.

Spectroscopic Analysis of Select Mutant RdRps. The conformation of the HCV RdRp is linked to the mode of RNA synthesis. To examine the effects of the mutations on NS5B conformation, we selected mutant proteins I432V (near the template channel) and Q438R/E440G (in the concave surface) as representing the two classes of mutant proteins. Differential scanning fluorimetry[27] was used to measure proteins' unfolding as a function of temperature. The assay uses SYPRO orange, which fluoresces when it binds to hydrophobic regions of proteins that are exposed upon thermal denaturation. Both I432V and Q438R/E440G differed distinctly in thermal denaturation profiles from Δ21 (Fig. 5A) and from each other, in agreement with the observed differences in RNA synthesis (Fig. 4C). The functional and spectroscopic analyses support the model that the CsA-resistant mutations affect the conformation of the NS5B protein.

RNA Binding by Recombinant HCV RdRps. A fluorescence anisotropy assay was used to determine the affinity of RdRp-RNA binding. The RNA used was chemically synthesized to contain 5′ fluorescein (Fig. 5B) and a stable hairpin needed for efficient de novo initiation of RNA synthesis.[28,29] The binding isotherms for the three proteins were complex to fit, perhaps reflecting that the proteins may exist in equilibrium of two or more conformers, but when fitted to the same hyperbola equation the affinities for SL-UC binding were 16 μM for Δ21 and less than 2 μM for I432V and Q438R/E440G (Fig. 5B). The apparent kD values were reproducible within 10% in two independent experiments. These results show that mutations that conferred CsA resistance can increase
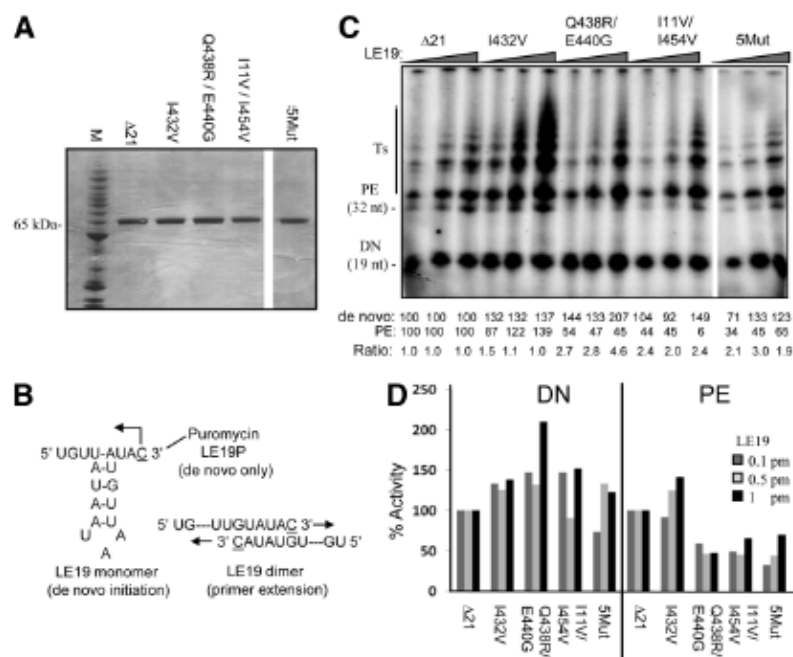
Fig. 4. Activity of recombinant NS5B proteins containing CsA-resistant mutations. (A) Coomassie blue-stained SDS-PAGE of the recombinant proteins purified for the experiments presented here and in Fig. 6. The purified proteins have been adjusted to be of comparable concentration. (B) Sequence and secondary structures of LE19, the template for the RdRp assay. The monomeric structure of LE19 can be used for de novo initiation, whereas the partially annealed dimer can direct primer extension. (C) Products of RNA synthesis by the Δ21 (wild-type for this study) and mutant RdRps. Each set of reactions was performed with increasing concentrations of LE19 in the reaction. The identities of the 19-nt de novo initiated the 32-nt primer-extended and the template-switch products are shown. Most proteins were named according to the mutated residues they contain. Mut5: the mutant that contained five mutations: I11V, I432V, Q438R, E440G, and I454V. (D) The amounts of products were determined by phosphorimage analysis and the ratios adjusted to the comparable reaction performed with Δ21. Results with Δ21, I432V and Q438R/E440G were confirmed in two additional experiments.

RNA binding by NS5B in the absence of other proteins. Strikingly, both I432V (near the template channel) and Q438R/E440G (the concave surface of the RdRp) conferred increased RNA binding by the HCV RdRp.

Rescue of P540A Lethal Phenotype by NS5B Mutations. We sought additional evidence for the functional relationship between the template channel and the concave surface of the HCV RdRp. A point mutation, P540A, that resides in the concave surface of the HCV RdRp abolished the replication of a genotype 1b replicon[13] and I432V rescued replication when engineered into the P540A background,[14] demonstrating communication between the mutations at the two patches. We tested all the CsA-resistance mutations for their ability to alleviate the lethal effect of P540A in a transient replication assay. Replicon RNAs carrying P540A or P540A plus the CsA-resistance mutations were delivered into Huh-7.5 cells by electroporation. Total RNAs were extracted and analyzed by real-time RT-PCR. The input RNAs were at comparable levels in all the replicon derivatives at

7 hours. After 4 days in culture, however, the P540A RNA had decreased to that of the negative control, whereas the replicon derivatives had levels close to that of the wt (Fig. 6). At day 10, the RNA levels of P540A/Q438R and P540A/E440G were lower than that of the wt but three orders higher than that of P540A (Fig. 6A). The colony-formation assay results confirmed these observations (Fig. 6B). These results provide additional evidence that the two patches in the NS5B protein affected by CsA are functionally related.

A Naturally Occurring I454V Variation Averts the Lethal Effect of P540A Mutation. The NS5B gene of GT2a carries a valine at position 454 instead of an isoleucine in the wt sequence. Importantly, the JFH-1 isolate of the GT2a genome can efficiently produce infectious particles in cell culture.[30] To examine if Val454 could counteract the lethal phenotype of P540A in this genetic background, we engineered the P540A mutation into the JFH-1 genome and examined its effect on viral replication and infection of this isolate. In the transient replication

Fig. 5. Spectroscopic characterizations of Δ21 and mutant proteins I432V and Q438R/E440G. (A) Differential scanning fluorimetry used to compare protein unfolding rates. Temperature increase was regulated by a Stratagene Mx3005P real-time PCR machine. The first derivative of the change in fluorescence is plotted. (B) Fluorescence anisotropy results revealing the affinities of the proteins for the RNA SL-UC (inserted in the graph to the left). The symbol attached to the 5′ terminus of the RNA represents fluorescein. Purified proteins were titrated into a cuvette fitted with a magnetic stir bar. Background fluorescence of the buffer and protein were small at the wavelengths used (emission: 520 nm; excitation: 560 nm) but were subtracted from the data. The fit to the binding isotherms was performed with a hyperbola equation (y = m1*x/[m2+x]; m2 = kD) and plotted with KaleidaGraph. The quality of the fit is shown by the R^2 value.
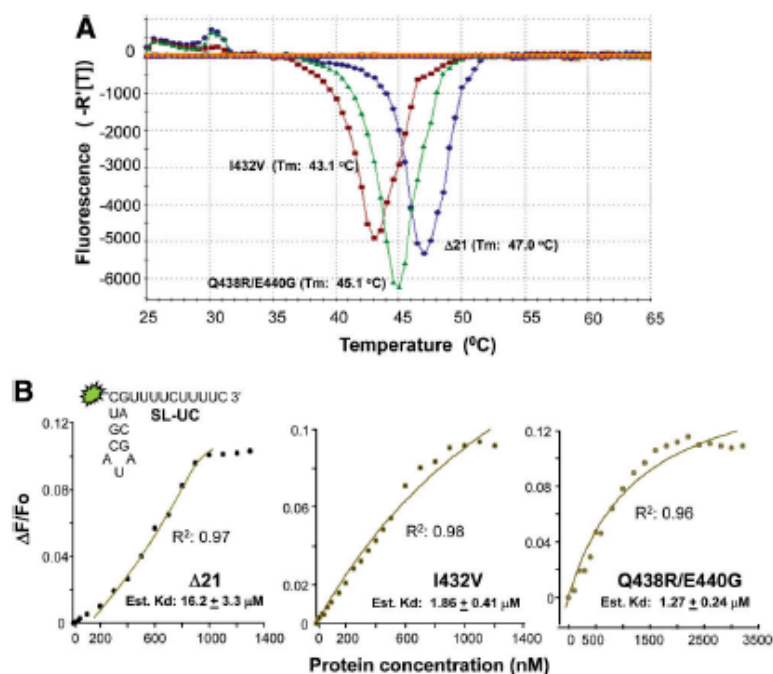
assay, the P540A mutant was impaired in its ability to replicate but accumulated to a level higher than a nonviable control virus (GDD changed to GND in the catalytic core of NS5B) (Fig. 7A). In contrast, the double mutant of V454I and P540A (PAVI) was not viable, whereas the V454I single mutant replicated close to the wt level (Fig. 7A). There is a significant decrease in RNA level from 7 hours to day 4 for all the samples, likely a result of the higher amount of input RNA (10 μg as opposed to 1 μg used for the replicons in Fig. 6A) needed to produce infectious viruses. Nevertheless, for the wt V454I, and P540A, the RNA level stabilized from day 4 through day 10, indicating sustained replication. Furthermore, when the supernatants from these cells were tested for their abilities to infect naïve Huh-7.5 cells, similar results were obtained (Fig. 7B). These results strongly suggest that the presence of a naturally occurring valine at position 454 could prevent the lethal effect of P540A in an experimental setting that recapitulates the full cycle of HCV infection.

Discussion

Here, we report that mutations in the HCV polymerase that confer CsA-resistant replication increased RNA binding by NS5B, which is an indirect viral target of CsA's inhibitory effect on HCV replication. Together with our previous report that CyPA interacts with NS5B and regulates HCV replication,[12] these results suggest a model in which CyPA assists NS5B in binding RNA for HCV RNA synthesis. When mutations arise within NS5B that improve RNA binding, CyPA is not as necessary for NS5B function. Structural analysis revealed that the mutations associated with CsA resistance and a lethal mutation for which they can compensate are located in two distinct patches in NS5B, one near the template channel and one on the back of the template channel. The two patches both affected the same activity, perhaps RNA binding with or without CyPA. Although the template channel certainly contacts the RNA, the patch behind the template channel may serve to stabilize RNA binding either directly or with assistance from CyPA.

NS5B exists in a closed conformation that is correlated with *de novo* initiation, which, on the basis of the ternary structure of the phage f6 RdRp, is likely to be the form that binds single-stranded RNA for *de novo* initiation.[31] The template channel is too narrow, however, to accommodate the double-stranded RNA intermediate that must form during RNA synthesis; the RdRp must assume a more open conformation during elongative RNA synthesis.[22] The open and closed conformations probably exist in equilibrium and we propose that CyP and/or mutations within the RdRp could affect the equilibrium. With
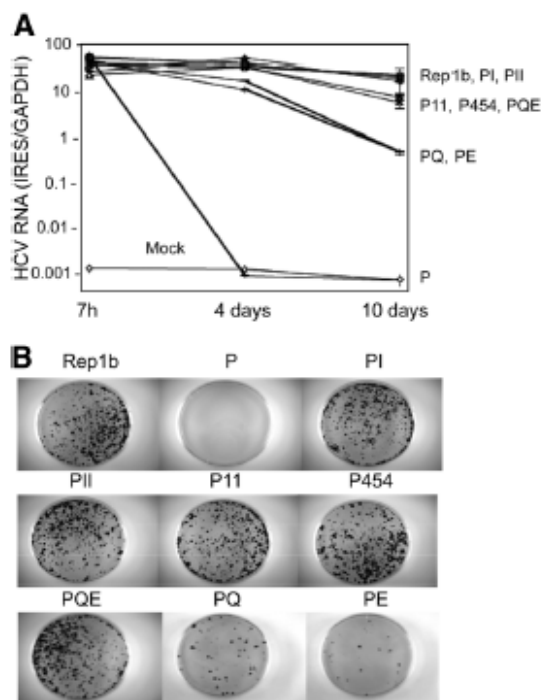
Fig. 6. CsA-resistance mutations alleviate a lethal mutation at the C-terminal domain of NS5B. (A) Transient replication of Rep1b, P540A, and the derivatives. One μg of in vitro transcribed replicon RNAs was electroporated into Huh-7.5 cells and total RNA was isolated 7 hours, 4 days, and 10 days after electroporation. The ratio of HCV RNA to the GAPDH RNA was plotted for each mutant at each timepoint. The mock-transfected cells were electroporated with buffer. P: P540A; PI: P540A/I432V; PII: P540A/I11V/I454V; P11: P540A/I11V; P454: P540A/I454V; PQE: P540A/Q438R/E440G; PQ: P540A/Q438R; PE: P540A/E440G. (B) Colony formation assay for the same set of mutants. The cells were selected with 500 μg/mL of G418 for 3 weeks to allow the formation of the colonies. The results shown are representative of three to four independent experiments.

the CsA mutations, the increased *de novo* initiation versus primer extension by several of the mutations led us to propose that at least some of the mutations affect the conformation of the RdRp, especially mutations I432V and I11A, which could contact the Δ1 loop.

The NS5B mutations did not completely restore CsA resistance when engineered into a Con1 replicon background. Mutations elsewhere in the genome, particularly in the NS5A region, can probably augment the CsA resistance in combination with the NS5B mutations.[14,15] NS5A has been proposed to serve as a cofactor for NS5B, and interactions between the two have been reported.[32,33] The NS5A-NS5B interaction may therefore modulate the conformation of NS5B and NS5A mutations may synergize with the NS5B mutations to increase CyP or RNA-binding. Interestingly, although the CsA-resistant replicons contained mutations in NS5A and NS3 (Supporting Table 4), these mutations were also found in GS5, which is a CsA-sensitive replicon.[12,14] It is possible that mutations in other NS proteins, although unable to confer resistance by themselves, can augment CsA-resistance when combined the NS5B mutations.

Polymorphism of the HCV NS genes may affect HCV replication fitness and drug sensitivity *in vivo*. Although P540A is clearly lethal to genotype 1b replicon, an alanine at position 540 exists in many naturally occurring isolates. Interestingly, all these isolates also contain at least one of the rescuing mutations that we identified as natural variations.[14] Taking advantage of the naturally occurring I454V variation in the JFH-1 isolate, we confirmed the intramolecular compensation using a full-length infection system. These results demonstrate that the mutations we found to confer CsA resistance in cultured cells could be found in natural HCV isolates. Also of note, the concentrations of CsA that we used here to select resistant replicons are in the same range of the blood concentra-
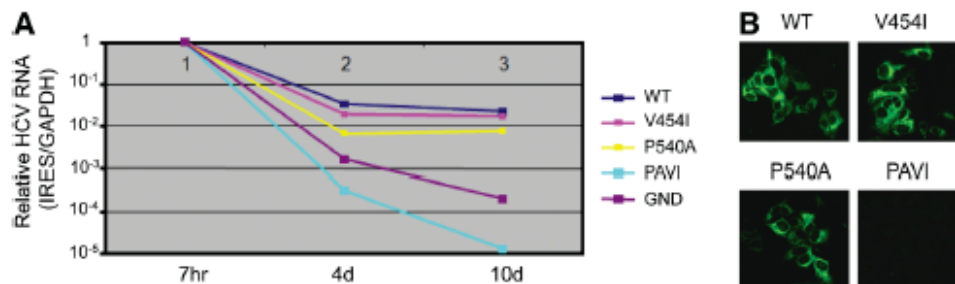

Fig. 7. Intramolecular compensation for P540A by valine at position 454 in an infection system. (A) Ten μg of in vitro transcribed JFH-1 and its derivative RNAs were electroporated into Huh-7.5 cells. Transient replication assay was performed as described in Fig. 6A using JFH-1-specific primers for RT-PCR. (B) Supernatant collected 19 days postelectroporation in (A) was used to infect naïve Huh-7.5 cells, which were then stained for the expression of core protein 7 days after infection. WT: wild type; PAVI: P540A/V454I. The results shown are representative of those from three experiments.

tions of CsA and DEBIO-025 in liver transplant and HCV-infected patients, respectively. These data suggest that CsA-based therapies may have varying effects based on the patient population.

Acknowledgment: We thank Drs. Takaji Wakita and Charlie Rice for reagents, Ruth Didier for assistance with flow cytometry, and Dr. Anne B. Thistle for proofreading.

References

1. Watashi K, Hijikata M, Hosaka M, Yamaji M, Shimotohno K. Cyclosporin A suppresses replication of hepatitis C virus genome in cultured hepatocytes. HEPATOLOGY 2003;38:1282-1288.

2. Nakagawa M, Sakamoto N, Enomoto N, Tanabe Y, Kanazawa N, Koyama T, et al. Specific inhibition of hepatitis C virus replication by cyclosporin A. Biochem Biophys Res Commun 2004;313:42-47.

3. Inoue K, Umehara T, Ruegg UT, Yasui F, Watanabe T, Yasuda H, et al. Evaluation of a cyclophilin inhibitor in hepatitis C virus-infected chimeric mice in vivo. HEPATOLOGY 2007;45:921-928.

4. Inoue K, Sekiyama K, Yamada M, Watanabe T, Yasuda H, Yoshiba M. Combined interferon alpha2b and cyclosporin A in the treatment of chronic hepatitis C: controlled trial. J Gastroenterol 2003;38:567-572.

5. Firpi RJ, Zhu H, Morelli G, Abdelmalek MF, Soldevila-Pico C, Machicao VI, et al. Cyclosporine suppresses hepatitis C virus in vitro and increases the chance of a sustained virological response after liver transplantation. Liver Transpl 2006;12:51-57.

6. Guitard J, Sandres-Saune K, Kamar N, Ribes D, Faguer S, Esposito L, et al. Hepatitis C virus viral load after conversion from tacrolimus to cyclosporine in liver transplant patients: a pilot study. Transplant Proc 2007;39:2603-2605.

7. Hilgard P, Kahraman A, Lehmann N, Seltmann C, Beckebaum S, Ross RS, et al. Cyclosporine versus tacrolimus in patients with HCV infection after liver transplantation: effects on virus replication and recurrent hepatitis. World J Gastroenterol 2006;12:697-702.

8. Martin P, Busuttil RW, Goldstein RM, Crippin JS, Klintmalm GB, Fitzsimmons WE, et al. Impact of tacrolimus versus cyclosporine in hepatitis C virus-infected liver transplant recipients on recurrent hepatitis: a prospective, randomized trial. Liver Transpl 2004;10:1258-1262.

9. Rayhill SC, Barbeito R, Katz D, Voigt M, Labrecque D, Kirby P, et al. A cyclosporine-based immunosuppressive regimen may be better than tacrolimus for long-term liver allograft survival in recipients transplanted for hepatitis C. Transplant Proc 2006;38:3625-3628.

10. Flisiak R, Horban A, Gallay P, Bobardt M, Selvarajah S, Wiercinska-Drapalo A, et al. The cyclophilin inhibitor Debio-025 shows potent anti-hepatitis C effect in patients coinfected with hepatitis C and human immunodeficiency virus. HEPATOLOGY 2008;47:817-826.

11. Nakagawa M, Sakamoto N, Tanabe Y, Koyama T, Itsui Y, Takeda Y, et al. Suppression of hepatitis C virus replication by cyclosporin a is mediated by blockade of cyclophilins. Gastroenterology 2005;129:1031-1041.

12. Yang F, Robotham JM, Nelson HB, Irsigler A, Kenworthy R, Tang H. Cyclophilin A is an essential cofactor for hepatitis C virus infection and the principal mediator of cyclosporine resistance in vitro. J Virol 2008;82:5269-5278.

13. Watashi K, Ishii N, Hijikata M, Inoue D, Murata T, Miyanari Y, et al. Cyclophilin B is a functional regulator of hepatitis C virus RNA polymerase. Mol Cell 2005;19:111-122.

14. Robida JM, Nelson HB, Liu Z, Tang H. Characterization of hepatitis C virus subgenomic replicon resistance to cyclosporine in vitro. J Virol 2007;81:5829-5840.

15. Fernandes F, Poole DS, Hoover S, Middleton R, Andrei AC, Gerstner J, et al. Sensitivity of hepatitis C virus to cyclosporine A depends on nonstructural proteins NS5A and NS5B. HEPATOLOGY 2007;46:1026-1033.

16. Ago H, Adachi T, Yoshida A, Yamamoto M, Habuka N, Yatsunami K, et al. Crystal structure of the RNA-dependent RNA polymerase of hepatitis C virus. Structure 1999;7:1417-1426.

17. Bressanelli S, Tomei L, Roussel A, Incitti I, Vitale RL, Mathieu M, et al. Crystal structure of the RNA-dependent RNA polymerase of hepatitis C virus. Proc Natl Acad Sci U S A 1999;96:13034-13039.

18. Lesburg CA, Cable MB, Ferrari E, Hong Z, Mannarino AF, Weber PC. Crystal structure of the RNA-dependent RNA polymerase from hepatitis C virus reveals a fully encircled active site. Nat Struct Biol 1999;6:937-943.

19. Di Marco S, Volpari C, Tomei L, Altamura S, Harper S, Narjes F, et al. Interdomain communication in hepatitis C virus polymerase abolished by small molecule inhibitors bound to a novel allosteric site. J Biol Chem 2005;280:29765-29770.

20. Nelson HB, Tang H. Effect of cell growth on hepatitis C virus (HCV) replication and a mechanism of cell confluence-based inhibition of HCV RNA and protein expression. J Virol 2006;80:1181-1190.

21. Zhong J, Gastaminza P, Cheng G, Kapadia S, Kato T, Burton DR, et al. Robust hepatitis C virus infection in vitro. Proc Natl Acad Sci U S A 2005;102:9294-9299.

22. Chinnaswamy S, Yarbrough I, Palaninathan S, Kumar CT, Vijayaraghavan V, Demeler B, et al. A locking mechanism regulates RNA synthesis and host protein interaction by the hepatitis C virus polymerase. J Biol Chem 2008;283:20535-20546.

23. Zhong W, Uss AS, Ferrari E, Lau JY, Hong Z. De novo initiation of RNA synthesis by hepatitis C virus nonstructural protein 5B polymerase. J Virol 2000;74:2017-2022.

24. Ranjith-Kumar CT, Kim YC, Gutshall L, Silverman C, Khandekar S, Sarisky RT, et al. Mechanism of de novo initiation by the hepatitis C virus RNA-dependent RNA polymerase: role of divalent metals. J Virol 2002;76:12513-12525.

25. Shim JH, Larson G, Wu JZ, Hong Z. Selection of 3'-template bases and initiating nucleotides by hepatitis C virus NS5B RNA-dependent RNA polymerase. J Virol 2002;76:7030-7039.

26. Kim MJ, Kao C. Factors regulating template switch in vitro by viral RNA-dependent RNA polymerases: implications for RNA-RNA recombination. Proc Natl Acad Sci U S A 2001;98:4972-4977.

27. Niesen FH, Berglund H, Vedadi M. The use of differential scanning fluorimetry to detect ligand interactions that promote protein stability. Nat Protoc 2007;2:2212-2221.

28. Kao CC, Yang X, Kline A, Wang QM, Barket D, Heinz BA. Template requirements for RNA synthesis by a recombinant hepatitis C virus RNA-dependent RNA polymerase. J Virol 2000;74:11121-11128.

29. Kim CH, Kao CC, Tinoco I Jr. RNA motifs that determine specificity between a viral replicase and its promoter. Nat Struct Biol 2000;7:415-423.

30. Kato T, Date T, Murayama A, Morikawa K, Akazawa D, Wakita T. Cell culture and infection system for hepatitis C virus. Nat Protoc 2006;1:2334-2339.

31. Butcher SJ, Makeyev EV, Grimes JM, Stuart DI, Bamford DH. Crystallization and preliminary X-ray crystallographic studies on the bacteriophage phi6 RNA-dependent RNA polymerase. Acta Crystallogr D Biol Crystallogr 2000;56:1473-1475.

32. Shirota Y, Luo H, Qin W, Kaneko S, Yamashita T, Kobayashi K, et al. Hepatitis C virus (HCV) NS5A binds RNA-dependent RNA polymerase (RdRP) NS5B and modulates RNA-dependent RNA polymerase activity. J Biol Chem 2002;277:11149-11155.

33. Dimitrova M, Imbert I, Kieny MP, Schuster C. Protein-protein interactions between hepatitis C virus nonstructural proteins. J Virol 2003;77:5401-5414.

34. Wiedmann B, Puyang X, Poulin D, Mathy JE, Ma S, Anderson LJ, et al. Characterization of mechanism of resistance to cyclophilin inhibitors in HCV replicon. In: 15th International Symposium on Hepatitis C Virus and Related Viruses. Oct. 5-9, 2008; San Antonio, TX.

APPENDIX III

SCREENING OF A NUCLEOSIDE/NUCLEOTIDE MIMIC COMPOUND

COLLECTION FOR BINDING AND INHIBITION OF NS5B

The differential scanning fluorimetry (DSF) assay described in Chapters IV and V
can be used to determine ligand binding to proteins as shown in those chapters and also
as reported by Niesen et al. (*212*) . In order to obtain inhibitors against NS5B we
purchased a nucleoside/nucleotide compound library from SIGMA (Sigma-Aldrich Inc.).
A total of ~125 compounds were purchased that were available directly from stocks or
custom synthesized. Before screening this collection we wanted to determine whether
the DSF assay can be used to determine NS5B interactions with its ligands/inhibitors
other than NTPs. The benzothiadiazine compounds described in Dhanak et al., (2002)
(*132*) were obtained from GlaxoSmithKline. The two compounds are potent inhibitors of
in vitro NS5B activity (*132*). The compounds named as C1 and C2 were included with a
poly-U column purified Δ21 at different concentrations and subjected to DSF assay (Fig.
B1A and B1B). As expected the presence of the compounds showed pronounced
increase in the stability of Δ21 showing compound binding and conformational changes
in the protein. This further confirmed that the DSF assay can be used to determine the
ligand-protein interactions. Next we subjected about 45 compounds from the SIGMA
collection to the DSF assay (Table B1). The remaining compounds had solubility
problems and had to be dissolved in very harsh acidic or basic solutions and therefore
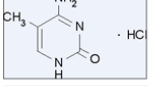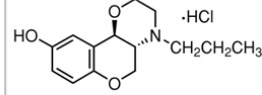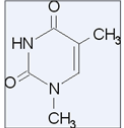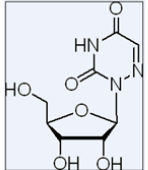were not further analyzed.
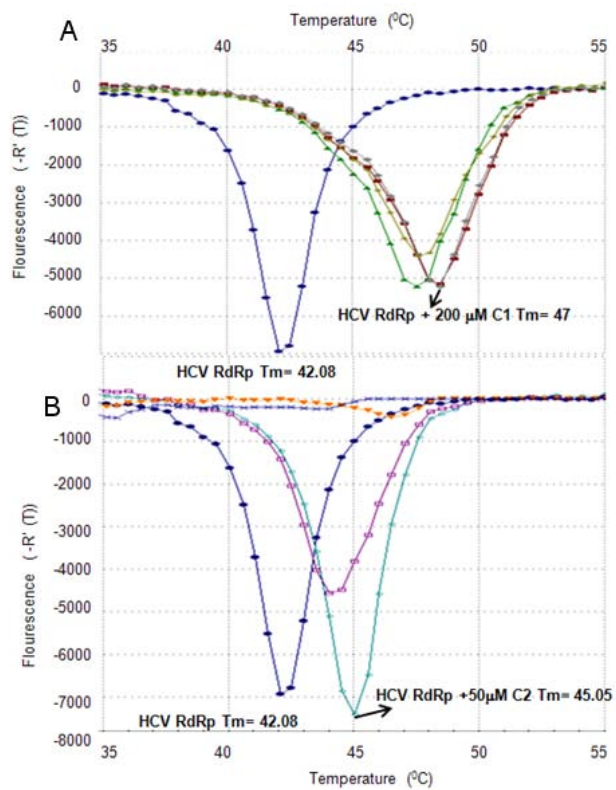
Figure B1: DSF assay of GSK compounds C1 and C2 with poly-U purified Δ21.
While Δ21 alone has a Tm of 42.08 $^{\circ}$C the presence of the compounds at different concentrations showed pronounced right shifts in the Tm as indicated.

Table B1: The compounds that were selected for screening by DSF assay

Compound	code
7-Methylguanosine	A1
5-Fluorouridine	A2
8-METHYLXANTHINE	A3
4-Thiouridine	A4
Thymidine	B3
Xanthine sodium salt	B4
Adenine 9-beta-D-arabinofuranoside	B5
5-Methylcytosine hydrochloride	C10
Uridine	B8
2-Aminopurine nitrate salt	B11
2'-Deoxyuridine	C8
Inosine	B7
2'-Deoxycytidine	D6
1,3,9-Trimethylxanthine	D11
6-Methylpurine	E9
2',3'-Dideoxyadenosine	G2
2-Amino-6-chloropurine riboside	G7
6-(Dimethylamino)purine	G10
(+/-)-PD 128,907 hydrochloride	C3
5-Methoxyuridine	A5
S-(2-HYDROXY-5-NITROBENZYL) -6-THIOINOSINE	A6
Isoxanthopterin	A7
5-Fluoro-2'-deoxyuridine	A8
3-Methyladenine	A10
6-AMINO-1,3-DIMETHYL -5-NITROSOURACIL	B2
6-ETHOXYPURINE	B10
N6-Benzoyladenine	C4
6-Chloropurine riboside	C7
1-Methyladenosine	C11
2'-Deoxyinosine	D1
5-Ethyl-2'-deoxyuridine	D2
1,N6-Etheno-2'-deoxyadenosine	D3
TEGAFUR	D4
5'-Deoxy-5'-(methylthio)adenosine	D5
1-Methylthymine	D10
6-Azauridine	E1
5-Carbethoxyuracil	E3
Indoxyl acetate	E5
2',3'-O-Isopropylideneuridine	E7
5-Iodo-2'-deoxycytidine	E8
6-Methylpurine	E9
IBU-DEOXYCYTIDINE	F1

(Structures of some of the compounds that affected the Tm of NS5B in DSF assay) (Code in parenthesis)

2-Aminopurine Nitrate (B11)

5-Methylcytosine hydrochloride (C10)

(+/-)-PD 128,907 hydrochloride (C3)

1-Methylthymine (D10)

6-Azauridine (E1)

The majority of the tested compounds did not affect the Tm of Δ21 (not shown) while compounds B11, C3 and C10 showed a destabilizing effect on Δ21 when included at 10 mM concentrations (Fig. B2). Intrigued by this result B11, C3 and C10 along with some other compounds were tested for effect on the RdRp activity of Δ21. However none of the compounds significantly affected RNA synthesis by Δ21 at three different concentrations tested (Fig. B3). To understand this better the DSF assay was done for Δ21 and compound B11 in presence and absence of GTP (Fig. B4). The presence of GTP masked the effect of B11 on the stability of Δ21 explaining partially the results of the RdRp assay. A few more compounds out of the ones listed in Table B1 showed a negative shift in Tm of Δ21 (Fig. B4) or a partial denaturation of Δ21 but none of them showed a positive shift in Tm like the C1 and C2 compounds from the GlaxoSmithKline collection (*133*) (Fig. B1). RdRp assays have not yet been performed with Δ21 in presence of the compounds shown in Fig. B4.
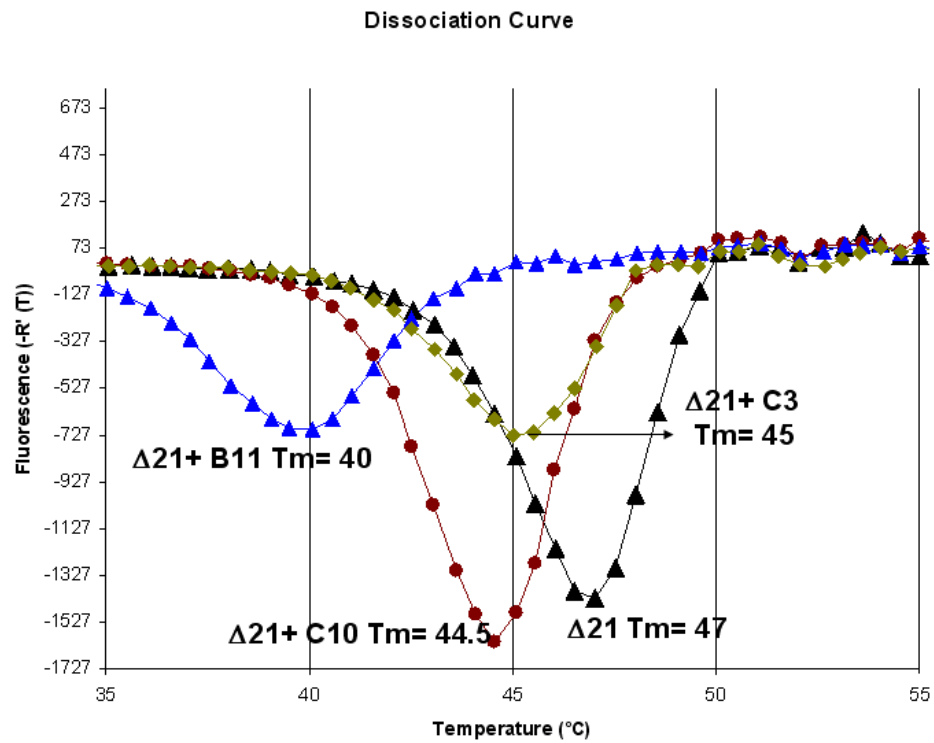
Figure B2: The results of DSF assay of 2 μM Δ21 in absence or presence of 10 mM B11, C3 and C10.

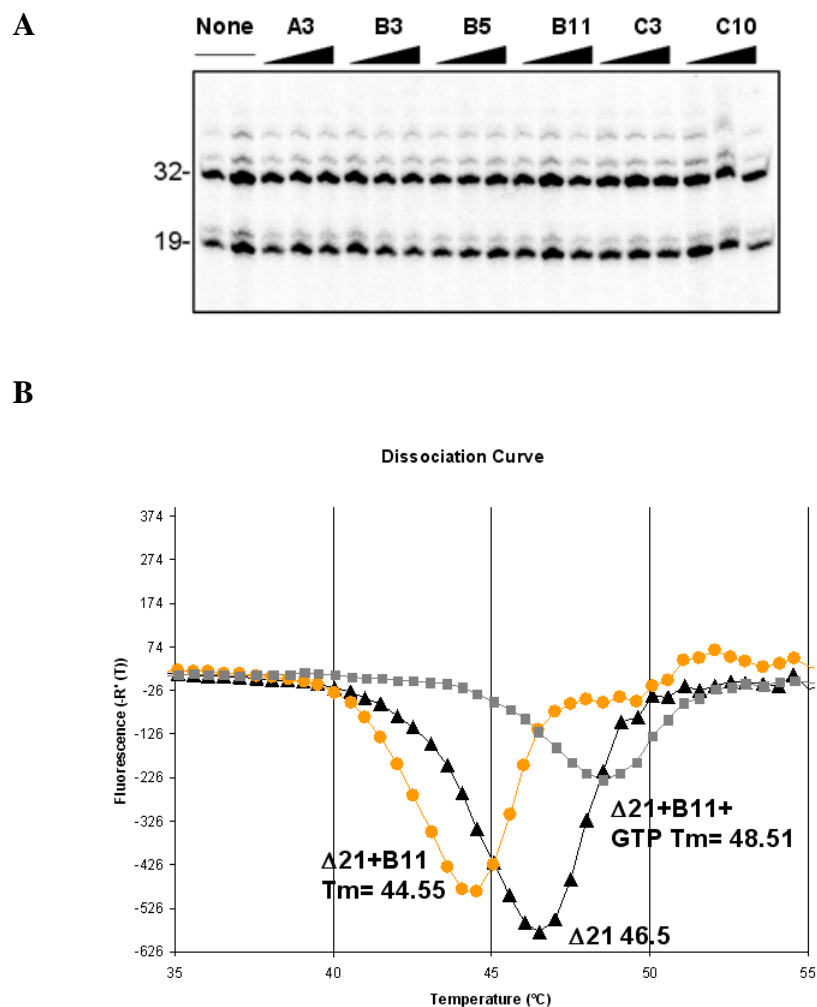Figure B3: A) RdRp assays of Δ21 in presence of 10, 50 and 100 µM of the compounds shown on the top of the gel. Template LE19 and standard RdRp assay conditions (see Chapter 3, Materials and Methods) were used. 19-nt is the de novo product and 32-nt is the primer extension product. B) DSF assay shows that the effect of compound B11 on the stability of Δ21 is masked in presence of GTP.
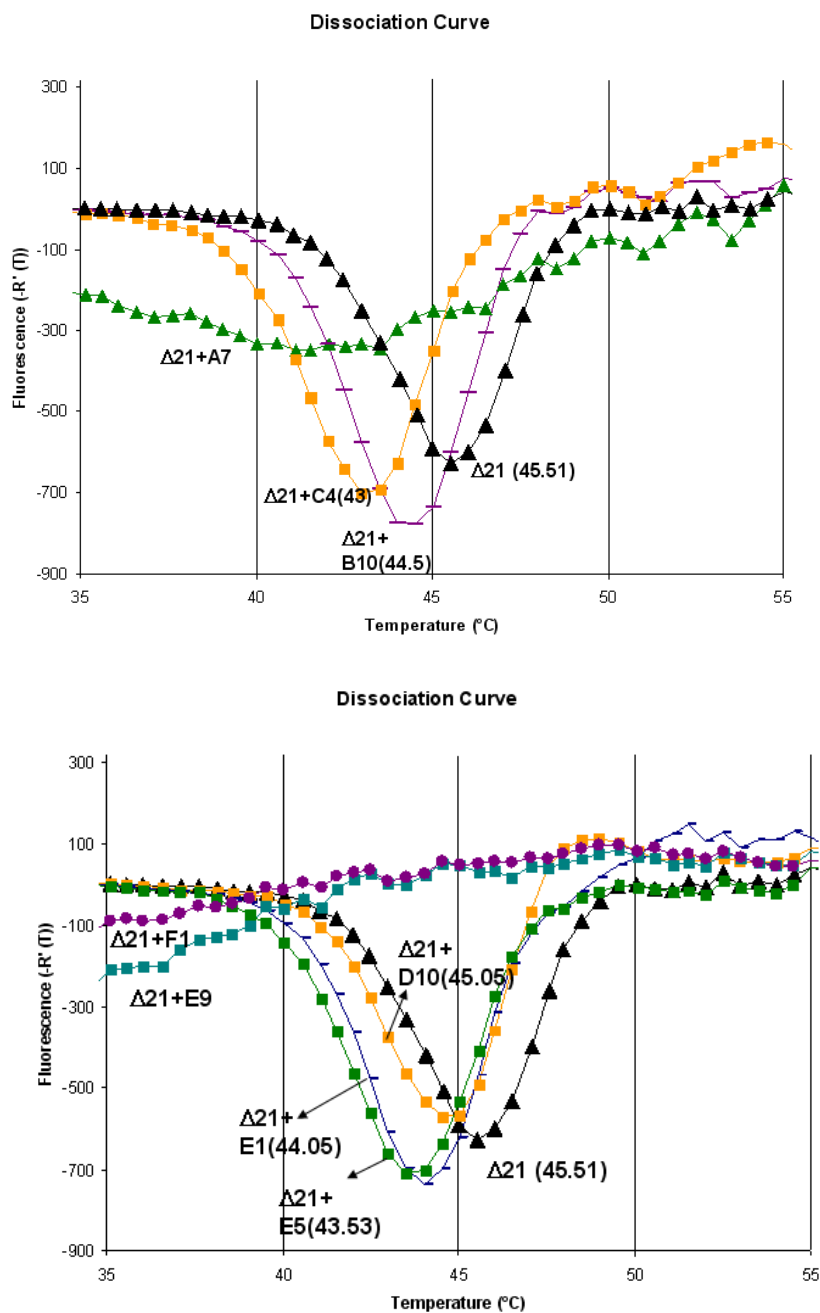
Figure B4: results of DSF assays of Δ21 in absence and presence of 10 mM of each of the compound specified. The Tms are indicated in parenthesis. The conditions of the assay are described in Chapter 4, Materials and Methods.

VITA

Name: Sreedhar Reddy Chinnaswamy

Address: Dept. of Molecular and Cellular Biochemistry
                   MSB I 209, Indiana University
                   Bloomington, IN-47405.

E-mail: sreedharc08@gmail.com

Education: BVSc &AH., Veterinary Sciences, University of
                          Agricultural Sciences, Bangalore, India, 1999.
                   MVSc., Animal Biochemistry, Indian Veterinary Research
                          Institute, Bareilly, India, 2003.
                   MS., Chemistry, New Mexico State University, Las Cruces,
                          NM, USA, 2005.
                   Ph.D., Biochemistry, Texas A&M University, College Station,
                          TX, USA, 2010.

Publications:

Chinnaswamy S, Yarbrough I, Palaninathan S, Kumar CT, Vijayaraghavan V, Demeler B, Lemon SM, Sacchettini JC and Kao CC (2008) A locking mechanism regulates RNA synthesis and host protein interaction by the Hepatitis C Virus RNA polymerase, *J Biol Chem* 283(29):20535-46.

McGivern DR, Villanueva RA, Chinnaswamy S, Kao CC and Lemon SM. (2009) Impaired replication of Hepatitis C Virus containing mutations in a conserved NS5B Retinoblastoma protein-binding motif. *J Virol* 83(15): 7422-33.

Liu Z, Robida JM, Chinnaswamy S, Yi G, Robotham JM, Nelson HB, Irsigler A, Kao CC and Tang H (2009) Mutations in the Hepatitis C virus polymerase that increase RNA binding can confer resistance to cyclosporine A. *Hepatology* 50(1): 25-33.

Chinnaswamy S, Ayaluru A, Li P and Kao CC. Regulation of de novo initiated RNA synthesis in the Hepatitis C virus RNA dependent RNA polymerase by intermolecular interactions. (Submitted to *J Virol*).